

**AN IN-SITU STUDY OF THE NUCLEATION
PROCESS OF POLYURETHANE RIGID FOAM
FORMATION**

**BY
EDEL MINOGUE B.Sc.**

**SUBMITTED TO THE
DEPARTMENT OF CHEMICAL SCIENCES**

**FOR THE DEGREE OF
DOCTOR OF PHILOSOPHY**

**AT
DUBLIN CITY UNIVERSITY
OCTOBER 2000**

Under the Supervision of

**Prof. J. G. Vos (Dublin City University)
Dr. A. Biedermann (BASF Schwarzheide GmbH)**

I hereby certify that this material, which I now submit for assessment on the programme of study leading to the award of **Doctor of Philosophy** is entirely my own work and has not been taken from the work of others save and to the extent that such work has been cited and acknowledged within the text of my work.

Signed: Edel Nkomo

ID No.: 97970697

Date: 30.01.01

Dedicated to my parents

Table of Contents

Abstract	1
Objective of Thesis	2
Thesis Overview	2
Glossary of Polyurethane Foams	3
1. Polyurethane Formation	6
1.1. Introduction	6
1.2. Chemical Background	8
1.3. General Composition	11
1.4. Formulation and Synthesis of Components	12
1.4.1. Isocyanates	12
1.4.2. Polyols	13
1.4.3. Blowing Agents	15
1.4.4. Catalysts	15
1.4.5. Surfactants	17
1.4.6. Prepolymers	19
1.5. Basic Principles of Foam Formation	20
1.5.1. The Gas Dissolution Stage	21
1.5.2. The Cell Nucleation / Bubble Formation Stage	22
1.5.3. Nucleation – Theories	23
1.5.3.1. Classical Nucleation Theory	24
1.5.4. The Bubble Growth Stage	32
1.5.5. The Bubble Stability Stage	34
1.6. Interfacial Phenomena	36
1.6.1. Surface Tension	36
1.6.2. Curved Interfaces - The Kelvin Equation	37
1.6.3. Capillarity	38
1.6.4. Viscosity	39
1.6.5. Colloids and Micelles	39
1.7. Fundamentals of Thermal Insulation - Polymer Physics	42
1.7.1. λ_s , Thermal Conductivity Through the Solid	42

1.7.2. λ_r , Radiative Heat Transfer	44
1.7.3. λ_g , Thermal Conductivity Through the Gas	45
2. Development of Experimental Methods	47
2.1. Introduction	47
2.2. In-Situ FTIR Spectroscopy	51
2.3. Thermal and Pressure Analysis	51
2.4. Dynamic Rheology	52
2.5. Positron Emission Tomography	52
2.6. Two- Colour Dynamic Light Scattering	53
2.7. In-Situ Microscopic Analysis – Part 1 – Method Development	54
2.7.1. Fundamentals of Light Microscopy	54
2.7.2. Determination of the Target	58
2.7.3. Determination of the Factors, Factor Ranges and Factor Constraints	58
2.7.3.1. The Mixing Process	59
2.7.3.2. Foaming under Controlled Temperature	63
2.7.4. Generation of Method Design	66
2.7.4.1. Image Processing	66
2.7.4.2. Implementation of Imaging Process	67
2.7.5. Realisation	70
2.7.6. Optimisation of the Method	73
2.7.6.1. Nucleation Number Corrected $[NZ_c]$	73
2.7.7. Experimental and Mathematical Validation	78
2.7.7.1. Statistics	78
2.7.7.2. Reproducibility	80
2.8. In-Situ Microscopic Analysis – Part 2 – A Study of the Nucleation Process	82
2.8.1. Influence of Gas Concentration on the Nucleation Process	82
2.8.2. Effect of Blowing Agent on the Nucleation Process	83
2.8.3. Effect of Surfactant Amount on the Nucleation Process	84
2.8.4. Effect of Surfactant Type on the Nucleation Process	84
2.8.5. Effect of Catalyst Amount on the Nucleation Process	85
2.8.6. Effect of Catalyst Type on the Nucleation Process	85
2.8.7. Effect of Emulsifier on the Nucleation Process	87

2.8.8. Effect of Prepolymer on the Nucleation Process	87
2.8.9. Influence of a Filler on the Nucleation Process	87
2.8.10. Opened-Cell Polyurethane Form	88
2.9. Measurement of End Cell Diameter	88
2.10. Calculation of Nucleation Number (NZ_{cal})	89
2.11. Surface Tension	90
2.11.1. The Lecomte du Noüy Tensiometer - Ring Method	90
2.11.2. The Pendant Drop Method	91
2.11.3. The Maximum Bubble Pressure Method	92
2.11.4. Surface Tension Measurements with a Cyclopentane Vapour Interface	93
2.12. Surfactant Analysis	95
2.12.1. Structural Analysis of Surfactants	95
2.12.2. Determination of the Turbidity Point of Surfactants	95
2.13. Vapour Pressure Measurements	96
2.14. CO ₂ Solubility	96
3. Results and Discussion	98
3.1. Foam Samples	98
3.2. Macroscale Analysis	99
3.2.1. In-Situ FTIR Spectroscopy	99
3.2.2. Thermal and Pressure Analyses	103
3.2.3. Dynamic Rheology	107
3.3. Positron Emission Tomography	110
3.4. Two-Coloured Dynamic Light Scattering	110
3.5. In-Situ Analysis of the Nucleation Process	111
3.5.1. Initial Study: A- and B-Components	111
3.5.2. Influence of Blowing Agent Concentration on the Nucleation Process	115
3.5.3. Effect of Blowing Agent on the Nucleation Process	117
3.5.4. Effect of Emulsifier on the Nucleation Process	122
3.5.5. Effect of Surfactant Amount on the Nucleation Process	127
3.5.6. Effect of Surfactant Type on the Nucleation Process	133
3.5.7. Effect of Catalyst Amount on the Nucleation Process	147

3.5.8. Effect of Catalyst Type on the Nucleation Process	152
3.5.9. Effect of Prepolymer on the Nucleation Process	156
3.5.10. Influence of Filler on the Nucleation Process	161
3.5.11. CO ₂ Solubility	165
3.5.12. Optimisations	168
4. Applicability to Commercial Systems	174
5. Conclusion	178
6. Future Work / Recommendations	184
7. Nomenclature	187
7.1. Greek Symbols	190
8. Acknowledgements	191
9. References	192
Appendices	i
A 1 - Key to Composition of Systems Used	i
A 2 - Examples of Gaussian Distributions Obtained form In-Situ Analyses	iii
A 3 - Positron Emission Tomography Results	v
A 4 - Two-Coloured Dynamic Light Scattering Results	vii
A 5 - A Method to Calculate the Maximum Number of Possible Nucleation Sites	viii
A 6 - Opened-Cell Polyurethane Foam Results	ix
A 7 - Surface Tension	x
A 8 - Surfactant Analysis	xv
A 9 - Measured Cell Diameter in Finished Foam	xviii
A 10 - CO ₂ Solubility – Method of Partial Pressures	xiv
A 11 - Publications	xx

Abstract

There have been many theoretical descriptions of the nucleation process but very few detailed experimental research has been carried out. The nucleation process was systematically analysed with the aim of gaining a deeper understanding of foam formation and the nucleation process, in order to develop possibilities in influencing it and to ultimately reduce the thermal conductivity.

A method was developed whereby the nucleation process could be observed in-situ and subsequently analysed by means of a PC-controlled camera attached to a stereo microscope. The increase in volume due to foam formation and its exothermic reactivity was taken into consideration. Thereby, the amount of cell nuclei in the initial phase was examinable and cell growth including coalescence could be followed. The initial nuclei compared favourably to the final number of cells and to their size, providing a consistency with real foaming conditions.

Detailed research was carried out on the effect of various types and amounts of blowing agents (e.g. carbon dioxide, cyclopentane, perfluoroalkanes), surfactants, catalysts, fillers and isocyanates on the nucleation process. Other important factors influencing the nucleation process are the component's viscosity and surface tension and their relationship with each other during the foaming process. The surface tensions and viscosities of the various systems used were also investigated using several known methods.

Perfluorohexane-blown foams have larger nucleation numbers than either CO₂- or cyclopentane-blown foams. This is only true when an emulsifier is present. Contrary to the literature, the initial number of nuclei did not vary with respect to surfactant type. Nucleation numbers proved to be independent of surface tensions values proving that lowering the surface tension does not automatically ensure higher nucleation numbers. Surfactants were shown to have either stabilising or emulsifying abilities. An improvement in nucleation numbers was obtained by improving the compatibility of the A- and B-components through the use of prepolymers. One can conclude that nucleation is a complex heterogeneous process in which surfactants, catalysts and fillers play a minor roll.

Objective of Thesis

In the search for a rigid foam which is an equally good thermal insulator as the banned CFC-produced foam, we need to take a closer look at the “roots” or “nucleus” of polyurethane rigid foam formation. A greater understanding of the nucleation process of polyurethane rigid foam is therefore necessary. In this thesis an in-situ study of the nucleation and foam formation processes has been developed. Using model systems with varying amounts and types of blowing agents, surfactants, catalysts, fillers etc. the nucleation process was analysed. The results, with the aid of surface tension, viscosity, temperature and pressure and other analysis, posited new theories on the nucleation process.

Thesis Overview

The thesis starts with an introduction to the fundamentals of polyurethane foam formation, discussing its general chemistry. This is followed by the theory of bubble formation and the nucleation process. The theory of thermal insulation is reviewed highlighting the current problems facing industry with regards to polyurethane as an insulation material. Chapter 1 is a description of the experimental, describing not only the procedures carried out but also the development of the methods implemented. The experimental results and discussion are presented in chapter 3. The work was conducted in co-operation with BASF Schwarzheide GmbH and therefore the applicability of the experimental results using model systems to commercial systems was study in chapter 4. Conclusions are presented in chapter 5. Chapter 6 offers recommendations for future work.

Due to the unfamiliarity of terms used herein, a glossary of polyurethane terminology subsequently follows.

Glossary of Polyurethane Terms

A-Component	A blend of polyol, catalyst, surfactant and blowing agent which, when reacted with the B-component, produces a polyurethane foam.
B-Component	The isocyanate material which will be reacted with the polyol or A-component.
Blowing Agent	The constituent of the foam mixture which physically or chemically causes gas production during the chemical reaction.
Cell	The cavity remaining in the structure of polyurethane foam surrounded by polymer membrane or the polymer skeleton after blowing is complete.
CFC-Free Foam	Polyurethane foams that have been made without the use of chlorofluorocarbons as an auxiliary blowing agent.
Core Density	The density of the foam sampled without skin, glue lines or compressed sections at or near the centre of the final foamed form.
Cure	A term referring to the process whereby chemical reactions approach completion. At 100% completion, a foam should have 100% of the physical properties attainable with that particular formulation.
Fine Cells	A term used to describe foam with a cell count of 80 or more per lineal inch.
Fire Retardants	A material that, when added to polyurethane foam, will cause the foam to be more difficult to ignite or burn less rapidly or lose less weight during a fire than without that material

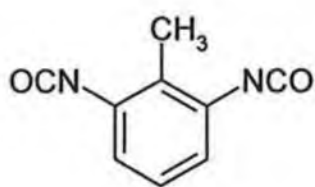
Foam	A lightweight cellular material resulting from the introduction of gas bubbles into a reacting polymer.
Formulation	The list of chemicals and their relative amounts to be used in the preparation of a foam.
Functionality	The number of hydroxyl groups per molecule of the polyol which are available as reaction sites. The higher the functionality the greater the reactivity of the polyol.
Hydroxyl Number	A factor used in the calculation of the equivalent weight of a polyol.
Nucleation	The process whereby, the gas nuclei which expand to form the cells of the foam, are formed.
Polyether	A polymeric polyol containing ether linkages (C-O-C) in the main molecular chain or in side chains.
Polyester	A polymeric polyol, ester based.
Polyol	A key chemical in foam formulation which, when mixed with diisocyanates and other specific ingredients, produces the reaction that causes polyurethane foam to form.
Polyurethane	Generally, a polymer connected by urethane groups. Urethane linkage and its supplements result from the reaction of polyol with isocyanate.
Prepolymer	A reacted, but not completely polymerised product. In the polyurethane industry this is usually a prereacted product formed by reacting polyol(s) or water with diisocyanate(s). The materials normally contain residual free isocyanates groups for further reaction with more polyol(s) or water to produce the final polymer.

Struts	The structural members of a foam material. These roughly triangular features contain most of the solid polymer and form the cell shape.
Surfactants	A term to describe substances that provide resiliency and stability to thin films and that markedly lower the surface tension of liquids.
Urethane	Actually a misnomer as applied to polyurethane foam. A colourless, crystalline substances used primarily in medicines, pesticides and fungicides. Urethane is not used in the production of urethane polymers or foams. The urethanes of the plastics industry are so named because the repeating units of their structures resemble the chemical urethane.

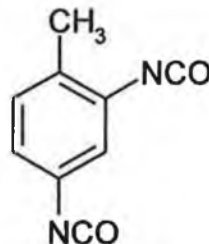
1. Polyurethane Formation ¹

1.1. Introduction

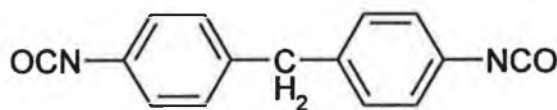
The foundation stone of polyurethane chemistry lies in the ability of the isocyanate group (-NCO) to react with both compounds containing active hydrogen and with itself. Otto Bayer, IG Farbenindustrie discovered in 1937 the polyaddition reaction from which he developed in the 1940s rigid polyurethane foams. These first foams were based on toluene diisocyanate (TDI) and polyesters terminated in both hydroxyl and carboxyl groups. Polyurethane has developed enormously both in its composition and production techniques over the last 60 years. To date, the largest markets for rigid polyurethane are in construction and thermal insulation. Current foams are based on branched polyether polyols terminated in hydroxyl groups. In most cases, polyfunctional isocyanates of the diphenylmethane diisocyanate (MDI) type have replaced TDI.



(1)



(2)



(3)

Fig. 1-1: Structure of 2,6-toluene diisocyanate (TDI) (1), 2,4-toluene diisocyanate (TDI) (2) and 4,4'-diphenylmethane diisocyanate (MDI) (3).

Chlorofluorocarbons (CFCs) initially replaced carbon dioxide as the foam blowing agent. These compounds (e.g. CFCl_3) have low boiling points, filling closed foam cells with the vapour that provides such foams with their typical low thermal conductivity. However, the Montreal Protocol criticised the use of CFCs due to their contribution to atmospheric ozone depletion and international regulations were developed in order to phase out their use by the year 2000. Since it was very difficult to introduce “drop-in” replacements which would have zero ozone depletion potential (ODP) and global warming potential (GWP), the 1990 Montreal Protocol Amendment introduced the concept of “transitional substances”. Hydrochlorofluorocarbons (HCFCs) were considered to be such a substance. However, the ban on all such substances implemented since the start of 2000 has continued the research on the thermal insulation properties of polyurethane foam with the hope of producing a foam with an equally good insulation capacity as the former CFC foams. The use of hydrocarbons since 1993 has been a step in the right direction. However, the ultimate goal of an environmentally sound super insulator is still just out of reach.

The amount and type of blowing agents available is limited and research^{2,3} has shown that none of the blowing agents produce a foam with an equally good insulation capacity as the former CFC foams. This prompts the supposition that the only possible way to reduce the thermal conductivity is the production of foams with finer cells. Several morphological studies have been carried out on rigid polyurethane foam^{4,5,6}. However, there is a paucity in the literature of studies of the formation and in particular the nucleation process of rigid polyurethane foam. Therefore, a fundamental and vital study in the search for an excellent thermal insulator is the in-situ analysis of the nucleation process of polyurethane rigid foam.

1.2. Chemical Background^{1,7}

Polyurethane has a wide spectrum of structural properties, which is influenced by the raw materials used. On a molecular scale the type of polyurethane is dependent on the variation of chain length and the amount of networking, resulting in either thermoplastic polyurethane (alternating segmented rigid and flexible polymer), flexible foam (large flexible, elastic polymer segments with rigid centres) or rigid foam (compact network polymer).

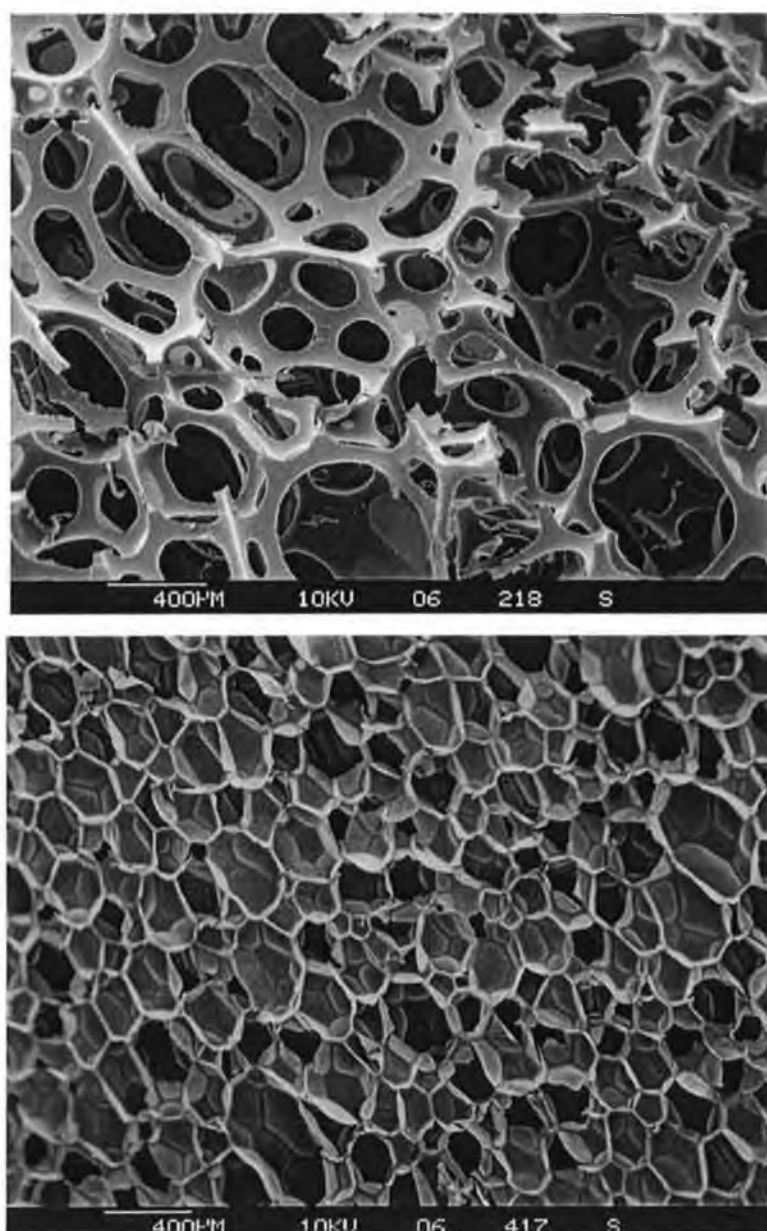
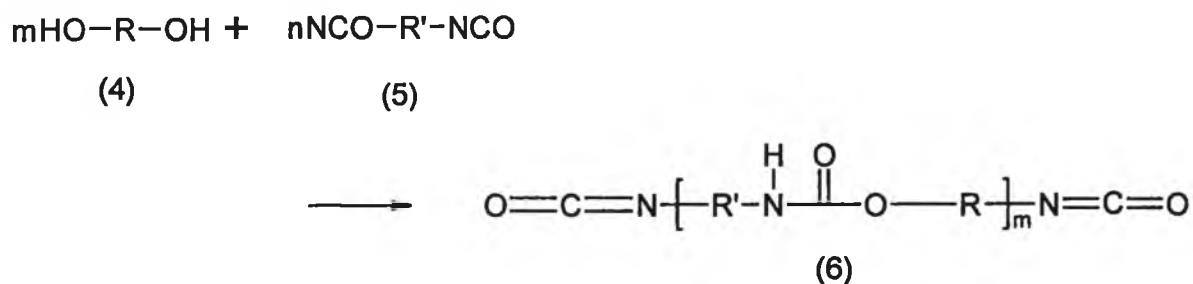


Fig.1-2: *Scanning Electron Microscope (SEM) images showing the structural differences between flexible open-celled PU foam (above) and rigid close-celled PU foam (below).*

The basic raw materials for polyurethane are isocyanates and polyols. Rigid polyurethane foam is formed by reaction of polyisocyanates and the polyol in the presence of selected catalysts, surfactants and blowing agents. The two main catalyst types for the reactions of rigid polyurethane foams are tertiary amines and metal salts. The fine, uniform cell structures of rigid PU foams depend on suitable surfactants or stabilisers. These are predominantly block copolymers of polyether and polysiloxane structures, which vary in molecular weight and branching. As has been previously mentioned, blowing agents have evolved from the traditional CFCs to HCFCs and now CO₂ and hydrocarbons (e.g. pentane) as a result of the increasing awareness of the ODP and GWP of the former. Additives such as flame retardants are also added to inhibit ignition of the foam.

A traditional rigid PU foam formulation consists of the above components combined in a chemically and physically balanced amount. Generally, the polyisocyanate is considered as the B-component and all other components combined considered as the A-component.

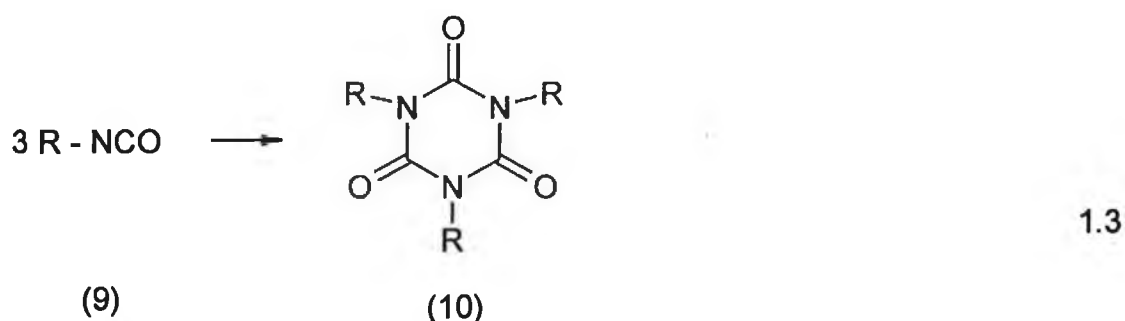
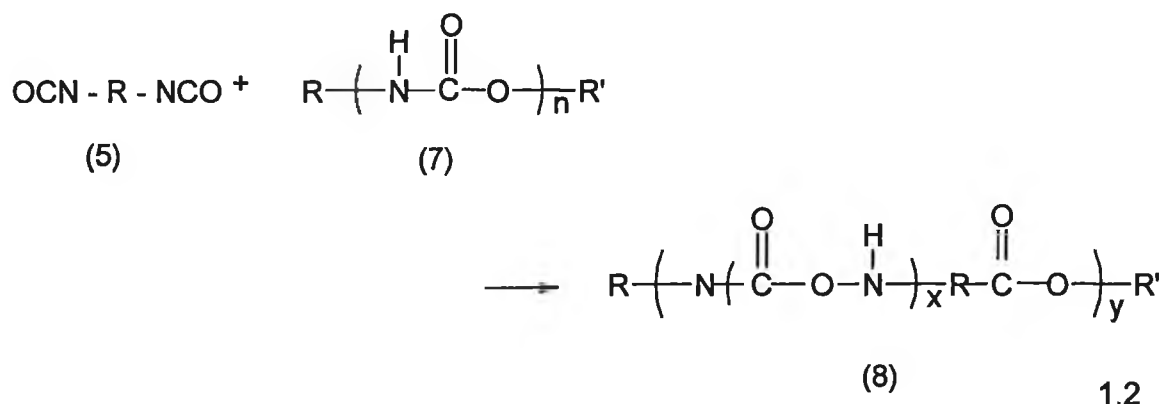
Rigid polyurethane foams are not polymers of ethyl carbamate, commonly known as urethane but are in fact block copolymers containing ether, ester and other functional groups. The principal reaction takes place between the polyfunctional isocyanates (5) and polyhydroxyl compounds (4), commonly known as polyols, forming the urethane linkage. This can be considered as a polyaddition reaction and accounts for the gelling process in foaming.



1.1

Fig. 1-3: The principle reaction in the formation of polyurethane.

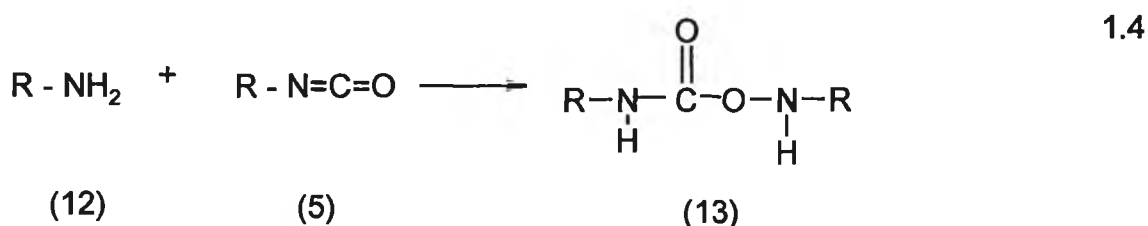
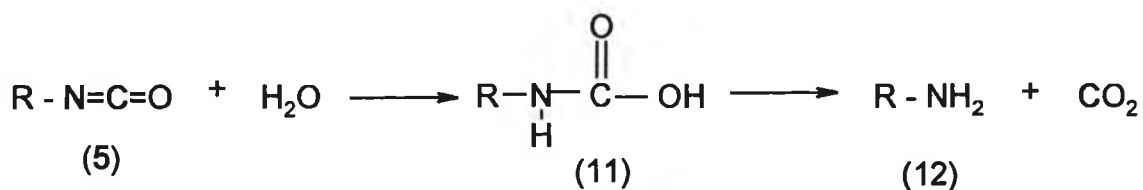
In the presence of excess isocyanate, further reaction can produce allophanates (8),



isocyanurates (10) and other secondary products:

Fig. 1-4: The presence of isocyanate can lead to further reaction, producing allophanates (8) and isocyanurates(10).

A second reaction, between the water and isocyanate, generates via an unstable intermediate, carbon dioxide and substituted ureas (12) and is responsible for the blowing of the foam. In the presence of excess isocyanate this reacts further to form substituted biurets (13).



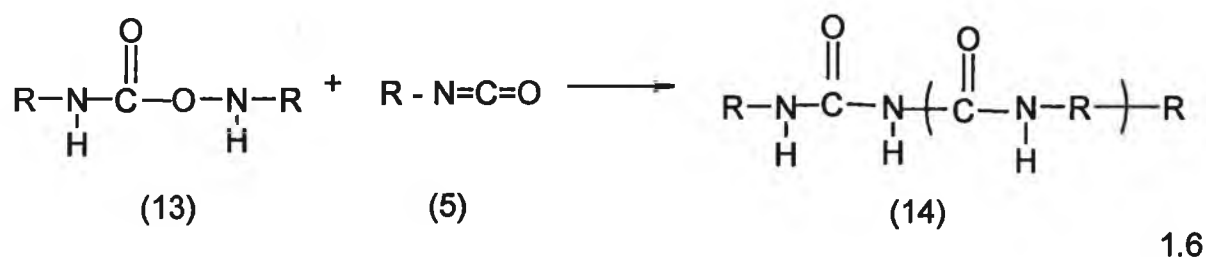


Fig. 1-5: The blowing reaction (reaction 1.4) caused by the production of CO₂ from the reaction of water and isocyanate. Excess isocyanate reacts further to form substituted biurets (13), (14).

Carbon dioxide is an effective blowing agent for polyurethane rigid foam but due to its high thermal conductivity it is a disadvantage in thermal insulation applications.

1.3. General Composition^{1,7}

Generally polyurethane rigid foam formulations contain the components listed below combined in chemically and physically balanced amounts.

Polyol:	One or more, hydroxyl number approximately 450mg KOH/g polyol
Isocyanate:	A polymeric MDI-type polyisocyanate in approximately 5% excess over hydroxyl groups.
Catalysts:	Up to 2wt%
Surfactants:	Up to 1wt%
Blowing Agent:	H ₂ O up to 5wt%; hydrocarbons, CFCl ₃ up to 15wt%
Flame Retardant:	Up to 30wt%.

The polyisocyanate is considered as the B-component and all other components are combined to form the A-component.

Rigid polyurethane foam is prepared in the following manner in the laboratory.

1. The A- component is premixed.
2. Components A and B are added together

3. The mixture is then mixed for approximately 8 seconds. At the start of mixing a stopwatch is started so as to measure the following characteristic time intervals:

3.1. Cream time: start of volume increase.

3.2. Gel time: the foam has developed enough gel strength to resist light impressions and is dimensionally stable.

3.3. Rise Time: end of the actual foaming process and the increase in volume.

3.4. Tack-free time: the surface of the foam is no longer adhesive.

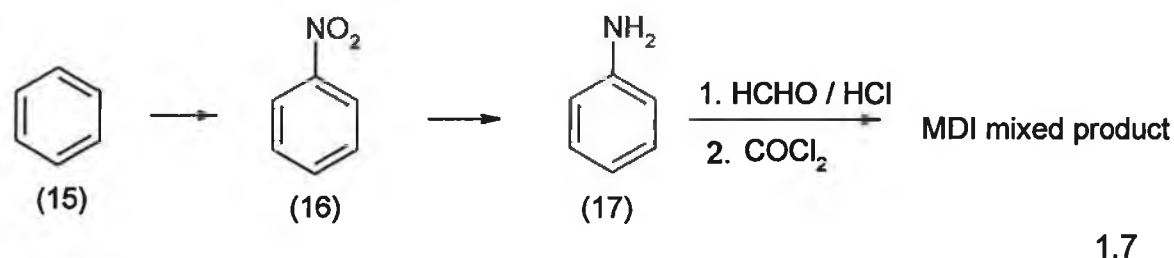
3.5. Curing: foaming is complete and the polyaddition product gels and solidifies.

1.4. Formulation and Synthesis of Components

1.4.1. Isocyanates^{1, 7}

For rigid polyurethane foams, polymeric isocyanates such as biphenyl methane diisocyanate or MDI (3) are mainly used. Its high isocyanate content and high vapour pressure limit the use of toluene diisocyanate (TDI)(1 and 2). Isocyanates are characterised by the %NCO content and their functionality, which describes the amount of NCO groups per molecule.

The first step in the production of polymeric MDI is the nitration of benzene (15) followed by reduction of the nitro-group (16) to produce aniline (17). The acid catalysed condensation of aniline in the presence of formaldehyde produces polyamines, which on phosgenation produce a mixture of MDI products (3), (18), (19). These products usually contain approximately 50% of the diisocyanate, predominately 4,4'-MDI(3), with decreasing amounts of oligomers having functionalities as high as 8 or 10. The composition of the polyisocyanates can be controlled by the aniline-formaldehyde condensation. Strong acid catalysts tend to result in the formation of the para-isomer, weaker acids in the ortho-isomer. Higher aniline/formaldehyde ratios produce higher concentrations of the diisocyanate.



MDI mixed product:

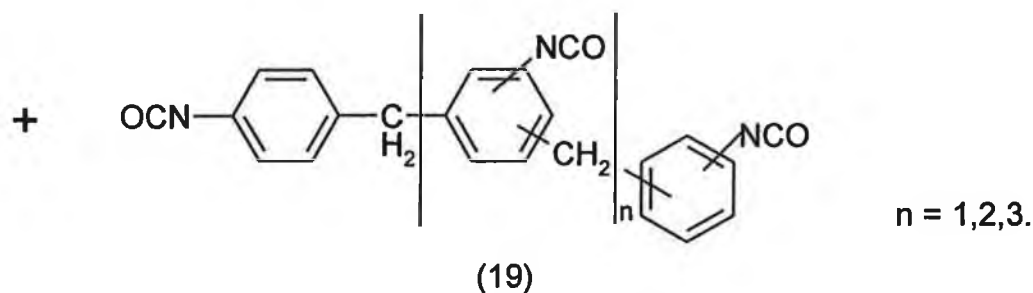
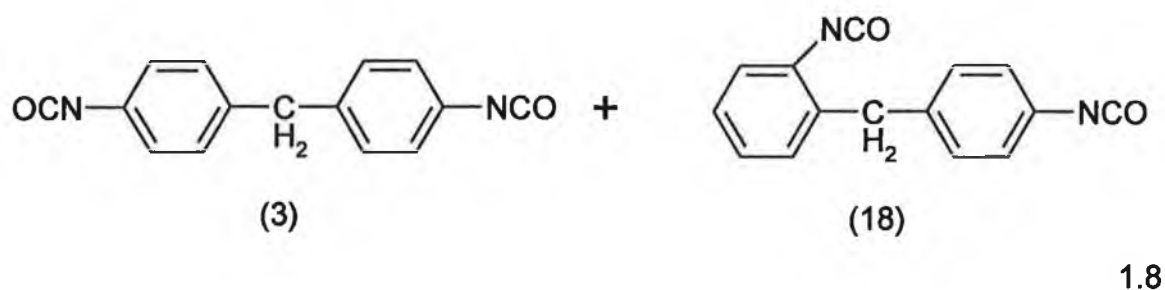


Fig. 1-6: Synthesis of polymeric MDI

1.4.2. Polyols^{1,7}

The main reaction partner for the isocyanates are polyhydroxyl compounds (polyols). These are characterised by the hydroxyl number (OH-No. in mg KOH/g) which is inversely proportional to the molecular weight. Polyols mainly used for rigid polyurethane foams are low molecular weight hydroxyl terminated polyethers, polyesters and natural products (e.g. castor oil).

Polyether polyols used in rigid foam are produced by addition of 1,2-propylene oxide (PO) (20) and ethylene oxide (EO) to the hydroxyl group (or amino groups) of low molecular weight molecules, usually by anionic chain mechanism:

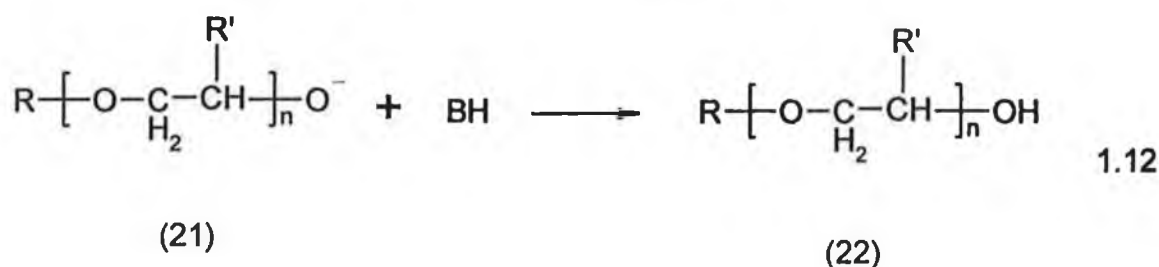
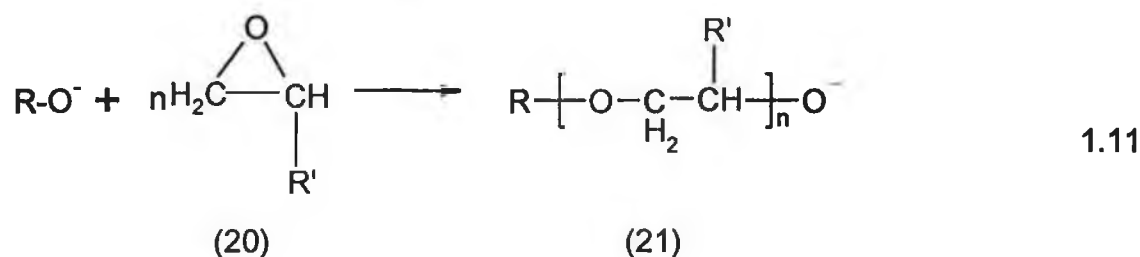


Fig. 1-7: Synthesis of polyether polyols by anionic chain mechanism.

Rigid polyurethane foams require polyols with a high functionality and short polyether chains.

Polyester polyols are prepared by the polycondensation reaction of di-, or polycarbonic acid or their anhydrides (e.g. phthalic acid, phthalic anhydride) with di- and polyalcohols (e.g. ethylene glycol).

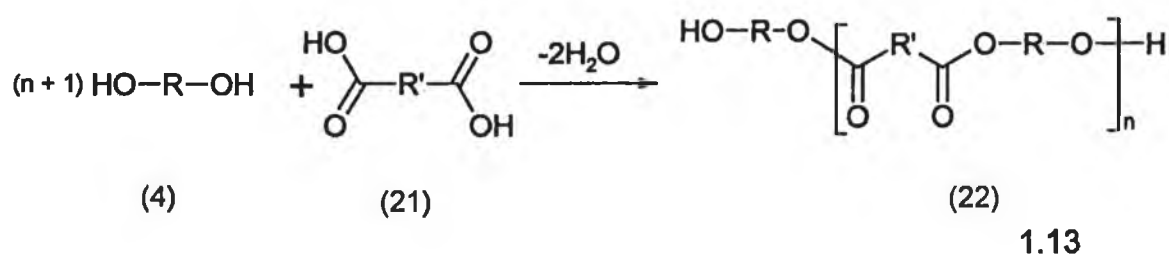


Fig. 1-8: Synthesis of polyester polyols by polycondensation.

1.4.3. Blowing Agents⁸

Foaming can be caused either chemically or physically. Foaming processes using chemical blowing agents (CBAs) are regarded chemical and those using physical blowing agents (PBAs) are regarded physical. CBAs are compounds or mixture of compounds that liberate gas as a result of a chemical reaction such as that which occurs during the reaction of isocyanate with water, liberating carbon dioxide. PBAs are compounds that liberate gas as a result of a physical process at elevated temperatures or reduced pressures. They do not undergo chemical reaction themselves and are mostly liquids with low boiling points, e.g. CFCs, pentane. They evaporate to gas by the heat of the exothermic reaction of foaming.

1.4.4. Catalysts⁷

Catalysts are used to increase the reaction rate and to establish the proper balance between the chain extension and the foaming reaction. They are either base-driven or nucleophile driven (see Fig. 1-9). The catalysts most commonly used are tertiary amines such as triethylamine, and alkali metal salts, e.g. potassium acetate. When a physical blowing agent is used, more catalyst or a more reactive catalyst is necessary due to the cooling effect of the evaporating solvent. In such cases, more active tertiary amine catalysts such as dimethyl-cyclohexylamine are helpful. Catalysts are used from 0.1 to 3.0% in varying concentrations of the total reactants. Certain catalysts such as tertiary amines affect both the isocyanate-hydroxyl and the water-isocyanate reaction, while others like dibutyltin dilaurate promote primarily the isocyanate-hydroxyl networking of the polyol reaction and chain propagation. The foam's properties can be controlled by the proper choice of catalyst.

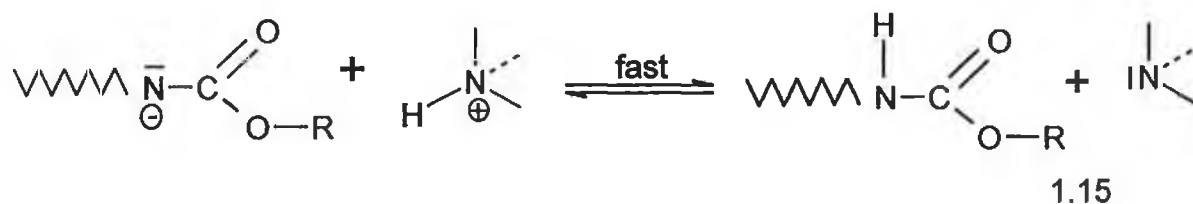
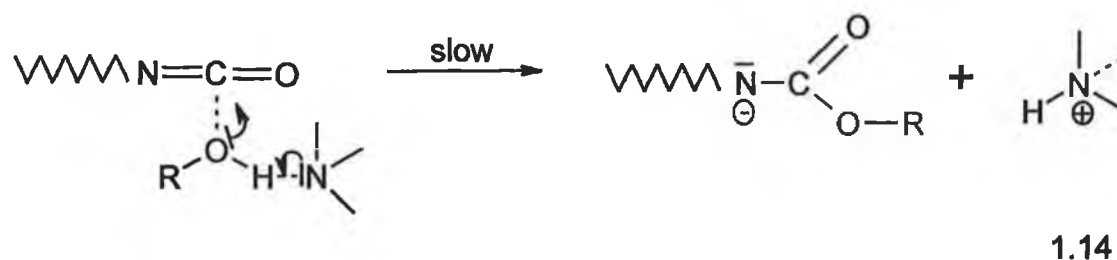


Fig. 1-9: Base driven catalysis

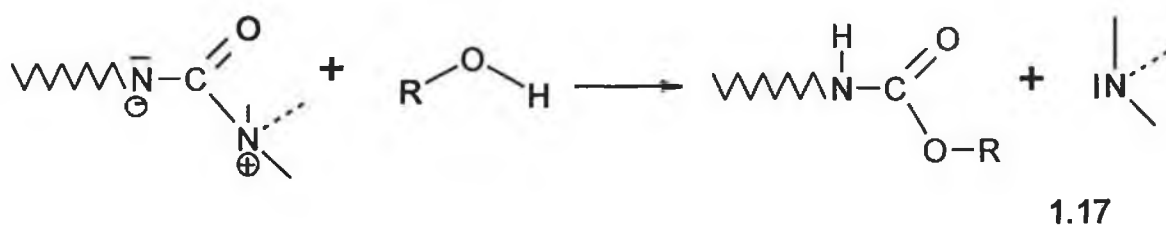
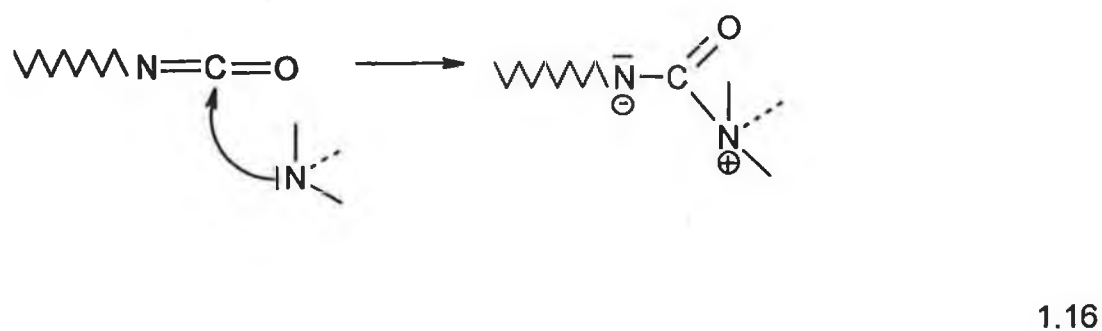
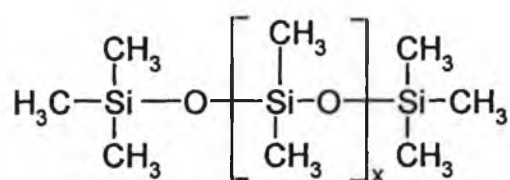


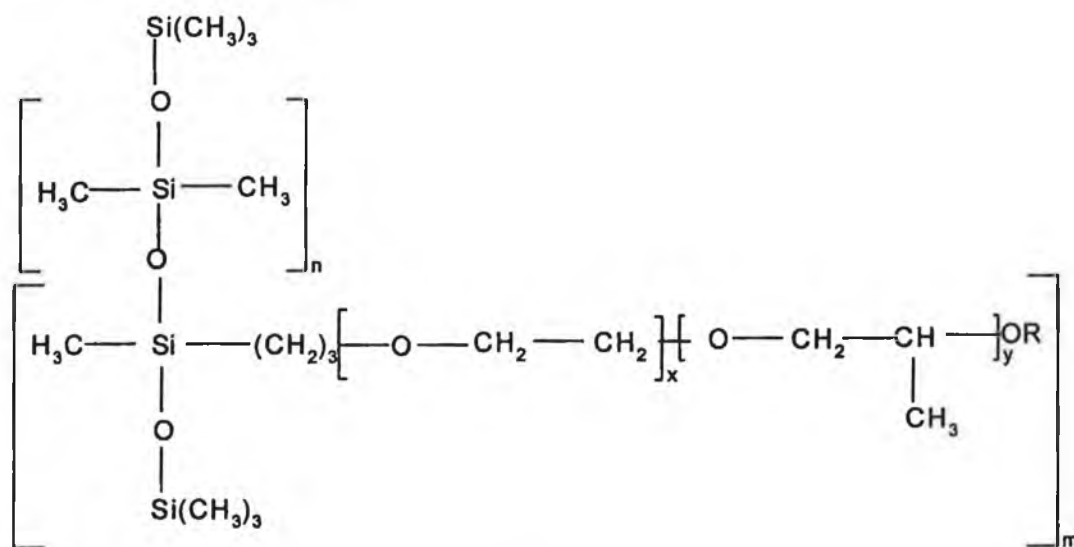
Fig. 1-10: Nucleophilic driven catalysis.

2.2.5. Surfactants⁹

Surface active agents, also known as surfactants or stabilisers have a large influence on the fine cell structure of rigid polyurethane foam. The well-known tail-head model ($\sim\text{O}$) is widely used in depicting simple surfactants, the tail (\sim) symbolises the hydrophobic group and the head (O) the hydrophilic group. The hydrophobic groups are mainly alkyl or alkylaryl hydrocarbon chains but siloxyl alkyl groups are also possible. Surfactants containing water-soluble silicones have proven to have an excellent ability to regulate cell size and cell wall stability. Two of the more common surfactants used in polyurethane foams are dimethyl polysiloxane (23) and dimethylpolysiloxane-polyalkylene oxide copolymer (24), the latter being primarily used.



(23)



(24)

Fig. 1-11: Chemical structure of dimethyl polysiloxane (23) and dimethylpolysiloxane-polyalkylene oxide copolymer (24)

Ethylene oxide-propylene oxide (EO/PO) block copolymers are prepared by sequential anionic polymerisation of alkylene oxides. The molecular weight and block composition of the copolymers determines the hydrophilic/hydrophobic balance and controls the surfactant properties. Block copolymers sterically stabilise the formed bubble nucleus by adsorbing onto the surface in a way that one block acts as an anchor and the second remains flexible and extends out into the polymer matrix.

Kanner and Decker¹⁰ highlighted that the unique surface-active properties of block copolymers are one of the principal reasons for the successful development of polyurethane foam. The most important function of the surfactant is the bubble stabilisation. Traditionally four different aspects of stabilisation have been investigated¹¹:

1. *Nucleation*. It is believed that the surfactant aids bubble nucleation by stabilising a dispersion of air, and essentially the nucleation centres for CO₂, in the foam-mixture.
2. *Emulsification*. This assists in the blending of the otherwise incompatible raw materials.
3. *Surface Elasticity*. This provides surface elasticity to the expanding films (Gibbs and Marangoni principle, see section 1.5.5.).
4. *Surface Viscosity*. This acts to retard the drainage within the membrane (cell wall) of the foam by building up surface viscosity.

Unfortunately it is not possible to predict the ability of a certain surfactant as its performance differs from formulation to formulation. Surfactants are generally used in the concentration range of 0.1 to 2.0% of the total reactants. Many studies have been conducted^{12,13,14,15} on surfactants and the theory behind their function is discussed later.

1.4.6. Prepolymers

In the context of polyurethane chemistry, prepolymers are understood to be intermediates of the isocyanate polyaddition. The following reaction scheme shows the production of NCO – terminated (6) and OH-terminated prepolymers (25).

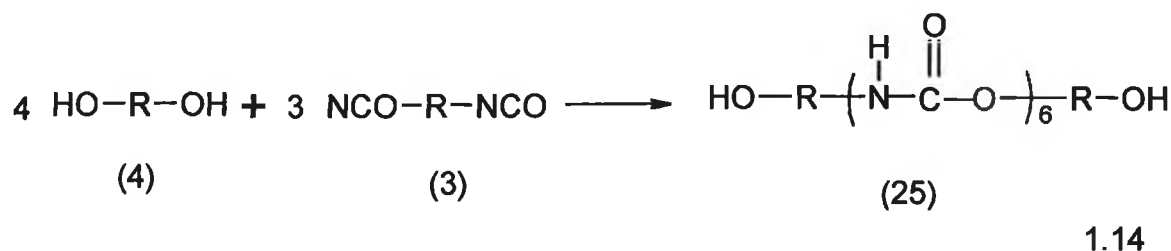
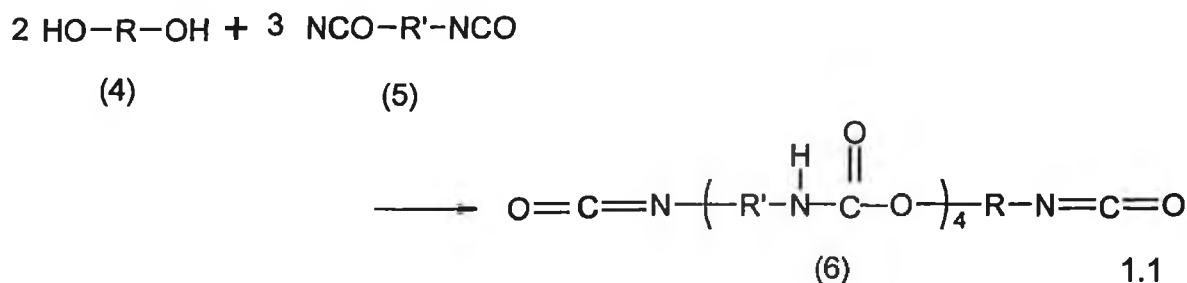


Fig. 1-12: The formation of prepolymers

Prepolymers are normally used in the production of polyurethane flexible foam rather than rigid foam due to curing problems. However, for the purpose of this study on the nucleation process and in the interest of being able to influence this process, prepolymers were implemented. They are obtained by reaction of di- or poly-hydroxy compounds with a molar excess of di- or poly-isocyanate at temperature between 70-100°C for approximately an hour. These are classified, as isocyanates, after the percentage free NCO groups and their functionality.

1.5. Basic Principles of Foam Formation

Pure liquids do not foam. Foam is also not prominent in mixtures of similar types of materials. Bubbles of gas introduced beneath the surface of an absolutely pure liquid rupture immediately on contact with each other or escape from the liquid as fast as the liquid can drain away from them. For true foaming to occur, the presence of a solute capable of being adsorbed at the liquid / gas interface of the bubble is required.

The most widely used system of producing foamed polymers involves dispersing a gas throughout a fluid polymer phase and stabilising the resultant foam. Rigid polyurethane foam formation occurs by reaction of polyisocyanates and polyols in the presence of selected catalysts, surfactants and blowing agents.

One can consider the foaming process as having four stages: the gas dissolution stage, the cell nucleation / bubble formation stage, the bubble growth stage, and the bubble stabilisation stage. The driving force for nucleation in a polymer is thermodynamic instability, which is a sudden solubility change. In polyurethane foaming the solubility change of a gas in a polymer occurs not only by saturation pressure and temperature change but also by polymerisation. That is to say, the solubility change occurs when isocyanate and polyol react with each other to form polyurethane. Normally the solubility of a polymer decreases as the polymer chain grows¹⁶, however in the case of the polyurethane foaming process we can consider the gas as the solute and the polymer as the solvent and therefore it is the solubility of the gas in the polymer which decreases. Physically we can understand the phenomenon by imagining the gas dissolved in the polymer being squeezed out by the growing polymer chains¹⁷.

The initial stages of the foaming process are now discussed under the following headings:

1. The Gas Dissolution Stage
2. The Cell Nucleation / Bubble Formation Stage
3. The Foam Growth Stage
4. The Bubble Stability Stage

1.5.1. The Gas Dissolution Stage¹

The first step of the foaming process is to form a gas / polymer solution. There are two factors that need to be taken into account for this process; the amount of gas required to saturate a polymer and the time it takes to saturate the polymer with gas. The amount of gas required to saturate a polymer can be expressed by its solubility. In the case of gas/polymer solution, the solubility is the maximum concentration of gas in the polymer. The concentration of gas in a polymer is also a critical variable in determining the cell morphology. The solubility of CO₂ in a polymer is uniquely determined by the saturation pressure and saturation temperature and is dependent of polymer type. For a particular polymer the solubility (S) relationship is represented as follows:

$$S = f(P_s, T_s)$$
$$= \int_0^{P_s} \left(\frac{\partial S}{\partial P} \right)_T dP + \int_0^{T_s} \left(\frac{\partial S}{\partial T} \right)_P dT \quad (1)$$

where P_s and T_s are the gas saturation pressure and the gas saturation temperature respectively.

The concentration of CO₂ in a polymer is equivalent to the solubility of CO₂ in the polymer if the gas saturation time is long enough to allow the polymer and the gas to mix and to reach a stable equilibrium condition. Fick's law is useful in the analysis of the gas dissolution process, whereby the time required to saturate gas in polymer can be investigated using the following equation:

$$F = -D \frac{\partial C}{\partial x} \quad (2)$$

where F is the molar rate of diffusion per unit area, D is the diffusion coefficient, C is the concentration of the dissolved gas and x is the distance in the direction of diffusion. This equation states that the rate of diffusion across a given plane is proportional to the concentration gradient across that plane. By taking time into account the following equation (Fick's second law) is derived:

$$\frac{\partial C}{\partial T} = \frac{\partial}{\partial x} \left[D \frac{\partial C}{\partial x} \right] \quad (3)$$

This then can be further simplified to

$$\frac{1}{t} = \frac{D}{x^2} \quad (4)$$

allowing for the calculation of the required gas saturation time.

1.5.2. The Cell Nucleation / Bubble Formation Stage

As discussed, the first step in producing a foam is the formation of gas bubbles in a liquid system. The second step is for cell nucleation or bubble formation to evolve. Bubble nucleation can only occur after the solubility of the gas dissolved in the liquid is exceeded. Therefore, anything that increases the concentration or decreases the solubility of the gas in the liquid will allow increased nucleation. If the bubbles are formed in an initially homogeneous liquid the process is called *self-nucleation* or *homogeneous nucleation*. *Heterogeneous nucleation* occurs when a second phase is initially present which allows the bubbles to form more readily at either a liquid-liquid or solid-liquid interface. In many processes without solid nucleating agents, the liquid phase actually contains many microbubbles of air, and they serve as sites for bubble growth with the formation of new bubbles not necessary. This can be achieved by mechanical agitation of the polymer liquid. The nucleation process is one of the most important in determining the morphology of the foam. The number and distribution of the nuclei can affect immensely the orientation and properties of the foam. It is very difficult to produce acceptable foams by a self-nucleation process. Most successful foam systems contain either nucleating agents or dispersed microvoids¹⁸. The majority of this study will be concentrated on the bubble formation i.e. the nucleation of polyurethane rigid foam.

1.5.3. Nucleation - Theories

Theoretical considerations on bubble nucleation by dissolved gas in liquids are rather limited as compared with the case of bubble nucleation by vapour molecules. There is even less known or understood about the nucleation of polyurethane foams. Although authors such as Park and Youn¹⁹ have studied the rate of nucleation of polyurethane microcellular foam, the majority of the literature reports studies of the nucleation of other polymers such as microcellular polyester composites²⁰ or poly methyl methacrylate²¹.

It is hoped that the theoretical and mathematical analyses derived from these studies can be adapted and applied to the study of the rate of nucleation of polyurethane rigid foams.

The processes of nucleation, growth and coarsening combine to dictate the final particle density produced by such a phase transformation²² that exists during the foaming of polyurethane foam. The complete process is indicated in the following diagram, which is a plot of the number of bubbles (cells) vs. time for a hypothetical transformation.

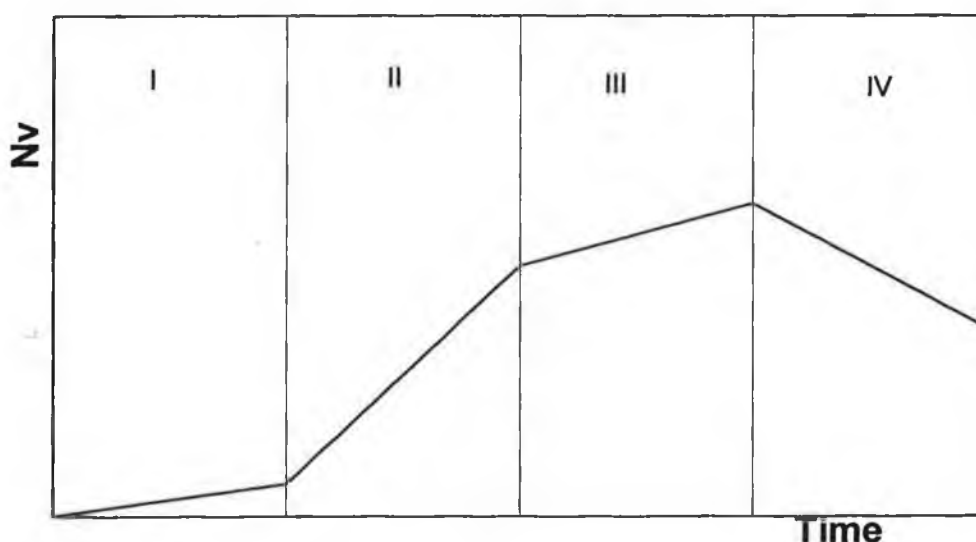


Fig. 1-13: Schematic sketch of bubble particle number density (N_v) versus time over the course of a phase transformation.

The diagram is divided into the following regions:

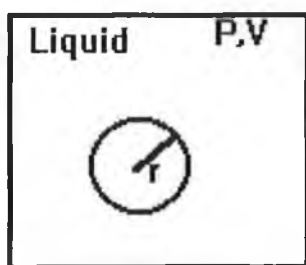
1. The induction period, τ , required to establish steady-state nucleation conditions.

1. The induction period, τ , required to establish steady-state nucleation conditions.
2. Steady state nucleation, where the number of bubbles increases linearly with time.
3. Decreasing nucleation rate, due to a reduction in supersaturation by growing bubbles.
4. Two possibilities exist for this region. If the system is stable (A) the amount of bubbles will remain constant. However, in an unstable system two processes for the elimination of bubbles take over – coalescence and / or disproportionation of gas bubbles. Coalescence can be described as the merging of two bubbles to create a bubble with a slight larger diameter. Disproportionation is the term used to describe the growth of large bubbles at the expense of smaller ones²³. This is also referred to in the literature as capillary-induced coarsening or Ostwald ripening¹¹. The number of bubbles in both processes then decreases with time (B).

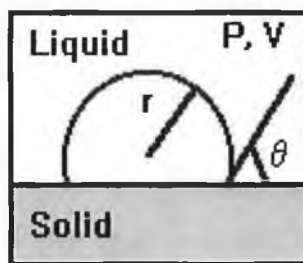
1.5.3.1. Classical Nucleation Theory^{1,18,19}

Classical nucleation theory addresses the process of condensation from vapour to liquid. The condensation mechanism is similar to that of cavitation in a pure liquid and therefore in the literature²⁰ the nucleation theory for condensation has been applied to bubble nucleation in a liquid supersaturated in gas.

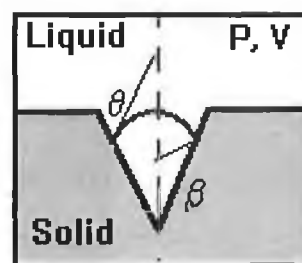
Homogeneous Nucleation



Heterogeneous Nucleation



At the interface



At the cavity

Fig. 1-14: Final States for different types of nucleation²⁰

Considering the free energy of initial and final states allows the associated free energy change in an isolated thermodynamic system to be derived. It is assumed that the initial state of the polymer liquid is supersaturated with gas at uniform temperature, pressure,

polymer liquid with a finite boundary. Assuming that the process is isothermal, gas in the bubble is ideal, and volume and temperature change of the system is negligible, the Helmholtz free energy change, ΔF , is given as

$$\Delta F = n_b RT \ln \left(\frac{P_b}{P_s} \right) + A\gamma - (P_b - P_0)V_b \quad (5)$$

where n_b is the mole number of the gas in the bubble, R is the universal gas constant, T is the absolute temperature of the system, P_b is the gas pressure inside the bubble, P_s is the saturation pressure, A is the interfacial area, γ is the interfacial energy (surface tension) between liquid and gas, P_0 is the environmental pressure, and V_b is the volume of the bubble. This is true for all cases shown in Fig. 1-14. However, the interfacial area, nucleus volume, and the mole number of gas in the bubble are different for each case, therefore resulting in three different kinds of critical free energy changes.

The minimum work required for homogeneous nucleation becomes :

$$\Delta F = n_b RT \ln \left(\frac{P_b}{P_s} \right) + \left[4\pi r_b^2 \gamma - (P_b - P_0) \frac{4}{3} \pi r_b^3 \right] \quad (6)$$

where r_b is the radius of the bubble. When the critical nucleus is generated, the free energy with respect to infinitesimal change of the radius becomes zero as follows:

$$\frac{d\Delta F}{dr_b} = 0 \quad (7)$$

Therefore the critical free energy change, ΔF^* , and critical radius, r_b^* are derived as

$$r_b^* = \left(\frac{2\gamma}{P_s - P_0} \right) \quad (8)$$

$$\Delta F^* = \left(\frac{16\pi\gamma^3}{3(P_s - P_0)^2} \right) \quad (9)$$

Similarly, the free energy change for heterogeneous nucleation at the interface is derived:

$$\Delta F = n_b RT \ln \left(\frac{P_b}{P_s} \right) + \left[4\pi r_b^2 \gamma - (P_b - P_0) \frac{4}{3} \pi r_b^3 \right] f(\theta) \quad (10)$$

where

$$f(\theta) = \frac{(2 + 3 \cos \theta - \cos^3 \theta)}{4} \quad (11)$$

For critical size,

$$r_b^* = \left(\frac{2\gamma}{P_s - P_0} \right) \quad (8)$$

$$\Delta F^* = \left(\frac{16\pi\gamma^3}{3(P_s - P_0)^2} \right) f(\theta) \quad (12)$$

For heterogeneous nucleation at the cavity:

$$\Delta F = n_b RT \ln \left(\frac{P_b}{P_s} \right) + \left[4\pi r_b^2 \gamma - (P_b - P_0) \frac{4}{3} \pi r_b^3 \right] f(\beta, \theta) \quad (13)$$

$$f(\beta, \theta) = \frac{1}{2} - \frac{3}{4} \cos \alpha + \frac{1}{4} \cos^3 \alpha + \frac{1}{4} \sin^3 \alpha \frac{\cos \beta}{\sin \beta} \quad (14)$$

where,

$$\alpha = \frac{\pi}{2} + \beta - \theta \quad (15)$$

$$r_b^* = \left(\frac{2\gamma}{P_s - P_0} \right) \quad (8)$$

$$\Delta F^* = \left(\frac{16\pi\gamma^3}{3(P_s - P_0)^2} \right) f(\beta, \theta) \quad (16)$$

The interfacial energy, γ [mN/m], which is used to calculate the free energy change for nucleation, is determined by surface tension measurement which measures surface tension, δ [mN/m]. Theoretically the interfacial facial tension refers to a liquid / liquid interface while the term surface tension is used when referring to a liquid / vapour interface. For our purposes the values are interchangeable and therefore, γ will be denoted by the surface tension value, δ , during the rest of this work.

The rate of nucleation, calculated by classical molecular kinetics is defined as the rate at which bubble nuclei, one molecule smaller than the critical size, gain the last molecule for further growth. The rate of nucleation, J , is given by the following equation:

$$J = Z\beta^* N \exp\left(\frac{-\Delta F^*}{k T}\right) \quad (17)$$

where Z is the Zeldovich nonequilibrium factor that takes into account that nuclei smaller than the critical size can be nucleated by large fluctuations near the critical size and is typically 10^{-2} to 10^{-3} . N is the number of available nucleation sites, ΔF^* is the critical free energy change, k is the Boltzmann constant, and β^* is described by

$$\beta^* = \frac{P_b}{\sqrt{2\pi m_c k T}} S(m_c) \quad (18)$$

where m_c is the mass of gas molecules in the critical nucleus, and $S(m_c)$ is the surface area of the critical nucleus. The number of available nucleation sites is the total number of saturated gas molecules in the unit polymer volume. The Zeldovich factor is applied to all types of nucleation.

As has been shown, there are two types of nucleation mechanisms: homogeneous and heterogeneous. However, these are not mutually exclusive. The presence of heterogeneous nucleation sites does not preclude homogeneous nucleation. Colton and Suh²⁴ have investigated this phenomenon and included an expression for the homogeneous nucleation rate in the presence of heterogeneous nucleation in their calculations

$$J_{\text{mod}} = f_0 C_0^* \exp\left(\frac{-\Delta F_{\text{mod}}^{**}}{kT}\right) \quad (19)$$

where J_{mod} is the homogeneous nucleation rate modified by the heterogeneous nucleation rate, f_0 the frequency factor for homogeneous nucleation and ΔF^{**} is the change in free energy needed to create a critical homogeneous nucleus after the change in potential energy has been subtracted. The reduced concentration of gas molecules, C_0^* , was evaluated using

$$C_0^* = C_0 - (J_{\text{het}} t n_b) \quad (20)$$

where C_0 is the concentration of the gas molecules, J_{het} the heterogeneous nucleation rate, t is the time since the first heterogeneous nucleations has occurred, and n_b is the number of gas molecules in a bubble nucleus.

Amon and Denson²⁵ have dealt with the analysis of bubble growth in purely a mathematical sense. However, as opposed to other work where the model is based on a single bubble growing in an infinite sea of liquid, they predict the growth of an individual gas bubble in a gas-liquid solution, which contains a collection of gas bubbles in close proximity to one another. The kinematics are modelled using the concept of a spherical unit cell which consists of a single gas bubble and a hypothetical concentric Newtonian liquid "envelope" of given mass (see Fig. 1-15). Five dimensionless parameters governing the isothermal-isobaric growth of a cell were identified. The relative magnitudes of the rates of mass and momentum transport were determined by the ratio of characteristic times, $\pi_{D\eta}$ defined as follows.

$$\pi_{D\eta} = \frac{t_D}{t_n} \quad (21)$$

where, t_D is the characteristic time scale for diffusion and is equal to

$$t_D = \frac{V^{2/3}}{9D} \quad (22)$$

where, $\underline{V} = V / R_e^3$, V being equal to the cell envelope divided by $(4\pi/3)$, R_e is the Reynolds number and D is the diffusivity of gas in polymer in cm^2/sec . \underline{V} was used to demonstrate the influence of the proximity of a large number of cells on the growing effect. The thermodynamic driving force for growth was related to the ambient pressure, and it was shown that increasing driving force resulted in a decreasing expansion time. They found the influence of the surface tension to be negligible and that the effect of the initial bubble radius was limited to the early stages of growth and had little influence on the long term progress of expansion.

Arefmanesh et al.^{26,27} compared their mathematical study of a similar model cell in a viscoelastic fluid with limited amount of dissolved gas, to that of a Newtonian fluid studied by Amon and Denson²⁵. It was found that the presence of initial stresses in the viscoelastic fluid significantly delayed the growth dynamics. With no initial stress, the growth rate was faster than in the Newtonian fluid. This is due to the stresses opposing the bubble expansion in a viscoelastic medium. However, this difference in growth rate has only a significant impact on the growth rate at the early stages of the process.

The following diagram, Fig. 1-15 illustrates the model cell as described in references 25, 26 and 27. The bubble comprises of a sphere of radius R , containing a mixture of polymer and gas, encapsulating a gas atmosphere with a internal pressure of P_g . The bubble is surrounded by the polymer.

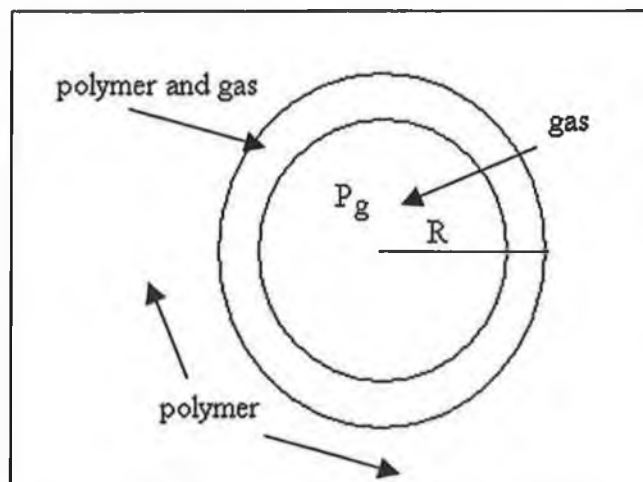


Fig. 1-15: Schematic diagram of a bubble and fluid "envelope" as described in references 25, 26 and 27.

In order for a nucleus with radius r to grow, an excess gas pressure Δp sufficient to overcome the surface tension, δ , (between the gas and the bulk) is needed. Otherwise the nucleus shrinks and disappears. As is described in the following section the pressure is given by the following equation:

$$\Delta p = \frac{2\delta}{r} \quad (23)$$

Therefore, a nucleus needs a critical radius, r^* , in order for it to grow

$$r^* = \frac{2\delta}{\Delta p} \quad (24)$$

This is equal to equation (8) and is calculable.

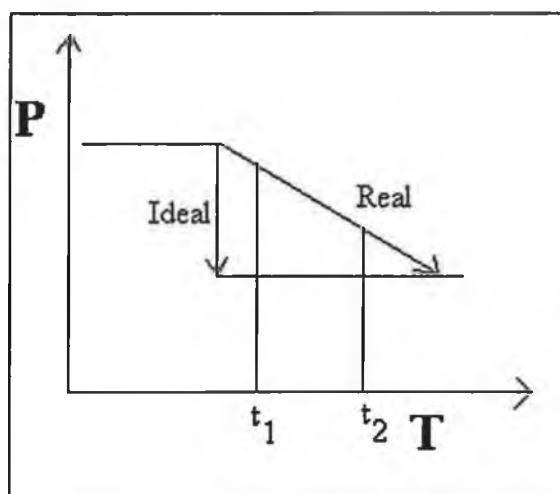


Fig. 1-16: Ideal and real pressure drops during the initial stage of foam formation.

For the maximum number of nuclei to form an ideal rapid pressure drop is necessary²⁸ as depicted in Fig. 1-16. Realistic is a pressure drop over a period of time. At t_1 a certain amount of nuclei form and grow. At time t_2 more nuclei form but comparatively less due to the competition from the nucleation and growth at t_1 . This is the reason why nuclei of various sizes are present resulting in a less homogeneous cell structure. For a homogeneous cell morphology a rapid pressure drop is necessary for the simultaneous production of nuclei with the same size.

1.5.4. The Bubble Growth Stage

A bubble once formed may grow by diffusion of gas from solution in the liquid phase into the bubble. For a given foam volume, the system will be more stable with fewer larger cells than with more smaller cells. This factor favours the coalescence of cells. One must also take into account that, at equilibrium the gas pressure in a spherical bubble is larger than the pressure in the surrounding fluid, as given by the equation 23. It also follows that the gas pressure in a small bubble is greater than that in a large bubble, with a difference, according to the Laplace equation, of,

$$\Delta p = \sigma \left(\frac{1}{r_1} + \frac{1}{r_2} \right) \quad (25)$$

where Δp is the difference in pressure between the two bubbles having a radii of r_1 and r_2 . Therefore the gas will tend to diffuse from the smaller bubble into the larger one, a process which is termed as disproportionation¹⁶.

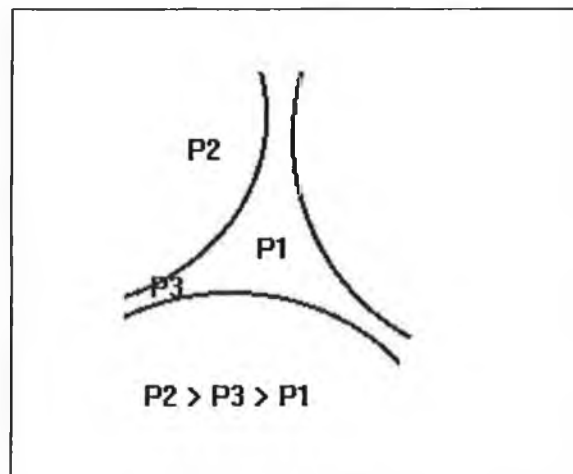


Fig. 1-17: Strut formation - the meeting of three bubbles (see also Fig 1-19). P_1 is the gas pressure in the strut, P_2 is the internal bubble gas pressure and P_3 is the gas pressure in the cell walls.

Since the curvature in the lamellae of the foam is greatest in the struts, there is a greater pressure across the interface in these regions than elsewhere in the foam. Since the

gas pressure inside an individual bubble is everywhere the same, the liquid pressure inside the lamella at the highly curved strut (P1) must be lower than in the adjacent, less curved parts of the strut (P3) (see Fig. 1-17). This causes drainage from the lamellae into the struts. Foams are destroyed when the liquid drains out from between two parallel surfaces of lamella, causing it to get progressively thinner. When it reaches a critical thickness (50 - 100Å) the film collapses.

During the early stages of foaming, when the gas volume is small, bubbles are spherical in shape. As the bubble volume grows, however, the fluid phase becomes insufficient to maintain the spherical shape, so the bubbles take on polyhedral shapes, with the polymer fluid distributed in thin membranes between two adjacent bubbles and in the struts where three bubbles have come into close proximity. Studies on the foam morphology of polyurethane rigid foam²⁹ have shown that the average bubble (cell) shapes of the finished foam are 4-, 5- and 6- sided polyhedral (see Fig. 1-18).

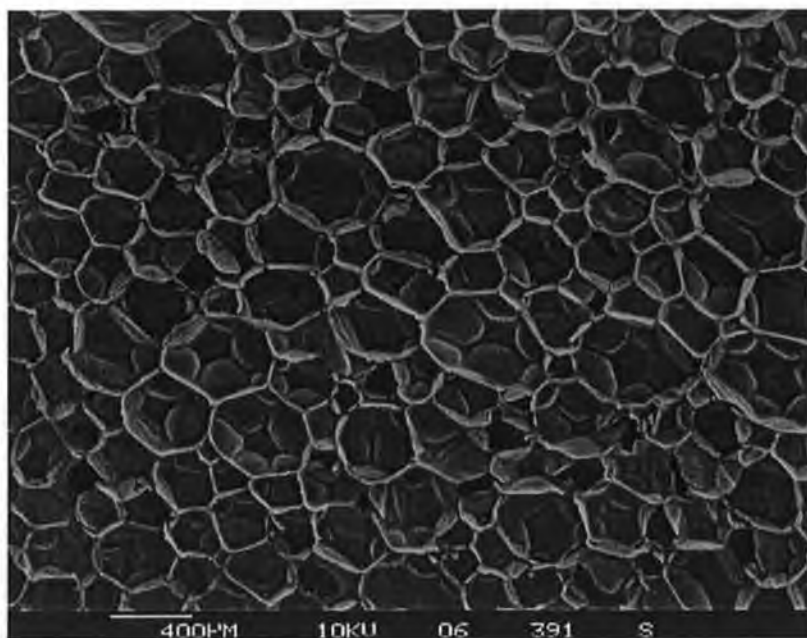


Fig.1-18: An SEM image of the polyhedral structure of polyurethane rigid foam.

1.5.5. The Bubble Stability Stage^{30,31,32}

When a cell expands, the concentration of adsorbed component is reduced. This concentration may be restored by one of two processes: The surface layer can flow from areas of low surface tension to those of high surface tension (low concentration), or surfactant in the interior of the liquid can diffuse to the surface. In the first case, called the *Marangoni Effect*, the surface flow is believed to drag underlying layers of liquid along with it, thus restoring film thickness. This process thus enhances film elasticity and resilience. The second process, known as the *Gibbs Effect* replenishes surfactant concentration at the surface, but does not restore liquid to the film, hence it is not self-healing.

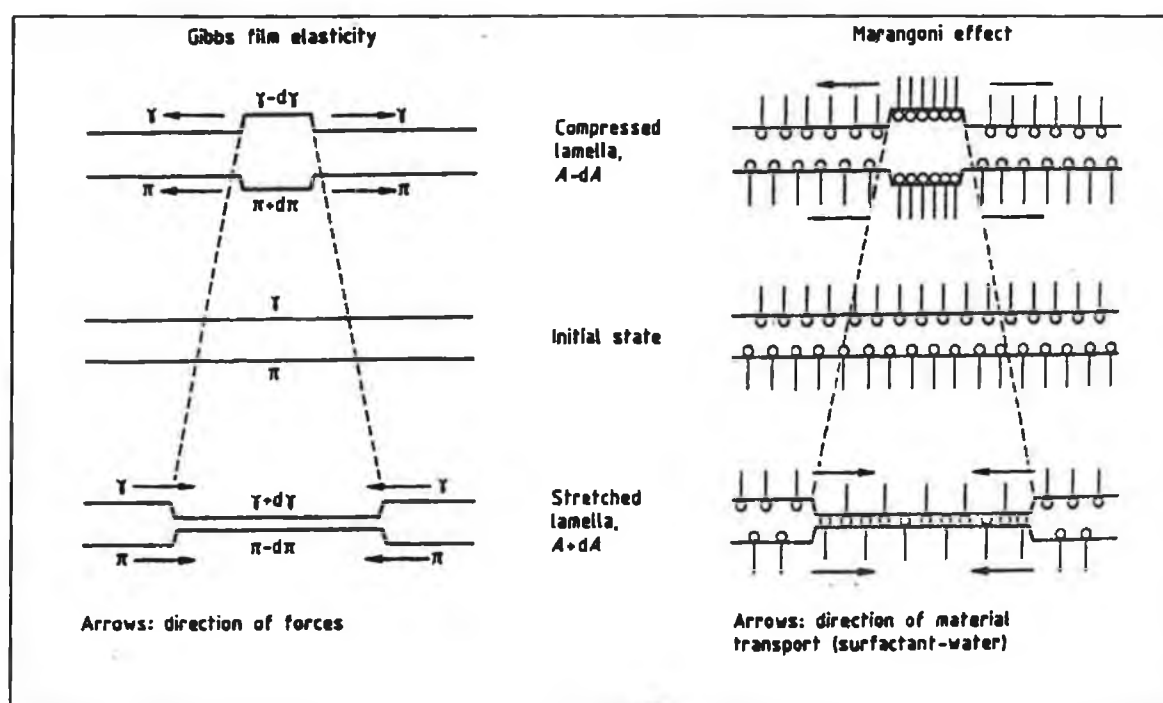


Fig. 1-19: The Gibbs and Marangoni effects³⁰ - π is the spreading pressure of the surfactants and is equal to $\delta_0 - \delta$. Note that γ is the interfacial tension and is equal to the surface tension, δ .

The temperature of the foam can also affect the stability. An increase in temperature reduces both viscosity and surface tension, making the thinning of membranes easier, and potentially leading to the rupture of membranes (cell walls) that are too thin to withstand existing stress. Conversely, a rise in temperature also increases reaction rates, which can

be favourable in those foams where ultimate stabilisation depends on further polymerisation.

Cell walls may be thinned by drainage due to gravity and capillary action, which sometimes can lead to excessive thinning, followed by rupture. In certain cases the surfaces of a very thin film attract each other by van der Waals forces, also favouring continuing thinning.

Polymeric foams have another major stabilising influence, that is, a rapid increase in viscosity. In polymerising foam systems, polymerisation proceeds at the same time as foaming, and reaction rates are catalysed so as to give at least moderate molecular weight and viscosity by the time the foam rise is complete.

Successful closed-cell foams are produced when the cell membranes are sufficiently strong (elastic) to withstand rupture at the maximum foam rise, and the modulus of the polymer is increased rapidly to a high level so that the cells are dimensionally stable in spite of the development of a partial vacuum within the cells. This is achieved most easily in relatively high-density foams or in highly cross-linked foams.

1.6. Interfacial Phenomena^{30,31,32}

1.6.1. Surface Tension

Cohesive forces of a condensed phase become anisotropic in the phase boundary region, and their normal component becomes smaller than the parallel component. This simplified is projected onto a two-dimensional surface (Gibbs "dividing surface"). The tensile stress resulting from the anisotropic forces in the boundary region is then termed the interfacial tension. This corresponds to the reversible work required to particles from the volume phase to the interface during enlargement of the former and thus thermodynamically corresponds to the increase in free enthalpy of the system per unit surface area:

$$\left(\frac{dG}{dA} \right)_{P,T} = \delta \quad (26)$$

where G is the free enthalpy, A the surface area, and δ the surface tension [mN/m].

Several methods - static, detachment and dynamic - are available to measure both the interfacial and surface tensions. Static methods measure the tension of practically stationary surfaces, which have been formed for an appreciable time and usually offer a greater potential for accurate measurements than detachment methods. Dynamic methods depend on the fact that certain vibrations of a liquid cause periodic extensions and contractions of its surface, which are resisted or assisted by the surface tension. Dynamic methods of measuring surface tension include capillary wave spectroscopy. The capillary height method and the maximum bubble pressure method are considered as static methods, while the drop weight method and the method of the sensile drop are detachment methods. Other detachment methods, which are based on the formation of a film of the liquid and its extension by means of a support which temporarily adheres to the liquid, are the plate method (Wilhelmy plate) and the ring method (Lecomte du Noüy tensiometer).

1.6.2. Curved Interfaces - The Kelvin Equation

Due to surface tension, there is a balancing pressure difference across any curved surface, the pressure being greater on the concave side. For a curved surface with principal radii of curvature r_1 and r_2 this pressure difference is given by the Laplace equation^{31,33}

$$\Delta p = \delta \left(\frac{1}{r_1} + \frac{1}{r_2} \right) \quad (25)$$

which, for a spherical surface, reduces to

$$\Delta p = \frac{2\delta}{r} \quad (23)$$

The vapour pressure over a small droplet, where there is a high surface/volume ratio, is higher than that over the corresponding flat surface. The transfer of liquid from a plane surface to a droplet requires the increase of energy, since the area and, hence, the surface free energy of the droplet will increase. If the radius of a droplet increases from r to $r+dr$, the surface area will increase from $4\pi r^2$ to $4\pi(r+dr)^2$ and the increase in surface free energy will be $8\pi\gamma r dr$. If this process involves the transfer of dn moles of liquid from the plane surface with a vapour pressure p_0 to the droplet with a vapour pressure p_r , the free energy increase is also equal to $dnRT \ln p_r/p_0$, assuming ideal gaseous behaviour. Equating these free energy increases,

$$dnRT \ln \frac{p_r}{p_0} = 8\pi\delta r dr \quad (27)$$

and since

$$dn = 4\pi r^2 dr \frac{\rho}{M} \quad (28)$$

then

$$dnRT \ln \frac{p_r}{p^0} = \frac{2\delta M}{\rho_r} = \frac{2\delta V_m}{r} \quad (29)$$

where ρ_r is the density of the liquid, V_m is the molar volume of the liquid and M is the molar mass.

1.6.3. Capillarity^{34,35}

An important phenomenon arising from surface tension is the elevation of a liquid in an open tube of small cross section, known as capillarity. If the tube is a cylinder of radius r , the liquid makes contact with the tube along a line of $2\pi r$. If the cylinder is considered to have a height h , then along with its liquid-vapour film, the total upward force is

$$F = 2\pi r \delta \cos\theta \quad (30)$$

The downward force, w , is equal to the weight-density ρg times the volume, which is approximately $\pi r^2 h$ i.e.

$$w = \rho g \pi r^2 h \quad (31)$$

Since the cylinder is in equilibrium ,

$$\rho g \pi r^2 h = 2\pi r \delta \cos\theta \quad (32)$$

From this we can clearly see the inversely proportionality of the surface tension to the radius of the capillary tube. If we take this basic physics and apply it to the physics of foam formation we can postulate that the higher liquid pressure (larger radius, r) in the cell walls and the lower liquid pressure (smaller radius, r) at the strut is the reason why the polymer matrix flows from the cell walls to the struts. This leads to the following assertion: in order to increase the flow of the polymer matrix from the cell walls to the struts the following parameters must be varied:

a) increase the surface tension value

- b) increase the difference in radii
- c) decrease the viscosity of the polymer.

1.6.4. Viscosity³⁶

Turner et al.³⁶ expressed the importance of the influence of the viscosity of the polymer on the foam formation, stating that the polymer viscosity should be as low as possible for adequate flow from the walls to the struts and then increase rapidly for foam stability. This thinning process is related to the viscosity as shown in the following equation:

$$v = \frac{\Delta p * c}{24\eta} \quad (33)$$

where v is the polymer flow from the wall in to the struts, η is the viscosity, c is the cell wall thickness and Δp^* is the pressure difference as a result of the increase in difference in radii as suggested in b) in section 1.6.3. In polyurethane rigid foam at least 90% of polymer flows into the struts leaving 10% or less in cell walls. Glicksmann³⁷ postulated that the strut fraction was probably due to the increase of polymer viscosity with respect to the surface tension during foam formation.

1.6.5. Colloids and Micelles³¹

A colloid is a dispersion of small particles ($< 500\text{nm}$) of one liquid in another. In general, colloidal particles are aggregates of numerous atoms or molecules, but are too small to be seen with an optical microscope. They are relevant to the discussion of surfaces because the ratio of their surface area to their volume is so large that their properties are dominated by events at the surfaces. The polymer bulk can be considered as an emulsion with the surfactant as an emulsifying agent, stabilising the product. Due to their large surface area, colloids are thermodynamically unstable with respect to the bulk. This expressed in the Gibbs equation (equation 26):

$$dG = \delta d\sigma \quad (26)$$

where δ is the surface tension and $d\sigma$ is the change in surface area.

Micelles are colloid-sized clusters of molecules. Micelles form only above the critical micelle concentration (CMC) and above the Kraft temperature. The Kraft temperature (or point) is the temperature at the triple point of mono-disperse solution-gel-micellar solution and is characteristic for each surfactant. The CMC is detected by observing a distinct discontinuity in physical properties of the solution such as turbidity, osmotic pressure and surface tension. Non-ionic surfactant molecules may cluster together in clumps of 1000 or more, but ionic species tend to be disrupted by the electrostatic repulsion between head groups and are normally limited to groups of between 10 and 100. Although spherical micelles do occur, micelles are more commonly flattened spheres close to the CMC. Some micelles at concentrations well above the CMC form extended parallel sheets (lamellar micelles) which are two molecules thick. In concentrated solutions micelles formed from surfactant molecules may take the form of long cylinders and stack together in close-packed hexagonal arrays (liquid crystalline phase).

A study of surface tension and viscosity using the aforementioned theories is necessary for a better understanding of the formation of polyurethane rigid foam in particular to the nucleation process. For this purpose the model systems which were implemented in the analysis of the nucleation process of polyurethane rigid foams were used.

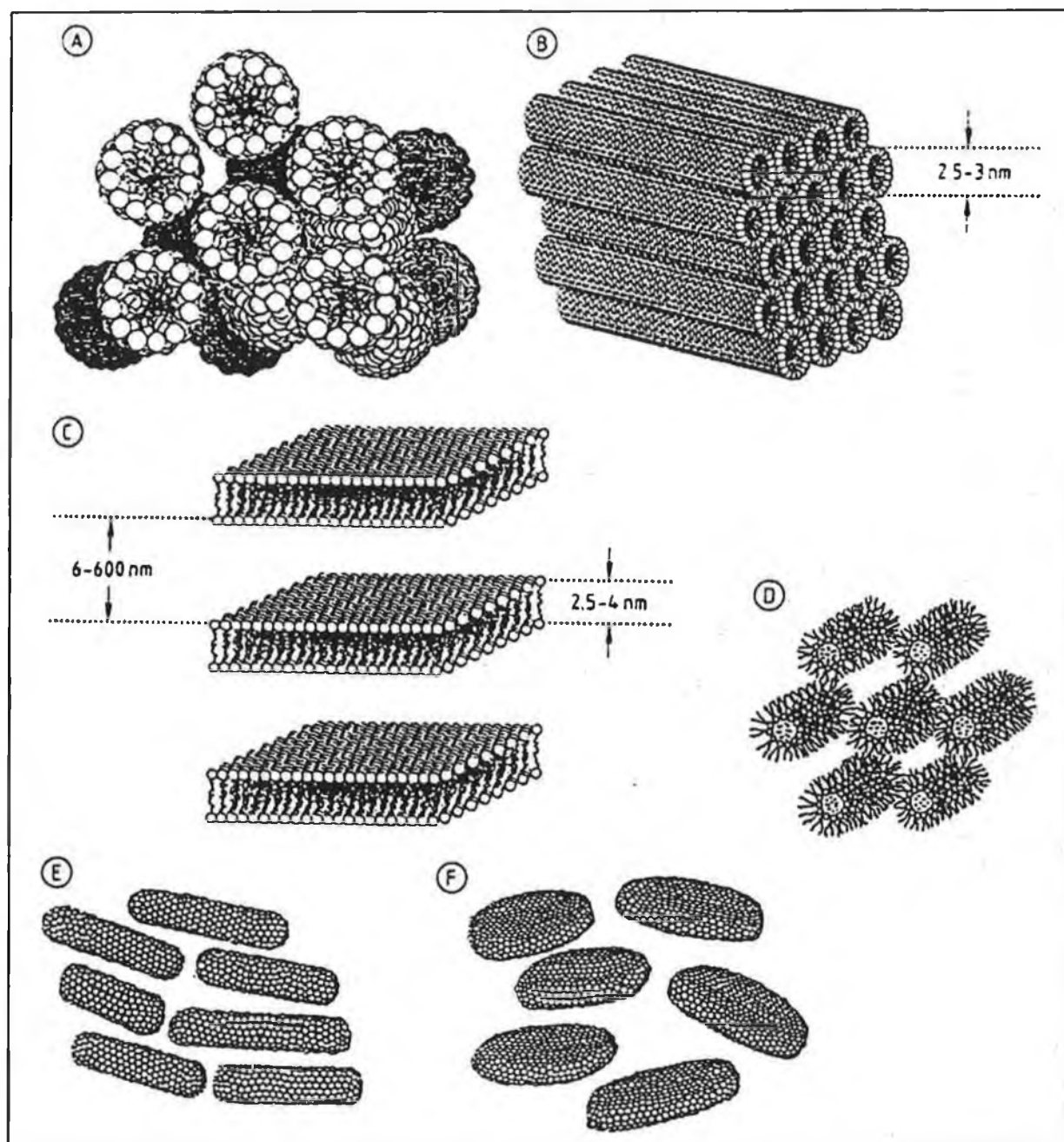


Fig. 1-20: Micelle structures: (A) Spherical (anionic) micelle, (B) spherical vesicle bilayer structure, (C) lamellar phases formed from laminar micelles, (D) inverse hexagonal phase, (E) nematic rod phase and (F) nematic disc phase³⁰.

1.7. Fundamentals of Thermal Insulation - Polymer Physics

A low thermal conductivity is one of the most important properties of polyurethane rigid foam. Heat transfer through insulating materials is defined by the thermal conductivity λ , which defines the ratio of the rate of heat transfer per unit cross-sectional area of a given thickness to the applied temperature difference and is represented by the Fourier equation for conduction through homogenous materials^{38,8}. This thermal conductivity λ , can be described in terms of three distinct contributions: conduction of heat through the solid matrix of the λ_s , conduction through the gas residing in the foam cells λ_g , and the radiative heat contribution λ_r . Skochdopole³⁸ proved that the contribution of thermal conductivity by convection is negligible at cell sizes below 3-4mm. The following is an expression for the total thermal conductivity, λ .

$$\lambda = \lambda_s + \lambda_g + \lambda_r \quad (35)$$

1.7.1. λ_s , Thermal Conductivity Through the Solid

In order to calculate λ_s (also known as the matrix thermal conductivity) it is necessary to understand the morphology of the foam. The solid polymer forms cells with cell walls of roughly constant thickness. At the intersection of three cells a thickening known as a strut is observed. The polymer cells are assembled in polyhedra with average diameters usually less than 500 μ m.

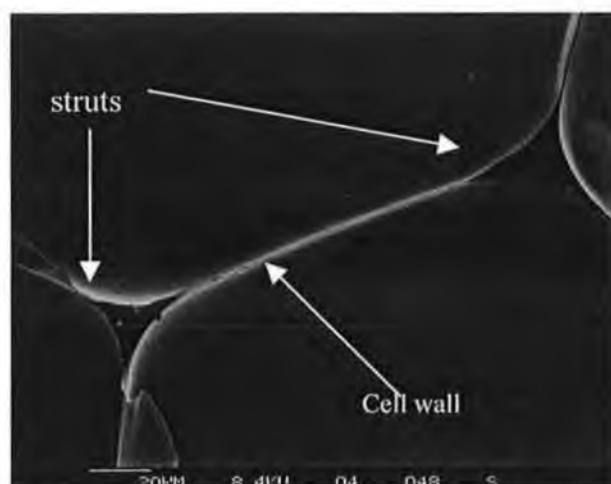


Fig. 1-21: An SEM image showing strut and wall formation

Several mathematical models have been developed for the estimation of conduction through the polymer matrix. A strut - wall design in which the majority of the polymer lies in the struts has been agreed upon with the following equation³⁷:

$$\lambda_s = \lambda_p (1 - \varpi) \frac{1}{3} (2 - f_s) \quad (36)$$

where f_s is the amount of polymer in the struts, ϖ is the porosity and λ_p is the thermal conductivity of the non-porous compact polymer. From this equation it can be seen that an increase in polymer content in the struts results in a decrease of λ_s . In order to do this thinner cell walls are necessary. This is highlighted in Fig. 1-22 which depicts the cubic cell model. The cell consists of walls of length y and thickness z . Where three walls meet a strut of thickness x is formed. The heat flowing in any given direction through this model is dependent on two walls and one strut of the cell (i.e. the dark shaded area in Fig. 1-22).

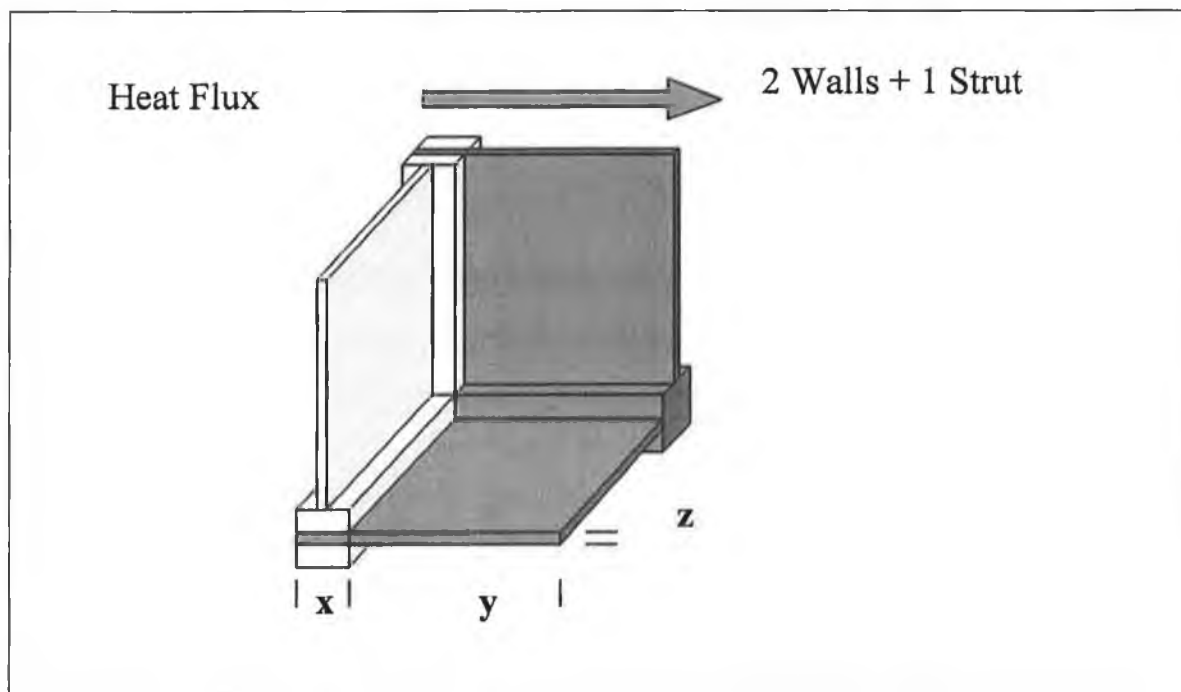


Fig. 1-22: The cubic cell model:– heat flowing through the cell in any given direction is dependent on two walls of length y and thickness z and one strut of thickness x .

High cellular anisotropy is also necessary for a reduction of thermal conductivity through the matrix. This is taken into consideration where a and b are the cell diameters perpendicular and parallel to the temperature gradient respectively:

$$\lambda_s = \lambda_p \frac{1}{3} (1-\omega) \left[f_s \sqrt{\frac{a}{b}} + 2(1-f_s) \left(\frac{a}{b} \right)^{1/4} \right] \quad (37)$$

1.7.2. λ_r Radiative Heat Transfer

The thermal conductivity λ_r contributed through radiation is 10-30% of the total conductivity. Glicksmann in early works modelled the radiative process as radiation across a series of parallel opaque planes with separation equal to the cell size. This leads to the following formula where ε is the cell wall emissivity, k_b is the Stefan-Boltzmann constant and d is the cell diameter³⁹:

$$\lambda_r = 4 \left(\frac{\varepsilon}{2-\varepsilon} \right) k_b T^3 d \quad (38)$$

Schuetz and Glicksmann³⁷ measured the transmissivity of various PU cell walls and showed that the cell walls were not opaque - this leads to a slightly higher λ_r calculated by the Rosseland equation:

$$\lambda_r = \frac{16}{3} \frac{k_b T^3}{K} \quad (39)$$

where K is the extinction coefficient. Experimental results show that struts of 30 μ m are opaque while walls <1 μ m are weakly absorbing.

$$K_{\text{strut}} = 4.10 \frac{\sqrt{\frac{f_s \rho_f}{\rho_s}}}{d} \quad (40)$$

$$K_{\text{wall}} = \left[\frac{(1 - f_s)\rho_f}{\rho_s} \right] K_w \quad (41)$$

By reducing the cell diameter and increasing the extinction it is possible to decrease the radiative thermal conductance λ_r .

1.7.3. λ_g , Thermal Conductivity Through the Gas

The thermal conductivity through the gas can be considered using the basic kinetic theory of gases whereby the thermal conductivity of the gas is indirectly proportional, by first order approximation, to its molecular weight. In a typical low density closed cell polymeric foam, of which 97% of the foam's volume is filled with a low gas conductivity, heat transfer through the gas comprises of over 50 % of the total heat transfer. The general expression for the conductivity of a gas mixture is given by the Wassilijewa equation⁶.

$$\lambda_{\text{mix}} = \frac{\sum_{i=1}^{N_c} y_i \lambda_{g_i}}{\sum_{j=1}^{N_c} y_j A_{i,j}} \quad (42)$$

where y_i is the mole fraction of the i^{th} component, N_c the number of components, and λ_{g_i} is the thermal conductivity of the pure i^{th} component.

Traditional polyurethane rigid foams for thermal insulation purposes were closed-celled. It is however possible to make opened-cell PU rigid foams and this type of foam has recently been developed for the implementation of rigid foam in vacuum insulation panels for the refrigeration industry^{40,41}. The basic principle behind it is the elimination by evacuation of the contribution of the thermal conductivity of the gas to the total thermal conductivity, reducing equation (35) as follows:

$$\begin{array}{ll} \lambda = \lambda_s + \lambda_r + \lambda_g & \text{(closed-cell)} \\ \downarrow \text{(vacuum)} & \\ \lambda_s + \lambda_r & \text{(opened -cell)} \end{array} \quad (43)$$

As can be seen from the previous equations, the thermal conductivity of polyurethane rigid foams is extremely dependent on the foam morphology. In order to find a way to minimise thermal conductance it is necessary to investigate further the foam morphology and its formation. Of utmost importance is a greater understanding of the previously described nucleation process during foam formation and a deeper knowledge of the influences of different additives such as blowing agents, stabilisers, catalysts etc. is required.

2. Development of Experimental Methods

2.1. Introduction

As already stated, there has been no previous detailed in-situ study of the nucleation and foaming processes of polyurethane rigid foam. Therefore, the initial aim of this work was to establish a possible method. This is described in detail in section 2.7. The influence of the various components on the parameters such as temperature, pressure (section 2.3.) viscosity (section 2.4.), and surface tension (section 2.11.) etc. was also analysed. Their effect on the nucleation process was subsequently studied using the method developed (section 2.8.). In this way it was hoped to determine possibilities for improving cell formation and ultimately reduce thermal conductivity. Diagram 2-1 schematically describes these aims and their relationship with each other.

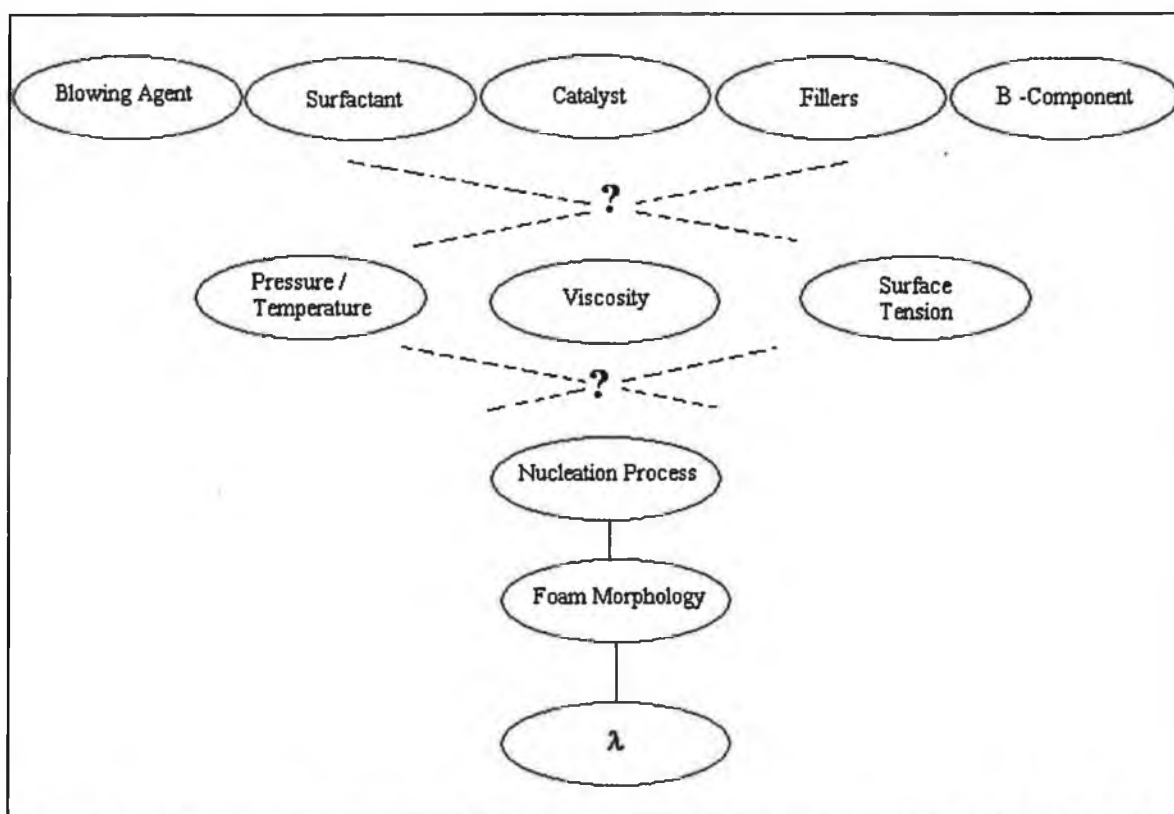


Fig. 2-1: Schematic representation of experimental aim. By studying the effect of the variables blowing agent, surfactant, etc. on the parameters of pressure, temperature, etc., it is hoped to determine their influences on the nucleation process and ultimately, by means of the foam morphology, on the thermal conductivity.

A model A-component was formulated for the purpose of this research. It was comprised of a mixture of polyols, a blowing agent (BA), a surfactant and a catalyst mixed in the following manner:

Polyol:	i) a polyol with starter materials of sucrose, glycerine and propylene oxide; OH No. 380 –420.	}	
	ii) a polyol with starter materials of propylene glycol and propylene oxide; OH No. 235-260.	}	96%
	Dipropyleneglycol	}	
Surfactant:	I		1%
Blowing Agent:	H ₂ O (A)		2.7%
Catalyst:	Dimethylcyclohexylamine (i)		0.3%

This system had at 25°C a density of 1.019g/cm³ and a viscosity of 819mPas. This was the basic formulation for all experiments, the components of which were only changed with respect to the experimental aim. In other words, for example, when the effect of the type of blowing agent in the A-component on the nucleation process was investigated, then the type of blowing agent was changed but all other components and amounts of the components of the formulation remained the same.

The B-component was a M20A, an MDI-type polyisocyanate with a free NCO content of 31.5%. At 25°C it had a density of 1.236g/l and a viscosity of 201mPas.

A and B components were mixed in a ratio of 40:60 at 25°C in the usual manner (as described in section 1.3.) with characteristic times as follows:

Cream time	≈	60s ±10s
Gel time	≈	200s ±10s
Rise time	≈	300s ±10s
Density	≈	55g/l ± 1g/l

This model system is considered very slow and therefore suitable for analysis. This is necessary as normal foaming systems with rise times of circa 10s would be impossible to

analyse. The applicability of the results obtained from the in-situ method to real systems with such fast reaction times, is studied later (section 4.1.)

Within this research the formulation of the A-component has been varied for the purpose of the analysis of the foaming process. As explained the basic content of the A-component remains the same. However, according to experiment the surfactant, blowing agent (BA), or catalyst, in each case amount and / or type, has been varied. For the purpose of clarity, the formulations will be abbreviated in such a manner throughout this work:

Blowing Agent (Surfactant / Catalyst)

where the blowing agents will be represented by a roman capital letter (A, B, C), the surfactants will be represented by a capital roman numeral (I, II, III, etc) while the catalysts by a small roman numeral (i, ii, iii, etc.). Under this system the former formulation is represented by A(I/i) since it is the first system introduced. Further formulations will be appropriately introduced before dealing with the experiment. An additional explanation of all formulations can be found in Table on the following page. For convenience purposes, enabling quick cross-referencing this table is repeated in Appendix 1 and on the bookmark provided.

Table 2-1: Clarification of the formulations of the A-components used throughout this work.

	A(I/i)	B(I/i)	B(II/i)	B(III/i)	B(IV/i)	B(V/i)	B(I/ii)	B(I/iii)	B(I/iv)	C(VI/i)
A-Component										
Polyol 1	✓	✓	✓	✓	✓	✓	✓	✓	✓	✓
Polyol 2	✓	✓	✓	✓	✓	✓	✓	✓	✓	✓
DPG*	✓	✓	✓	✓	✓	✓	✓	✓	✓	✓
Water	✓✓	✓	✓	✓	✓	✓	✓	✓	✓	✓
Cyclopentane		✓	✓	✓	✓	✓	✓	✓	✓	
Perfluorohexane										✓
Surfactant										
(HLB-Value):										
I (1.38)	✓	✓					✓	✓	✓	
II (1.15)			✓							
III (1.77)				✓						
IV (4.18)					✓					
V (5.35)						✓				
VI (0.87)										✓
Catalyst:										
C ₈ H ₁₇ N	✓	✓	✓	✓	✓	✓				✓
C ₆ H ₁₂ N ₂							✓			
C ₁₁ H ₂₁ O ₂ N								✓		
C ₃₂ H ₆₄ O ₄ Sn									✓	
Emulsifier:										
C ₁₂ H ₁₀ O ₃ SF ₁₇										✓

Polyol 1 = a polyol with starter materials of sucrose, glycerine and propylene oxide; OH No. 380–420.

Polyol 2 = a polyol with starter materials of propylene glycol and propylene oxide; OH No. 235-260.

*DPG = dipropylene glycol

Initial experiments included in-situ FTIR, thermal and pressure analyses and dynamic rheology. These provide information on the macro process during foam formation and are intended as both an overview of the process and to later support theories on the micro processes.

In the search for a suitable in-situ method, positron emission tomography and two-colour dynamic light scattering were considered. The successfully developed in-situ method of analysis using a stereo microscope is then discussed in detail as are the experiments carried out using this method.

2.2. In-Situ FTIR Spectroscopy

A 50cm³ cubic cardboard mould through which an AgCl/Br MIR fibre (1000µm) was sewn horizontally 1.5cm from the base was used as the sample “cell”. The fibre was connected to a Nicolet Magna IR Spectrometer 750. The A-component used was of the type A(I/i). A total weight of components A and B of 500g (ratio 40:60) was mixed for 9s and subsequently poured into the mould. Spectra were taken at 2-second intervals for 10 minutes.

2.3. Thermal and Pressure Analysis

The foaming process is a highly exothermic reaction. The temperature of the reaction was followed using two methods. The first method involved the insertion of a NiCr-Ni thermocouple into the base of a 50cm³ cubic cardboard mould. The thermocouple was initially placed 1cm from the base. The A- and B-components were mixed (A-component: A(I/i)) in a ratio of 40:60 at 25°C for 9s and then poured into the mould. Temperature readings were taken at set intervals and a plot of temperature against time demonstrated the exothermic process of foaming. The experiment was repeated and the thermocouple moved to 5 cm from the base in order to account for the foam growth. The entire process was repeated for the A-component B(I/i), with cyclopentane as the blowing agent, and subsequently for the A-component C(VI/i), with perfluorohexane as the blowing agent (see Appendix 1 for clarification of the formulations of B(I/i) and C(VI/i)).

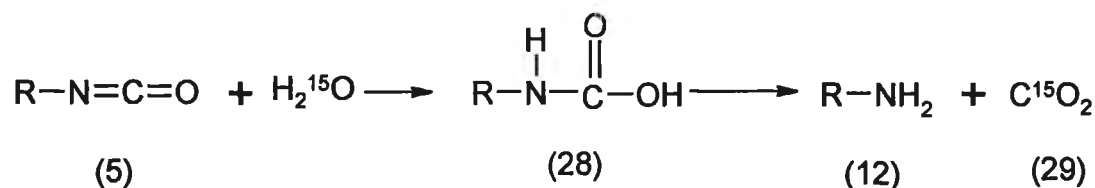
The second method was coupled to the measurement of the internal pressure using ultrasound. The foaming took place in a form placed beneath an ultrasound sensor. Again, the A- and B-components were mixed (A-component: A(I/i)) in a ratio of 40:60 at 25°C for 9s and then poured into the mould. Using a foam height measuring instrument (LRS3V3 from Vogt / Prosa GmbH, Hannover, Germany) the increase in foam height during foaming was measured by ultrasound, from which the rate of volume increase was obtained. A built in thermocouple simultaneously observed the reaction temperature. The internal pressure was computationally obtained from the change in temperature and change in volume at a given time. Again, the experiment was repeated using B(I/i) and C(VI/i) as the A-components.

2.4. Dynamic Rheology

Rheological measurements were carried out on a Haake VT500 rheometer using a neofrakt®-mixer at a mixing speed of 700rpm with 40g cup samples at 25°C. The samples resistance to flow against a given rate of revolution is measured from which its viscosity is calculated. The change in viscosity as a function of time was noted and graphically represented.

2.5. Positron Emission Tomography

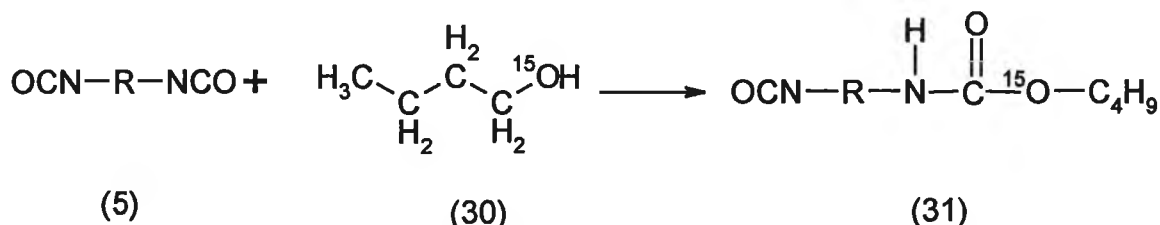
Positron emission tomography is more or less exclusively a medical imaging technique, few attempts being made on its implementation in non-clinical applications⁴². With the aid of short-lived positron emitting radionuclides it was hoped to visualise the nucleation process. For this purpose a Siemens ECAT HR Positron Emission Tomograph at Århus University Hospital, Denmark was used. ¹⁵O was the short-lived positron emitting radionuclide used. Two different radiolabelled compounds, [¹⁵O]water and [¹⁵O] butanol, were added respectively to the B-components (A(I/i)). The reaction between isocyanates and [¹⁵O]H₂O generates an amine and [¹⁵O]CO₂. The [¹⁵O]CO₂ is trapped in the gas bubbles and should therefore enable the visualisation of nucleation and foam growth:



2.1

Fig. 2-2: The reaction between isocyanates and radio-labelled H₂O generates an amine and radio-labelled detectable CO₂.

The results obtained were compared to those from labelling with [¹⁵O] butanol, which is introduced directly into the molecular chain of the polyurethane as an ending block:



2.2

Fig. 2-3: Isocyanate (5) and radio-labelled butanol (30) produces a radio labelled NCO terminated prepolymer (31).

The [^{15}O]water A-component was mixed with the B-component in the usual manner (ratio of 40:60 at 25°C) at which time scanning was started. The method was repeated using the [^{15}O] butanol A-component. It was assumed that [^{15}O]water and [^{15}O]butanol reacted with the diisocyanate as postulated above.

2.6. Two- Colour Dynamic Light Scattering

A- and B-components were sent for two colour dynamic light scattering analysis to ALV-Laser Vertriebsgesellschaft mbH, Langen, Germany. The aim was to measure the size of the initial nuclei formed, providing perhaps an experimental value for the critical nucleus radius, r^* (Equation 8). The components (A-component: A(I/i)) were mixed in the usual manner (total weight 10g) and analysed using an ALV- NIBS/HPPS High Performance Particle Sizer which operates on the two-colour dynamic light scattering principal⁴³. The cross-correlation function and light scattering was measured with respect to time.

2.7. In-Situ Microscopic Analysis – Part 1 – Method Development

Nuclei formed during rigid foam formation have initial sizes in the range of $1\mu\text{m}$ – $40\mu\text{m}$, $40\mu\text{m}$ being their average size at cream time. It is possible to visualise these sizes, even in the opaque medium of foam, using light microscopy. However, it is not possible to observe nuclei under $1\mu\text{m}$ using this method. For this purpose the two-colour dynamic light scattering experiment in section 2.6. was conducted. Therefore, an in-situ microscopic analysis of polyurethane rigid foam was developed using an Olympus SZX-12 stereo microscope, proving to be the only viable method of analysis. A brief description of the fundamentals of light microscopy follows. The steps taken in the development of the process are subsequently discussed in detail.

2.7.1. Fundamentals of Light Microscopy⁴⁴

Light is a form of radiant energy absorbed or emitted by spontaneous energy changes of bonding electrons initiating transitions between energy levels in the outer electron shell of an atom. In the electromagnetic theory by Maxwell, light is regarded as superimposed oscillating electric and magnetic fields carrying energy through space in the form of continuous waves. According to quantum theory, energy is transported discontinuously in individual bundles called photons. The effects of interaction of light with matter observed in optical microscopy are primarily wave-like in nature and can therefore be explained by wave mechanics.

A simple microscope consists of two convergent lenses. The principal beam paths for microscopical imaging are (see Fig.2-4):

- Beams, which propagate parallel to the optical axis, pass the back focal point.
- All beams, which pass the lens through the optical axis, do not change direction.

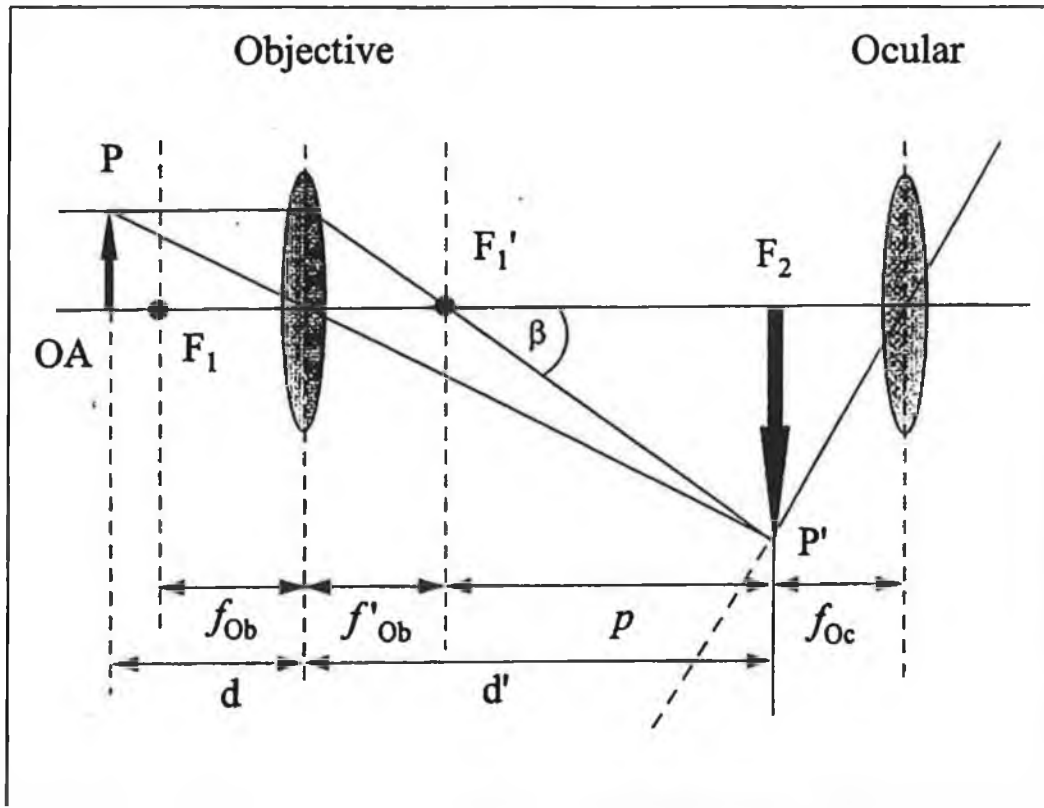


Fig. 2-4: Schematic illustration of a simple microscope with an objective and an ocular lens with focal points of F_1 and F_2 and distances of f_{Ob} and f_{Oc} respectively on the optical axis (OA). Beam paths indicate the generation of a real, inverted and magnified image P' of an object P .

Using these principal beam paths the imaging of convergent lenses can be found. The lens equation describes the relationship between the focal distance f and the object and image distances (d_o, d'_o)

$$\frac{1}{f} = \frac{1}{d_o} + \frac{1}{d'_o} \quad (44)$$

The lateral amplification of the objective A_1 and the total magnification of the optical system M_t are given by

$$A_1 = \frac{d'_o}{d_o} = \frac{d'_o}{f - 1} \quad (45)$$

$$M_t = A_1 M_{oc}, \quad \text{where } M_{oc} = \frac{250}{f}$$

However, scientific microscopes generally incorporate optical elements such as prisms, polarisers and mirrors into the beam path between the objective and the ocular lenses. This can be achieved by using objectives with an infinite image distance. If the object is then placed in the focal plane, all beams emitted from one point of the object are parallel after passing the objective. To obtain an image at infinite distance a third lens, the tube lens, is needed. This lens produces a real image, which can be magnified by the ocular lens. The tube lens is characterised by the tube factor q_{∞} . The total magnification then, is written as:

$$M_t = M_{obj} q_{\infty} M_{oc} \quad (46)$$

The wavelength of light ranges from 360nm (violet light) to 780nm (red light). When light impinges on a bubble it is partially reflected at the surface without preference for any colour. The rest of the light enters the substance and propagates as refracted wave within it. Therefore, the bubble appears colourless. Their outlines are however visible because of the reflection of the light at the surfaces.

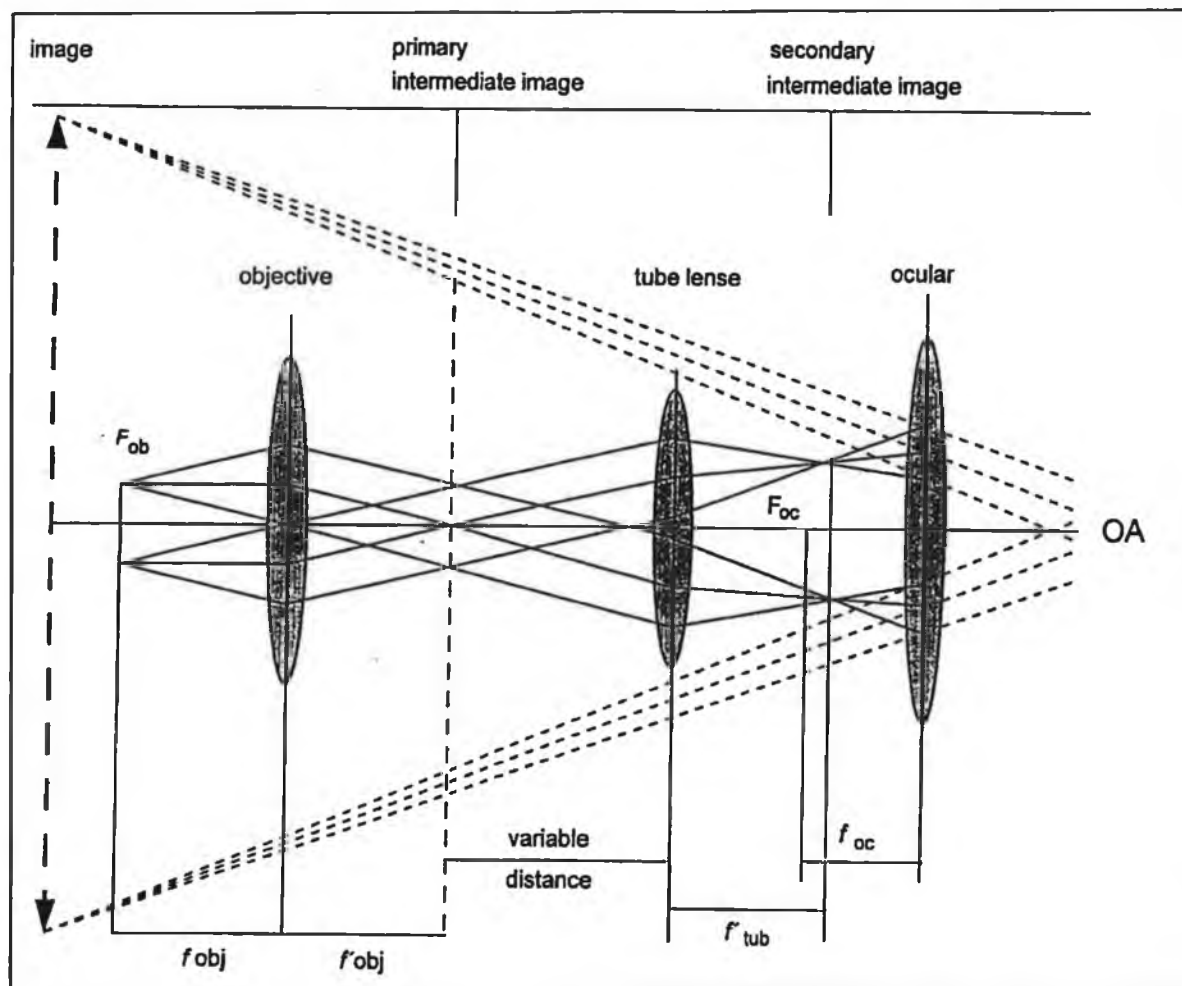


Fig. 2-5: Beam path in a compound microscope (taken from reference 44) with a tube lens to convert the intermediate image of the objective from infinity into a finite distance. In the region of parallel beam paths between the objective and the tube lens, additional optical elements, e.g. polarisers or prisms, can be assembled without disturbing imaging.

As with any method development the relationship between the responses and the factors of a given experiment is exploited by optimising the technique. In detail the method development process consists primarily of the following steps:

1. Determination of the target (In-situ analysis of the nucleation process)
2. Determination of the factors, factor ranges and factor constraints (temperature dependency, speed of reaction, size of nuclei)
3. Generation of method design
4. Realisation
5. Optimisation of the method (correction of observed nucleation number)
6. Experimental and mathematical validation (reproducibility and statistical viability of method).

These steps will be discussed more clearly to give an accurate account of the development of the method.

2.7.2. Determination of the Target

The aim of this research is the in-situ analysis of the nucleation and formation of polyurethane rigid foam. By studying the effect of the various components it is hoped to exploit these influences for the production of rigid foam for thermal insulation purposes.

2.7.3. Determination of the Factors, Factor Ranges and Factor Constraints

Factors influencing this method included the mixing process and the temperature dependency. Mixing must be fast, and, ideally, lead to a homogenised reaction mixture while the temperature development of the sample under observation must be the same as the temperature gradient during foaming in the beaker. These were accounted for in the following manner:

2.7.3.1. The Mixing Process

The principle aim of mixing is to create as large an interfacial area as possible between the two components and the blowing agent⁴⁵. Fine primary droplets or gas bubbles have a tendency to coalesce, i.e. a part of the work done in forming interfacial area is wasted. During the production of fine bubbles the size distribution of the bubbles is as a result of a continuous process of dispersion and coalescence. The coalescence process depends chiefly on the state of flow in the mixing device.

With this in mind, the mixing process was studied under the following key points: amount of reactants, type of stirrer and duration of mixing. The amount of reactants must be substantial enough to allow for homogenous mixing and yet small enough to enable a short mixing time. For mixing purposes the system had a viscosity of 984mPa. Four different stirring methods were studied. Method 1 was carried out using a turbine mixer, methods 2 and 3 using a paddle mixer and method 4 using a propeller type mixer (see Fig. 2-6). Speed is essential. One must homogeneously mix the components, take a sample, place it in the sample chamber, place the chamber under the microscope and start following the process within a matter of seconds.

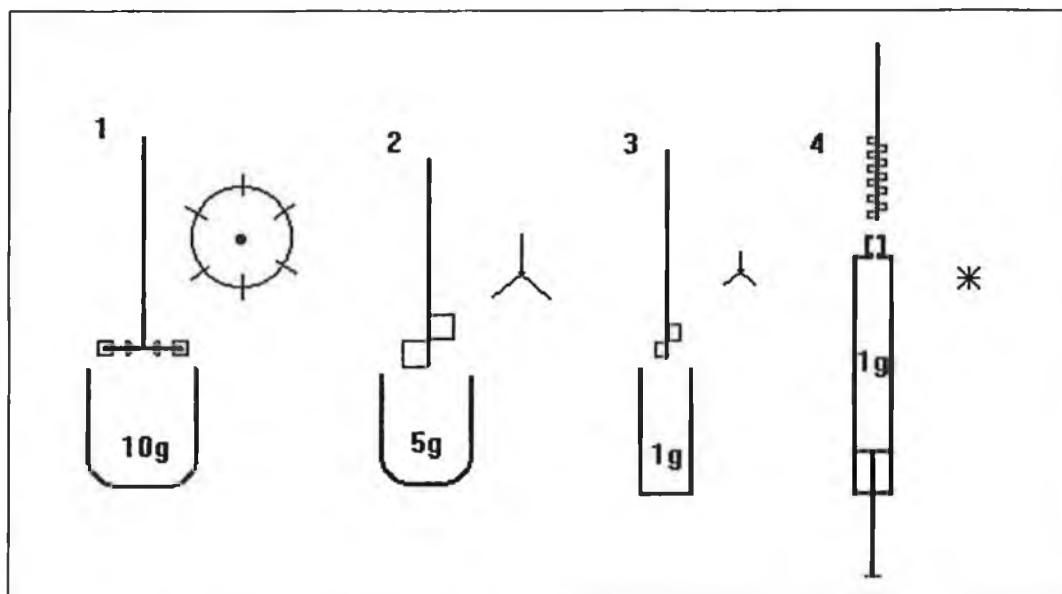


Fig. 2-6: The four different stirring methods as described in text including a schematic representation of the stirrers used; 1 is a turbine mixer, 2 and 3 are paddle mixers and 4 is a propeller type mixer.

The previous diagram shows the various methods studied. Initially a 150ml Lupolene[®] beaker was used in which 10g of reactants were mixed using a turbine mixer (Vollrath[®] –Mixer) with a 36.50mm diameter. The second and third attempts involved the use of a 10ml (5g of reactants) and 2ml (1g of reactants) vials with customised paddle mixers with diameters of 11.50mm and 4.25mm respectively. Finally, a syringe was considered. By using a 1ml single-use syringe and a customised propeller type mixer with a diameter of 1.80mm, it was hoped to minimise the amount of air entering the sample during mixing. An additional advantage was the reduction of the sample transfer time from the bulk to the sample chamber by injecting the mixed reactants directly onto the microscope slide. The B-component followed by the A-component was drawn up into the syringe. The stirrer was inserted through the top of the syringe and after mixing, a sample was injected on to the slide. Mixing times for each experiment are 5sec with a turning rate of 2400rpm.

The four methods of mixing were tested and each proved to be a feasible method. The injection method (method 4) was compared with the beaker method. For both methods the model A-component A(I/i) and the B-component (M20A) was mixed in a ratio of 40:60 at room temperature. Each analysis was carried out ten times from which an average number of bubbles per area observed and average bubble diameter was calculated. The results were surprising. It was expected that by using the injection, where the amount of air introduced by mixing would be minimised, smaller bubbles would be produced. However, the size (see Fig. 2-7) and the amount of the bubbles (Fig. 2-8) increased. This was probably due to the inhomogeneity of the mixture, which was as a result of the design of stirrer. Similar tests were carried out on the other stirring possibilities with the result that the initial stirring method suggested proved to be the most suitable due to the homogeneity and speed of mixing.

Of the four different methods studied, the first stirring method (turbine mixer) studied was considered the most suitable. Using this method the model A-component A(I/i) was mixed with the B-component in the usual manner. The stirrer, stopwatch, and macro (see section 2.7.4.2.) were started simultaneously. Using a spatula, a sample with a diameter of approximately 2.5mm was placed in the sample chamber which was quickly placed under the microscope.

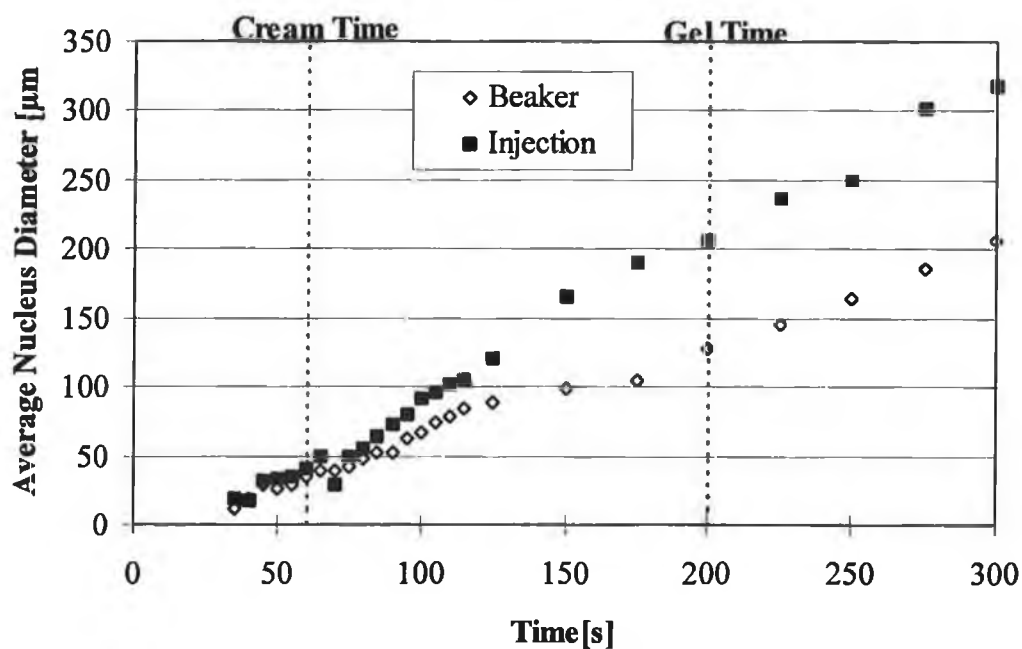


Fig. 2-7: Average bubble diameter growth; comparison of the beaker and injection methods, described as method 1 and 4 in Fig. 2-6, using the A-component A(I/i).

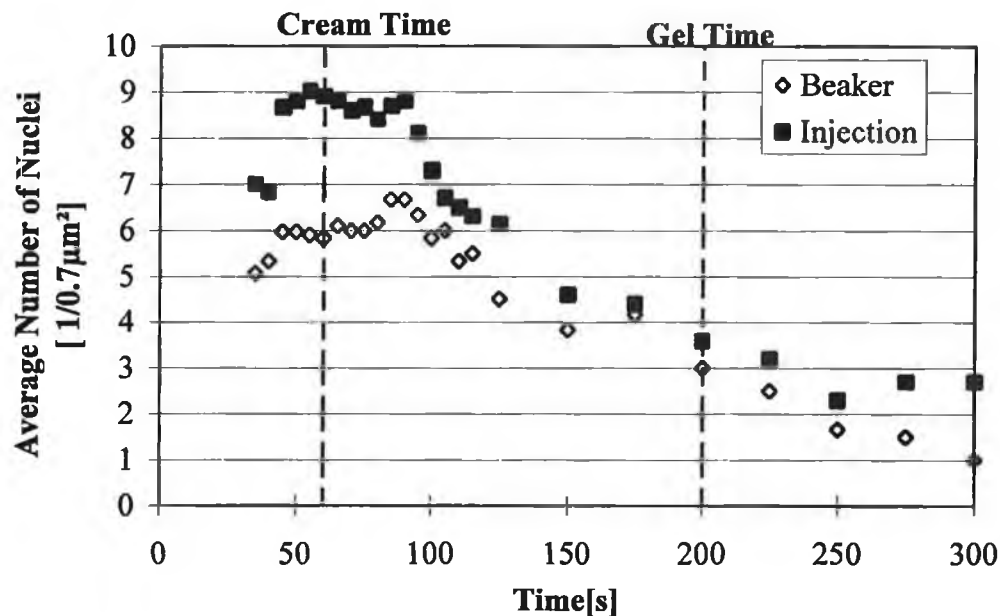


Fig. 2-8: The average number of bubbles analysed per photomicrograph (area equal to $0.7\mu\text{m}^2$); comparison of the beaker method to the injection method. The A-component A(I/i) and the B-component (M20A) were mixed in a ratio of 40:60 at room temperature.

Each experiment was repeated ten times and the total number of bubbles at a given time analysed. This ensured that a maximum of at least one hundred bubbles was counted at the earlier stages of foaming, including cream time. This allowed for a more statistically valid value of the nucleation number (NZ) and bubble diameter (see section 2.7.6.1.). Due to bubble growth the amount of bubbles to be seen in any one photomicrograph decreased after that.

The duration of mixing is as influential as the type of mixing. Over agitation could destroy bubbles while under agitation could lead to inhomogeneity.

In order to examine the effect of the mixing time on the foaming process and to ensure homogeneous mixing, photomicrographs of the unreacted A-component A(I/i) were taken after 0 sec, 5 sec and 9 sec of mixing. As expected, an increase in bubbles is observed (see Fig. 2-9) which is due to the longer mixing time indicating that mixing up to 9s does not destroy the bubbles. This is long enough to ensure homogeneous mixing and yet fast enough to allow for a quick transfer of the sample from the bulk to the microscope for analysis of the early stages of foaming.

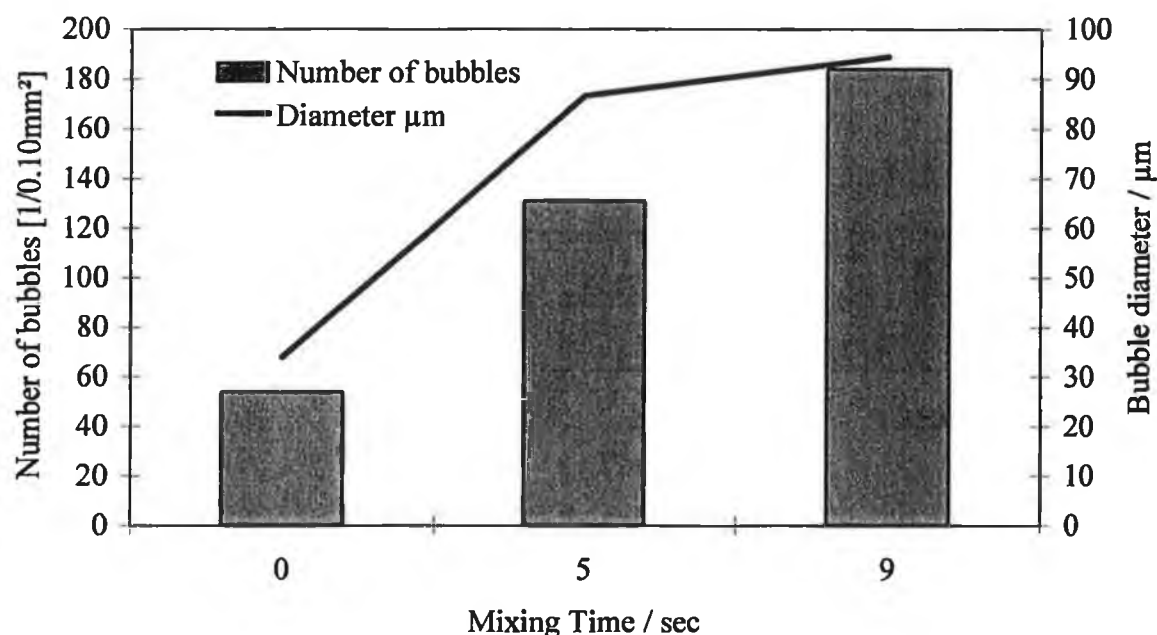


Fig. 2-9: A study on the influence of the increased mixing times on the size and number of bubbles per $10\mu\text{m}^2$ of unreacted A(I/i). (Using stirring method 1 in Fig. 2-6 at 2400rpm).

It is hoped to draw a relationship between the bubbles appearing due to the mixing and the bubbles, which are suspected nucleation sites which, appear within the foams cream time. Kanner and Decker¹⁰ have also studied foam formation under similar conditions. They noted that the number of bubbles observed at this early stage, which are introduced by the process of mixing, is more than sufficient to account for all of the cells present in a final foam.

2.7.3.2. Foaming under Controlled Temperature Conditions

As has already stated in section 1.4.3. the foaming process is a highly exothermic process. Therefore, if a significant amount of heat was lost from the sample under observation to its surroundings, the temperature development of the sample under observation would not represent the temperature development of the sample in the beaker. The surface to bulk ratio of the sample is quite large, resulting in a large heat loss to its environment. In order to compensate for this heat loss and thus making the results comparable to those obtained from the beaker, a heating mantle was attached to the microscope's table, thus preventing the loss of energy in the form of heat to its surroundings, providing an adiabatic system. Using compounds with known melting points, the heating mantle was calibrated. The results obtained from the thermal analysis (section 3.2.2.) of the foaming process established the programmable heating rates. Sample preparation was carried out as normal however, the time of the first images recorded was delayed due to the extra time needed to insert the sample chamber into the heating chamber. A further disadvantage generated by the heating mantle was the reduced field of view as there was only a pinhole for viewing to prevent heat loss. The foaming of model A-components A(I/i), B(I/i) and C(I/i) was analysed.

For each experiment the temperature was held constant at 25°C up until cream time, from which time the following heating rates were used: for the foaming of the A-component A(I/i) a rate of 10°C/s was used, for B(I/i) a heating rate of 12°C/s was used and for C(VI/i) a rate of 7°C/s was used. These rates are equivalent to the temperature increase during foam formation obtained from the thermal analysis in section 3.2.2.

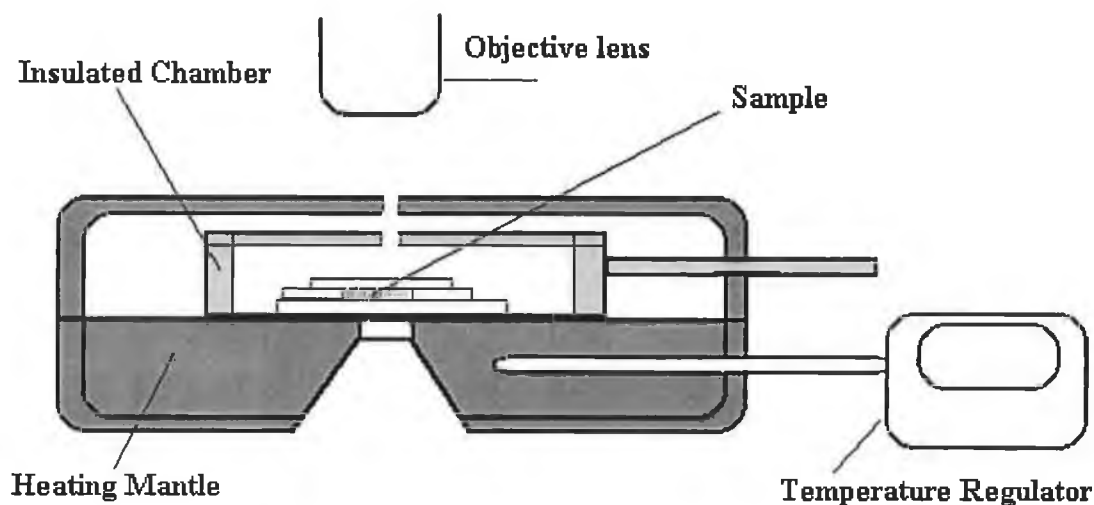


Fig. 2-10: Heating Mantle.

The results were compared to those obtained without a heating mantle. It was noted that due to the experimental set-up (i.e. the delay needed for accuracy due to smaller sample chamber) it was difficult to clearly visualise the initial nuclei before 40s. This is the time region of most interest. The results were independent of A-component used (i.e. the blowing agent used). The size of the nuclei (see Fig. 2-11) deviated only after 150-200s, which is outside our primary region of interest. Nucleation numbers for each system (see Fig. 2-12) varied little from the results obtained without a heating mantle. Considering this and the disadvantages to the speed and accuracy of the method, it was agreed to continue without a heating mantle as heat loss could be considered negligible. The applicability of the results to commercial systems is tested later in this work (section 4.1.).

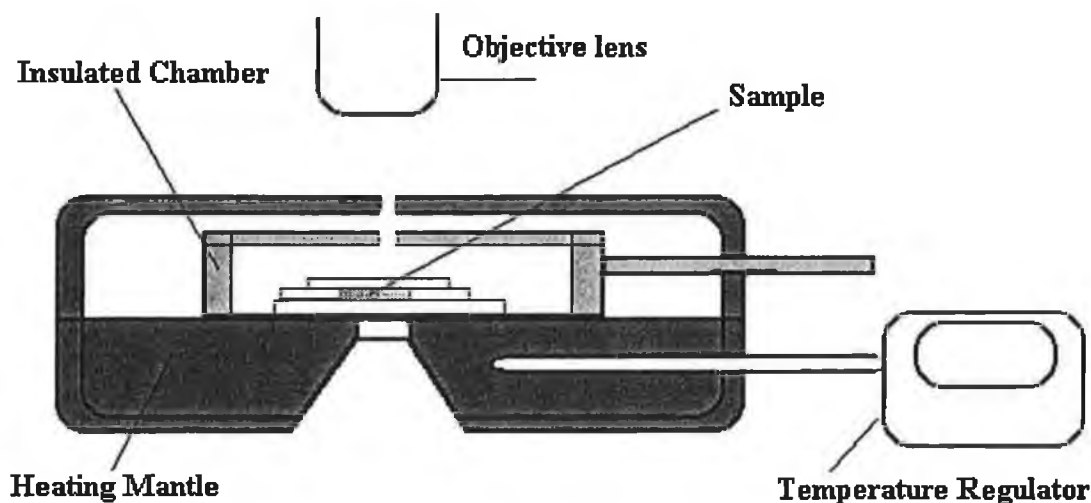


Fig. 2-10: Heating Mantle.

The results were compared to those obtained without a heating mantle. It was noted that due to the experimental set-up (i.e. the delay needed for accuracy due to smaller sample chamber) it was difficult to clearly visualise the initial nuclei before 40s. This is the time region of most interest. The results were independent of A-component used (i.e. the blowing agent used). The size of the nuclei (see Fig. 2-11) deviated only after 150-200s, which is outside our primary region of interest. Nucleation numbers for each system (see Fig. 2-12) varied little from the results obtained without a heating mantle. Considering this and the disadvantages to the speed and accuracy of the method, it was agreed to continue without a heating mantle as heat loss could be considered negligible. The applicability of the results to commercial systems is tested later in this work (section 4.1.).

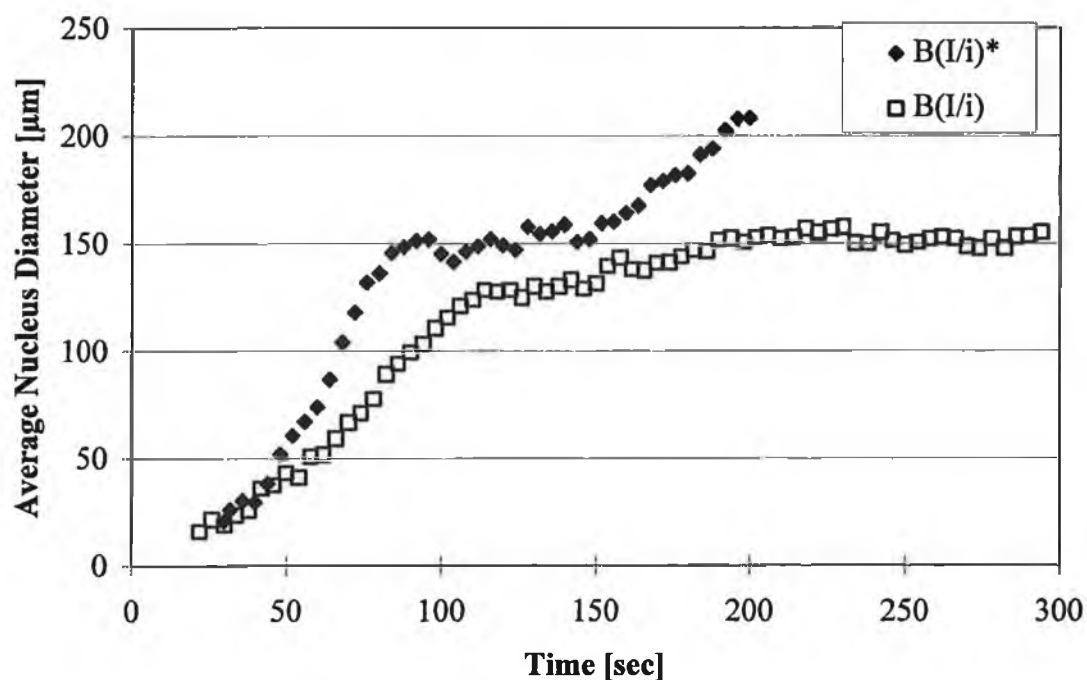


Fig. 2-11: Comparison of nucleus diameters obtained while foaming (A-component: A(I/i)) with (♦) and without (□) controlled temperature conditions. * system foamed under temperature controlled conditions.

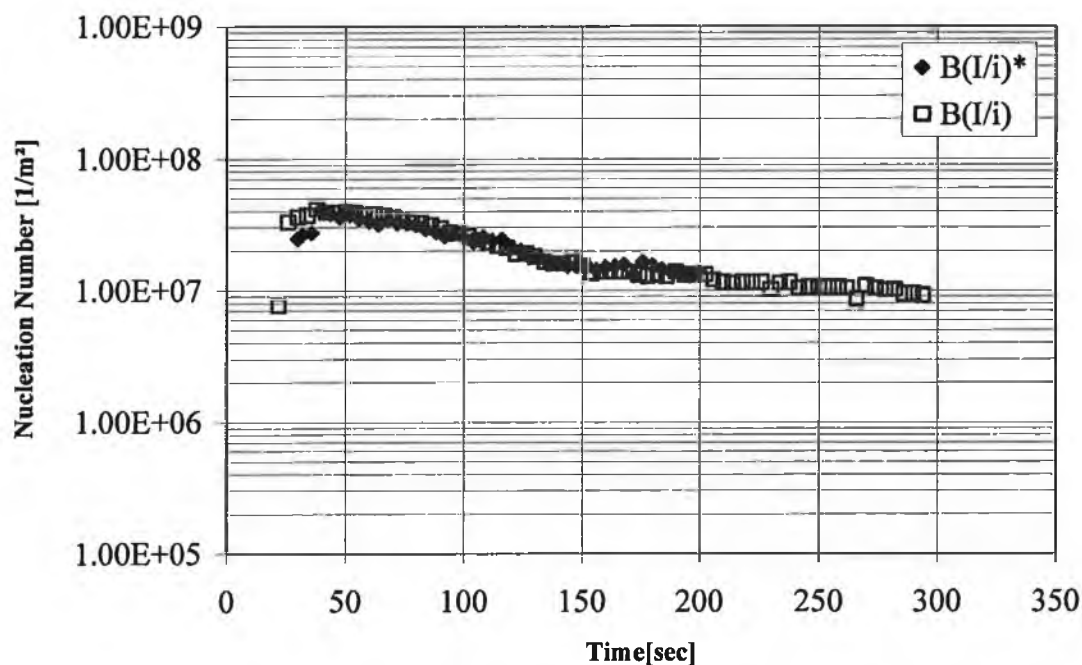


Fig. 2-12: Comparison of nucleation numbers obtained while foaming with and without controlled temperature conditions. Differences in nucleation numbers are negligible. *under temperature controlled conditions.

2.7.4. Generation of Method Design

2.7.4.1. Image Processing^{46,47}

Image processing is a generic term, which covers several activities related to digital images, i.e. images that have been converted into arrays of pixels. It is used not only to improve the visual images to the viewer, but also to prepare the images for measurement of the features and structures present. The path from data acquisition to image analysis is usually as follows:

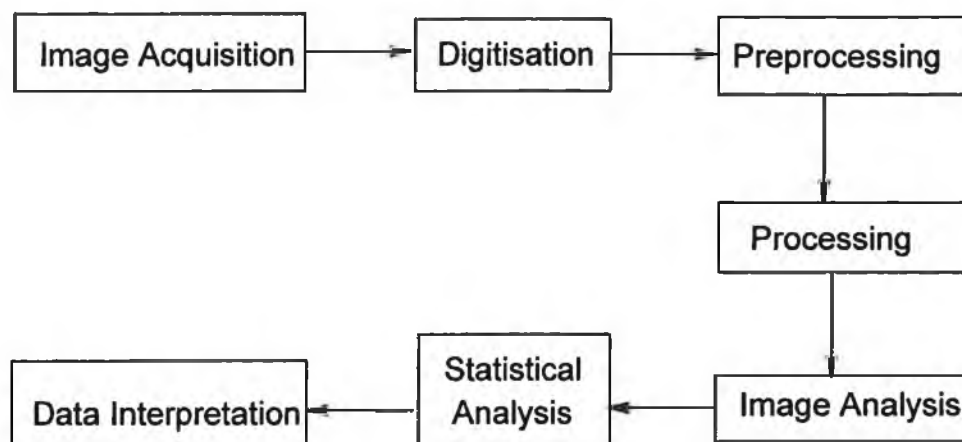


Fig. 2-13: Flow diagram of the imaging process.

Image pre-processing consists of preparing images for subsequent operations. Two main concepts which can be varied here are contrast, a fairly intuitive concept, and the signal to noise ratio, due to electronic fluctuations or low-count signals. One can consider these methods as purely “cosmetic” because, although it improves the appearance of the picture, it does not modify the fundamental image content. Image processing consists of transforming an image into another one, which is intended to be more manageable, either in terms of interpretation or in terms of subsequent analysis. Such methods are image segmentation and image binarisation.

Due to the lack of contrast between the nucleated cell centre and the surrounding matrix and the growing cell diameter, it was not possible to carry out any further

processing techniques other than contrasting. If it had been possible to binarise the images, i.e. to get a black and white solid image, it would have been possible to write a macro to automatically measure and categorise the nucleated cell diameters. This was not possible and so the growing cell diameters were automatically saved at set intervals, digitised and were subsequently measured manually and statistically analysed.

Image analysis has previously been used for the characterisation of foams and plastic⁴⁸, in evaluation of cell and strut size. It is also useful for such areas as the study of catalysts in gas phase polymerisation⁴⁹. Kanner and Decker¹⁰ have carried out similar work in the sixties. In this respect, it is not a new method of analysis. Be that as it may, no in-situ studies of the foaming process of polyurethane rigid foam and especially the nucleation process have been previously carried out in such a fundamental manner. This is partially due to the speed of the new technology used.

2.7.4.2. Implementation of Imaging Process

As discussed in the previous section, the nucleation process was examined by foaming the model system under the microscope (Olympus SZX-12 Stereomicroscope). Before actually analysing the nucleation process under the microscope, it was first necessary to find a suitable imaging system for the process. Imaging processing is used not only to improve the visual images to the viewer, but also to prepare the images for measurement of the features and structures present. Using a video camera (JVC TK-C1380 Colour Video Camera) connected to a computer equipped with an imaging system (analySIS 2.1, Soft Imaging System GmbH, Münster, Germany), snapshots or photomicrographs of the foaming process were taken (see Fig. 2-14). To acquire the maximum information from the photomicrographs the following procedures were taken prior to analysis:

1. The microscope and the imaging system were calibrated and subsequently tested.
2. The microscope was adjusted to a suitable magnification.
3. A suitable light contrast was found and set, i.e. held constant thereafter.

Finally, a macro program was written whereby photomicrographs were automatically taken by the imaging system at a set interval of 3sec. This not only saved precious time during the foaming process but also allowed the viewer to concentrate on focusing on the growing bubbles. A method was developed whereby a maximum of 10g of reagent was mixed from which a sample was taken and placed on a microscope slide between two coverslips 0.15mm thick. A third cover slip was placed over the sample, resting on the other two, as depicted in Fig. 2-14. This gives a 20mm x 20mm x 0.15 mm chamber for foam growth at set intervals. The stirrer, a stopwatch and the macro were all started simultaneously. From the photomicrographs the number of nuclei per area and their diameter could be measured with respect to time. The rate of bubble growth could also be calculated. Experiments were carried out at room temperature unless where otherwise stated (for implementation of heating mantle see previous section).

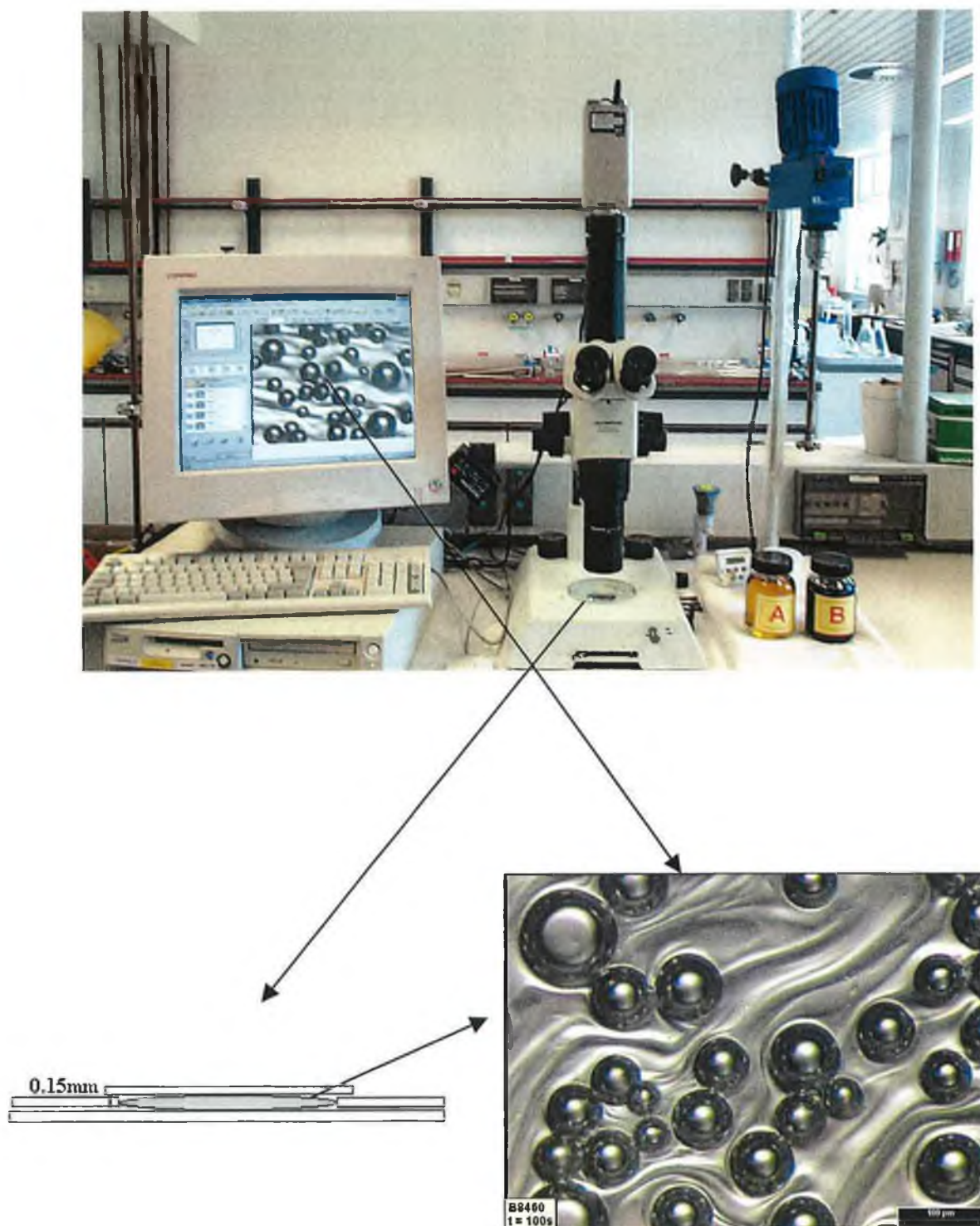


Fig. 2-14: Experimental set-up; A- and B-components were mixed in their appropriate ratios using the stirring method 1 in Fig. 2-6. A sample was taken from the mixture and placed under the microscope where the stages of the foaming process were followed.

2.7.5. Realisation

Before continuing the discussion on method development the following terms need to be clarified: nucleus, bubble, cell and nucleation number.

Within this work, the following words appear frequently: *nuclei, bubbles and cells*. A *nucleus* is that which is initially formed from gas dissolution, i.e. from the nucleation process and is in the size range $< 40\mu\text{m}$, $40\mu\text{m}$ being their average size during cream time. Within the foaming process these nuclei grow resulting in spherical *bubbles* which undergo radial growth until they are hindered by each other. They then take on the polyhedral shape of foam *cells* normally with cell size $> 150\mu\text{m}$. These words are interchanged in this work. However, they occur at various times and stages of the whole process which is polyurethane rigid foam formation. The nucleation number (NZ) is the number of nuclei counted per area observed and is converted to nucleation number per meter squared for convenience ($\text{NZ}[1/\text{m}^2]$).

Initial experiments exhibited the four characteristic regions of development as described previously in this work and in reference 22 and can be correlated to the regions identified in the rheological studies by Mora et al⁶⁴. These regions are as indicated in the following Fig. 2-15 and can be described as follows:

Region I: this indicates the induction period, i.e. the time required to establish steady state nucleation conditions. This is assumed since, although the sample is under the microscope in under 20 seconds from the start of mixing time, the first bubbles (nucleation sites) are seen after 30 seconds. It is this region which is of the most interest. (bubble nucleation)⁶⁴

Region II: the number of bubbles increase linearly with time. This appears to be due to the spontaneous appearance of more bubbles. (Liquid foam and microphase separation)⁶⁴

Region III: the number of bubbles begin to reduce per observed area due to the growth of the bubbles present. (Physical gelation)⁶⁴

Region IV: depending on the stability of the system these bubbles grow to an end size of approximately 250 μm or are unstable, coalescence then resulting in fewer but larger bubbles.

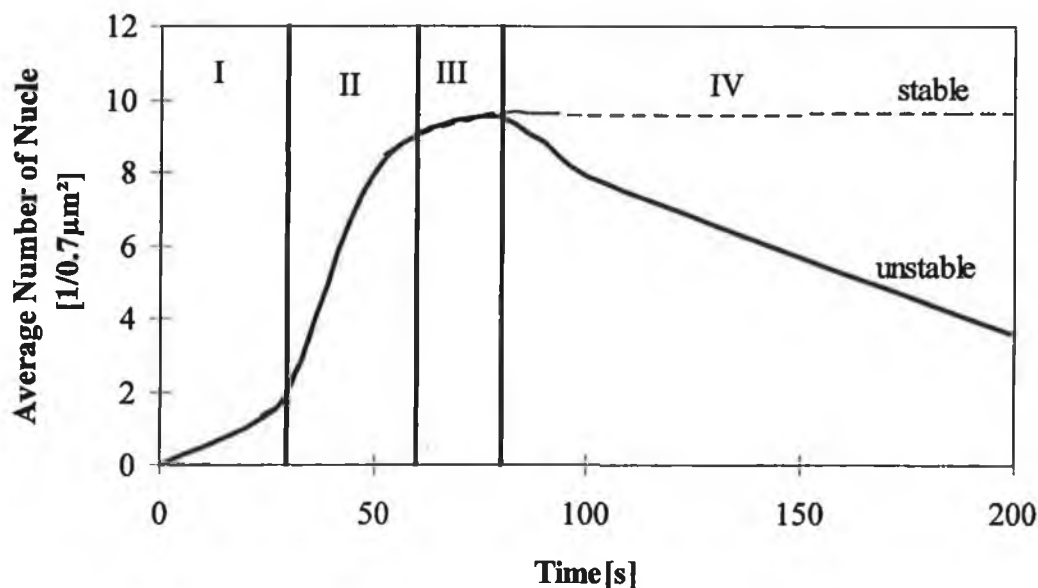


Fig. 2-15: Schematic Sketch of experimentally analysed bubble growth with respect to time in agreement to that described in ref. 22.

The nucleation number was initially counted per observed area and converted to per square meter [$1/\text{m}^2$]. This was not strictly representative of the nucleation number as it took neither the volume increase nor density decrease of the foam into consideration. This is important when analysing foams with various densities or nucleation numbers. One needs to eliminate the error in assuming that higher density foams with finer cells, indicates a higher nucleation number. Therefore, we convert the nucleation number observed per meter squared [$1/\text{m}^2$] to nucleation number per gram [$1/\text{g}$] (see section 2.7.6.)

Fig. 2-16 on the following page shows typical photomicrographs taken at set intervals during these experiments, remembering that each experiment consists of a minimum of ten “runs” (analyses) under the microscope. The nucleus diameter and nucleation number values shown are the calculated average values from the ten analyses.

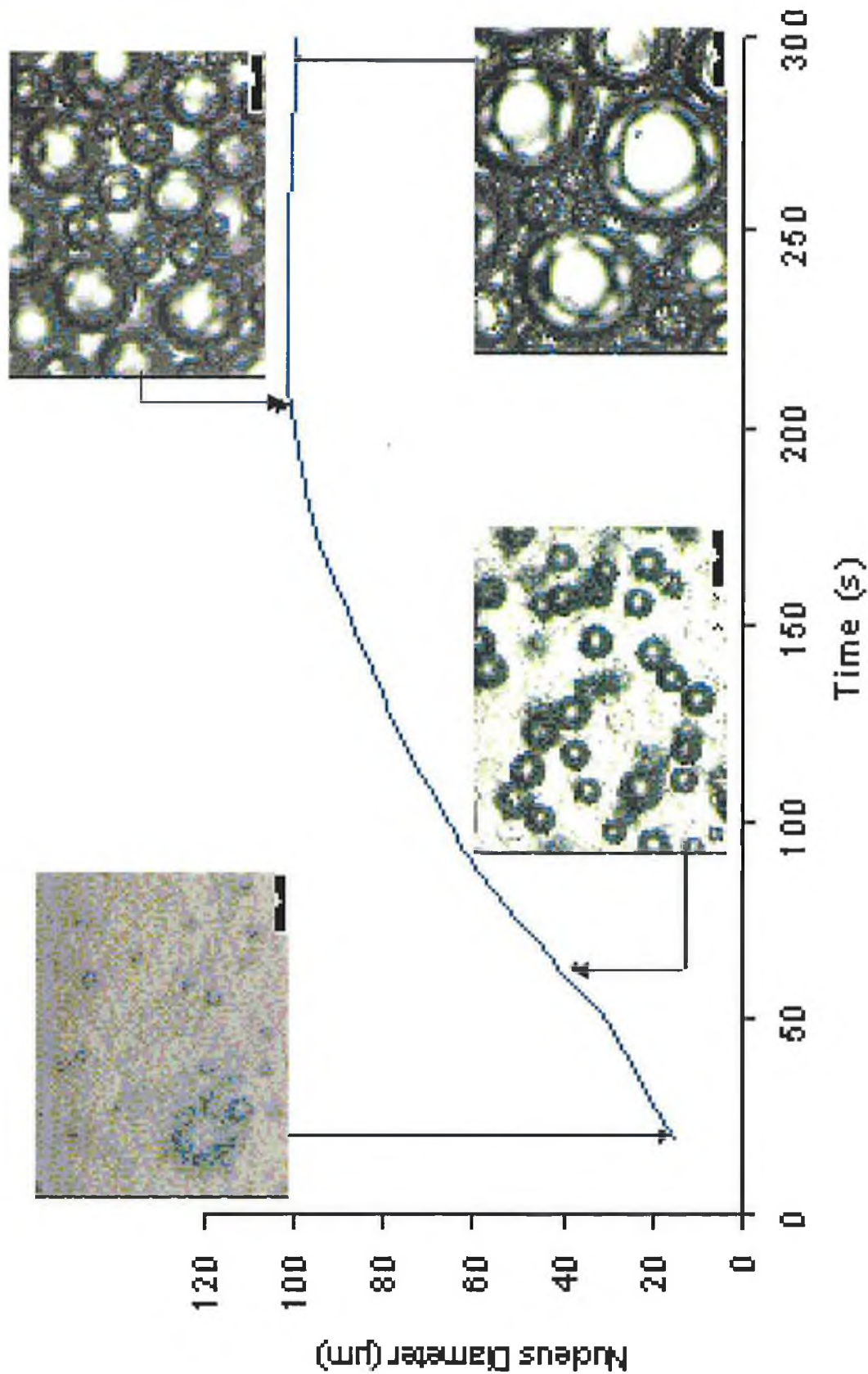


Fig. 2-16: Typical photomicrographs taken at set intervals during the nucleation and foam growth process. The photomicrographs were saved, digitised and manually analysed.

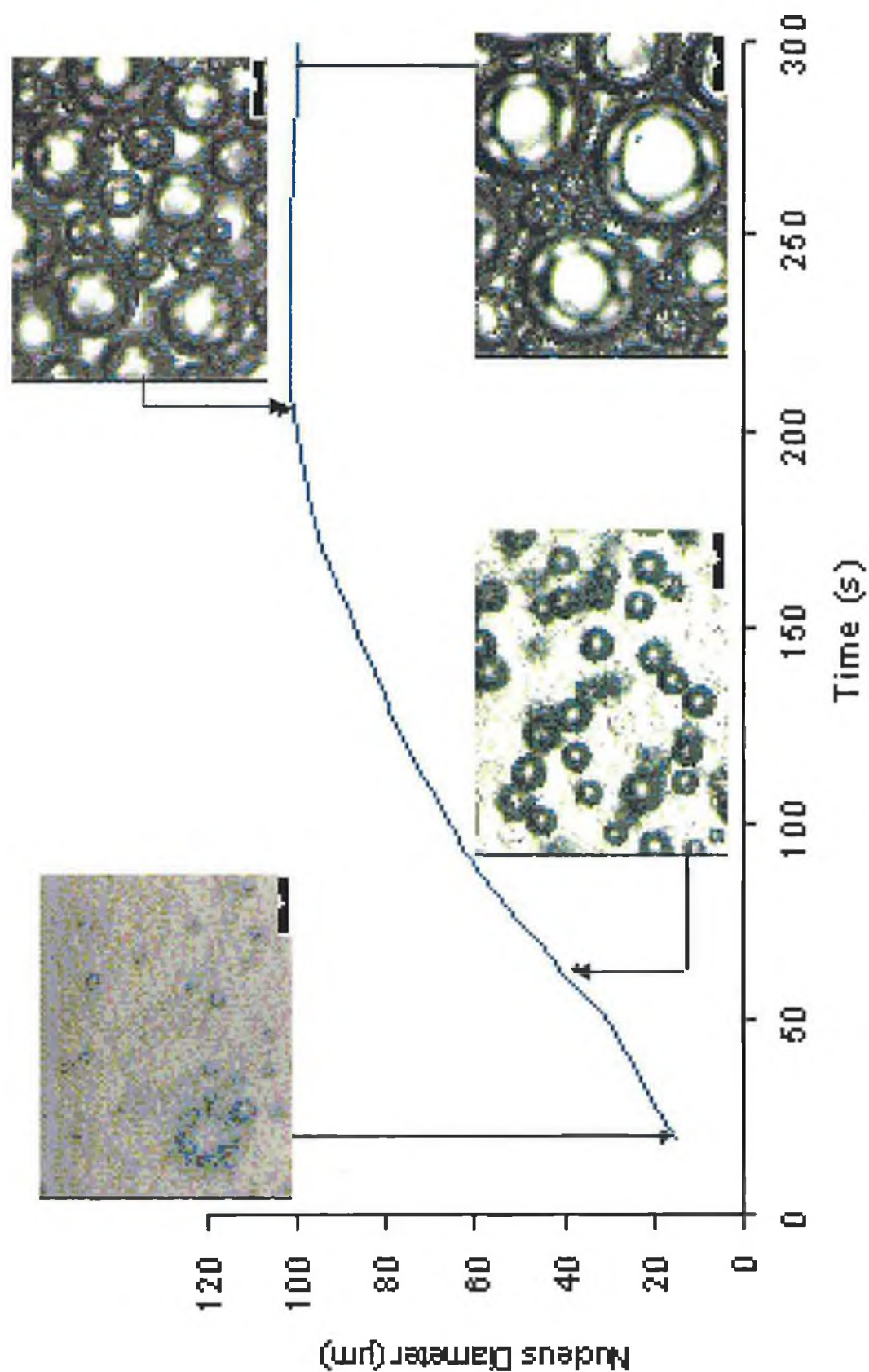


Fig. 2-16: Typical photomicrographs taken at set intervals during the nucleation and foam growth process. The photomicrographs were saved, digitised and manually analysed.

2.7.6. Optimisation of the Method

2.7.6.1. Nucleation Number Corrected [NZ_c]

The former diagram indicates the typical growth curve for the observed nucleus diameter during foam formation. The typical curve obtained for the nucleation number per square meter with respect to time is shown in the following diagram, Fig. 2-17. The decrease in the nucleation number with time is effectively a reduction in observed nuclei as a direct result of sample growth and not a physical reduction of nuclei. Therefore, in order to obtain an accurate nucleation number the observed number had to be corrected with respect to the growth and density decrease of the sample.

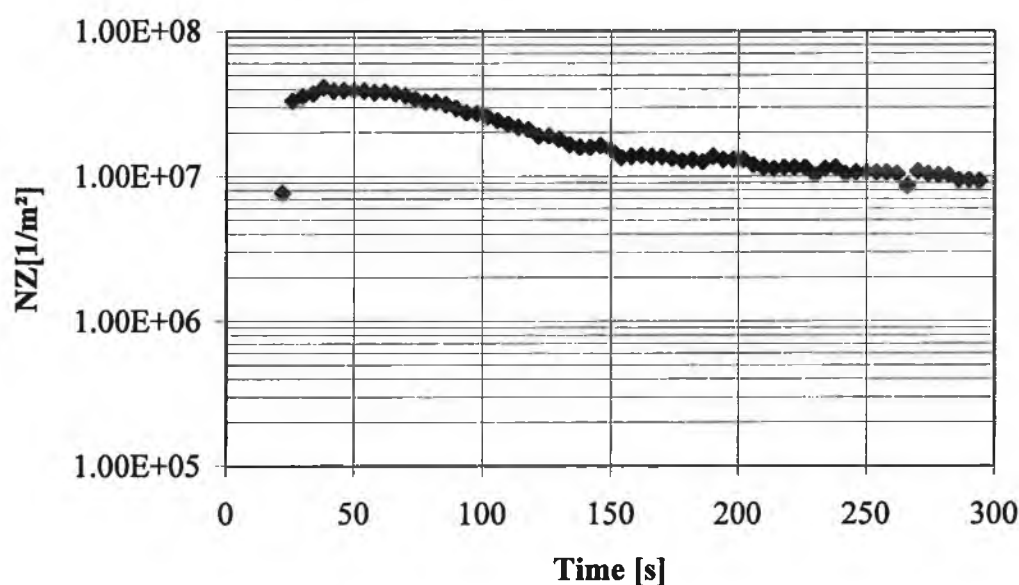


Fig. 2-17: Typical curve obtained when measuring the number of nuclei per area during foaming. Model system B(I/i) under the conditions developed in section 2.6.2.

The area of observance remains the same while the nuclei grow in an expanding medium (see Fig. 2-17). For this purpose, an auxillary ocular lens onto which concentric circles were engraved was fitted to the ocular lens of the microscope. The circles' diameters at a set magnification were measured. To calculate the volume increase and subsequently the density decrease, a sample with diameter approximately equal to 1.0mm was placed in the sample chamber and under the microscope.

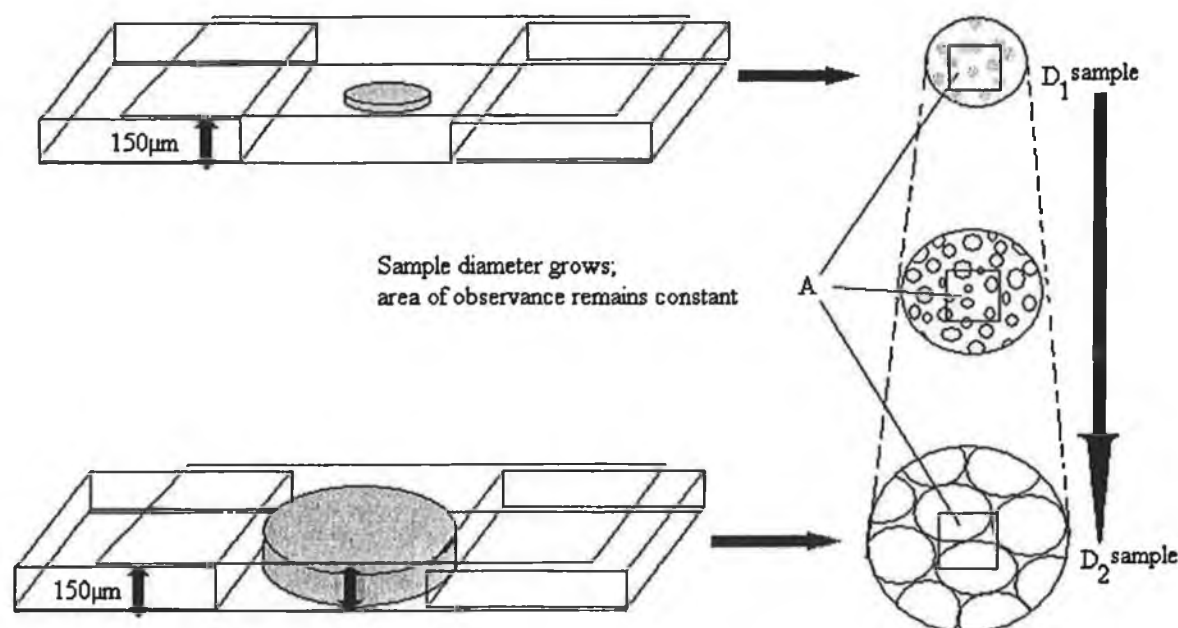


Fig. 2-18: The nucleation number per observed area (A) needs to be corrected to include such factors as the sample growth (growing from D_1 to D_2).

The sample's diameter growth was analysed with respect to time and using the chamber's height (150µm) equal to the maximum sample height, the volume increase with respect to time was calculated (see Fig. 2-19). The sample was weighed and the density during the foam process calculated. Both volume and density could be mathematically expressed as a function of time and these functions were used to correct the nucleation number [$NZ_c = 1/g$] as depicted in Fig. 2-20.

It should be noted that nucleation numbers obtained at times less than 30s are inaccurate (see Fig. 2-17). This is as a direct result of the lack of clarity due to the incompatibility of the reaction mixture. After this time the sample begins to turn a creamy opaque colour, improving visualisation.

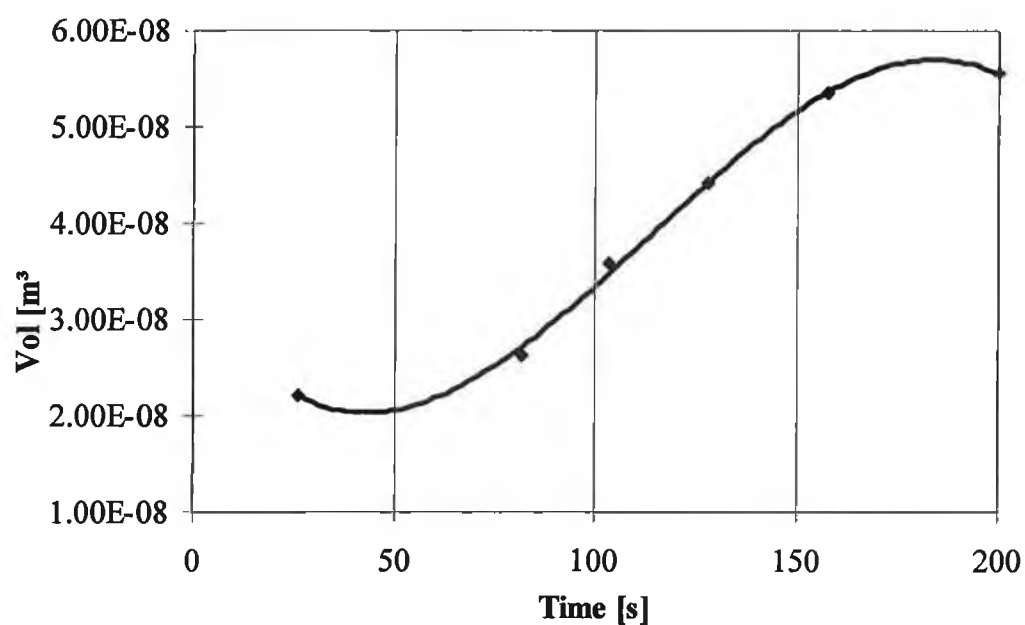


Fig. 2-19: Sample foam growth with respect to time as calculated with the aid of concentric circles.

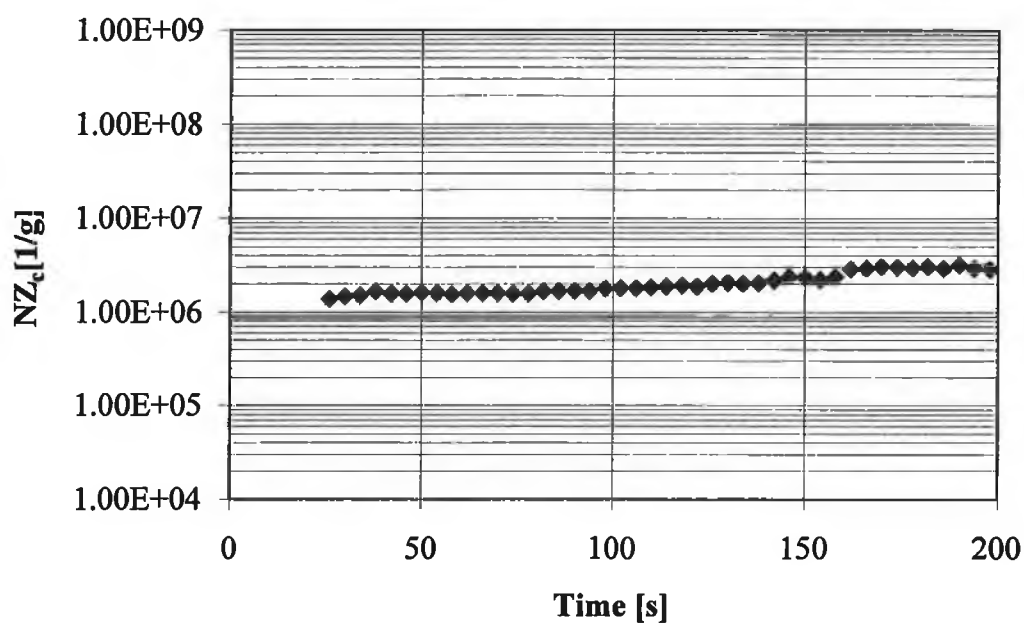


Fig. 2-20: The corrected nucleation number (NZ_c) [1/g] with respect to time, i.e. the nucleation number per square meter as shown in Fig. 2-17 corrected using the volume increase (Fig.2-19) and the density decrease of the sample.

A further correction was necessary when the bubble diameter was greater than or equal to the chamber height ($150\mu\text{m}$). At this point the growing bubble, which up until then was growing radially unhindered, is hindered and begins to take on an ellipse form (see Fig. 2-21). The diameter of these "squashed" bubbles was measured and the volume of an ellipse calculated. This volume was then equated to the volume of a spherical bubble and its diameter calculated. The ellipse:sphere factor was included in the calculation of the nucleation number where the bubble diameter was greater than or equal to $150\mu\text{m}$. As can be seen from Fig 2-19 this correction factor is only needed after approx. 150s and therefore has no influence on the nucleation process.

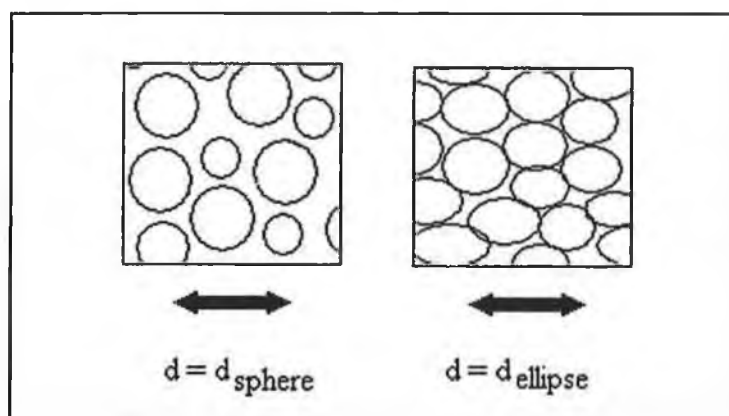


Fig. 2-21: Bubble growth $2r < 150\mu\text{m}$, i.e. the diameter is the diameter of a sphere; $2r > 150\mu\text{m}$, i.e. the diameter is the diameter of an ellipse.

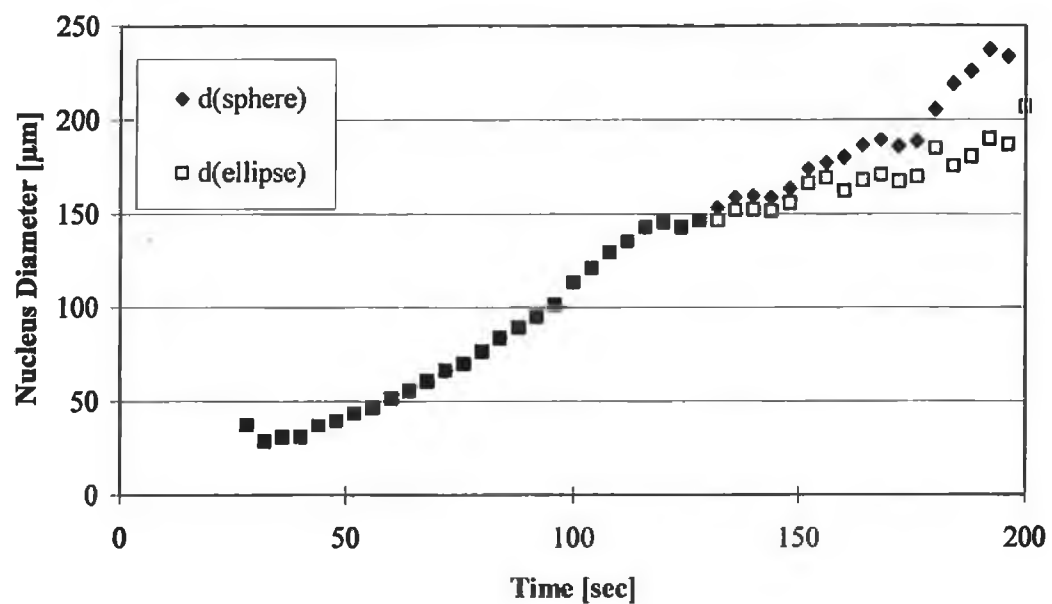


Fig. 2-22: A comparison of the nucleus diameter values with (\square) and without (\blacklozenge) the ellipse correction factor for bubbles larger than $150\mu\text{m}$.

2.7.7. Experimental and Mathematical Validation

2.7.7.1. Statistics⁵⁰

Statistics has always played an important part in analytical experiments particularly in the analysis of particle or cell size^{51,52,53}. It is important that average values obtained are statistically correct and for this purpose each analysis was repeated up to ten times under the same conditions. In other words, for the purpose of this work, an “experiment” is ten analyses of the same system, the results of the experiment being an average of these analyses. This provided, at the start time, a maximum number of bubbles (approximately over 100) for analysis. Average (μ) values and standard deviation (σ) were calculated in the usual manner:

$$\mu = \frac{1}{n} \sum_{i=1}^n x_i \quad (47)$$

$$\sigma = \sqrt{\frac{\sum_{i=1}^n (x_i - \mu)^2}{n - 1}} \quad (48)$$

where, n is the number of experiments and x is any given diameter value.

The precision of any analytical method is usually indicated by its confidence interval - that is the range of values about the mean that includes a specified value of the standard deviation. This assumes that the distribution is Gaussian, i.e. of the form e^{-x^2} , the precise form being:

$$y = \frac{1}{\sigma\sqrt{2\pi}} e^{-\frac{1}{2}\left(\frac{x-\mu}{\sigma}\right)^2} \quad (49)$$

In order to test whether the obtained distribution range was actually Gaussian a probability net was set up. The values were classified into ten groups, according to diameter size and the percentage frequency for each group was calculated. A graph known

as the probability net was drawn where the y-axis was the Gaussian distribution, equal to equation 49, exponentially distributed and the x-axis was the classification. A straight line indicated a Gaussian distribution, with an average value at $y=50$. A standard deviation could be got from the graph by obtaining x values where y is equal to 15.9 and 84.1, subtracting one from the other and dividing by two. (The values 15.9 and 84.1 are the turning points of the integrated Gaussian curve⁵⁰). Substituting these values into the above Gaussian function, provides a value for y for every given x, i.e. it is now possible to draw the typical bell-shaped Gaussian curve for any given set of experiments. All experiments obtained results that proved to be Gaussian (see Appendix 2 for examples).

It is useful to depict the foaming process statistically and informatively in one diagram. When this is done in the normal way, i.e. the absolute frequency divided into diameter size classes, the overview is unclear, giving no real information; a narrow tall peak in the initial stages flattening out to a broad spread by the end. If we take a growth factor into account it is possible to produce graphs giving more information.

Assuming that the nucleation process has finished by start time (in these processes at 60s) and that all nuclei present grow at the same rate up until rise time (200s). Using the ocular lens with concentric circles the area growth of the sample can be followed. The area of observation (a) remains the same at set magnifications [$M_t = 4 \times 10^5$ (i.e. $1\text{cm} = 1\mu\text{m}$); $a = 3.16 \times 10^{-7}\text{m}^2$] and a growth factor f_{gr} from 60s to 200s can be calculated as follows:

$$\frac{a}{A_{60}} = \frac{a}{A_{200}} \Rightarrow \frac{A_{200}}{A_{60}} = f_{gr} \quad (50)$$

where, A_{60} and A_{200} are the sample area at 60s and 200s respectively.

Continuing the assumption that all nuclei grow unhindered, we would therefore expect an overlapping of the distribution at 200s and that of at 60s multiplied by f_{gr} . This, however, does not happen due to several destabilising factors including phenomena such as coalescence and disproportionation of gas bubbles. Therefore, this growth factor approach can also be used as a measure of the amount of coalescence or the instability of a given foaming process.

2.7.7.2. Reproducibility

Having developed the method (i.e. stirring of 5g of A- and B-components in a ratio of 40:60 in a beaker for 7s; from this mixture a sample is placed on a microscope slide which is quickly positioned under the microscope, during which time photomicrographs are taken at set intervals) and obtained results (based on an average of 10 analyses/runs per experiment) for the A-component A(I/i), the reproducibility of the method was tested by repeating in full the experiment under the same conditions using the same system A(I/i). Both the average nucleus diameter results (Fig. 2-23) and the nucleation number result (Fig. 2-24) correlated well, lying well within their standard deviations, the standard deviations of the average nucleus diameter for the first and second trial being $8.84\mu\text{m}$ and $7.98\mu\text{m}$ respectively. Therefore, the method was accepted as viable.

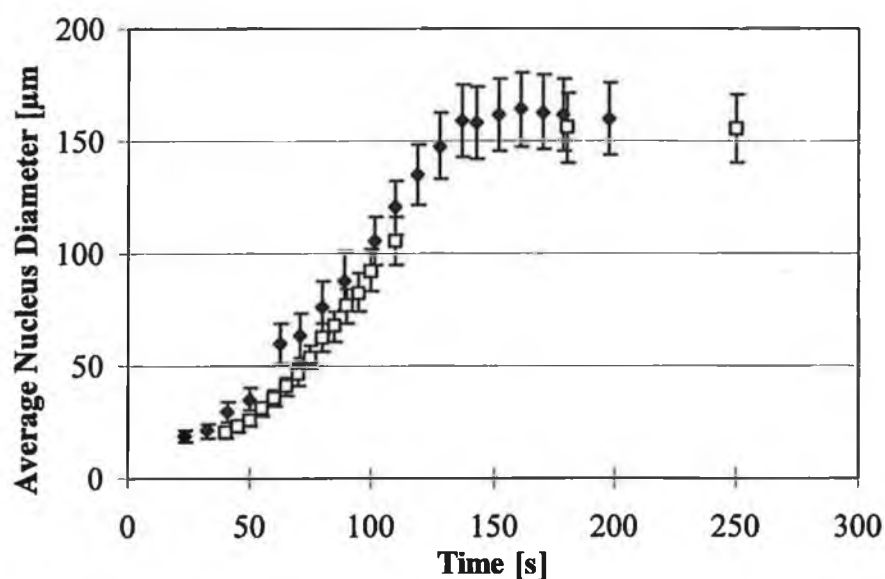


Fig. 2-23: The results of two separate independent experiments, each the average nucleus diameter obtained from an average of ten repeat analyses of the foaming of A(I/i) under the usual conditions.

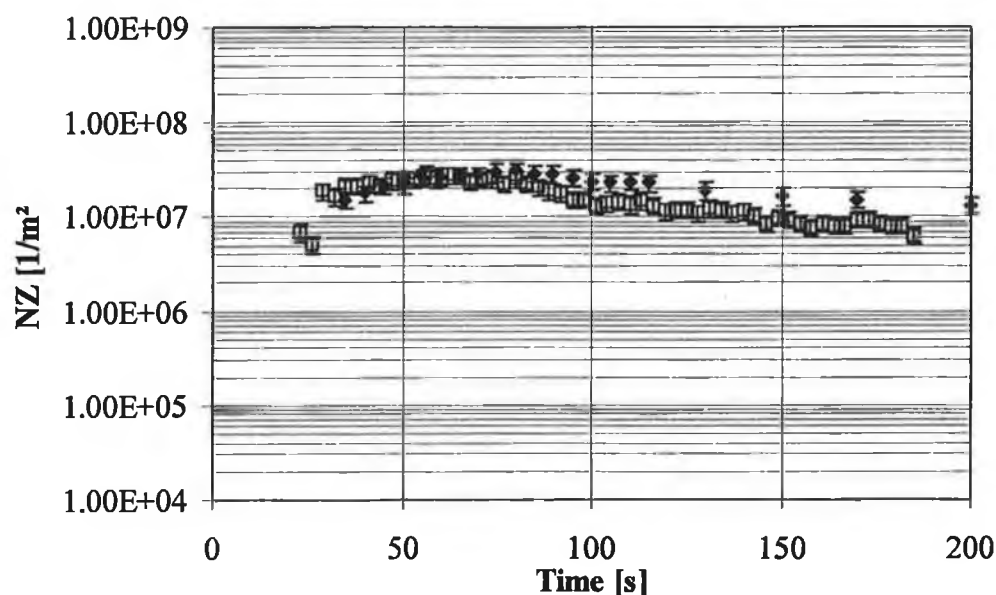


Fig. 2-24: The results of two separate independent experiments each nucleation number being an average of ten repeat analyses.

Table 2-2: Ranges of significant difference.

	Before Cream Time	Cream Time – Gel Time	After Gel Time
Nucleus Diameter [μm]	$\pm 5\mu\text{m}$	$\pm 10\mu\text{m}$	$\pm 20\mu\text{m}$
Nucleation Number [1/g]	$\pm 20\%$		

We can say that the cell size is reproducible when the cell size before cream time is $\pm 5\mu\text{m}$, between cream time and gel time $\pm 10\mu\text{m}$ and after gel time $\pm 20\mu\text{m}$. In other words outside these values the results are “significantly different”. Likewise, we can say that nucleation numbers outside, for example $1.0(\pm 0.02) \times 10^7$ are significantly different. These “significantly different” ranges are summarised in Table 2-2 above. In other words, we can say that above the positive range of deviation more nuclei exist and beneath the negative range of deviation less nuclei exist.

2.8. In-Situ Microscopic Analysis – Part 2 – A Study of the Nucleation Process

For the systematic analysis of the nucleation and foaming process of polyurethane foam the effect of the various blowing agents, surfactant, catalyst, fillers etc have been investigated microscopically. These experiments are described below. For each system photomicrographs were taken at 3s intervals. These photomicrographs were subsequently analysed with respect to the number of nuclei / bubbles per area and the average diameter of these nuclei / bubbles at a given time. The number of nuclei / bubbles and their diameters were measured manually and averaged with the aid of the previously described imaging system (section 2.7.4.2.).

2.8.1. Influence of Gas Concentration on the Nucleation Process

The influence of the initial gas concentration on the rate of nucleation was more closely studied by comparing experiments conducted using the model A-component A(I/i) untreated, degassed and containing excess air. Placing it under pressure (0.8mbar) for 3 hours degassed the A-component. The system was saturated with moist air by flushing the A-component with air for 3 hours. This was considered a sufficient amount of time for saturation while also avoiding the possibility of flushing the blowing agent (H_2O) out which would prevent foaming. The treated A-components A(I/i) were mixed with the B-component M20A in a ratio of 40:60. From the mixture a sample was taken, placed on a microscope slide between two cover slips, a third cover slip being placed on top of the sample and quickly placed under the microscope for analysis. Photomicrographs automatically taken at set intervals enabled the subsequent analysis of the nucleation process. This is the experimental process carried out for all analyses.

In order to establish the effect of the concentration of the blowing agent cyclopentane in the A-component B(I/i) the amount of cyclopentane added to the A-component was varied. The A-components containing 0%, 10% and 20% cyclopentane were mixed with the B-component (M20A), foamed and analysed as previously described.

2.8.2. Effect of Blowing Agent on the Nucleation Process

As already previously discussed (section 1.4.3.) foaming can be chemically or physically induced. The reaction of isocyanate with water produces CO₂, a chemical blowing agent. Two further systems with different physical blowing agents were analysed. These blowing agents were cyclopentane (Bp. 49°C at 1mbar) (B(I/i)) and perfluorohexane (Bp.54-55°C at 1mbar) (C(VI/i)), which are converted to gas by the heat of the exothermic reaction of foaming. Cyclopentane was a drop-in replacement of water in the model system A(I/i). An emulsifier, which is required when using fluorinated compounds had to be added to perfluorohexane-blown system. For a more detailed explanation of the formulations of the A-components A(I/i), B(I/i) and C(VI/i) check Appendix 1.

Table 2-3: Characteristic foaming times of the model systems with various blowing agents.

	Blowing Agent	Cream Time [s]	Gel Time [s]	Core Density [g/l]
A (I/i)	Carbon dioxide	62 ± 5	218 ± 10	55.6 ± 1
B (I/i)	Cyclopentane	60 ± 5	202 ± 10	56.0 ± 1
C (I/i)	Perfluorohexane	64 ± 5	220 ± 10	54.0 ± 1

The formulation of the A-component A(I/i) including polyols blowing agent, catalyst, surfactant as described in section 2.1. was premixed. Cream times and gel times as shown in Table 2-3 were set to coincide by varying the catalyst amount. The densities of the end foams were also equal. Each system was analysed with (1%) and without surfactant.

The A-component was then added to the B-component M20A in a ratio of 40:60 and subsequently mixed for 7s. The macro for the imaging system coupled to the microscope was started simultaneously to the mixing., enabling the automatic shooting and saving of photomicrographs during the process. After mixing, a sample was taken from the mixture placed on a microscopic slide as depicted in Fig. 2-14 and placed under the microscope in a matter of seconds. The nucleation and foaming process were followed microscopically and the nucleation number and average nuclei diameter per ten analyses were calculated

as previously described (section 2.7.5). This is the process that was carried out for all experiments, varying either the A-components or B-components formulation.

2.8.3. Effect of Surfactant Amount on the Nucleation Process

The amount of surfactant I in the A-component B(I/i) was varied from 0% to 2%. The modified A-components were foamed with M20A as the B-component under microscope using the method described in the previous section and the nucleation number and bubble diameter analysed as already described.

2.8.4. Effect of Surfactant Type on the Nucleation Process

Table 2-4: A preview of the structure of the various surfactants used; m and n are the siloxane blocks of the backbone, m being the siloxane block containing the polyol sidechain. x and y are the ethylene oxide and propylene oxide parts of the sidechain m. Values given are absolute values.

Surfactant No.	Silicone backbone			Side chain	
	n	m	%SiH	x	y
I	39	5	9.33	13	6
II	53	7	9.70	26	15
III	26	5	13.10	20	9
IV	10	4	18.90	29	1
V	9	3	17.20	47	3

The surfactants used were commercial surfactants which are marketed under code names. Therefore, as their structures were not known, all surfactants were structurally analysed (see section 2.12.) the results of which are partially shown in Table 2-4 above. They are all silicone block copolymer surfactants of type (24) shown in Fig.1-11. A more detailed description of the formulations is found in Appendix 3. The type of surfactant in system B(I/i) was varied with a constant concentration of 1%. The new A-components B(II/i), B(III/i), B(IV/i) and B(V/i) were foamed under microscope using the method developed and the nucleation number and nucleus diameter analysed in the usual manner.

2.8.5. Effect of Catalyst Amount on the Nucleation Process

The amount of catalyst i (dimethyl cyclohexylamine) in the A-component B(I/i) was varied, reducing the cream time. The aim was to determine whether the fact that foams with more catalyst had finer cells, was due to the decrease in time for coalescence to occur due to the faster reaction time or whether the catalyst itself had an effect on nucleation and consequently foam and morphology formation. The modified A-components were foamed with M20A as the B-component under the microscope using the method developed and the nucleation number and nucleus diameter analysed as already described.

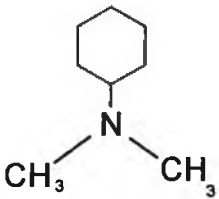

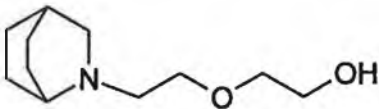
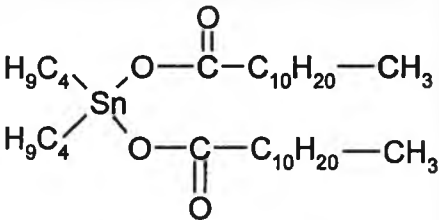
2.8.6. Effect of Catalyst Type on the Nucleation Process

The type of catalyst in A-component B(I/i) was varied, concentration remaining constant. The new systems were known as follows (see Appendix 1 for a more detailed description):

A-Component	Catalyst
B(I/i) -	Dimethyl-cyclohexylamine
B(I/ii) -	2,2,2-Diaza-bicyclo-octane
B(I/iii) -	2-(2-Hydroxy-ethoxy-ethyl)-2-azanorbornan
B(I/iv) -	Dibutyltin dilaurate

The A-components were foamed with the B-component M20A under the microscope using the method developed and the nucleation number and nucleus diameter analysed using the developed method.

Table 2-5: Chemical structure and formula of the various catalysts used.

Catalyst	Name	Chemical Structure	Formula
I	Dimethyl - cyclohexylamine		$C_8H_{17}N$ 127g/mol
ii	2,2,2-Diaza- bicyclooctane		$C_6H_{12}N_2$ 112g/mol
iii	2-(2-Hydroxy ethoxy-ethyl) 2-azanorbornane		$C_{11}H_{21}O_2N$ 199g/mol
iv	Dibutyltin dilaurate		$C_{32}H_{64}O_4Sn$ 630.7g/mol

2.8.7. Effect of Emulsifier on the Nucleation Process

In the A-component C(VI/i), the perfluorohexane blown foam, an emulsifier of the type $(C_8F_{17}SO_2)N(C_2H_4OH)(C_2H_5)$, is used. The effect of this emulsifier was observed by analysing foaming with the A-component C(VI/i) with the B-component, where C(VI/i) contains no emulsifier. The experiment was repeated using the A-component C(VI/i) containing emulsifier and the results obtained compared.

2.8.8. Effect of Prepolymer on the Nucleation Process

Up till now the B-component, M20A, has remained constant. Here the effect of the B-component on the nucleation process is analysed. This is done by means of prepolymers. As already stated prepolymers are a prereacted product formed by reacting polyol(s) or water with diisocyanate(s). The materials normally contain residual free isocyanates groups for further reaction with more polyol(s) or water to produce the final polymer. Prepolymers are not usually used in rigid foam as they retard curing. However, if one was to improve the compatibility (by decreasing the percentage free NCO groups) between A- and B-components, what influence would that have on the nucleation process?

To test this, three prepolymers were produced by reacting 100g of the B-component with 2g, 4g and 6g of methanol respectively at 70°C for 3 hours. After cooling, the prepolymers were reacted with the model A-component B(I/i) and systematically analysed using the developed method.

2.8.9. Influence of a Filler on the Nucleation Process

If solid particles are in the system, heterogeneous nucleation will occur⁵⁴. In order to see the effect of micro particles on the nucleation process, 1% carbon and 1% latex (in an aqueous solution) were added to A-components B(I/i). With the aid of a Coulter LS Particle Size Analyser, using distilled H₂O as the solute, the particle sizes of the carbon and the latex was measured proving to have average particle sizes of 7.0µm and 0.3µm respectively. After foaming under the microscope, the number and size of the nuclei for each system were measured in the usual manner.

2.8.10. Open-Celled Polyurethane Foam

Rigid polyurethane (PU) foam can either be closed-celled or open-celled⁵⁵ (section 1.7.3.). Until now we have been analysing the nucleation of closed-celled PU foam. In this experiment it was hoped to analyse the nucleation of open-celled PU foam with particular emphasis on the observation of the cell-opening process. For this purpose, a model A-component (Codename: DB006), which produces opened-cell rigid foam, was foamed with the B-component M20A and analysed in the usual manner. Results are given in Appendix 6.

2.9. Measurement of End Cell Diameter

Using the standard test method for measuring the cell size of rigid cellular plastics (ASTM D3576 - 77) the average cell diameter on the finished foam was measured. This method involves cutting the foam into a 5cm x 5cm-specimen sample using a microtome. A grey dye is then sprayed on the sample enabling imaging of the otherwise opaque cells with the aid of a stereo zoom microscope (Olympus SZH). The images were printed using a Sony Video Graphic Printer UP-860. The average chord length was obtained by counting the cells or cell wall intersections and averaging this value to an average cell diameter using the following equation:

$$d = \frac{t}{(0.785)^2} \quad (51)$$

where d is the cell size and t is the average cell chord length, which is got by dividing the length of the line of counting by the number of cells counted. This was automatically carried out using a PC coupled to a Calcomp Drawing Board™. A maximum of 250 cells was measured in order to obtain a statistically acceptable diameter average.

2.10. Calculation of Nucleation Number (NZ_{cal})

It is possible to estimate the number of nuclei (NZ_{cal}) present at the start of foam growth by using the value of the cell size of the finished foam. The cell sizes of finished foam samples were measured according to the method previously described.

Assuming that the cell is spherical the cell volume (V_z) can be calculated:

$$V_z = \frac{4}{3}\pi r^3 \quad (\mu m^3) \quad (52)$$

where r is the cell radius. The volume of gas (V_g) is calculated using the following equation, whereby the volume of the polymer matrix (1ml/1g) is subtracted from the foam's total volume (V_f):

$$V_g = \left(\frac{1000}{V_f} - 1 \right) \times 10^{12} \quad (\mu m^3) \quad (53)$$

The maximum of nuclei required to contain this volume (V_g) of gas is considered as the nucleation number (NZ) per gram and is obtained simply in the following manner:

$$NZ_{cal} [1/g] = \frac{V_g}{V_z} \quad (54)$$

In this way the experimental values can be compared to predicted values of the nucleation number. Therefore, it is possible to both measure and estimate the amount of nuclei per gram of foam. This equation is also useful in understanding that it is possible for foams with a higher core density to have smaller cells, but the same number of nuclei. When measuring the cell diameter values these have a standard deviation of circa. $\pm 50\mu m$, this consequently results in a standard deviation of $\pm 0.2 \times 10^5 [1/g]$ for calculated nucleation numbers.

2.11. Surface Tension^{56,31,32}

The surface tensions of various A-components were measured using three different methods:

The Lecomte du Noüy tensiometer - ring method ⁵⁶	(detachment method)
The pendant drop method ³¹	(detachment method)
Maximum bubble pressure method ³¹	(dynamic method)

2.11.1. The Lecomte du Noüy Tensiometer - Ring Method⁵⁶

In order to examine the surface tension between a liquid and vapour phase, a Lauda Tensiometer TE1C/3 coupled to a SAE / KM5 Epson HC 20 data handler was used. This is based on the ring method (DIN 53 914-80). In this method the force required to detach a ring from the surface is measured by using a torsion wire arrangement. The detachment force is related to the surface tension, δ , by the expression

$$\delta = \frac{\beta F^+}{4\pi R} \quad [\text{mN/m}] \quad (55)$$

where F^+ is the pull on the ring, R is the mean radius of the ring and β is a correction factor.

The instrument was calibrated using chromatographic H_2O ($\delta = 72 \text{ mN/m}$ at 20°C). To ensure a zero contact angle the platinum ring was carefully cleaned by flaming. It is essential that the ring lie flat in a quiescent surface. The polyol sample was pre-treated by heating to 23°C for two hours. 250ml of the sample to be measured was placed in a beaker and heated to 25°C . The ring was automatically lowered, immersed in the sample, drawn out of the sample and a surface tension value obtained as described in Fig.2-25. Initial experiments were carried out on CO_2 blown model system A(I/i) with varying surfactant amounts. All experiments were carried out at 25°C .

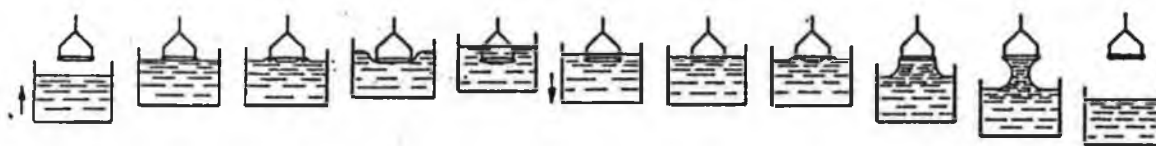


Fig. 2-25: *The du Noüy ring method:- the ring is held at a constant height and the sample container is slowly moved upwards against the ring, initially pushing the sample surface inwards and eventually immersing the ring in the sample. At this point the sample changes direction. The ring slowly pulls the surface of the sample, just before contact breaks the value is taken.*

In order to see whether the results correctly related to the activity of the surfactant in the bulk, i.e. to see whether it was possible, using this method, for the surfactant to reach the surface, a second method was considered - the pendant drop method.

2.11.2. The Pendant Drop Method³¹

Samples were sent to BASF AG Ludwigshafen (ZKM/D), Germany, where their surface tension was measured using the pendant drop method. The device which is depicted in Fig. 2-26 consisted of a light source to illuminate the drop, which hangs from a needle containing 10ml of the sample, and a camera linked to an image processor. The drop profile is transformed into a digitised image. A computed fit between a theoretical drop profile and the measured profile is done in order to obtain the surface tension. All measurements were carried out at 25°C.

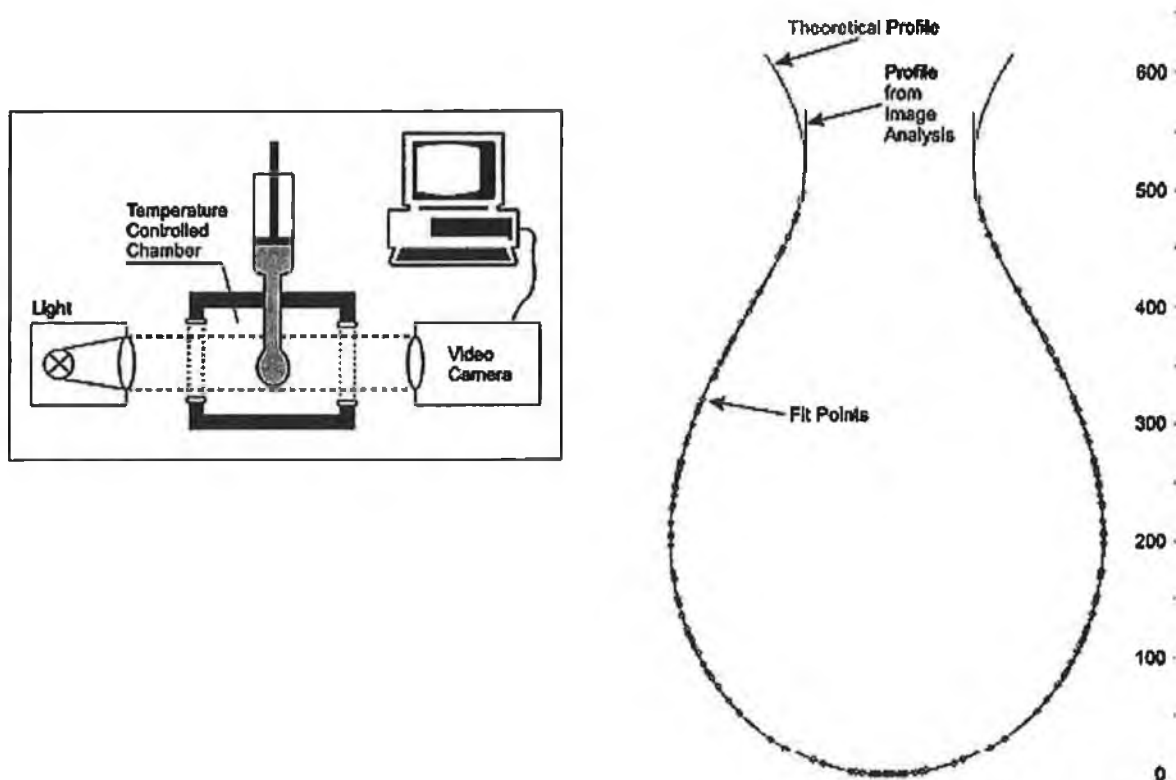


Fig. 2-26: The pendant drop method. Left: the standard apparatus used for the pendant drop method. Right: the standard shape of a pendant drop.

If we consider this method as the liquid interface being blown or expanding into the gas interface, then we can consider it as a "photographic negative" or the reverse of the foaming process, where the gas phase is blown or expanded into the liquid phase. Keeping this in mind, a third method was tried.

2.11.3. The Maximum Bubble Pressure Method³¹

The SITA-online f10, a mobile online-tensiometer for measuring the dynamic surface tension was used. Its principle of working is based on the maximum bubble pressure method. The pressure, which is needed for the bubble formation, according to the Young Laplace equation (Equation 25), is proportional to the surface tension.

Air bubbles were blown through a capillary tube into the 100ml of the sample liquid at a set frequency. The pressure was measured and the surface tension calculated. Parallel

to this the bubble frequency, bubble lifetime and the temperature, which remained constant at room temperature, were measured.

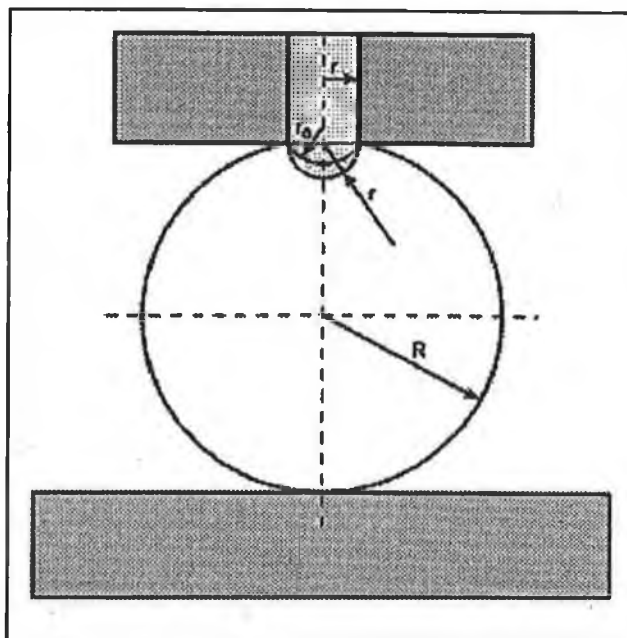


Fig. 2-27: The maximum bubble pressure tensiometer. When the bubble radius, R , has reached the capillary radius, r , a spherical bubble of constant volume is formed at the tip of the capillary, and the pressure inside increases to a maximum.

2.11.4. Surface Tension Measurements with a Cyclopentane Vapour Interface

An additional bubble cap (bell cap) was integrated into the apparatus for the du Noüy ring method (Fig. 2-25) in order to have the cyclopentane in the sample at equilibrium with its surroundings by creating a cyclopentane atmosphere directly above the sample. This is illustrated in Fig. 2-28. Again the ring was cleaned and the sample was pretreated by heating to 23°C for two hours. Cyclopentane vapour was produced by gently heating it to 49°C (the boiling point of cyclopentane at 1mbar is 49°C) and maintaining it at this temperature. Surface tension values were obtained as for the du Noüy ring method described in section 2.11.1.

The first objective of this experiment was the establishment of an adequate vaporisation time. This was done by measuring the surface tension of the sample at various time intervals during the promotion of cyclopentane vapour, at constant surface tension values the cyclopentane was assumed to be in equilibrium.

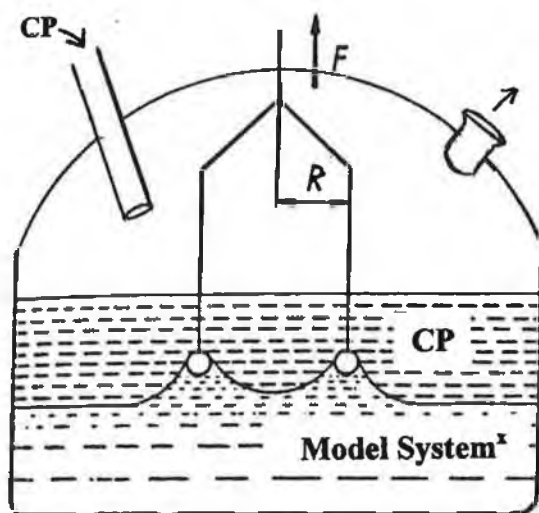


Fig. 2-28: A schematic representation of the apparatus used to measure δ of the model system in a cyclopentane atmosphere; x = model system with varying surfactant amounts; CP = cyclopentane, R = radius of the ring and F = force.

Once the vaporisation time was determined the loss of cyclopentane from the sample to the cyclopentane atmosphere were measured. For this purpose a sample containing 10 parts cyclopentane was weighed as was the amount of cyclopentane to be vaporised. After a time interval the sample and cyclopentane were weighed and the cyclopentane loss calculated and concluded to be insignificant.

Subsequently the surface tensions of the A-component B(I/i) containing 10 parts cyclopentane, without cyclopentane and with 30 parts cyclopentane, each containing various amounts of surfactants were measured. This was carried out under both air and cyclopentane atmosphere. All measurements were carried out at 25°C.

2.12. Surfactant Analysis

The surfactants implemented in the formulation of the A-components in this research are commercial silicone surfactants, of which the general structure is known. However, for a comprehensive analysis of the effect of these surfactants a detailed knowledge of the surfactants is necessary. Therefore, structural analysis using quantitative ^1H - and ^{29}Si -NMR spectroscopy was carried out. The hydrophilic/hydrophobic strength of the surfactants was also established.

2.12.1. Structural Analysis of Surfactants

All surfactants were structurally analysed in BASF AG Ludwigshafen, Germany, using quantitative ^1H - and ^{29}Si - NMR spectroscopy. Consequently it was possible to estimate the average length of the siloxane backbone, the number of side chains and the ethylene oxide: propylene oxide (EO:PO) ratio.

^{29}Si has a natural frequency of 4.7% and due to its gyromagnetic relationship it is approximately twice as sensitive as ^{13}C . However, the addition of a paramagnetic relaxation reagent is necessary as the relaxation time of ^{29}Si is comparatively long and the nuclear Overhauser effect (NOE) results in a reduced signal intensity. For this purpose chromacteyl acetone (ca. 0.05 - 0.1 Mol) was added to the sample's solvent of deuteriated CHCl_3 (CDCl_3).

The polymer surfactant was derivatised using trichloro-acetyl-isocyanate in order to differentiate between primary and secondary alcohol end groups.

2.12.2. Determination of the Turbidity Point of Surfactants⁵⁷

The hydrophilic / hydrophobic strength of a surfactant is measured by its turbidity point. The turbidity point of each surfactant was experimentally determined by dissolving the surfactant in a 4% aqueous solution. The clear solution was slowly heated until it turned turbid or cloudy. This temperature or turbidity point is characteristic of the surfactant and is reversible. Therefore, on cooling the turbidity point could be verified.

2.13. Vapour Pressure Measurements⁵⁸

To investigate the physical effect of the siloxane surfactant on the nucleation process the vapour pressure of model A-component A(I/i), however, with three times the amount of surfactant and without surfactant was measured in ZAT/D BASF Ludwigshafen AG, Germany.

100ml of the sample was placed in a pressurised cell. The cell was cooled to -80°C and subsequently evacuated to eliminate any air present. The sample was then heated to a given temperature, which was then held constant. The pressure increase was noted and the point where the sample began to vaporise, i.e. where the pressure remained constant, was noted as the equivalent pressure of vaporisation. This was repeated for various temperatures. The estimated experimental error lay below 1%.

2.14. CO₂ Solubility

The solubility of CO₂ was analysed with the aid of infra-red spectroscopy (Nicolet Impact 420 IR Spectrometer). Three A-components were measured; A(I/i), with and without surfactant and A(II/i) - with the intention of ascertaining the surfactant's influence on the solubility of the blowing agent, CO₂, and ultimately on the formation of nucleation sites.

The samples were placed in a 0.0525mm CaF₂ cuvette. Firstly, background IR spectra were obtained with untreated samples, paying particular attention to the CO₂ region. The samples were then treated by flushing with CO₂ for two hours after which time another IR spectra was taken of each sample. The samples were compared to their background spectra for an increase in CO₂ peaks.

The solubility CO₂ was also measured by ZAT/D in BASF Ludwigshafen AG, Germany using the method of the partial pressure of CO₂⁵⁸(see section 2.13). The sample, A(I/i), was placed in a pressurised glass cell which had a volume of 100cm³. It was maintained at a constant temperature of 25°C. CO₂ (M = 44.01g/mol, 99.9993% purity, Messer-Griesheim) was added step-wise to the sample and the pressure of the cell and the

gas cylinder was noted. The mass of soluble CO₂ in the liquid phase could be calculated from the fall in pressure in the gas-providing cylinder and the additional correction factor for the area of gas above the liquid phase. The method was repeated using the model system without surfactant.

3. Results

As discussed in the introduction to the development of the experimental methods (section 2.1.) the aim of this work is the analysis of the nucleation process with respect to the different components of the formulations, e.g. surfactants, catalysts, fillers etc. Due to the paucity in the literature of analyses of such a detailed nature, the results obtained from the experiments described in the previous chapter are fundamental in the understanding of the nucleation process of polyurethane rigid foam.

3.1. Foam Samples

The A-components nomenclature has been described in an earlier section (section 2.1.). Depending on the experiment, the appropriate A-component A(I/i) was mixed with the B-component which was an MDI-type polyisocyanate (M20A), with a free NCO content of 31.5%, at a ratio of approximately 40:60. In a 70g-paper cup mould, this resulted in the following characteristic times and density:

Cream time	≈	60s ± 10s
Gel time	≈	200s ± 10s
Rise time	≈	300s ± 10s
Density	≈	55g/l ± 1g/l

As already stated, this is considered a very slow system and is therefore suitable for in-situ analysis. The B-component remained M20A, except where otherwise stated.

3.2. Macroscale Analyses

Due to the lack of experimental data regarding the nucleation process of rigid polyurethane foam in the literature, a systematic exploration of foam formation and growth was carried out. In order to gain a better understanding of the dynamics of the foaming process it was decided to examine the formation of rigid form using the following methods:

- In-Situ FTIR spectroscopy
- Temperature and pressure analyses during foam formation
- Rheology (viscosity analysis)

Although admittedly, it is the microscopic behaviour of the foam that is of main interest in the study of the nucleation process, it is hoped that information on the macroscopic behaviour will help with the overall understanding of the process.

3.2.1. In-Situ FTIR Spectroscopy

The application of several spectroscopic techniques is popular in the analyses of foaming as they give a clear overview of the macroscopic behaviour of the developing process. Grünbauer et al^{59,60} applied dynamic mechanical spectroscopy (DMS) and on-line FTIR in their study of flexible foams. The formation of urethane, soluble urea and hydrogen - bonded urea species during the fast bulk copolymerisation has been studied using the adiabatic reaction method and forced-adiabatic, time-resolved FTIR spectroscopy.

In this work the conversion of the isocyanate functional groups during the foam formation of model system A(I/I) was monitored by in-situ infrared spectroscopy. The isocyanate band occurs at approximately $2300\text{--}2270\text{cm}^{-1}$ in the mid-infrared spectrum and the decay in intensity of this absorbance is used to monitor the reaction. Restricting the analysis to the carbonyl region of the spectrum, the formation of polyurea and polyurethane groups could be followed, along with the reduction of the isocyanate during the foaming process (see Fig. 3-2).

Between cream time (60s) and gel time (200s) a urea band develops at around 1660cm^{-1} as the foaming reaction proceeds. The formation of urea is at least a three-step process, its reaction scheme shown in Fig.3-1. The reaction of water with isocyanate (5) produces carbon dioxide and an amine. Further reaction of the amine with the isocyanate produces polyurea (12) via an unstable intermediate carbamic acid (27). After the gel time the broad bands between 1690cm^{-1} and 1710cm^{-1} develop. These are assigned to both free and hydrogen bonded urea and urethane linkages, respectively. Values obtained correlated well to values reported in the literature⁵⁹(see Table 3-1).

Table 3-1: Comparison of band assignments obtained to those in the literature⁵⁹

Group	Band Assignment, cm^{-1}	
	Obtained	Literature
Urea	1673	1660
Hydrogen bonded urea	1690 - 1700	1710
Urethane	1722	1730

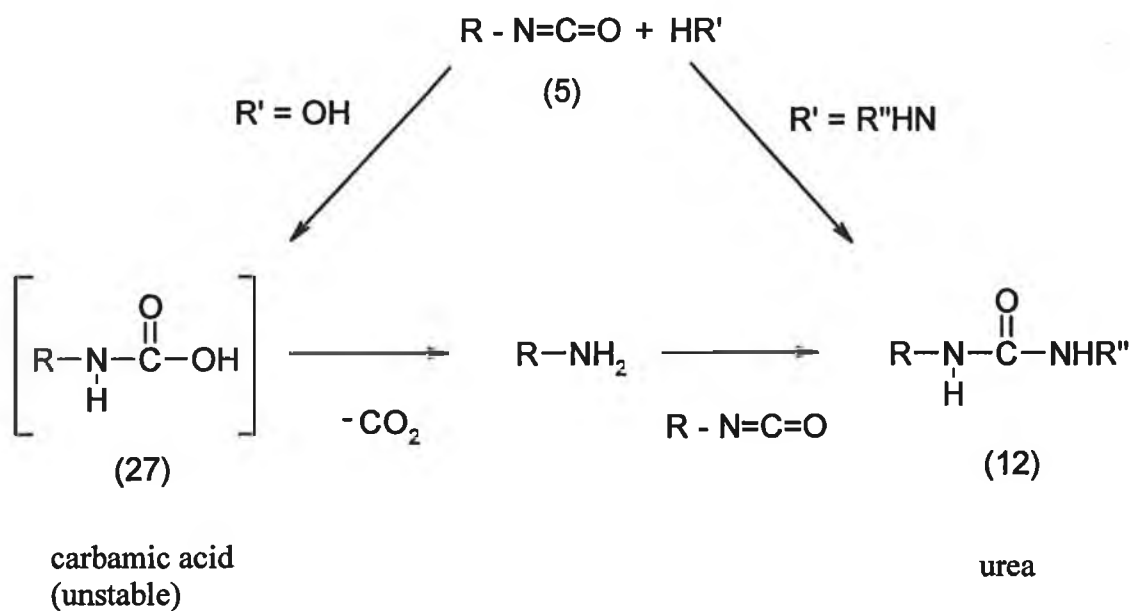


Fig. 3-1: Formation of urea; The reaction of water with isocyanate (5) produces carbon dioxide and an amine. Further reaction of the amine with the isocyanate produces polyurea (12) via an unstable intermediate carbamic acid (27).

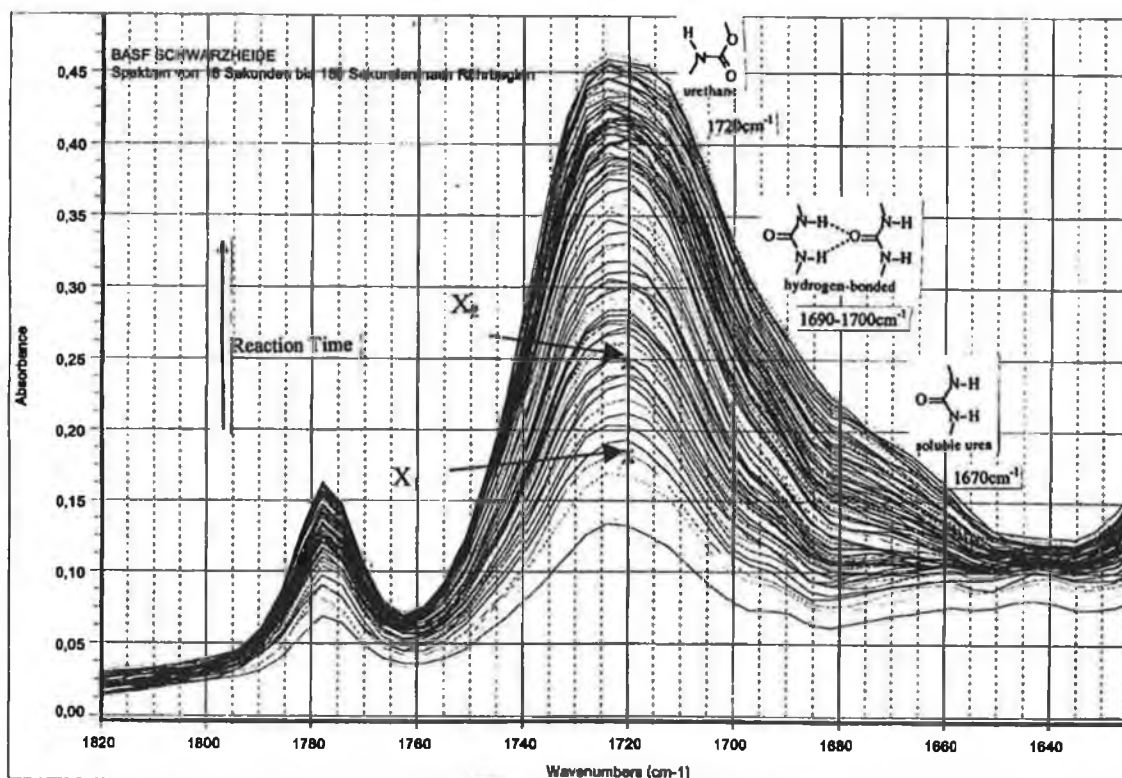


Fig. 3-2: In-situ IR analysis of polyurethane rigid foam; carbonyl region of the spectra. x_1 and x_2 indicate cream time of 60s and gel time of 200s respectively. The reduction in isocyanate is not indicated in this diagram.

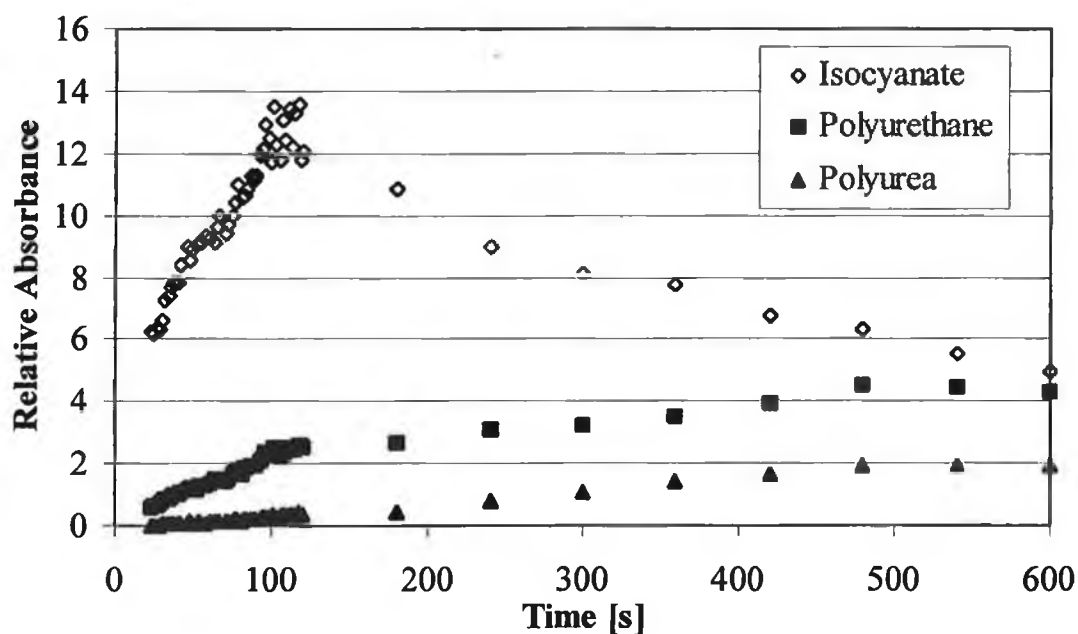


Fig. 3-3: Determination of the formation of polyureas (at 1673cm⁻¹) and polyurethanes (at 1722cm⁻¹) at the expense of the isocyanate (at 2300-2270 cm⁻¹) during formation of A(I/i).

By plotting the relative absorbances of the various groups against time (Fig. 3-3), a reduction in free isocyanate is demonstrated, while simultaneously an increase in polyurethane and polyurea concentration is observed. This is in agreement with the reaction equations already discussed. It should be noted that the apparent increase in isocyanate before 100s in Fig. 3-3 does not indicate isocyanate formation but is due to the rise of the foaming sample which initially touches and finally covers the sensor during the experiment.

In conclusion, urea formation is a dominant process during the initial stages of foam rise. This is then followed by the disappearance of the isocyanate due to its reaction with the polyol to form polyurethane. Little information could be gathered before 60s, the time of interest for nucleation studies and so no further studies were carried out using in-situ FTIR.

By plotting the relative absorbances of the various groups against time (Fig. 3-3), a reduction in free isocyanate is demonstrated, while simultaneously an increase in polyurethane and polyurea concentration is observed. This is in agreement with the reaction equations already discussed. It should be noted that the apparent increase in isocyanate before 100s in Fig. 3-3 does not indicate isocyanate formation but is due to the rise of the foaming sample which initially touches and finally covers the sensor during the experiment.

In conclusion, urea formation is a dominant process during the initial stages of foam rise. This is then followed by the disappearance of the isocyanate due to its reaction with the polyol to form polyurethane. Little information could be gathered before 60s, the time of interest for nucleation studies and so no further studies were carried out using in-situ FTIR.

3.2.2. Thermal and Pressure Analyses

Reaction temperatures affect both viscosity and reaction kinetics. An analysis of the reaction temperature during the foaming process was therefore carried out as described in section 2.3. Combining the results obtained when the thermocouple was 1cm and 5cm away from the base of the mould (to compensate for foam growth and the self-insulation effect caused by the growing foam), the reactions overall temperature profile was extracted. This is graphically presented for system A(I/i) in Fig. 3-4. There is no temperature change before the cream time of 60s. The temperature then increases gradually until the gel time where the temperature is approximately 50°C. Between gel time and rise time the temperature increases rapidly to 170°C. This is the reaction time, according to the FTIR analysis (Fig. 3-2), during which the polyurethane network is formed. The maximum temperature reached is 180°C. The foaming process is a highly exothermic. However, the temperature remains constant during the time of nucleation.

It is important to keep these reaction temperatures in mind when dealing with the nucleation process under controlled temperature conditions (see section 2.6.2.2.).

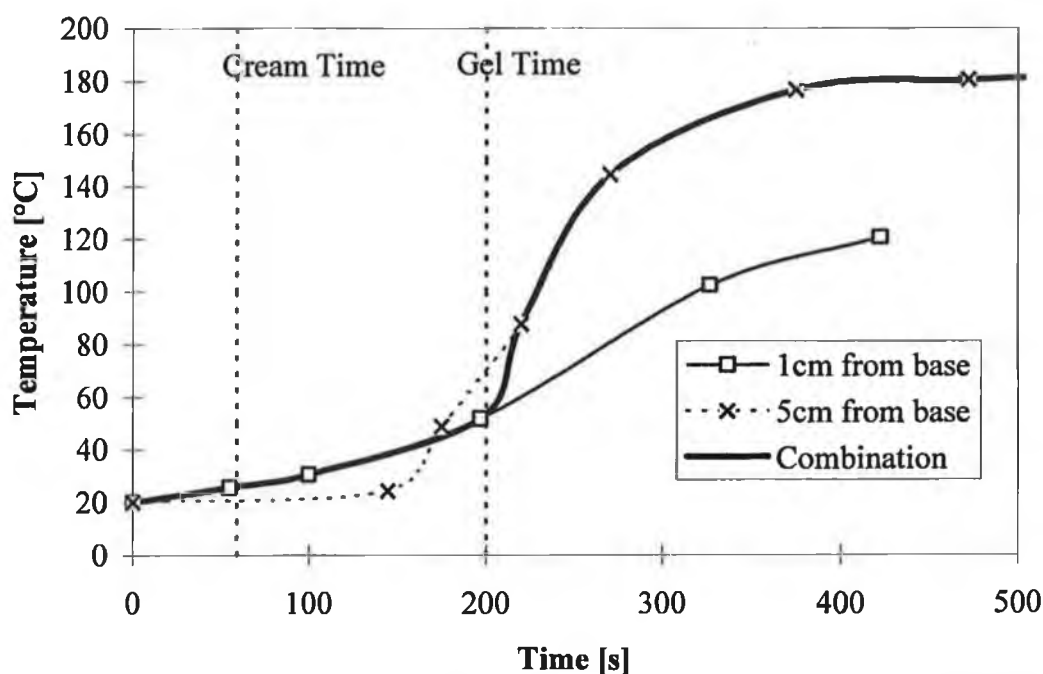


Fig. 3-4: The temperature measured during foaming of the A-component A(I/i) with the B-component M20A. Temperatures were measured with the thermocouple 1cm and 5cm from the base of the mould. Combining these results gave the overall temperature increase.

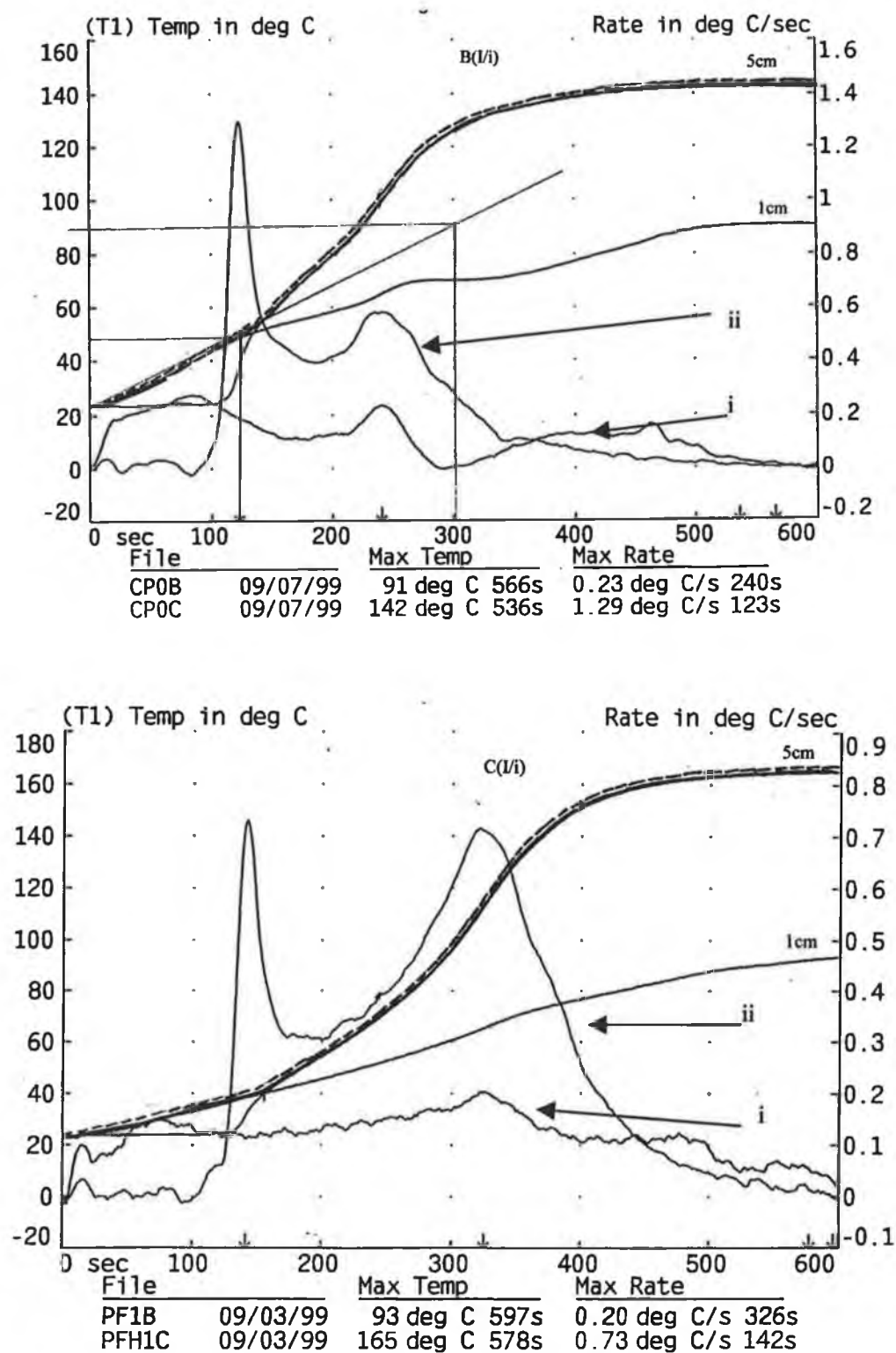


Fig. 3-5: Temperature analysis of the foaming system: Systems B(I/i) (top) and C(I/i) (bottom). — is a combination of the results obtained from 1cm and 5cm from the base (as in Fig. 3-4). The curves i and ii are derivatives of the curves for 1cm and 5cm.

Due to the presence of the physical blowing agents cyclopentane and perfluorohexane in the systems B(I/i) and C(VI/i) the temperature analysis has a different roll. Again, in each case the experiment was repeated with the thermocouple 1cm and 5cm away from the base. The blowing agent cyclopentane has a boiling point of 49°C and this point is reached at approximately 120s indicated by the maximum temperature rate of 1.29°C/s in Fig. 3-5 (top). The maximum heating rate of C(VI/i) in Fig. 3-5 (bottom) also indicates the boiling point of perfluorohexane of 54°C. The “blowing” action coupled to the isocyanate –hydroxyl reaction between gel time and rise time leads to foam formation and end temperatures of 140°C and 160°C for systems B(I/i) and C(VI/i) respectively. This is somewhat lower than the value for A(I7i) (180°C).

Table 3-2: Maximum temperature and pressure rates for the model systems with different blowing agents. Values obtained from Fig. 3-5 and Fig. 3-6.

System	Maximum Rates	
	Temperature [°C/s]	Pressure [psi/s]*
A(I/i)	1.01	0.0004
B(I/i)	1.29	0.0029
C(VI/i)	0.73	0.0002

*1 psi = 68.95mbar

Simultaneously a pressure analysis of the three model systems was carried out. In all cases the pressure increased well after the gel time had been reached as shown in Fig. 3-6. Maximum pressure rates are also given in the table above. This is a measure of the overall pressure of the system and does not reflect the microscale pressure differences which are created prior and during nucleation. Therefore, a more detailed evaluation of these results is not present in this work as it is not applicable to the time of interest, i.e. the period of nucleation .

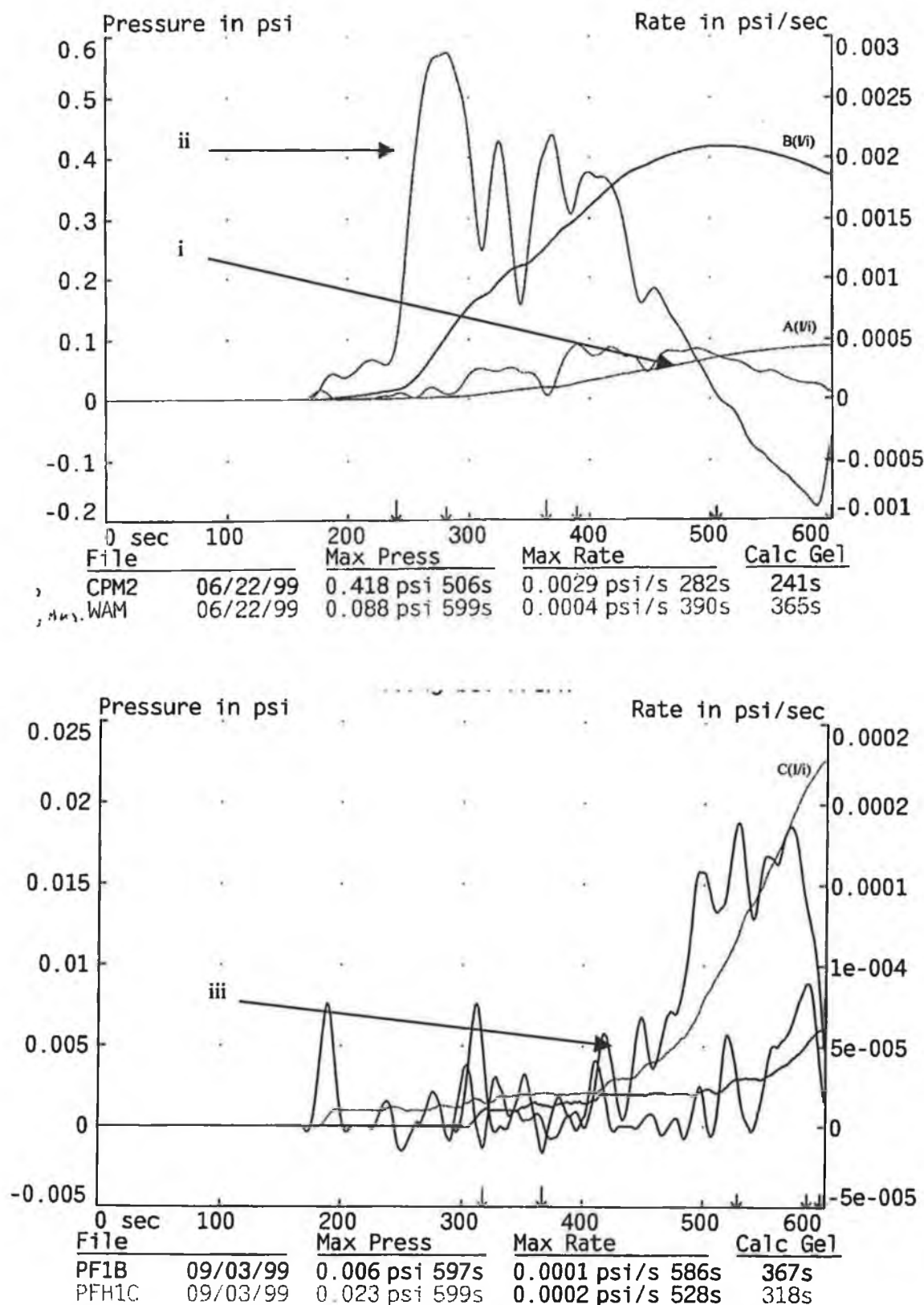


Fig. 3-6: A pressure analysis of the model systems A(I/i), B(I/i) (above) and C(VI/i) (below), i, ii and iii being their derivatives. Each system had a cream time of circa 60s and a gel time of circa 200s.

3.2.3. Dynamic Rheology

Rheology is accepted as a powerful tool in the study of reactive foaming systems^{61,62}. This involves the measurement of viscoelastic changes, the profile of which can help in the prediction of mould filling behaviour, when applied to rigid foaming systems. The foaming process involves a large volume increase (20 - 50 times) and it is, as already discussed, exothermic ($>100^{\circ}\text{C}$). The measurement probe must accommodate the foam expansion without changing the material and cope with the extremely fast curing time.

However, rheological studies in the literature are primarily based on polyurethane flexible foam^{60,63,64}. The gelling of the foam into a rigid polymer network causes difficulties in measuring the viscoelastic changes during foaming. Despite this, an attempt was made at establishing the apparent viscosity during foaming of a PU rigid foam. Another draw back in the method was that the sensing unit interacted mechanically with the growing foam resulting in a possible distortion of the rise profile.

The influence of the blowing agents CO_2 in A(I/i), C_5H_{10} in B(I/i) and C_6F_{14} in C(VI/i) on the viscosity of the system (Fig. 3-7), as was the influence of the surfactant type (Fig.3-8) and the compatibility of A- and B-components through the use of prepolymers (Fig. 3-9), was investigated. The viscosity of the A-components are given in Appendix 1.

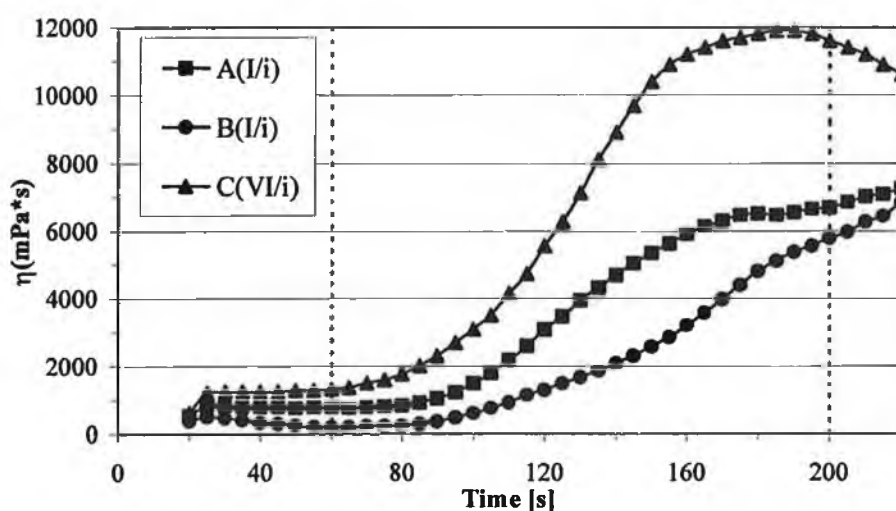


Fig. 3-7: Influence of the blowing agents A, B and C on the viscosity, η , of the foaming systems. Foaming carried out as described in section 2.4. (cream time $\approx 60\text{s}$, gel time $\approx 200\text{s}$ and density $\approx 55\text{g/l}$).

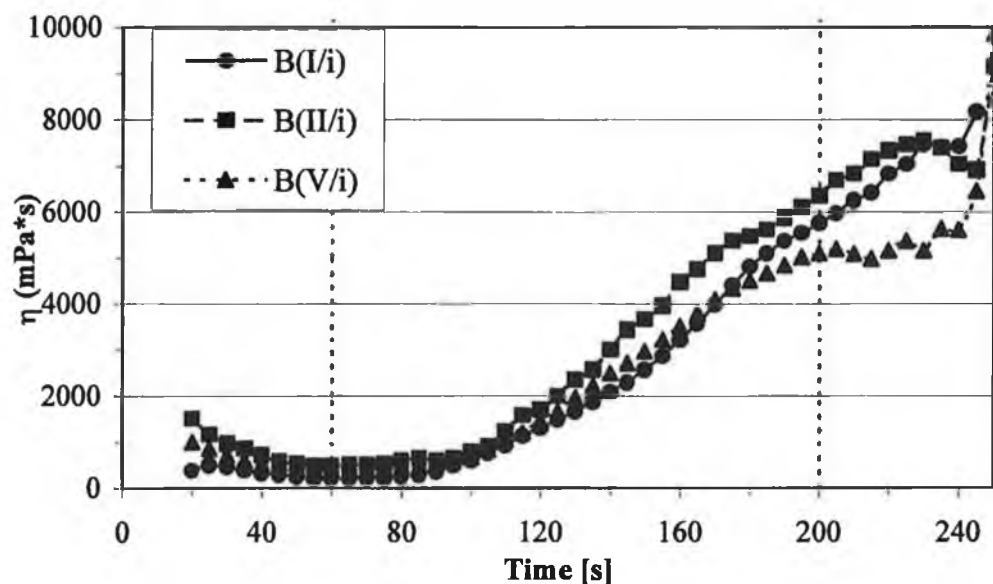


Fig. 3-8: Influence of surfactant type (I, II and V) on the viscosity, η , of the foaming systems. Foaming carried out as described in section 2.4. (Cream time ≈ 60 s, gel time ≈ 200 s and density ≈ 55 g/l)

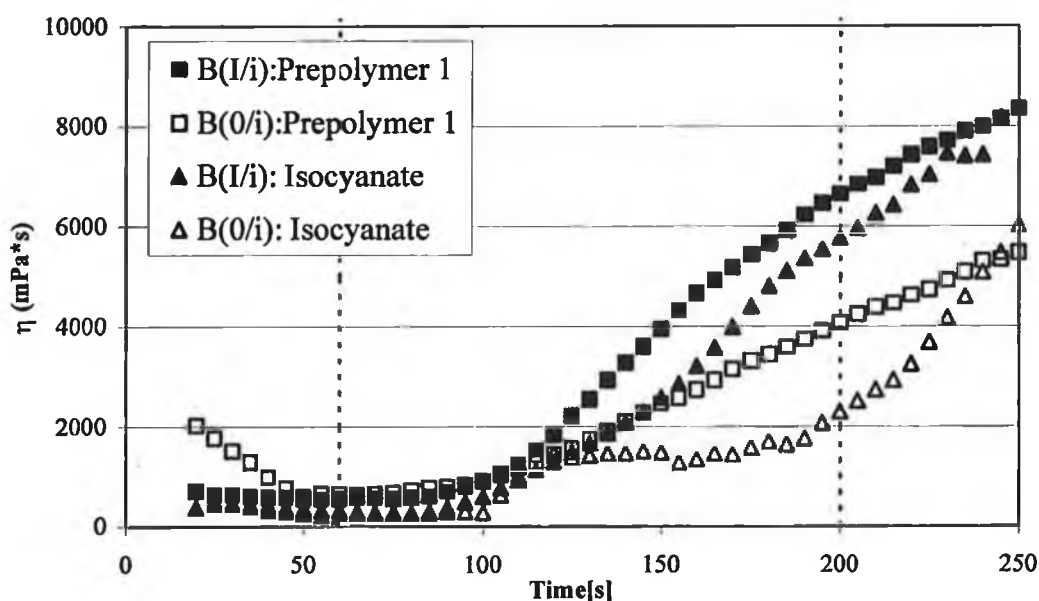


Fig. 3-9: Influence of prepolymers as the B-component on the viscosity, η . Foaming was carried out with the A-component B(I/i) containing 1% surfactant and without surfactant B(0/i) (cream time ≈ 60 s, gel time ≈ 200 s and density ≈ 55 g/l).

The in-situ viscosity measurements is an indication of the behaviour of the polymer matrix during foam formation. From the in-situ temperature measurements we know that the boiling point of C_5H_{10} ($49^{\circ}C$) in B(I/i) is reached at 120s at which point there is a marked increase in viscosity due to blowing. C_6F_{14} in C(VI/i) works on the same principle, reaching its boiling point at approximately the same time. However, as C_6F_{14} is in the system in the form of an emulsion this blowing agent has more nucleation sites. Hence, the extreme difference in viscosity. On the other hand, the chemical blowing agent CO_2 in A(I/i) has first to be formed and then evaporate in order to function as a blowing agent. It therefore has a different rate of viscosity, reaching however, approximately the same end viscosity.

Table 3-3: *The influence on the blowing agent on the viscosity, η at various foaming times. Values at 0s are the viscosities of the A-components, all other values obtained from Fig. 3-7.*

	η [mPa*s]			
Reaction Time:	at 0s	at 20s	at 60s	at 200s
A(I/i)	819	539	790	6690
B(I/i)	240	383	209	5780
C(VI/i)	967	620	1320	11600

The surfactant type influences the viscosity during the nucleation period, B(I/i) having the greatest value of the systems measured at 20s (see Table 3-4). The viscosity drops until cream time where the values lie closer together. The stabilising ability of the surfactants then takes over showing that the surfactant V deviates from the other stable systems, which have similar viscosity rates, indicating instability.

Table 3-4: *The effect of surfactant type on the viscosity during the nucleation period (20s), at cream time (60s) and gel time (200s). Values obtained from Fig. 3-8.*

	η [mPa*s]		
Reaction Time:	20s	60s	200s
B(I/i)	383	209	5780
B(II/i)	1510	488	6360
B(V/i)	999	441	5110

The implementation of a prepolymer increases the viscosity of the foaming system with surfactant from 383mPa·s to 720mPa·s at 20s. Fig. 3-9 show that the curve trends are similar. However, in the absence of surfactant, the system foamed with M20A shows its inability to foam while that foamed with the prepolymer proves to be more stable .

3.3. Positron Emission Tomography

Positron Emission Tomography analysis was carried out using the radiolabelled compounds [^{15}O]H₂O and [^{15}O]butanol according to the reactions schemes described in Fig. 2-22 and Fig. 2-23. However, due to the bad spatial resolution of the technique and the velocity of the foaming process Positron Emission Tomography was considered not to be suitable for the analysis of the nucleation process. A more detailed description of the results is given in the appendix (see Appendix 3).

3.4. Two-Coloured Dynamic Light Scattering

Ideally, nucleation should be instantaneous. However, in reality nucleation takes place over a short time span resulting in the formation and growth of nuclei of various sizes. During the two-coloured dynamic light scattering analysis this lack of instantaneous nucleation resulted in a complicated feed back. Therefore, two-coloured dynamic light scattering was also considered ineffective for our purposes. A more detailed description is given in Appendix 4.

Imaging using positron emission spectroscopy and two-colour dynamic light scattering, proved to be unsuccessful. This left the following microscopic method as the principal tool in the investigation of the nucleation process of polyurethane rigid foam in this research.

3.5. In-Situ Microscopic Analysis of Polyurethane Rigid Form

3.5.1. Initial Study: A- and B-Components

It is important to have a reference sample for all analysis and for this purpose A- and B- components were analysed separately. The unreacted A- components A(I/i), B(I/i) and C(VI/i) were submitted to the same treatment as when being foamed, i.e. mixed at 2400rpm for 7s in a beaker, from which a sample was taken with a spatula and placed on the microscopic slide. This was carried out without any isocyanate present. The aim was to estimate, by means of the number of bubbles formed, the maximum amount of nucleation sites possible. The experiment was repeated with the same model systems minus the surfactant.

This showed some remarkable results. The presence of a surfactant somewhat reduces the amount of possible nucleation sites (see Fig. 3-10) – however, not significantly - suggesting the surfactant has a tendency to inhibit nucleation. Popular theories^{9,10} would lead us to believe that the presence of a surfactant reduces the surface tension of the system allowing easier nucleation.

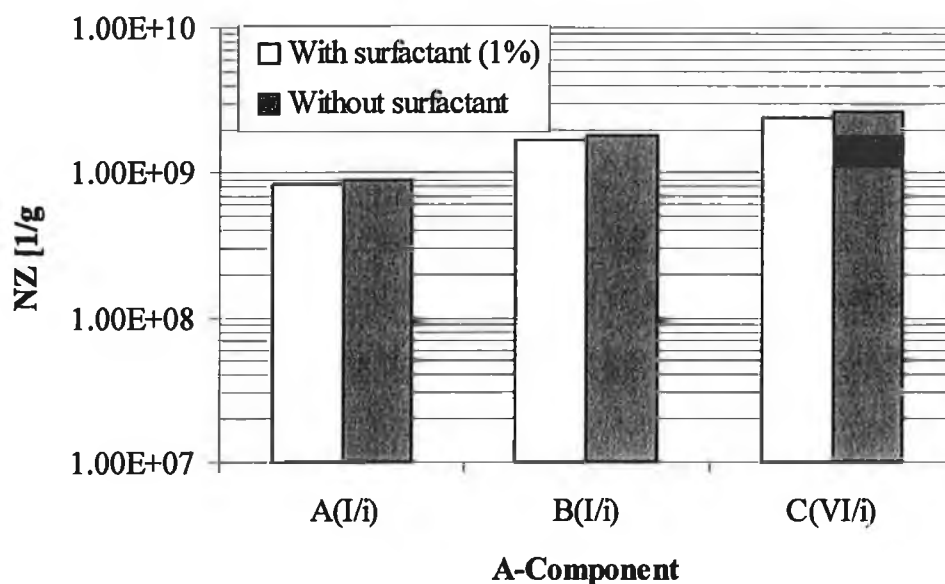


Fig. 3-10: The nucleation number (NZ) per gram of unreacted A-component with (1%) and without surfactant. Surprising is the slight decrease NZ with added surfactant.

These results concurred with the observation made by Kanner and Decker¹⁰, i.e. that the number of bubbles introduced by mixing is more than sufficient to account for the number of cells present in the final foam.

Table 3-5 below shows the observed nucleation number converted to nucleation number per gram for the systems mentioned, including also the percentage increase due to absence of surfactant. There is an increase in the number of possible nucleation sites when going from system A(I/i) to B(I/i) to C(VI/i) indicating either an increased potential in forming nucleation sites or a decrease in the potential to destroy these sites by mixing¹⁰. The former premise leads to an examination of the viscosities of the systems. The assumption that an decrease in viscosity would increase the mixing ability and result in more bubbles does not support these results. On the other hand, it is possible that bubbles once formed are unable to coalesce due the high viscosity and are subsequently stabilised. This could explain why the maximum nucleation sites of C(I/i) is greater than B(I/i) despite the viscosity of B(I/i) being lower than C(I/i). The latter hypothesis is quite probable inhibiting the destruction due to mixing, of bubbles (or nucleation sites). This is irrespective of the presence of a surfactant.

Table 3-5: *Experimental estimation of the maximum nucleation numbers (NZ) for the model A-components with surfactant (1%) and without surfactant, including the percentage difference between the two. The viscosity of the A-components are also given.*

	Viscosity [mPa*s]	NZ _{With} Surfactant [1/g]	NZ _{Without Surfactant} [1/g]	Difference [%]
A(I/i)	819	8.3×10^8	8.91×10^8	6.85%
B(I/i)	240	1.7×10^9	1.82×10^9	6.68%
C(VI/i)	1101	2.4×10^9	2.63×10^9	8.74%

Using the same method the B-component was analysed. Considerably less nucleation sites were formed suggesting that the A-component is primarily responsible for the formation of nucleation sites during the initial stages of foaming. The A-component is also more important as it contains the surfactant which stabilises the formed nuclei. There

Using the same method the B-component was analysed. Considerably less nucleation sites were formed suggesting that the A-component is primarily responsible for the formation of nucleation sites during the initial stages of foaming. The A-component is also more important as it contains the surfactant which stabilises the formed nuclei. There are no surfactants in the B-component. The photomicrographs following clearly show the difference between the number and type of bubbles formed, i.e. nucleation sites, in the two components. The A-component, irrespective of type, contains more and smaller bubbles than component B.

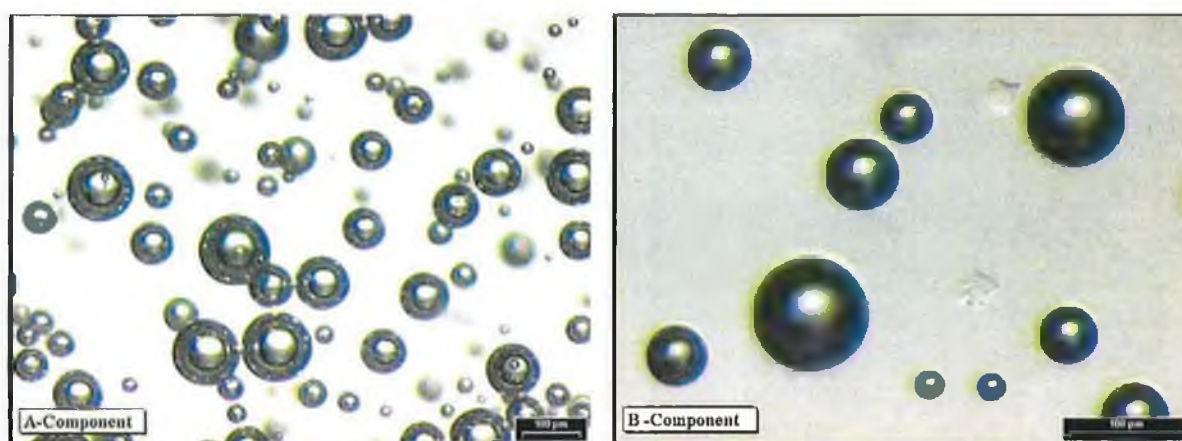


Fig. 3-11: Photomicrographs exhibiting the difference in the number and size of nucleation sites between unreacted A- (left) and B- components (right).

Another method in predicting the maximum number of nucleation sites is purely mathematical and suited for the ideal scenario. By assuming that each molecule of blowing agent when vaporised is a potential nucleation site, the maximum number of nucleation sites per gram can be calculated. An example of A(I/i) where $\text{H}_2\text{O} / \text{CO}_2$ is the blowing agent is detailed in Appendix 5. After taking the critical radius (see section 3.5.6.) into consideration a maximum number of nucleation sites of 1.3×10^{19} [1/g] was obtained. Experimentally less than 90% of the theoretical number of nuclei is observed. This is due to either the incapability of the method to visualise nuclei under $1\mu\text{m}$ or there is actually less than theoretically expected. Reasons for this will be discussed in the following sections.

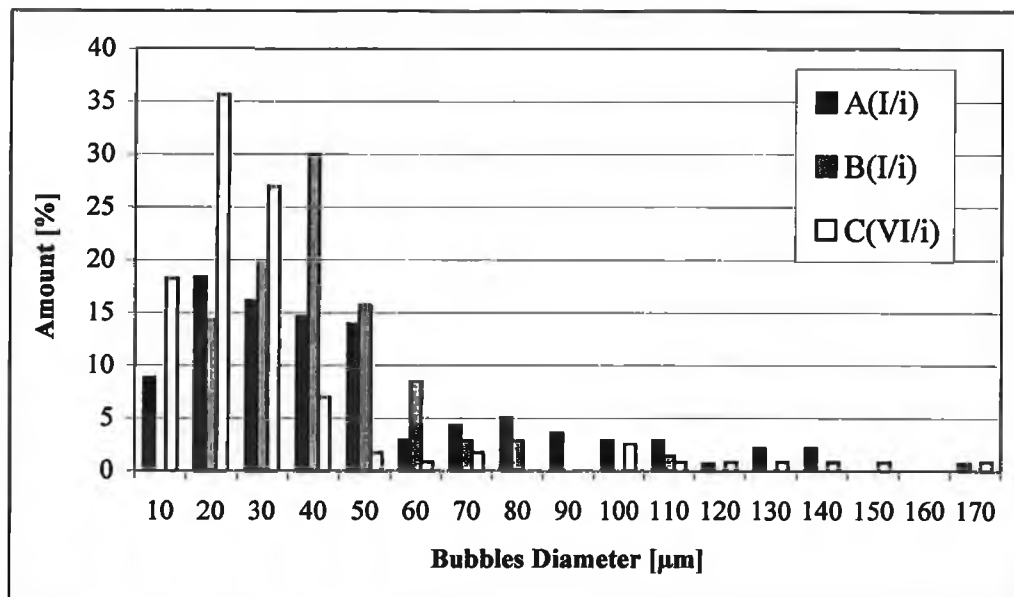


Fig. 3-12: Bubble size distribution for the three model A-components A(I/i), B(I/i) and C(VI/i) unreacted. Number of bubbles: $A(I/i) < B(I/i) < C(VI/i)$; size of bubbles: $A(I/i) > B(I/i) > C(VI/i)$.

Distribution curves (Fig. 3-12) obtained during the former method for the three A-components unreacted gave interesting predictions for the foam structures of the said systems. Average bubble size for A(I/i) was 29.16μm, smaller than that for B(I/i) (38.07μm). However, B(I/i) shows a narrower distribution which possibly under foaming conditions would lead to a more homogeneously structured foam. A-component C(VI/i) has a small average bubble diameter (27.44μm) and an even more narrow distribution than B(I/i) and A(I/i), predicting that C(VI/i) when foamed should have the finest cell structure of the three systems. These size distributions are also clear from the Gaussian distributions in Appendix 2 which are distributions of the nuclei size at the cream time of the foaming of the A-components A(I/i), B(I/i) and C(VI/i) with the B-component M20A. Here, as predicted, the amount of nuclei is greatest in the system foamed with the A-component C(VI/i). This system also has the smallest average nuclei diameter.

3.5.2. Influence of Gas Concentration on the Nucleation Process

With the intention of establishing the effect of the blowing agent concentration on the nucleation process the amount of blowing agent in the A-component was varied. For the A-component A(I/i) this was done by comparing the foaming of an untreated sample, to that of the foaming of a sample containing excess gas and to a third sample which was degassed (as described in section 2.8.1.). As can be seen from Fig. 3-13 and Fig. 3-14 the difference in both the amount of bubbles and the size of the bubbles with varying amounts of gas is negligible. This is initially surprising. One would expect to have fewer and smaller bubbles in the degassed system and an increase and larger bubbles in the system containing excess air⁶⁵. The degassed system does exhibit a tendency for smaller bubbles than the untreated model system. One could not completely exclude the inclusion of air introduced by mixing. However, all systems have nuclei of approximately the same size at circa 250s.

A different method was used for the analysis of the effect of the amount of blowing agent in system B(I/i) on the nucleation process. The blowing agent in this system is cyclopentane, which is volatile and therefore unsuitable for the previous method. In this case the systems was varied by altering the amount of blowing agent from 0%, 10% to 20% cyclopentane (CP). These new A-components were foamed with the B-component M20A and analysed under the microscope using the method described earlier. Distribution curves for the bubble diameters of the three systems shows that the presence of the blowing agent increases the average bubble size from 27.16 μ m (0% CP) to 38.98 μ m (10% CP). Increasing the amount of blowing agent to 20% CP does not however increase the average bubble size (37.98 μ m) but increases the percentage of such sized bubbles by 5% (see Fig. 3-23).

This is possibly due to the change in viscosity with added cyclopentane, decreasing from 743mPa*s (0% CP) to 206mPa*s (10% CP). This improves mixing, forming larger bubbles. It is also possible that due to the mixing of air bubbles the solubility of cyclopentane increases as the vapour pressure point, the point at which cyclopentane no longer dissolves, takes longer to obtain. Increasing the amount of blowing agent to 20% does not however comparatively increase the bubble size as the viscosity decrease to 159mPa*s is not significant.

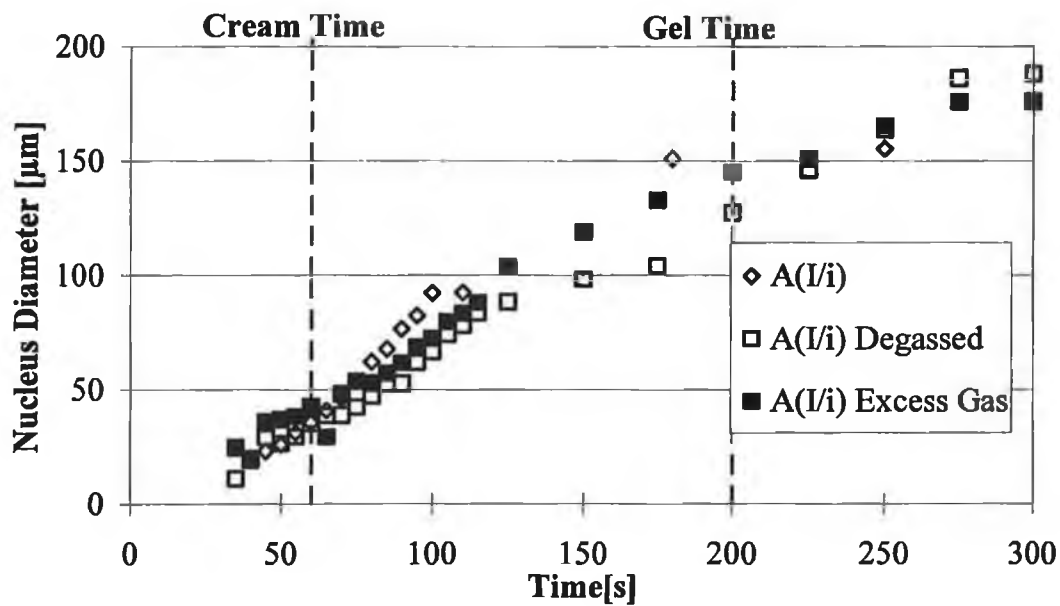


Fig. 3-13: Influence of blowing agent concentration on the nuclei size during foaming of the B-component (M20A) with the model A-components A(I/i) untreated, degassed and containing excess air, under conditions described in section 2.8.1.

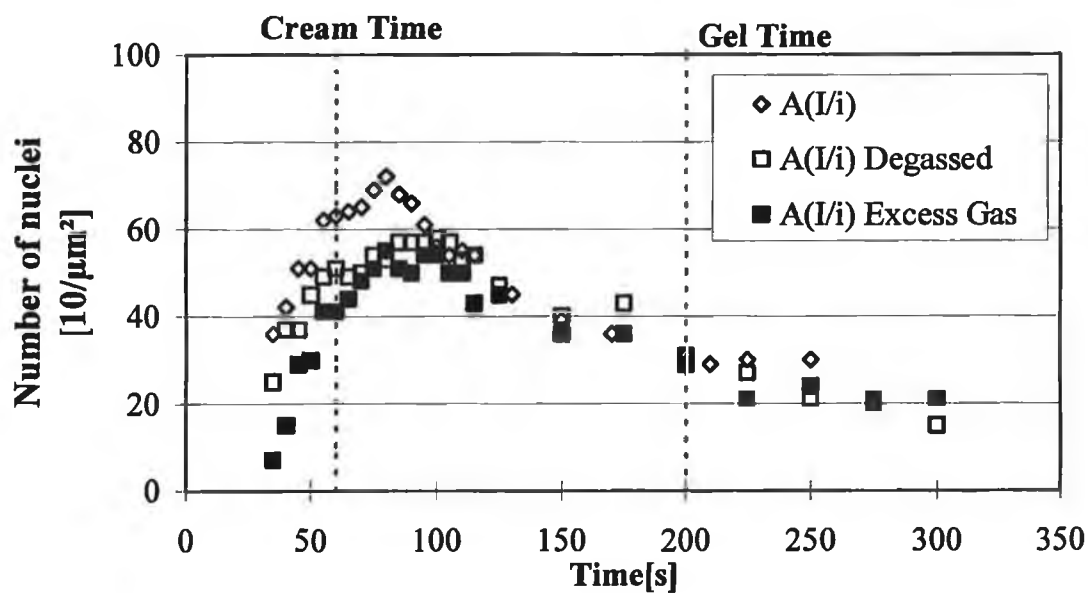


Fig. 3-14: Influence of blowing agent concentration on the number of nuclei per analysed area using the same criteria as in the diagram above.

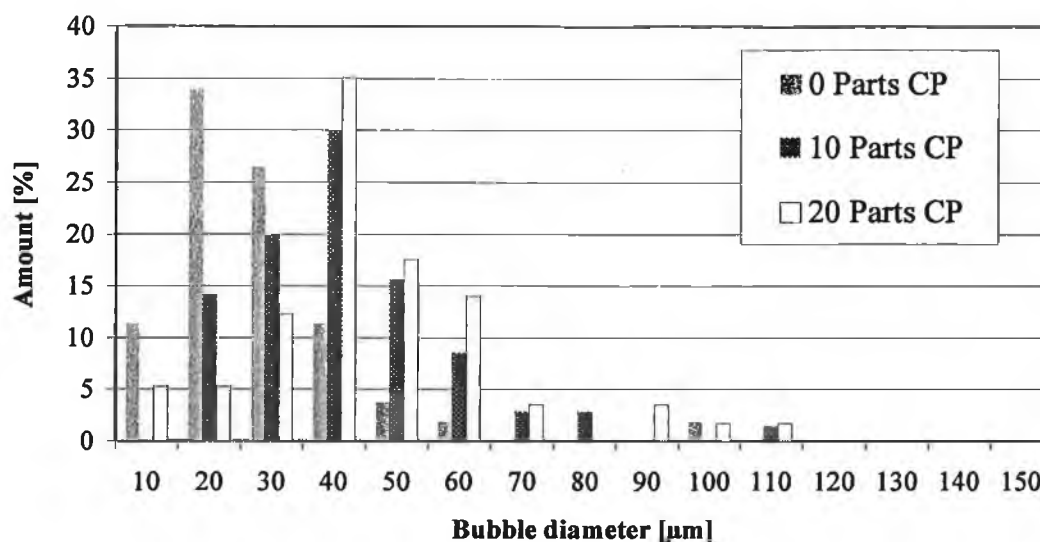


Fig. 3-15: A study of the A-component B(I/i) with 0%, 10% and 20% cyclopentane. The presence of the blowing agent (10% CP) initially increases the average bubble size; increasing the amount of blowing agent to 20% CP however, only increases the percentage of such sized bubbles.

3.5.3. Effect of Blowing Agent on the Nucleation Process

Here we wanted to study the difference between the nucleation due to a chemical blowing agent to that due to a physical blowing agent. As previously described, a chemical blowing agent liberates gas as a result of a chemical reaction such as occurs during the reaction of isocyanate with water, liberating CO₂. A physical blowing agent liberates gas as a result of a physical process at elevated temperatures or reduced pressures. The physical blowing agents studied here are cyclopentane, C₅H₁₀, and perfluorohexane, C₆F₁₄. The physical characteristics of the blowing agents used are tabulated in Table 3-6.

Table 3-6: The various blowing agents implemented and their physical data, including their boiling points B_p and gas thermal conductivity, λ , at 25°C.

A- Component	Blowing Agent	Type	Bp [°C]	λ_g [mW/m·K] @ 25°C
A(I/i)	H ₂ O / CO ₂	Chemical	*	16.8 ⁶⁶
B(I/i)	C ₅ H ₁₀	Physical	48-49	12.1 ⁶⁷ †‡
C(VI/i)	C ₆ F ₁₄	Physical	54-58	15.3 ⁰

† C₅H₁₀: Air (38:62) mixture; $\lambda_{25^\circ\text{C}} = 19.4 \text{ mW/mK}$ ⁶⁸

‡ C₅H₁₀: CO₂ (38:62) mixture; $\lambda_{25^\circ\text{C}} = 15.0 \text{ mW/mK}$ ⁶⁸

⁰ C₆F₁₄: C₅H₁₀ (38:62) mixture⁶⁸

The effectiveness of C(VI/i) is clearly evident in the results shown in Fig. 3-16 and Fig. 3-17. The average nucleus diameter is twice as small as those produced from foaming of the A-components A(I/i) or B(I/i). The amount of nuclei increased 100% and these nuclei are more homogeneous than the other systems studied as demonstrated by the narrower frequency distribution for C(VI/i) in Fig. 3-18. By cream time, as shown in the photomicrographs in Fig. 3-19, the nuclei produced by A(I/i) are B(I/i) are similar in size (note that the photomicrographs of A(I/i) and B(I/i) have different magnifications!) while the size of the nuclei in C(VI/i) is smaller and considered significantly different. As previously described (section 2.6.6.2.), “significantly different” is a difference of greater than 20%. The difference between the number of nuclei formed by B(I/i) and C(VI/i) is in the region of 90% and therefore justifiably considered significant.

The blowing agents in A(I/i) and B(I/i) prove to be easily soluble in their A-components. However, since CO₂ has first to be formed before it subsequently reaches the solubility maximum and crosses over to the vapour phase, nucleation takes slightly longer than with cyclopentane, which is present from the start, as the blowing agent. On the other hand the nucleation sites in system C(VI/i) are not formed during the induction period before cream time but are present from the start of mixing. A possible reason for this is that the blowing agent perfluorohexane is neither in A- nor in B-component soluble and therefore very small emulsion droplets are formed. These provide sites for nucleation.

A discussion of the effect of the blowing agent on the surface tension, end cell size and consequently the calculated nucleation number, NZ_{cal} , is given in the next section.

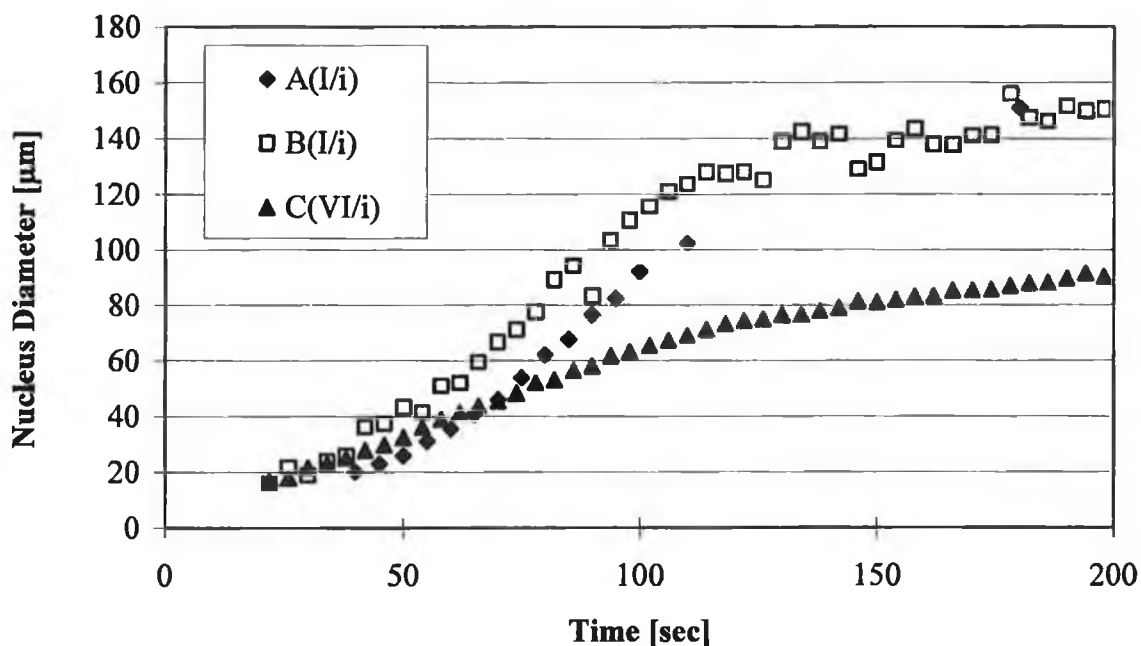


Fig. 3-16: The average nucleus diameter [μm] measured with respect to time for the A-components with CO_2 (A(I/i)), C_5H_{10} (B(I/i)) and C_6F_{14} (C(VI/i)) as blowing agents foamed with M20A as the B-component, in a ratio of 40:60 at room temperature (cream time $\approx 60\text{s}$, gel time $\approx 200\text{s}$ and density $\approx 55\text{g/l}$).

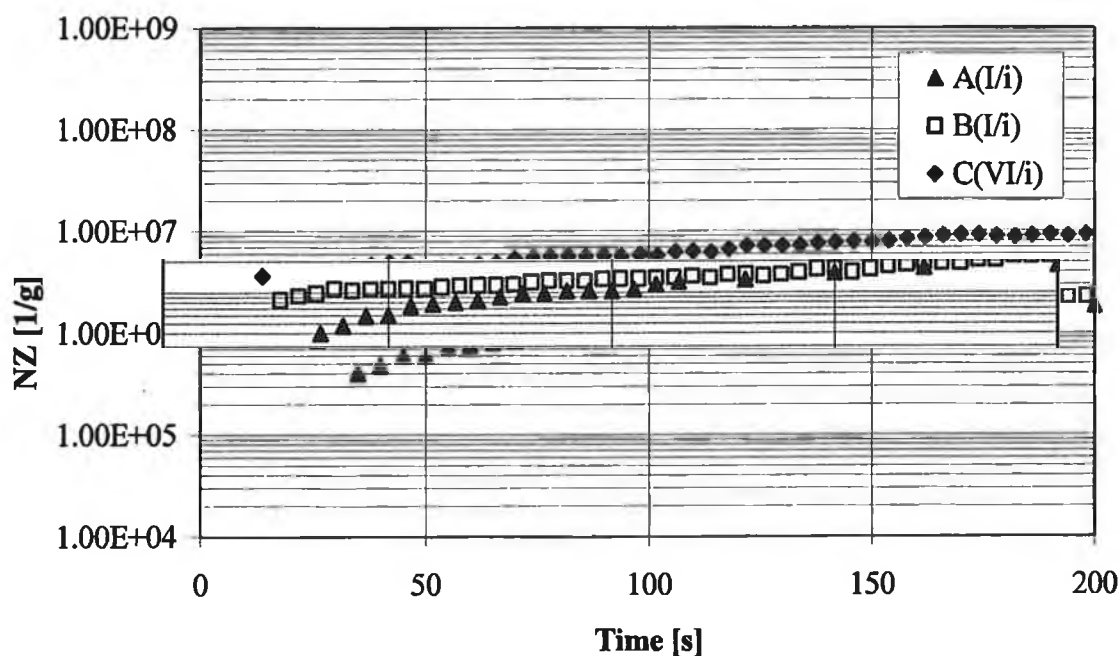


Fig. 3-17: The average nucleation number, NZ [1/g] measured with respect to time for the A-components with CO_2 (A(I/i)), C_5H_{10} (B(I/i)) and C_6F_{14} (C(VI/i)). Experimental conditions were as in Fig. 3-16.

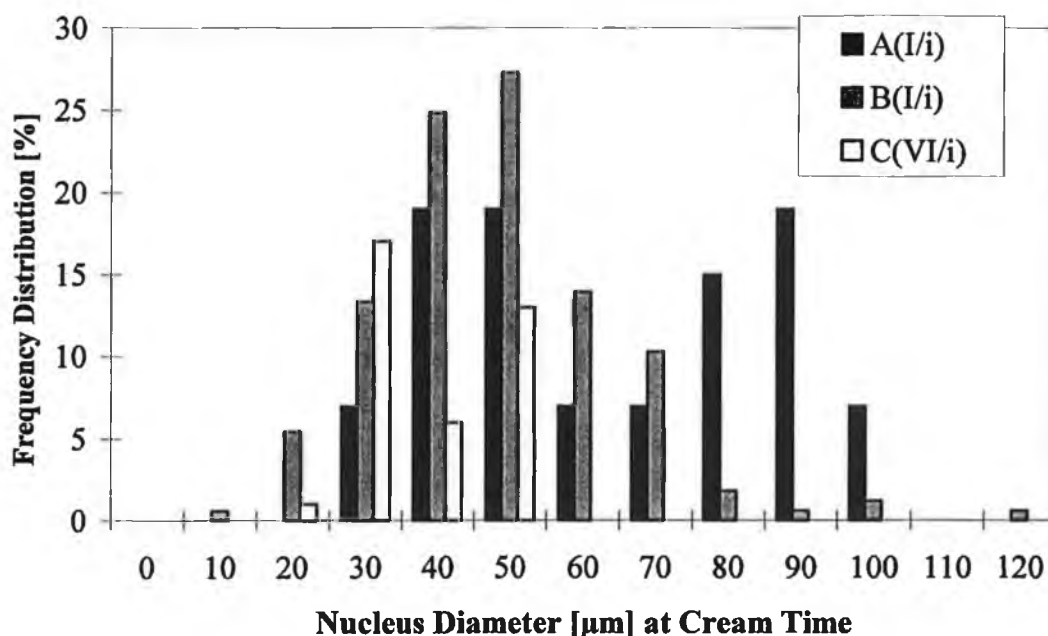


Fig. 3-18: Frequency distribution curves of the measured nucleus diameters for systems A(I/i), B(I/i) and C(VI/i) at their cream times of circa 60s.

In the systems foamed with the A-component A(I/i) a minimum amount of coalescence was observed. Foaming with B(I/i) resulted in what is described as disproportionation (section 1.5.3.) and less, if not a negligible amount of coalescence. C(VI/i) showed a negligible amount of disproportionation. These phenomena, their origins and their affect on the foaming process is described in detail in section 3.5.5.

It is well known that perfluoroalkane blown foams have finer cells than traditional water-blown and hydrocarbon-blown foams^{1,6}. As previously stated, the blowing agent does not stay in the mixed A- and B- components but falls out forming an emulsion, i.e. a dispersed system in which both phases are liquid. In order to stabilise an emulsion a third substance is necessary, an emulsifying agent or emulsifier. The effect of the emulsifier on the nucleation process was subsequently studied.

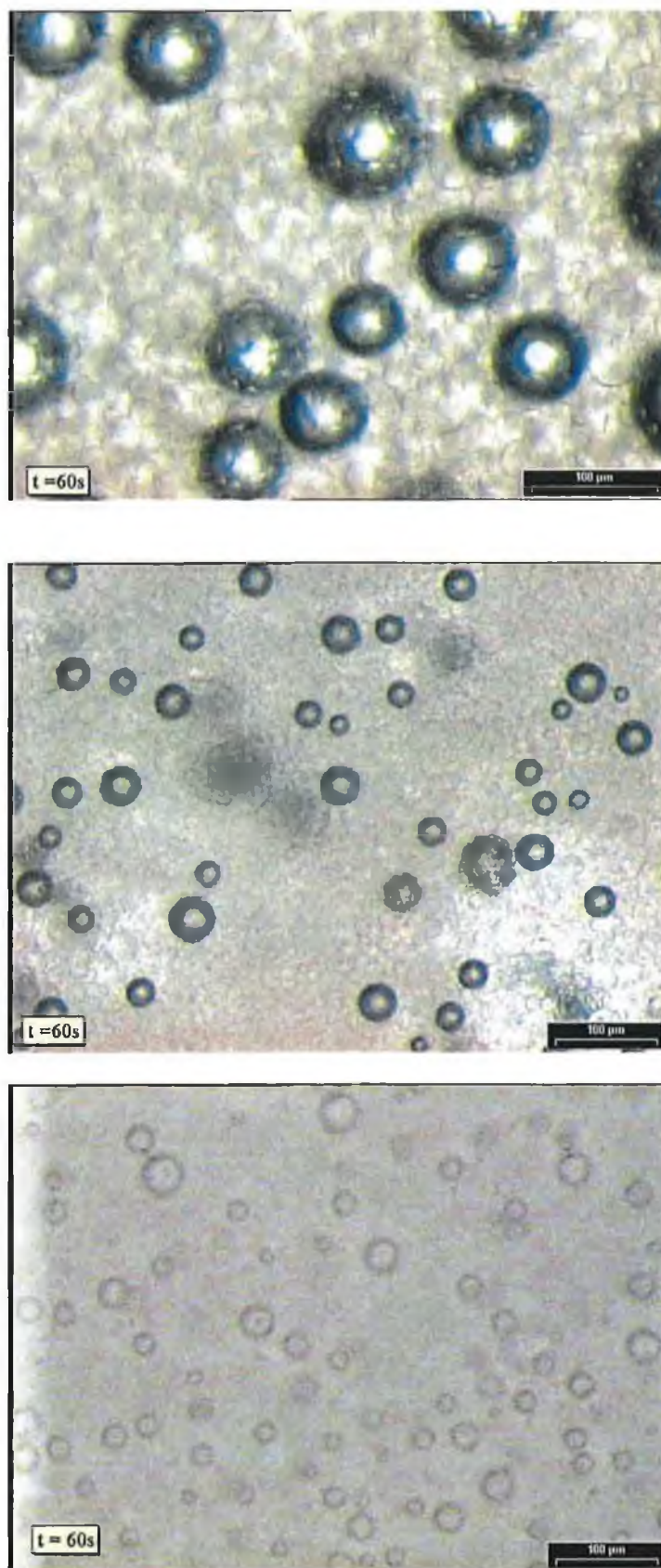


Fig. 3-19: Photomicrographs at cream time (60s) of systems A(I/i) – CO₂-blown, B(I/i),- C₅H₁₀-blown and C(VI/i) - C₆F₁₄-blown foams. The decrease (from top to bottom) in size and the increase in the number of the nuclei is clearly seen.

3.5.4. Effect of Emulsifier on the Nucleation Process

The perfluorohexane-blown foam, using A-component C(VI/i), resulted in the finest cell structure of all the systems investigated. This was expected as in practice such foams have lower thermal conductivity values⁸, a direct result of the homogeneity of the fine cells produced. The effect of the emulsifier, $(C_8F_{17}SO_2)N(C_2H_4OH)(C_2H_5)$, in this process was therefore analysed.

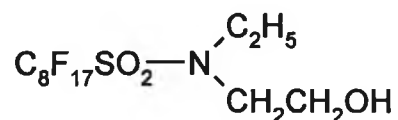


Fig. 3-20: *The emulsifier used in the foaming systems analysed.*

The emulsifier, $(C_8F_{17}SO_2)N(C_2H_4OH)(C_2H_5)$, as shown in Fig. 3-20, is a long chain compound with the hydrophilic sulphonyl-amino-ethanol which projects itself into the polyol and a hydrophobic part consisting of perfluoratoalkyl. The emulsifier therefore helps to create an emulsion of perfluorohexane droplets which are hydrophobic in the A-component which is hydrophilic. These droplets are stabilised by the surfactant in the A-component and are possible nucleation sites. In the absence of an emulsifier nucleation does take place. Surprisingly enough however, without an emulsifier and despite the presence of a surfactant, foaming does not proceed and nuclei sizes remain constant (see Fig. 3-23). Gas does not diffuse from the liquid phase into the nuclei which would enable nuclei growth. The absence of growth verifies this assumption. Neither coalescence nor disproportionation occurs as the formed nuclei in the emulsion tend to assemble into clusters rather than merge together (Fig. 3-22).

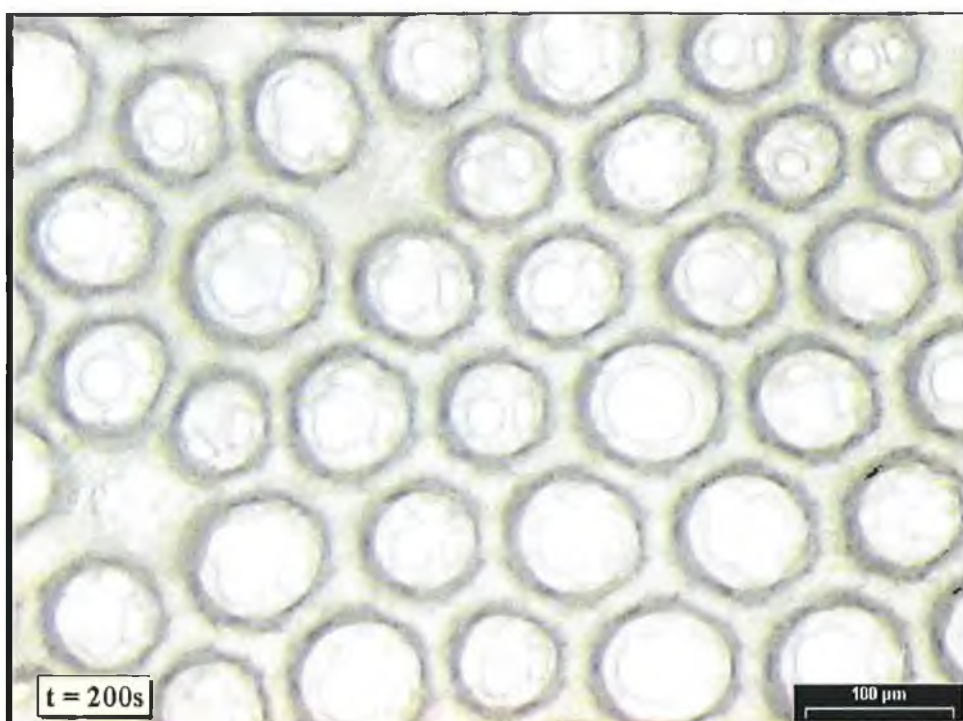


Fig. 3-21: Photomicrograph of foamed system with C(VI/i) including emulsifier as the A-component at gel time of 200s. A fine homogeneous structure favourable for an insulation material is depicted.

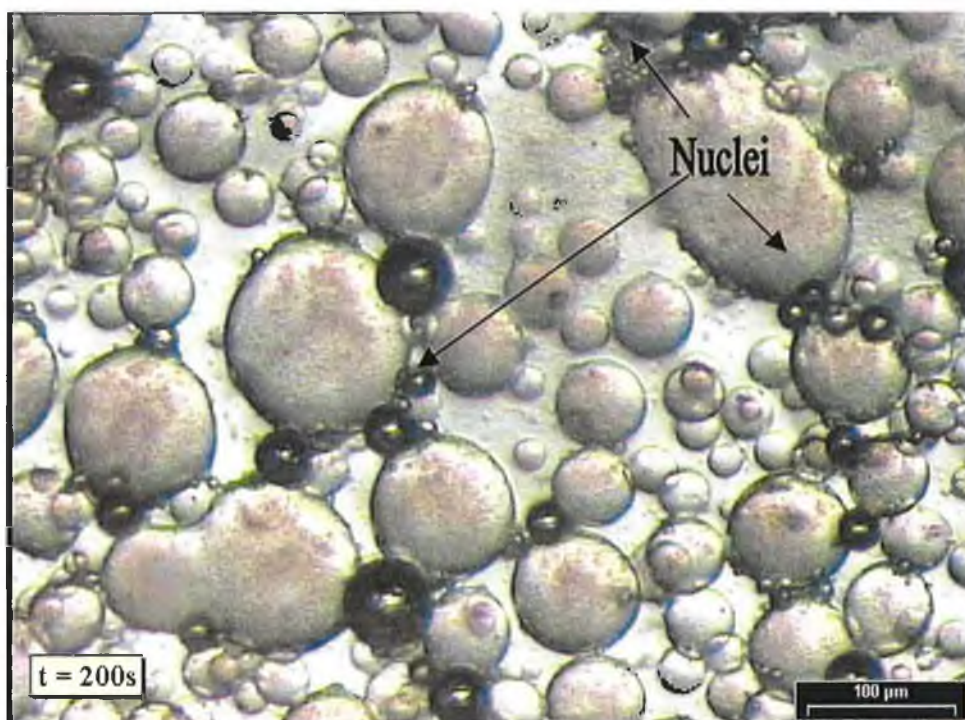


Fig. 3-22: Photomicrograph of foamed system with C(VI/i) without emulsifier as the A-component at 200s. Nuclei have been formed but no foaming occurred. The A-component remains unreacted as dispersed droplets in the B-component.

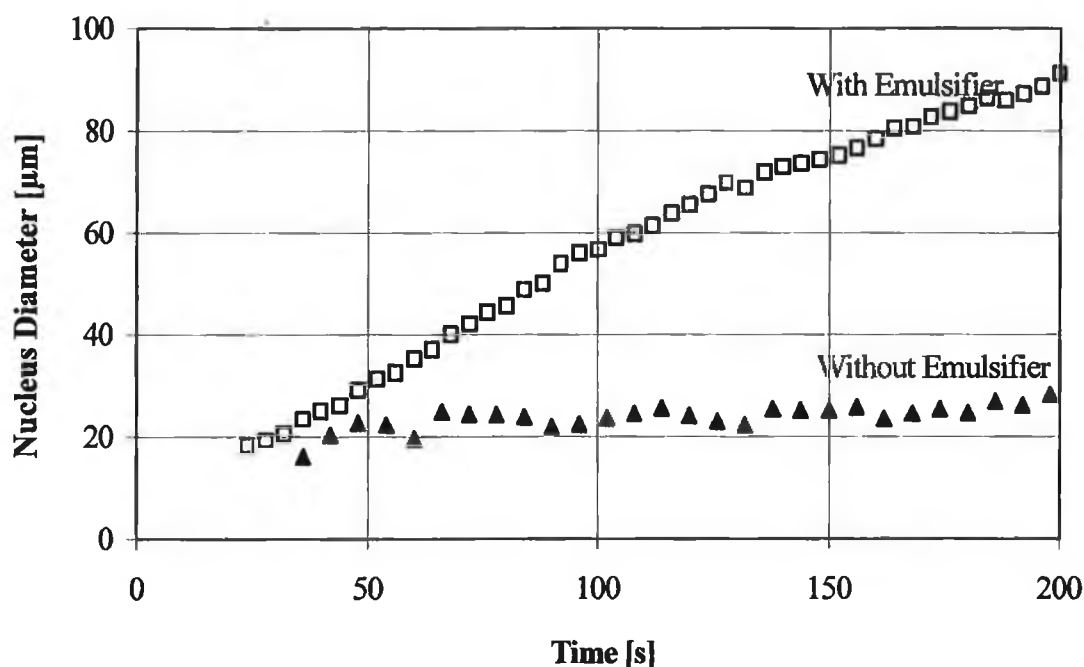


Fig. 3-23: The average nucleus diameter measured with respect to time for the foaming of the A-component C(VI/i), with (0.9%) and without an emulsifier, with the B-component M20A under the standard conditions.

Surface Tension Analysis

What role do the surface tensions of the systems have on the nucleation formation? One would expect that by decreasing the surface tension an increase in nucleation would result. For a more detailed account of the surface tension measurements see Appendix A7.

Using a Lecomte du Noüy tensiometer (section 2.11.1) the surface tensions, δ [mN/m], of each of the model A-components A(I/i), B(I/i), and C(VI/i) containing various amounts of their respective surfactants, were measured and are tabulated in Table A7-1 (see Appendix 7). The dependence of the surface tension on the amount of surfactant in the system was clearly seen (see Fig. 3-24). An amount as low as 0.05% can lower the surface tension considerably. The difference between the surface tensions of the A-components C(I/i) without surfactant and containing 0.05% surfactant is equal to 11.60mN/m. A critical micelle concentration (c.m.c.) could be obtained from the graph indicating the minimum amount of surfactant required for the maximum effect of

lowering the surface tension. This is obtained between 0.2 - 0.3% surfactant, after which point the amount of surfactant added has no significant effect on the surface tension.

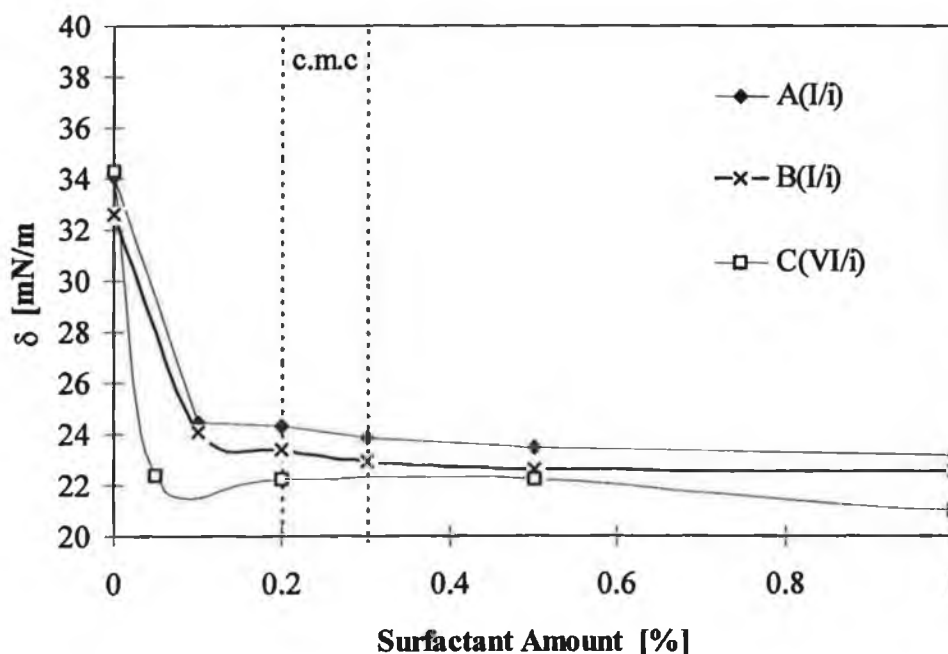


Fig. 3-24: Relationship between surface tension and surfactant amount for the various blowing agents measured using the Lecomte du Noüy tensiometer as described in 2.11.1. The critical micelle concentration (CMC) is indicated between 0.2–0.3% surfactant amount.

Systems with the lowest surface tensions, i.e. systems foamed with C(VI/i) as the A-component, have also the highest number of nucleation sites. Whether this is directly as a result of the surface active agents will be established in section 3.5.6.

The size of the end cells gives a good indication of the influence of the blowing agent on the nucleation process. Perfluorohexane blown foams, i.e. the A-component was C(VI/i) showed finer cell structures than those blown with either cyclopentane, B(I/i) or carbon dioxide, A(I/i). This is clearly illustrated in the following diagram, Fig. 3-25. The influence of the surfactant amount can also be seen in Fig. 3-25. This is the topic of our analysis in section 3.5.6.

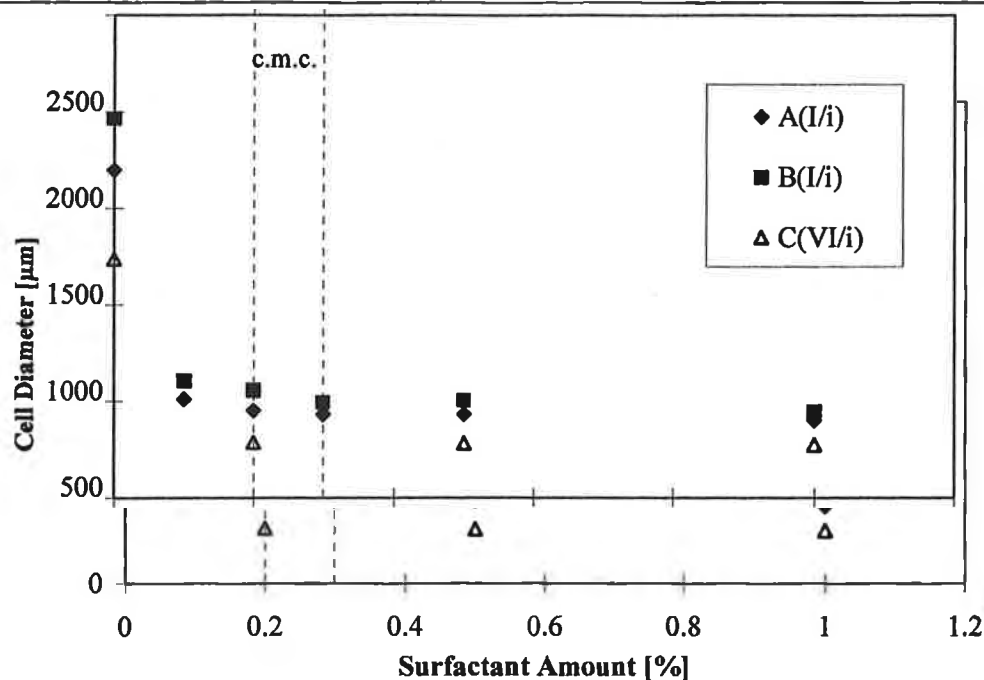


Fig. 3-25: The dependency of the end cell size with respect to surfactant amount on the blowing agent. Critical micelle concentration (CMC) correlates to c.m.c. in Fig. 3-24. End cell sizes obtained as described in section 2.9.

Table 3-7: Using the cell diameter, foam density and equations 53 and 54, where V_z is the cell volume V_g is volume of gas, the nucleation numbers (NZ_{cal}) for the various A-components A(I/i), B(I/i) and C(VI/i), each containing 1% surfactant I, were calculated.

A-Component	Cell Diameter [μm]	Foam Density [g/cm ³]	V_z [cm ³]	V_g [cm ³]	NZ_{cal} [1/g]
A(I/i)	399.5	56.8	1.66×10^{13}	3.34×10^7	4.98×10^5
B(I/i)	444.7	55.0	1.72×10^{13}	4.60×10^7	3.73×10^5
C(VI/i)	272.6	55.0	1.72×10^{13}	1.06×10^7	1.62×10^6

Using the above cell diameters (Fig. 3-25) and the known density of the foams, the nucleation number was calculated (NZ_{cal}) using equation 53 and 54 from section 2.10., the results of which are tabulated above. Predictably, calculated nucleation numbers indicate that the system foamed with C(VI/i) contain more nuclei than either A(I/i) or B(I/i) agreeing with the experimental.

3.5.5. Effect of Surfactant Amount on the Nucleation Process

Does the amount (or type) of surfactant at the gas/liquid interface hinder or promote nucleation? This was the principal question governing the analysis of the nucleation process pertaining to the surfactant.

The amount of surfactant I in the A-component B(I/i) was varied and the new A-component foamed with the B-component M20A as described in section 2.8.3. Fig. 3-26 and 3-27 show the results of the average nucleus diameter and nucleation number (NZ) respectively. The system containing no surfactant is used as a reference sample. Interestingly, the amount (1×10^6 [1/g] approx.) and size ($20 \mu\text{m}$) of the initial nuclei at 20s does not vary significantly with respect to surfactant amount. This is remarkable as traditionally it was thought that by lowering the surface tension (see Fig. 3-24), the possibility of more nuclei forming would increase. One can therefore, surprisingly, deduce that the amount of surfactant has no effect on the nucleation process but on the actual stabilising of the formed nuclei. Also notable is the comparison to the reference A-component. The number of nuclei is drastically reduced on reaction with the B-component from 1.7×10^9 [1/g] to circa 1×10^6 [1/g]. Values at circa 18s are invalid due to the inability to clearly see the nuclei, resulting in inaccurate analysis.

One of the principal functions of the surfactant is to stabilise the growing foam and this can be clearly seen with a levelling off of the curves by cream time (200s). The system without surfactant undergoes coalescence resulting in nuclei diameters out of range, i.e. $>250 \mu\text{m}$ at 120s. In systems with insufficient amounts of surfactant, i.e. 0.1%, 0.2% surfactant (I), coalescence (see Fig. 3-28) and disproportionation (see Fig. 3-29) play a significant roll resulting in larger cells and a less fine structure. With surfactant amounts greater than the critical micelle concentration (0.2-0.3%) sufficient stabilisation occurs with only a negligible amount of disproportionation sometimes observable.

In order to mathematically observe these phenomena relative distribution curves were used. With the aid of equation 50 growth factors, f_{gr} , were calculated as described in section 2.7.6.1. and the relative frequencies of the measured nuclei diameter measured at 60s and 100s were corrected by f_{gr} with respect to the relative frequencies of the measured

nuclei at 200s. Where these distribution curves overlapped the system was considered stable, i.e. minimum coalescence (Fig. 2-30). The system without surfactant showed no overlapping and it was impossible to measure the nuclei/bubbles at 200s as, due to coalescence, they were out of range (Fig. 2-31). These curves represented therefore a very unstable system with maximum coalescence.

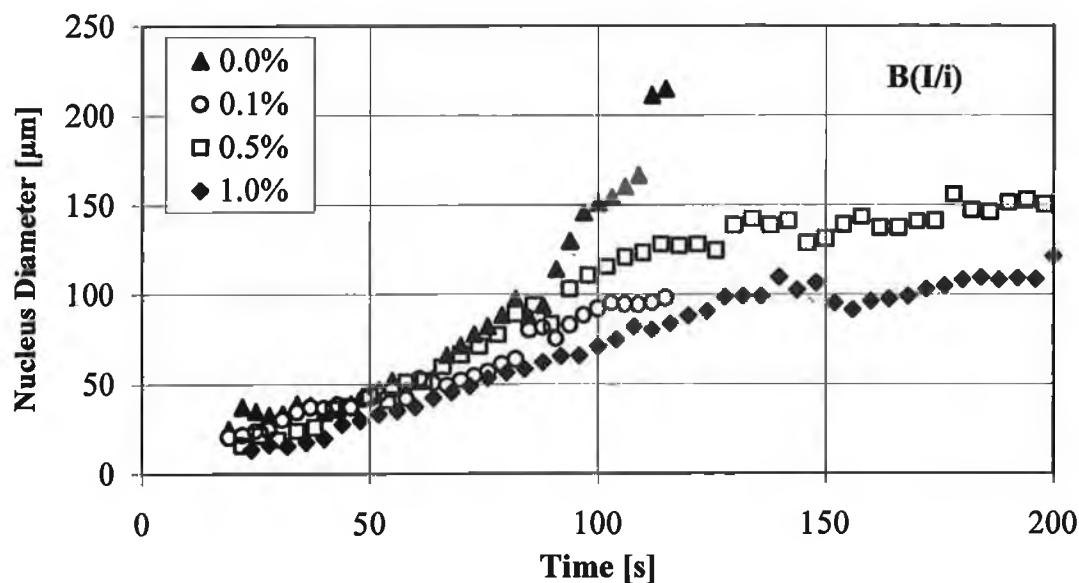


Fig. 3-26: The influence of the amount of surfactant (*I*) in the A-component *B(I/i)* on the average nucleus diameter during foaming under the usual conditions. Cream time ≈ 60 s, gel time ≈ 200 s and density ≈ 55 g/l.

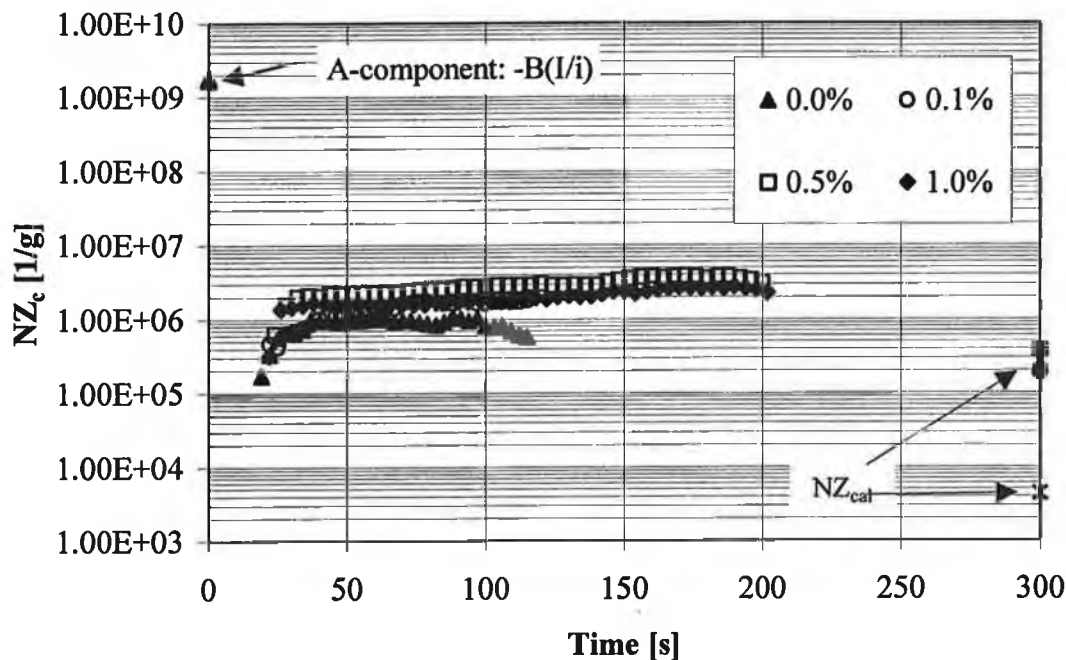


Fig. 3-27: The influence of the amount of surfactant (*I*) in the A-component *B(I/i)* on the nucleation number (NZ_c). At 0s the “nucleation number” for the unreacted *B(I/i)* is shown. At 300s the calculated NZ_{cal} is depicted, agreeing in general with the initial nucleation number observed.

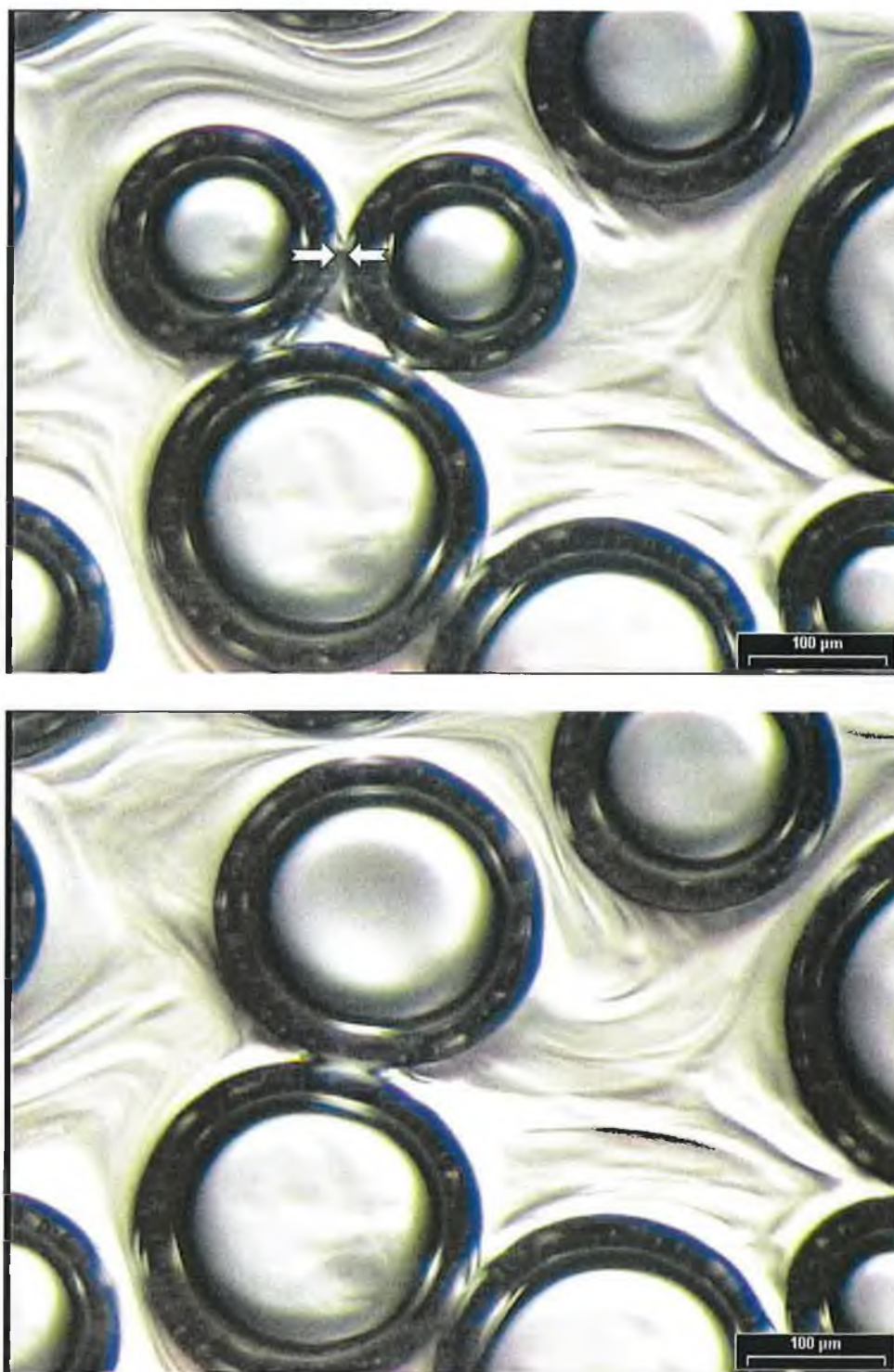


Fig. 3-28: Typical example of coalescence observed with systems foamed with the A-component without surfactant. Surfactants act as stabilisers inhibiting such phenomena which result in large-celled foam and in certain cases foam collapse.

Disproportionation has already been described in section 1.5.3. as the growth of larger bubbles at the cost of smaller bubbles. This occurrence was also microscopically observed, decreasing in frequency with increasing surfactant amount.

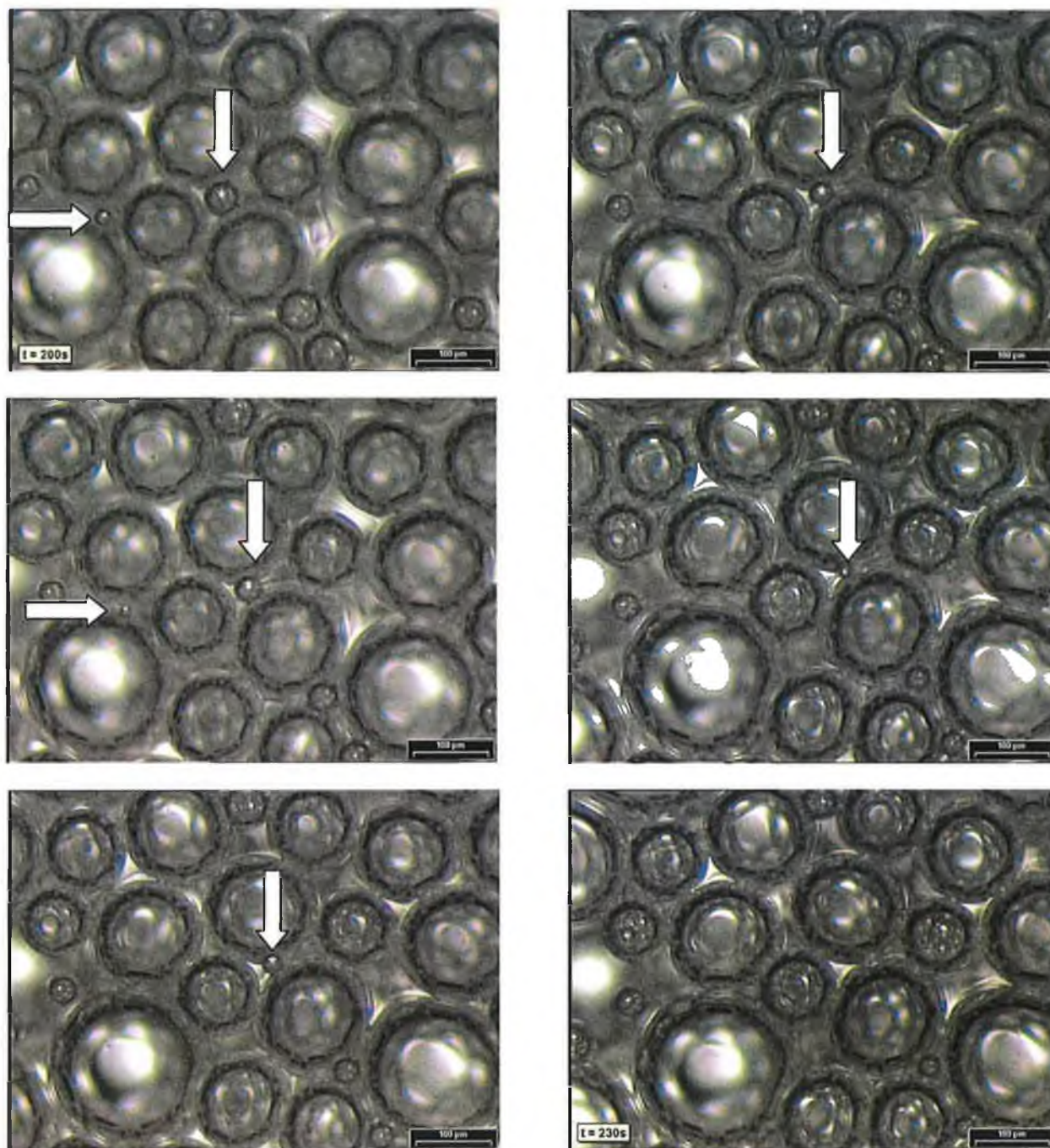


Fig. 3-29: Disproportionation – bubble growth at the expensive of the smaller bubbles. The arrows indicate the disappearing bubbles.

As a measure of the instability of a given system relative frequency distributions were calculated and compared to the curves for minimum and maximum coalescence below.

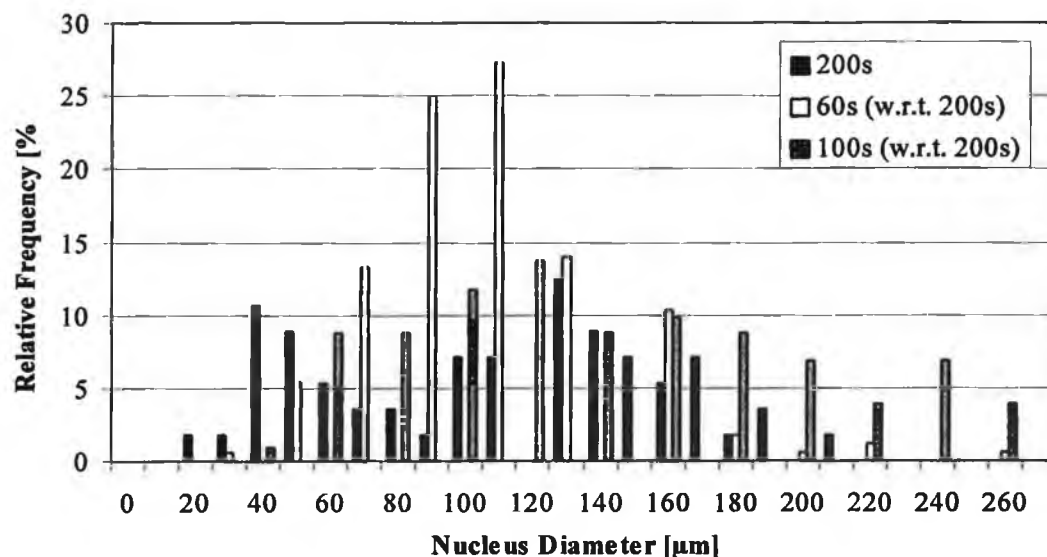


Fig. 3-30: The relative distributions for the stable system foamed with the A-component B(I/i). The curves overlap indicating no coalescence. Note that the relative frequency at 60s is higher than at 200s; this is because more nuclei are counted per area at 60s. These grow resulting in less nuclei counted per area at 200s. (w.r.t. = with respect to).

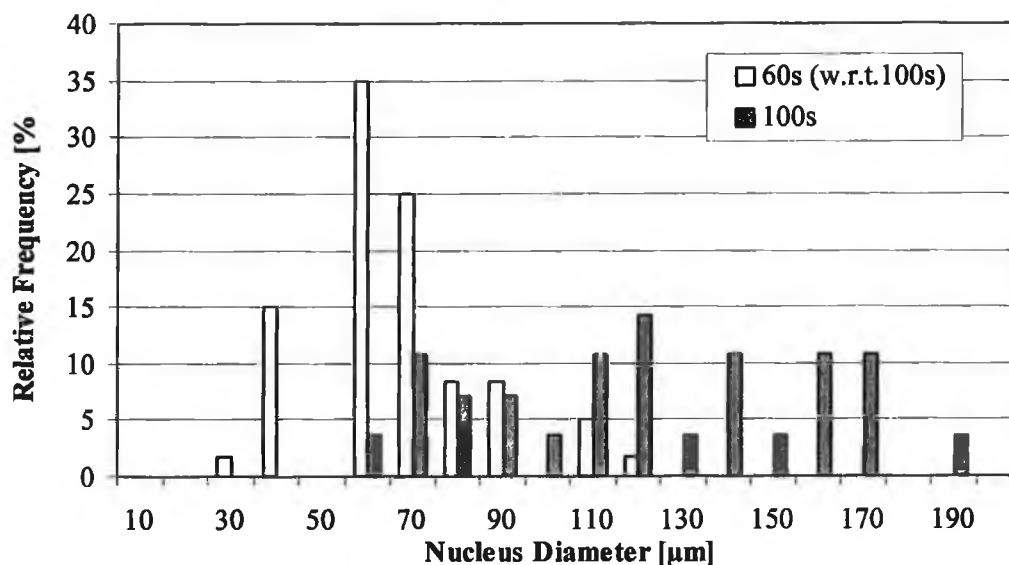


Fig. 3-31: The relative distributions for the unstable system foamed with the A-component B(I/i) without surfactant. The distributions are calculated using the growth factor from equation (54), with respect to (w.r.t.) 100s, where 100s are the experimental values. Nuclei diameters at 200s were out of range.

3.5.6. Effect of Surfactant Type on the Nucleation Process

For clarity purposes the results of the surfactant structural analysis are first introduced before going on to discuss the results of the microscopic analysis.

Structural Analysis of Surfactants

Structural analyses was carried out using quantitative ^{29}Si -NMR and ^1H -NMR as described in section 2.12.1. providing values for the length of the siloxane backbone, the number of polyol sidechains, and the ratio of ethylene oxide to propylene oxide (EO:PO) in the sidechain. For a detailed explanation of the spectra evaluation see Appendix 5.

The basic structure is that of a dimethyl polysiloxane-polyoxialkylene copolymer as shown in Fig. 3-32 below:

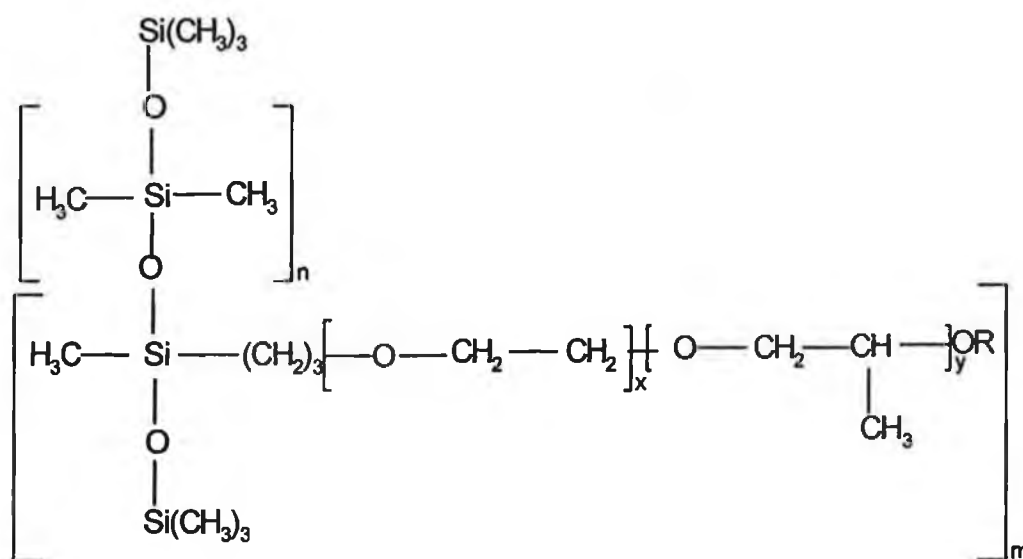


Fig. 3-32: The general structure of the surfactants used in this work. For values for m , n , x and y see Table 3-8.

The following table summarises the results obtained for the surfactants used in this thesis. It is important to be able to use these results to explain the results obtained during the in-situ analysis.

Table 3-8: The results of the NMR surfactant analysis; *m* and *n* are the siloxane blocks of the backbone, *m* being the siloxane block containing the polyol sidechain. *x* and *y* are the ethylene oxide (EO) and propylene oxide (PO) parts of the sidechain *m*. Values given are absolute values. *M* is the mass of the compound in grams.

Surfactant No.	Backbone		Side Chains			M [g]
	n	m	x	y	EO:PO	
I	39	5	13	6	1:0.43	8254
II	53	7	26	15	1:0.60	19694
III	26	5	20	9	1:0.45	9970
IV	10	4	28	1	1:0.05	5937
V	9	3	47	3	1:0.07	7725
VI	97	8	38	40	1:1.05	38606

A-components containing the surfactants described in Table 3-8 were used in the in-situ analysis. The actual formulations of the A-components B(II/i), B(III/i), B(IV/i) and B(V/i) are given in Appendix 1. Turning to the results of the microscopy results, one fact is immediately obvious – the initial nucleus size of approximately 20µm is independent of surfactant type (see Fig. 3-33). The nucleation number in Fig. 3-34 varies less than 20% and is therefore considered insignificant. This is an important and interesting result. The literature^{10,11} would lead us to believe that different stabilisers, nucleate and stabilise the nucleated sites at different rates resulting in foams with different cell size. However, from these results this assumption is only partially validated. After the cream time of 60s the nuclei size deviate from each other showing the stabilising efficiency of the various surfactants. Both the average nucleus diameter and the nucleation number formed by the foaming of A-components containing surfactants which sufficiently act as a stabiliser, such as I and II and III, levels off to a constant at circa 100s. Unstable foaming systems coalesce creating larger nuclei after 100s as shown by surfactant IV in Fig.3-33. Surfactant IV's inability to stabilise adequately is also highlighted in its nucleation number which gradually decreases with time. There is also a gradual increase in the nucleation number (NZ) with respect to surfactant type. In order to explain this a closer look at the chemical structure of the surfactants is needed.

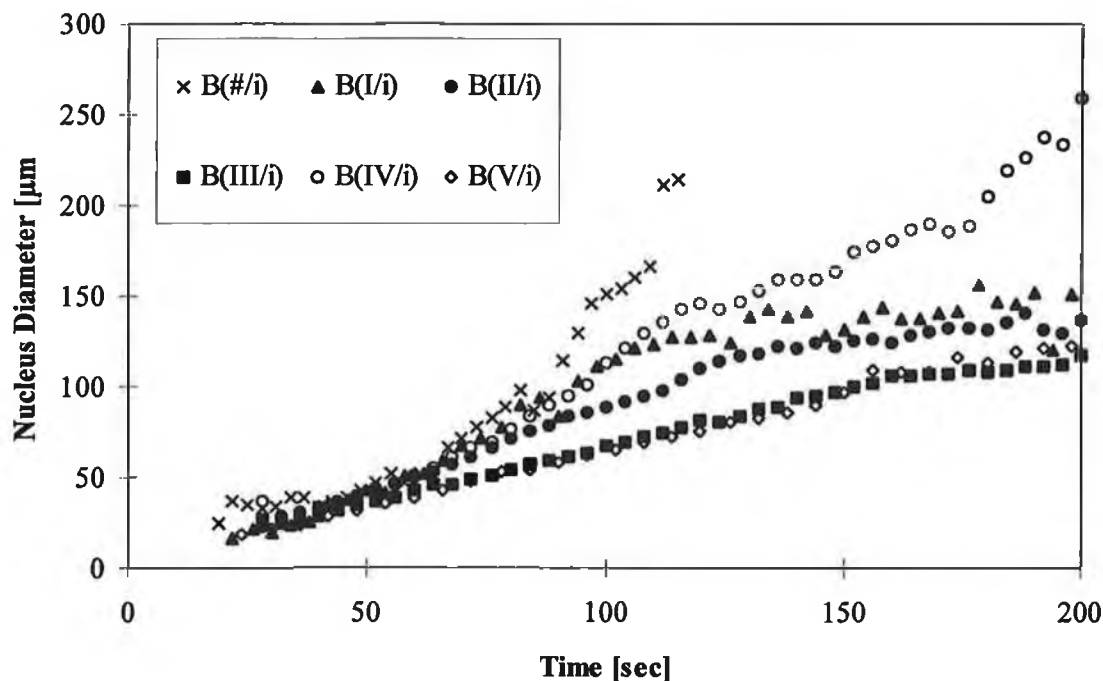


Fig. 3-33: The average nucleus diameter formed during the foaming of the A-components $B(I/i)$, $B(II/i)$, $B(III/i)$, $B(IV/i)$ and $B(V/i)$ (each with 1% of their respective surfactant) with the B-component M20A under the usual conditions. $B(\#/i)$ represents the A-component without surfactant. Cream time $\approx 60s$; gel time $\approx 200s$; density $\approx 55g/l$.

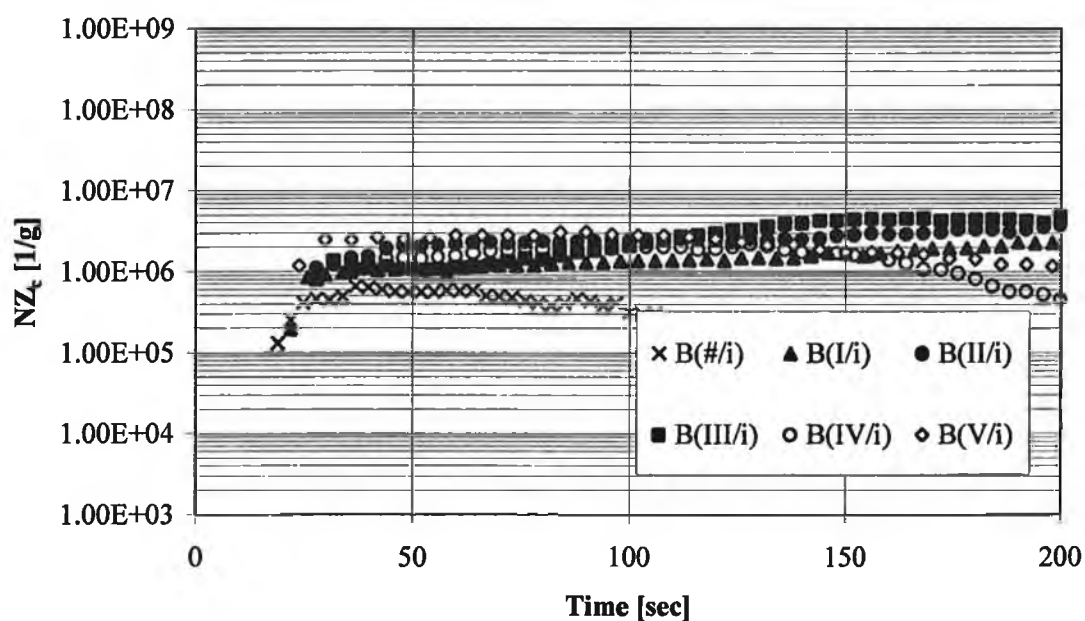


Fig. 3-34: The average nucleation number (NZ_c) formed during the foaming of the A-components as described in Fig. 3-33. Cream time $\approx 60s$; gel time $\approx 200s$; density $55g/l$. (# represents 0% surfactant).

The rigid Si-O backbone of the surfactant (as shown in Fig. 3-32) is important for the foam stability and is a hydrophobic part of the compound. The PO group on the side chain is also hydrophobic whereas the EO group is the hydrophilic part of the compound. This is probably the most influential part of the compound, having a positive effect on the emulsifying ability of the surfactant. In order to measure the hydrophilic strength of the surfactants the turbidity points and hydrophilic-lipophilic values for the various surfactants were obtained (see the experimental section 2.12.2).

Determination of the Turbidity Point of Surfactants^{30,57}

The solubility of non-ionic surfactants in water results from the hydration of the oxygen groups by hydrogen bonding. The degree of hydration decreases with increasing temperature, therefore so too does the water solubility of non-ionic surfactants.

Correlations exist between the turbidity points and the hydrophile-lipophile balance (HLB) values or phase inversion temperatures of surfactants. The HLB allows a rough classification of non-ionic surfactants to be arranged on a scale from 0 to 20, increasing in polarity. It can be calculated from the ratio of the molecular mass of the hydrophilic fraction (the EO part), M_h , to the total molecular mass M of the surfactant, multiplied by 20^{30,57}:

$$\text{HLB} = 20 \frac{M_h}{M} \quad \text{i.e.} \quad \frac{\% \text{EO}}{5} \quad (56)$$

These values are also presented in the Table 3-9. From the diagram, Fig. 3-35, a correlation in the trends is clearly seen. As the turbidity points increase so does the hydrophile-lipophile balance values. These have been correlated to the stabilisation and emulsification abilities of the surfactants. Surfactants with a lower turbidity point / HLB-value such as surfactants I, II, III and VI, exhibited stabilising abilities, as discussed with respect to Fig. 3-33 and Fig. 3-34. Increasing the surfactant's turbidity point / HLB-value increases emulsification abilities. Surfactants IV and V did not sufficiently stabilise the foaming system resulting in a decrease in nucleation number at 200s but showed an increase in emulsification. This can be seen in the photomicrographs in Fig. 3-36.

Table 3-9: Measured turbidity points as described in section 2.12.2. and calculated HLB-values (as described in the text) for the various surfactants.

Surfactant No.	Turbidity Point [°C]	Hydrophilic-Lypophilic Balance		
		M	M _b	HLB-Value
I	59.8	8253	568	1.38
II	63.2	19694	1131	1.15
III	54.1	9970	880	1.77
IV	83.0	5937	1241	4.18
V	86.9	7725	2068	5.35
VI	43.3	38606	1672	0.87

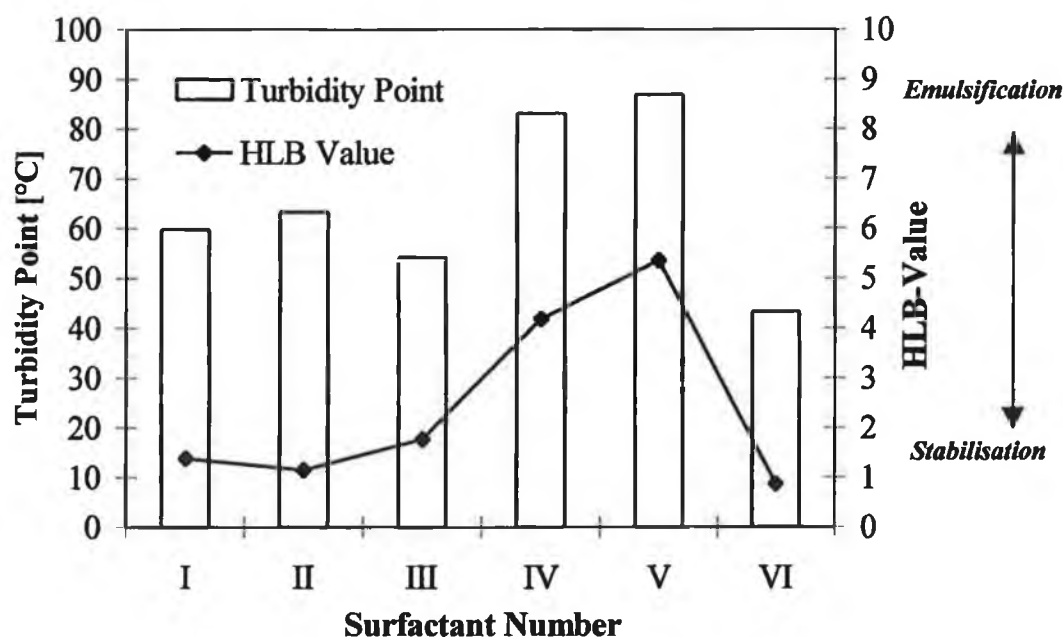


Fig. 3-35: The turbidity points and hydrophile-lipophile balance (HLB)-values for the surfactants used in this thesis. Surfactants with higher HLB-values showed emulsification properties while decreasing the HLB-value increase their stabilisation abilities.

The higher the percentage EO groups the more hydrophilic the compound. Surfactants IV and V have a very high %EO in their comparatively longer sidechains with EO:PO ratios of 1:0.05 and 1:0.07 respectively. As a result they have a high HLB-value.

These values correlate well with their high turbidity points of 83°C and 86.9°C respectively. The decrease in molecular weight improves the surfactants ability as an emulsifier (see Table 3-8). Surfactants IV and V have a lower molecular weight than the surfactants implemented in this study. With these attributes, one would expect surfactants IV and V to act more as an emulsifier than a stabiliser. This expectation is confirmed in the microscopic analysis (see Fig. 3-34 and the photomicrographs in Fig. 3-36) with these surfactants tending to give a larger nucleation number at the beginning but having a reduction in nucleation number due to instability at the end.

Despite this, 1% of the surfactant IV or V was not sufficient to stabilise the nuclei formed, resulting in coalescence and hence larger cells and consequently a smaller end nucleation number than, for example, the more stable B(I/i) (all having the same density, 55g/l) (See Table 3-10 for values). The inability of V to stabilise sufficiently was also highlighted during the rheological studies. The frequency distribution for system B(V/i) (Fig. 3-37) highlights the instability of that system. In comparison to the frequency distributions for the unstable system without any surfactant, i.e. maximum coalescence and the stable system B(I/i) with minimum coalescence the distributions show that the surfactant V is not a sufficient stabiliser.

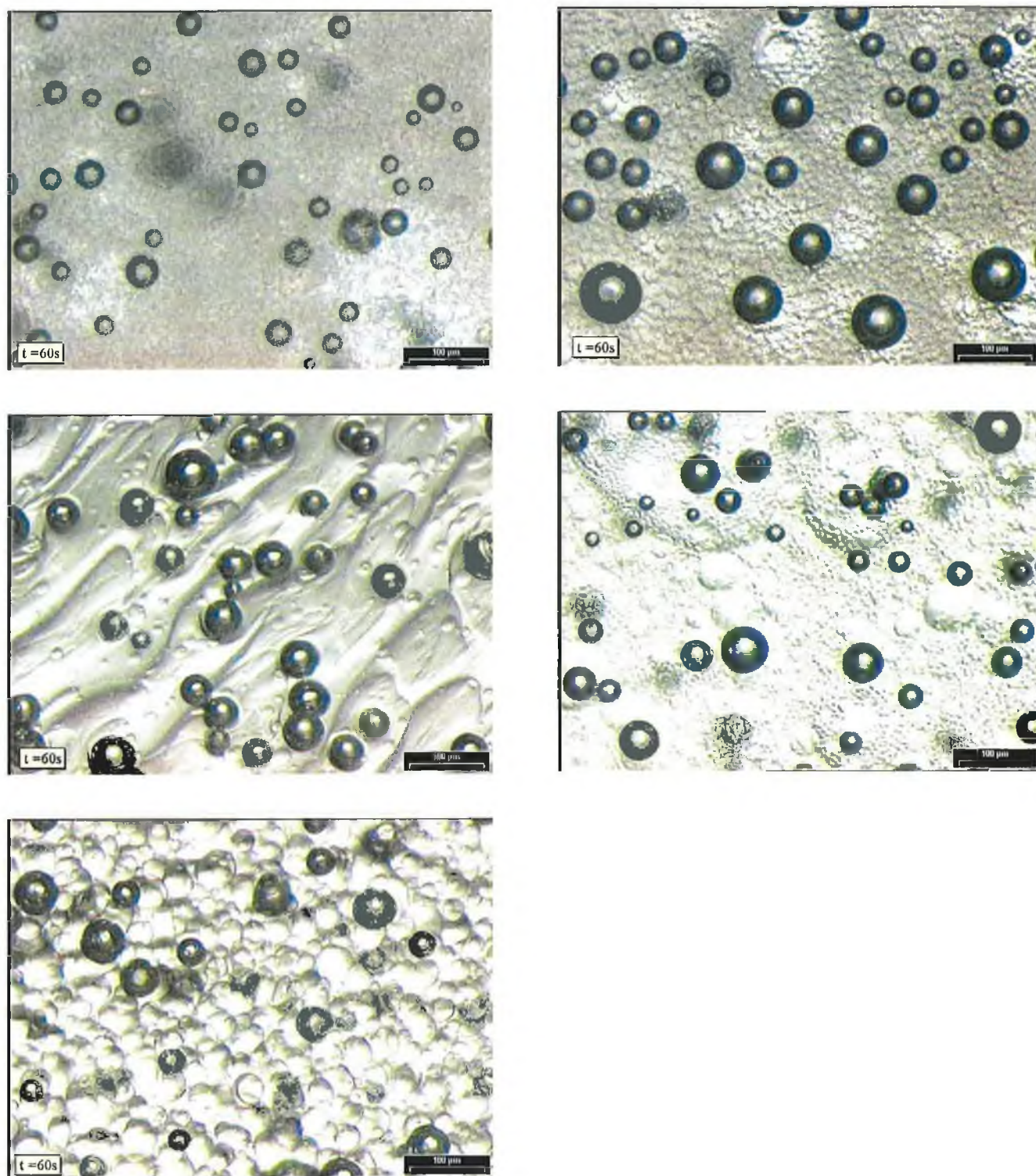


Fig. 3-36: Photomicrographs of systems foamed with A-components B(I/i), B(II/i), B(III/i), B(IV/i) and B(V/i), from top to bottom, left to right. All photomicrographs were taken at cream time of 60s. The emulsification tendency of surfactant IV and V is illustrated by the emulsion-type formation of the polymer matrix in B(IV/i) and B(V/i) and the lack of such “smears” as clearly shown with B(II/i)

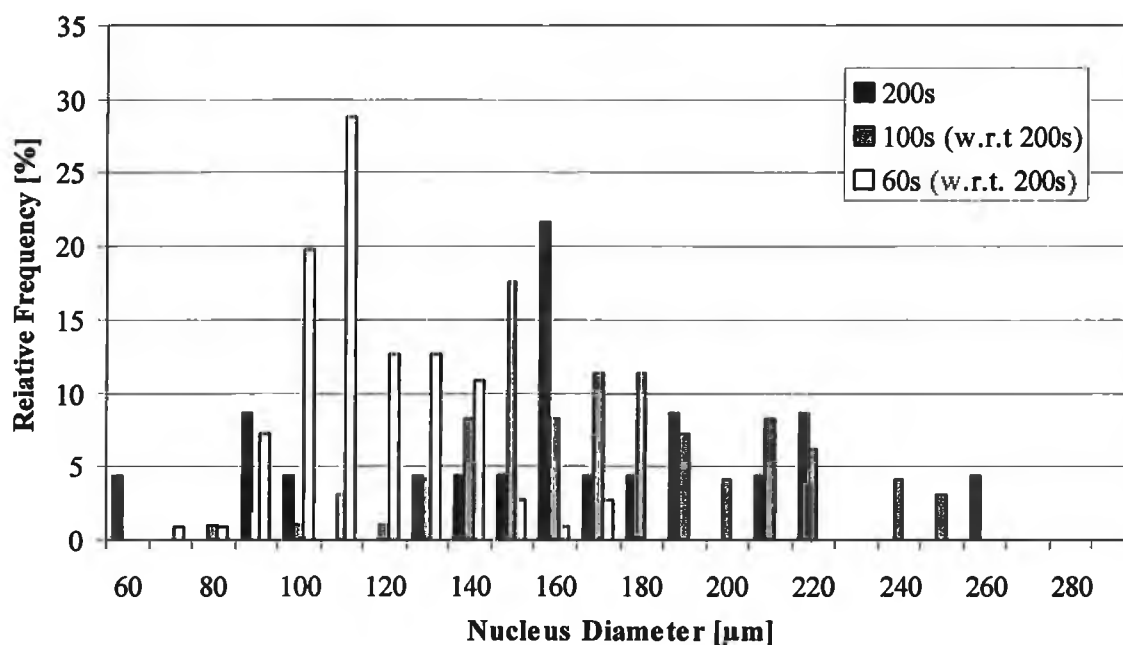


Fig. 3-37: Frequency distributions for the unstable system B(V/i). Distribution at 200s are actual values; distributions at 60s and 100s are calculated with respect to (w.r.t.) 200s with the aid of equation 50.

Although the nucleus diameter range at 200s (60-260μm) is not as wide as the nucleus diameter range obtained for foaming without surfactant which was out of range by 200s (Fig. 3-31), the distributions do not overlap as with the stable system B(I/i) (Fig. 3-30), indicating coalescence or disproportionation, i.e. instability.

Systems B(I/i) and B(III/i) have a slightly less nucleation number (observed at 60s) than B(II/i). Considering the %EO in these three systems one would expect similar stabilising abilities with I and III and a slightly less stabilising ability due to the slight increase in %PO (i.e. decrease %EO) in II. Nevertheless, the molecular weight of II is considerably higher adding to the overall stabilising ability of the surfactant. Surfactant III has a turbidity point at 54°C and a HLB-value of 1.77, which leads to its classification on the border of stabilising and emulsifying abilities. Its backbone (%backbone = 100% - %sidechain) is smaller than I, comparatively improving its hydrophilic ability. This possibly explains why system B(III/i) has the smallest nucleus diameter and ergo the highest NZ_{cal} of the systems analysed.

Table 3-10: The effect of the surfactant structural properties (molecular weight, M ; %Sidechain; %EO (with respect to the molecular weight)) on the nucleation number, NZ_c of the foaming systems (*observed at 60s, * calculated from finished foam, NZ_{cal}).

Surfactant No.	NZ_c [1/g]*	NZ_{cal} [1/g]*	M [g]	Sidechain %	EO %
I	1.12×10^6	3.73×10^5	8254	59.5	6.88
II	2.12×10^6	3.47×10^5	19694	77.2	5.74
III	1.15×10^6	4.76×10^5	9970	76.1	8.83
IV	1.56×10^6	2.73×10^5	5937	81.3	20.29
V	2.77×10^6	2.58×10^5	7725	87.0	26.77
VI	4.73×10^6	1.63×10^6 *	38606	79.72	4.33

*Surfactant VI was used in the foaming of the perfluorohexane-blown system with the A-component C(VI/i) and therefore has a larger NZ_{cal} .

It is interesting to note the values obtained for the surfactant VI. This surfactant was only used with system C(VI/i). It has the lowest turbidity and HLB-values of 43.3°C and 0.87 respectively. The excess %PO in its sidechain coupled to its larger molecular weight suggests that this surfactant is extremely stabilising but in no way capable of emulsifying. This reconfirms the results seen when the emulsifying agent was taken out of C(IV/i) (see previous section). No foam formed, however, a very stable system was produced whereby neither coalescence nor disproportionation, which are typical in an unstable environment, occurred. In this case, the addition of an emulsifier is need for foaming to occur.

Interesting was to see whether the surface tensions of these systems can help us in understanding their nucleating ability. Theory would lead us to believe that by lowering the surface tension more nuclei are formed as less energy is needed (see section 1.5.3.). The affect of the type of surfactant on the surface tension was investigated. Each system showed the same tendency with critical micelle concentrations (CMCs) between 0.2-0.3% surfactant but reached different minimum surface tension values (see Fig. 3-38).

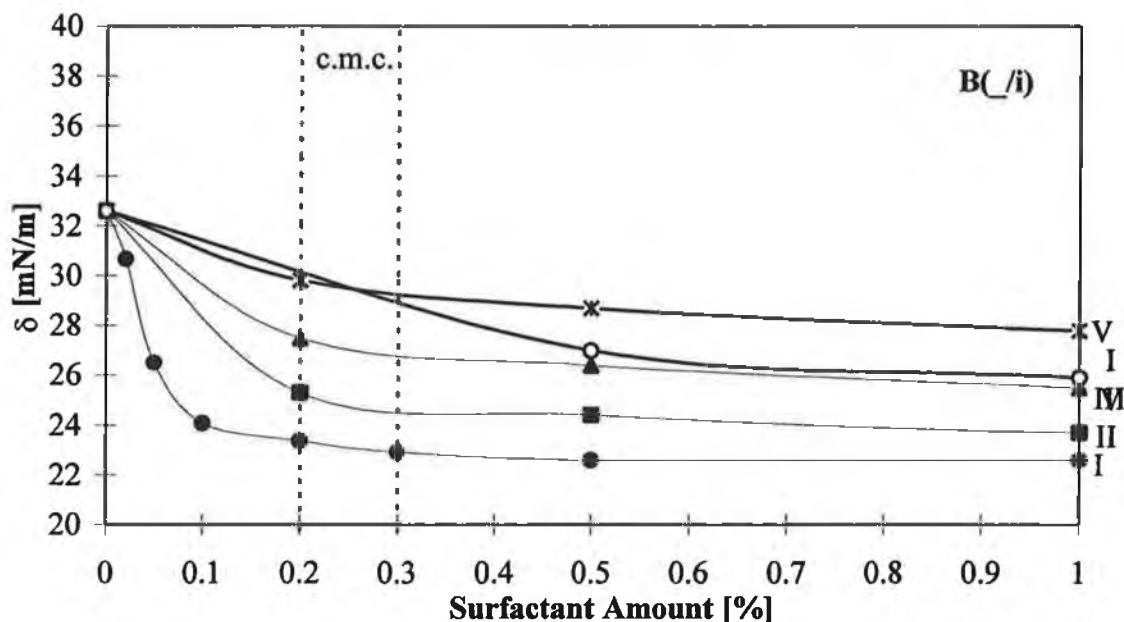


Fig. 3-38: The surface tensions (measured as described in section 2.11.1.) of the A-components B(I/i) containing various types (I, II, III, IV and V) and/or amounts of surfactants, indicating their critical micelle concentrations (CMC).

From these results one would expect that system B(I/i) would have the most nucleation sites and hence produce the foam with the finest cell structure. This contradicts what we see under the microscopic analysis.

A comparison of the end cell sizes for the various surfactants with varying concentration revealed a curve (Fig. 3-39), which levelled off at a point (0.2-0.3%) which correlates well with the critical micelle concentration obtained in the surface tension analysis of these systems. However, the order of value is inverted. The order is consistent to that obtained from the in-situ study. This indicates that the influence of the surfactant on the nucleation process is complex and cannot be described by the surface tension values. In other words, the surface tension does not support the search for a fine-celled rigid foam system.

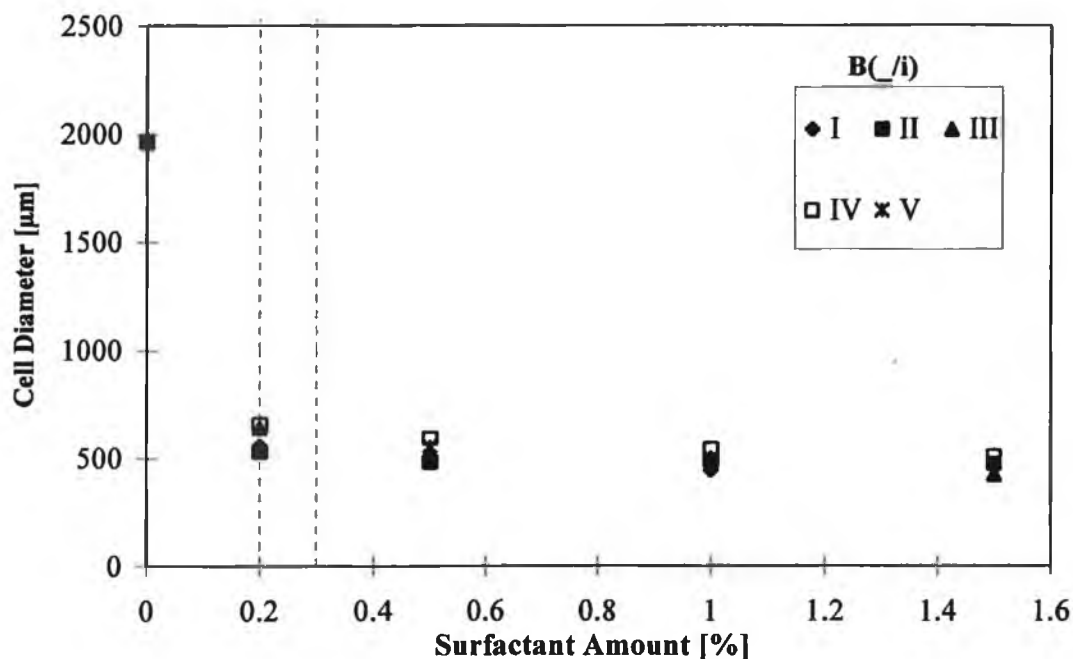


Fig. 3-39: The effect of various types and amounts of surfactants on the end cell size measured using the method described in section 2.9.

Table 3-11: The influence of surfactant type and amount on the nucleation number (NZ_{cal}).

Surfactant [%]	Nucleation Number (NZ_{cal}) [1/g]				
	B(I/i)	B(II/i)	B(III/i)	B(IV/i)	B(V/i)
0.00	4.33×10^3	4.33×10^3	4.33×10^3	4.33×10^3	4.33×10^3
0.20	1.87×10^5	2.41×10^5	2.38×10^5	1.27×10^5	-
0.30	2.55×10^5	3.21×10^5	2.87×10^5	1.76×10^5	-
0.50	2.74×10^5	2.08×10^5	4.04×10^5	2.25×10^5	1.84×10^5
1.00	3.73×10^5	3.47×10^5	4.76×10^5	2.73×10^5	2.58×10^5

Inserting the cell diameter values (see Appendix 7) and the density of the foams into the equations 52, 53 and 54 which are described in the section 2.10., the number of nuclei formed, i.e. the nucleation number (NZ_{cal}) could be estimated. Important is to note that this assumes that the amount of cells in the end foam is equal to the amount of nuclei formed and does not take phenomena such as coalescence or disproportionation into account.

Comparing Theory to Practice

In section 1.5.3. the classical nucleation theory has been discussed. Here we compare theoretical results with those obtained from experiment.

Due to the cyclopentane blowing agent which has a vapour pressure of 0.53 bar at 20°C, 0.8 bar at 30°C, 1 bar at 49°C and 2 bar at 80°C, an estimated pressure difference of less than 1 bar is present during the gas dissolution stage of foam formation. Using the Young-Laplace equation (i.e. $r_b^* = 2\delta / (P_s - P_0)$ – equation 8) and the obtained surface tension values, the critical radius r_b^* was determined. This is the critical nuclei size for nucleation to take place. Table 3-12 below shows the values for $2r_b^*$, i.e. nucleus diameter [μm]. This shows that with increasing surfactant amount the critical radius slightly decreases. In this way one would theoretically expect more nuclei due to the more favourable nucleation environment with increasing surfactant amount. The comparative tendency for a smaller critical radius is I<II<III<V<IV. However, the difference is well within the 20% significance level. This backs up the experimental results that the surfactant type has no influence on the formation of nuclei, i.e. nucleation process.

Table 3-12: The critical nucleus diameter values, $2r_b^*$, (calculated from equation (8)) for systems foamed with A-components of B(I/i), B(II/i), B(III/i), B(IV/i) and B(V/i).

Surfactant Amount [%]	$2r_b^*$ [μm]				
	B(I/i)	B(II/i)	B(III/i)	B(IV/i)	B(V/i)
0	1.30	1.30	1.30	1.30	1.30
0.2	0.93	1.01	1.10	1.19	-
0.5	0.90	0.98	1.06	1.15	1.08
1.0	0.90	0.95	1.02	1.11	1.04

It was not feasible to validate these critical radii values with experimental evidence. It is possible to obtain images of approximately $1\mu\text{m}$ with the stereo microscope but due to the incompatibility between the components, initial nuclei with a minimum size of circa $10\mu\text{m}$ were only observed. In the search for a method to measure nuclei of $1\mu\text{m}$ and smaller, two-colour back scattering was implemented (see section 3.4.). However, as

nucleation took place over a period of time, resulting in various sizes of nuclei, an unhelpful, complicated feed back was obtained.

For the calculation of the free energy, ΔF , we assume, for simplicity, homogeneous nucleation. Fig. 3-40 shows the free energy associated with the homogeneous nucleation, lying in agreement to free energy diagrams in the literature^{24,69}. The curves are obtained from the second and third terms of equation 6:

$$\Delta F = 4\pi r^2 \gamma - (\Delta P_0) \left(\frac{4}{3} \right) \pi r^3 \quad (56)$$

Since the interfacial term increases with r^2 and the volume free energy increases with r^3 , the formation of small bubbles always leads to a free energy increase until the radius of the bubble nucleated is larger than the critical size. Also shown in the diagram is the maximum free energy, ΔF^* associated with the critical radius r^* . With the aid of equation 9 and the calculated critical radii in Table 3-12, the maximum free energy for the systems studied in this work was calculated, the results of which are tabulated in Table 3-13.

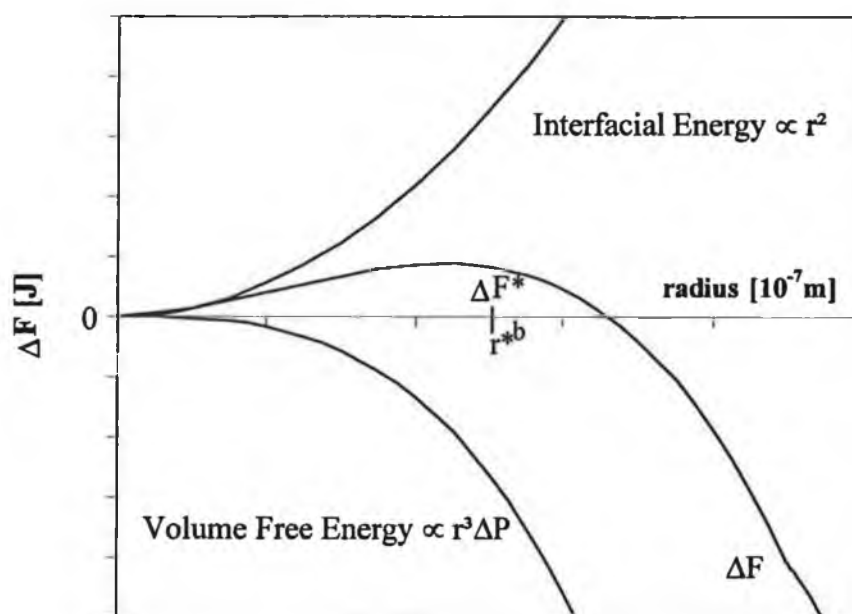


Fig. 3-40: The free energy change ΔF , associated with the homogeneous nucleation of a sphere of radius r as described in references 24, 69.

Table 3-13: The critical nucleus diameter values, $2r_b^*$, (from Table 3-12), free energy change, ΔF^* , associated with the homogeneous nucleation of a sphere of radius r_b^* and the nucleation rate, J , for systems foamed with A-components of B(I/i), B(II/i), B(III/i), B(IV/i) and B(V/i).

A-Component	$2r_b^*$ [μm]	ΔF^* [$1 \times 10^{-14} \text{J}$]
B(I/i)	0.90	5.56
B(II/i)	0.95	6.44
B(III/i)	1.02	8.02
B(IV/i)	1.11	10.40
B(V/i)	1.04	8.41

The critical nucleus diameters for the model A-components B(I/i), B(II/i), B(III/i), B(IV/i) and B(V/i) with 1% of their respective surfactant are tabulated above. The minimum work required for the formation of the critical nucleus, i.e. the free energy change was subsequently calculated from equation 9. Although the deviation in critical radii values is less than 20%, the maximum difference, between ΔF^* of B(I/i) and ΔF^* B(IV/i) is approximately 45%. Therefore, one would expect that the system foamed with the A-component B(I/i) would need less energy for the formation of critical radii than the system foamed with the A-component B(IV/i) and hence would have a greater nucleation number. If we look at Table 3-11 which gives the calculated nucleation numbers NZ_{cal} this proposition is verified – the nucleation number for the system foamed with the A-component B(IV/i) ($2.73 \times 10^5 [1/\text{g}]$) is less than the NZ_{cal} for the system foamed with the A-component B(I/i) ($3.73 \times 10^5 [1/\text{g}]$). However, as already pointed out this effectively ignores the coalescence which occurs in the unstable system B(IV/i). The in-situ analysis showed that in fact slightly high initial nucleation number was observed for B(IV/i), the results which are compared to the calculated nucleation numbers in Table 3-10.

In this way the in-situ results contradict theory. This is possibly due to the inclusion of a surface tension dependency in the theory. However, as shown in the previous section the nucleation number is not dependent on the surface tension value. In other words, a low surface tension, resulting in a low critical radius value and consequently a lower free energy is not a prerequisite for an increase in nucleation numbers.

3.5.7. Effect of Catalyst Amount on the Nucleation Process

The catalyst (i) was varied in the system B(I/i) producing foams with the following cream times: 30s, 45s, and 60s. See Appendix 1 for a detailed description of the formulations. Gel times were 115s, 135s, and 200s respectively. Increasing the catalyst amount leads to increased reaction times. This was observed in the rate of temperature rise, the pressure measurements, and the earlier gel times, the results of which are tabulated in Table 3-14. Decreasing the nucleation time lead to a larger pressure difference over a shorter period of time leading to the simultaneous nucleation of more nuclei, increasing homogeneity. This was reflected in the in-situ studies, reflected in the photomicrographs in Fig. 3-44. Although differences in the average nucleus size were negligible as can be seen in Fig. 3-42, a comparison in Fig. 3-41 of the relative distributions of the nucleus diameter at their cream times show a narrow distribution at 30s which broadens with increasing cream time. However, relative distributions at the gel time overlapped indicating no influence on the end cell size. The nucleation number increased slightly as illustrated in Fig. 3-43, however, this difference is greater than 20% and is therefore considered significant.

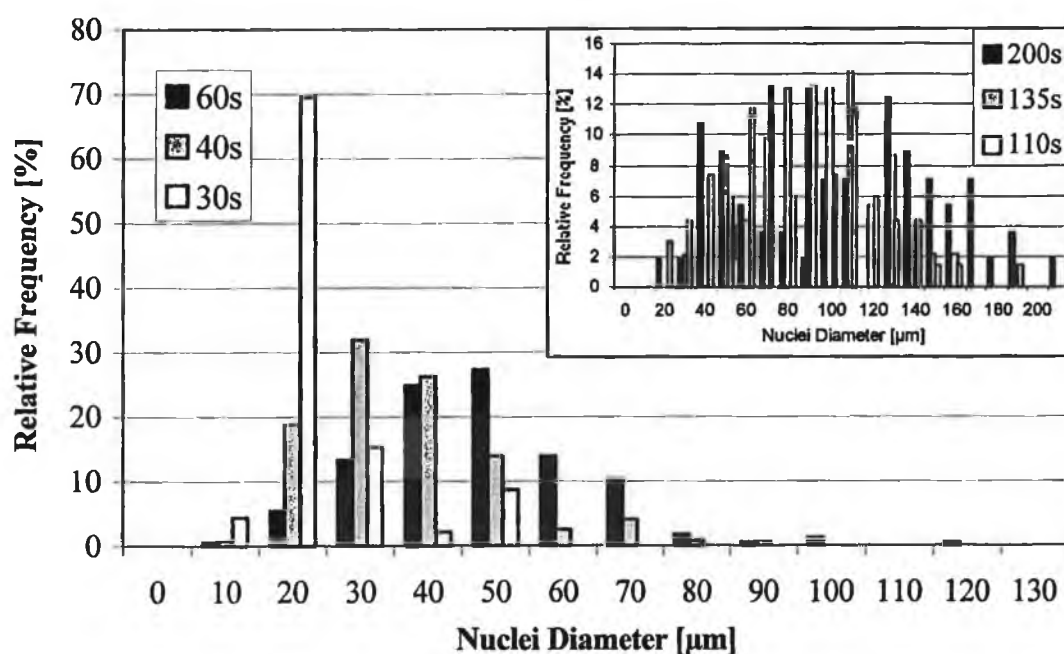


Fig. 3-41: Relative distribution of the nucleus diameter at cream times of 30s, 45s, and 60s. Inlay shows the relative distributions of the said systems at their respective gel times.

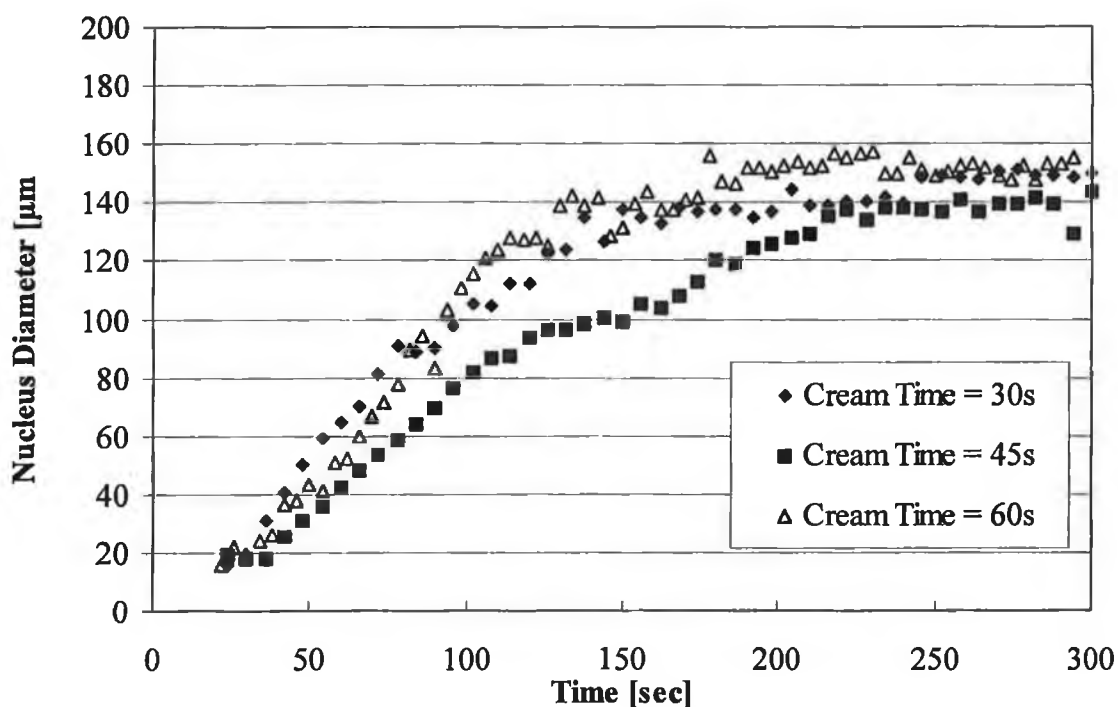


Fig. 3-42: The average nucleus diameter with respect to time during foaming with the A-component B(I/i) with 1.8%, 1.4% and 0.8% catalyst i, dimethyl cyclohexylamine. This resulted in cream times of 30s, 45s and 60s with gel times of 200s, 135s and 110s.

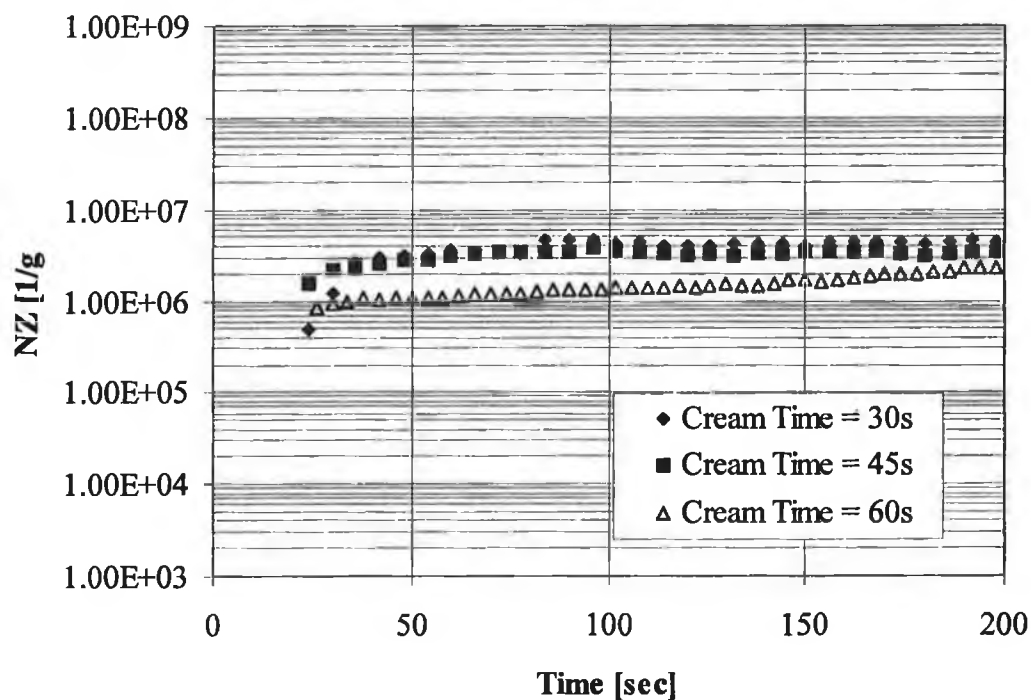


Fig. 3-43: The average nucleation number with respect to time during foaming of the A-component B(I/i) with various amounts of catalysts as describe in Fig.3-42.

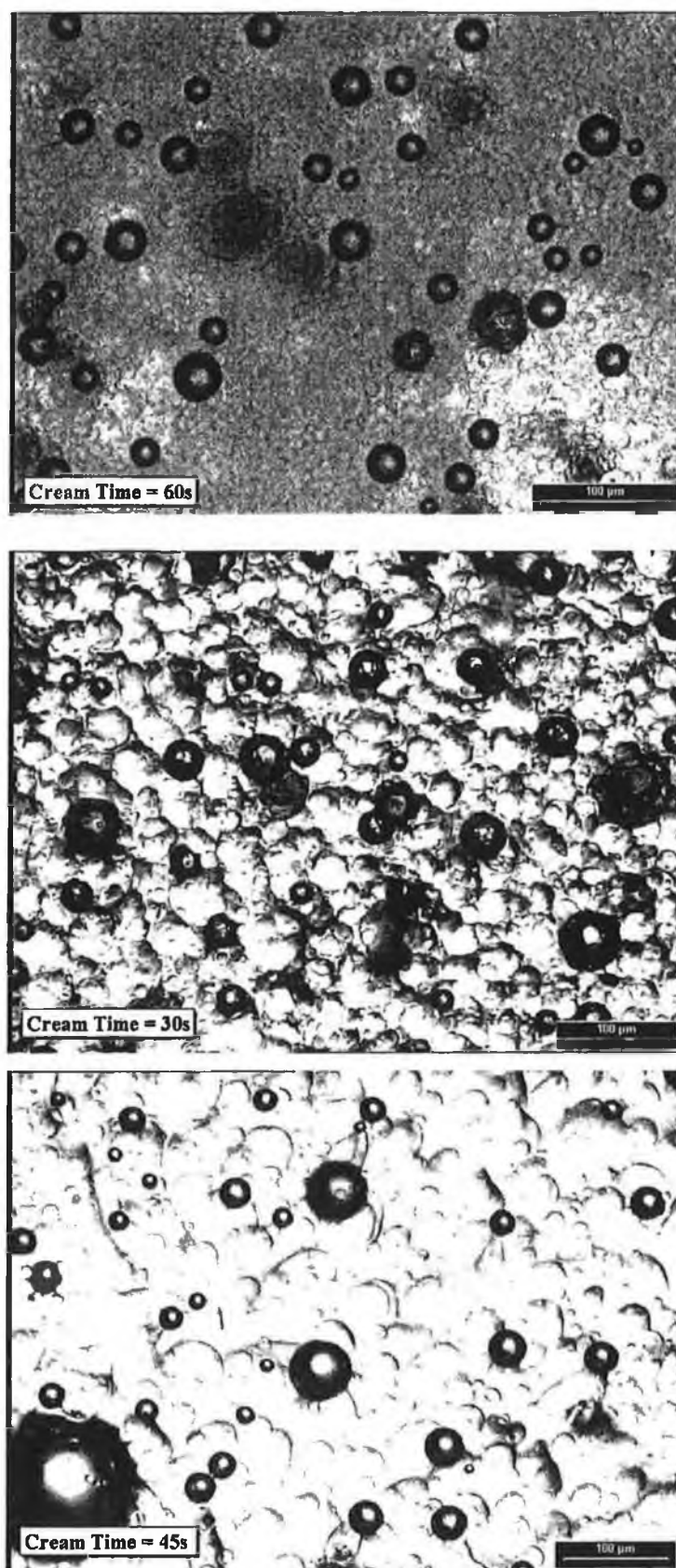


Fig. 3-44: Photomicrographs of system B(I/i) with various amounts of catalysts at their respective cream times. (top 1.8%, middle 1.4% and bottom 0.8% catalyst). Increasing the catalyst decreases the cream time resulting in slightly more nuclei of the same size.

Table 3-14: The effect of different amounts of catalyst (different cream and gel times) on the surface tension, δ , end cell diameter, d , and the mathematical estimation of the nucleation number, NZ_{cal} as described in section 2.10.

Catalyst [%]	Cream Time [s]	Gel Time [s]	δ [mN/m]	d [μ m]	NZ_{cal} [1/g]
1.8	30	115	22.80	423.5	4.23×10^5
1.4	45	135	22.60	428.3	4.18×10^5
0.8	60	200	22.57	444.7	3.73×10^5

Next we needed to establish whether the catalyst amount has an effect on the surface activity of the polymer. This was tested by measuring the surface tensions of the A-components B(I/i) with various amounts of the catalyst i with 1% surfactant the results of which are tabulated above. The amount of catalyst in the A-component exhibits no effect on the surface tension of the system with surface tension values of 22.53 ± 0.23 mN/m. The end cell diameter and calculated nucleation number (NZ_{cal}) are also given in Table 3-14, showing a significant difference (see section 2.10.) between foaming with a cream time of 30s and 60s. It was shown that the quicker the cream times and gel times the finer the cells in the end foam. This tendency is also apparent in the in-situ analyses.

Table 3-15: The faster the maximum temperature (T_{max}) and the maximum pressure (P_{max}) are obtained the larger the nucleation number. T_{max} and P_{max} measured as in section 3.2.2.

Cream Time [s]	Gel Time [s]	Time T_{max} [s]	Time P_{max} [s]	NZ_{cal} [1/g]
30	115	290	120	4.23×10^5
45	135	417	180	4.18×10^5
60	200	555	270	3.73×10^5

Increasing the catalyst amount increases the rate of reaction producing foams with quicker cream and gel times (Table 3-15). The maximum temperature of approx. $150 \pm 40^\circ\text{C}$ and maximum pressure of approx. $0.08 \pm 0.03\text{MPa}$ are also obtained quicker. This quicker pressure difference over a shorter period of time improves the homogeneity of the nucleation. This authenticates results obtained from the in-situ analyses.

3.5.8. Effect of Catalyst Type on the Nucleation Process

The type of catalyst in system B(I/i) was varied maintaining a cream time of 60s and a gel time of 200s. See Table 2-5 in section 2.8.6. for the structural details of the catalysts implemented and Appendix 1 for clarification of the A-components B(I/ii), B(I/iii), B(I/iv). When dibutyl tin dilaurate (catalyst iv) was used and a cream time of 60s was set a rise time of 75s followed. Setting the gel time to 200s resulted in moving the cream time to 175s. However, since a time of approximately 150s had elapsed from the time the sample was placed under the microscope until cream time, the sample (which had cream time of 175s and a gel time of 200s) had lost the reaction energy to foam and so no analysis could be carried out. This highlighted one of the restrictions of the method - the cream time must be fast enough (35s) to allow visualisation of the initial nuclei but also slow enough (60s) so as to promote foaming.

Analysis of the foaming of the A-components mentioned containing various showed deviations in the nucleation number. The observed end nucleus size varied significantly from each other with values of $120\mu\text{m} \pm 25\mu\text{m}$ as shown in Fig. 3-45. In search for an explanation the chemical structure of the catalysts needed to be examined.

The catalytic activity of the catalysts depends on their strength as a base and / or their nucleophilic strength, i.e. the strength of the electron pair on the nitrogen in the amino group. Therefore, one would expect that catalyst ii, 2,2,2-diazabicyclooctane, with its two pairs of lone-pair electrons, one on each side, which are sterically unhindered, would be ideal. Results from the in-situ study show an improvement in nucleation number when compared to the initial less basic catalyst dimethyl-cyclohexylamine. The 2,2,2-diazabicyclooctane average nucleus size at gel time (200s) is halved from circa $160\mu\text{m}$ to circa $80\mu\text{m}$ with B(I/i) (Fig. 3-45) but has a larger nucleation number per gram (Fig. 3-46). What would happen if this sterically favourable catalyst could be built into the polymer network? For this purpose catalyst iii, 2-(2-hydroxyethoxyethyl)-2-azanorbornane was examined. This catalyst has a nitrogen (one lone-pair) less than catalyst ii and the hydroxy group on the ethoxylated carbon chain increases the polarity of the compound. It is sterically unhindered and can take part in the polymer formation due to the presence of the active hydrogen atom in the molecule.

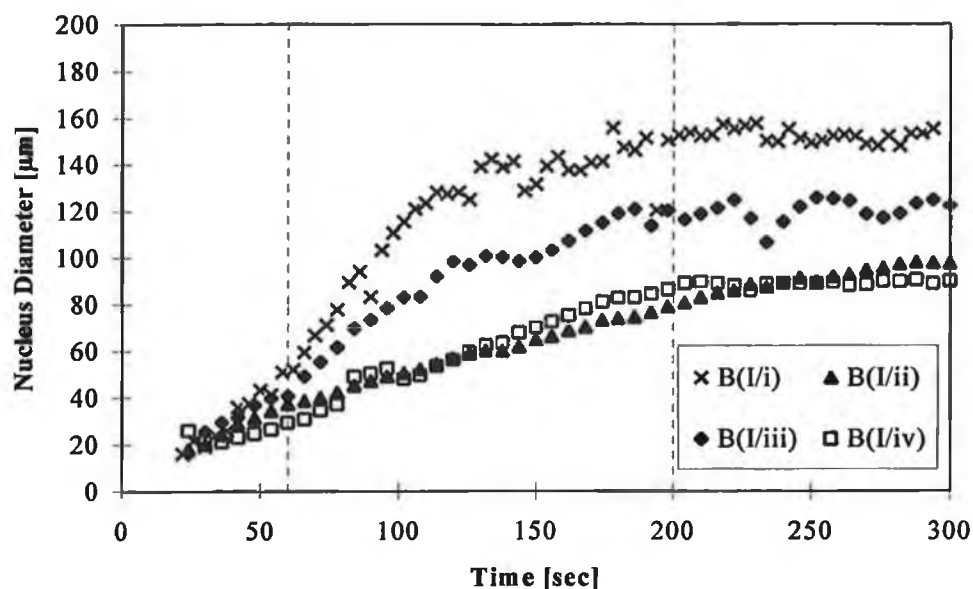


Fig. 3-45: The nucleus diameter measured with respect to time indicating the influence of the various catalysts as discussed in the text. Cream time and gel time were 60s and 200s for all foams except B(I/iv) which were 60s and 75s respectively. Density of all foams \approx 55g/l.

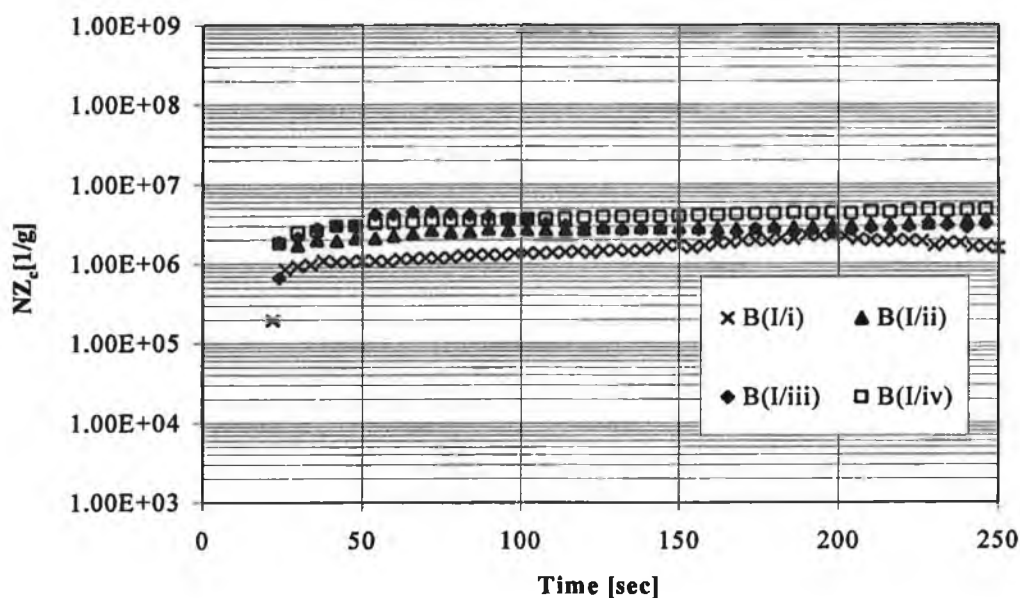


Fig. 3-46: The influence of the catalyst type on the nucleation number (NZ_c). Cream time and gel time were 60s and 200s for all foams except B(I/iv) which were 60s and 75s respectively. Density of all foams \approx 55g/l.

Although the nucleation number (Fig. 3-46) are similar for both systems B(I/ii) and B(I/iii), catalyst iii results in comparatively larger nuclei (Fig. 3-45). The organo-tin complex catalyst iv, dibutyltin dilaurate, is traditionally implemented in flexible foams and is known to enhance the nucleation¹. The microscopic analysis shows, in the case of polyurethane rigid foam, that although dibutyltin dilaurate had the greatest nucleation number as illustrated in Fig. 3-46 (however, comparatively minimal) and the finest cell structure (Fig. 3-45), it does not induce excessive nucleation as expected.

Overall one can deduce that the catalyst type has little influence on the nucleation number but the reactivity of the catalyst influences somewhat the nucleus size. As already mentioned, tertiary amines, such as in catalysts i, ii and iii affect both the isocyanate-hydroxyl and the water-isocyanate reaction, while, the dibutyltin dilaurate catalyst promotes primarily the isocyanate-hydroxyl reaction and chain propagation. Unfortunately, it was not possible within the scope of this work to ascertain from these experiments which process, if any, affects the nucleation process. This is a topic, which could be investigated in the future.

Catalysts are not surface active agents and therefore the type of catalyst used had no effect on the surface tension of the systems. This is however, not a prerequisite for nucleation. A direct relationship between the surface tension of a system and the nucleation number of that system foamed was not found in this work. The fact that the catalyst type influenced the size of the nuclei proves that nucleation is a complex process which is not surface tension dependent.

Table 3-16: *The effect of catalyst type on the end cell diameter and the nucleation number NZ_{cal} . Cream time and gel time were held constant at 60s and 200s.*

Catalyst Type	Cell Diameter [μm]	NZ_{cal} [1/g]
I	444.7	3.73×10^5
Ii	411.5	4.71×10^5
Iii	428.6	4.17×10^5
Iv	406.0	4.25×10^5

The cell diameter in the end foams were measured and subsequently the nucleation number (NZ_{cal}) was calculated. The results are shown in Table 3-16 above. These correlate quite well with nucleation numbers obtained from the in-situ analyses, however, the total trend being in a lower range.

3.5.9. Effect of Prepolymer on the Nucleation Process

Prepolymers are used in the production of flexible foams, ensuring complete reaction of all polyols and allowing the selective synthesis of a segmented chain structure through pre-organised structural units. The compatibility of the suitably chosen A- and B-components notably increases. This is primarily due to the decreasing percentage NCO available for reaction, leading to the complete reaction of all diols. As the compatibility has already proved to be of importance (see section 3.5.6.), the improvement of the compatibility of B(I/i) through the use of prepolymers and its effect on the nucleation process was investigated.

For this purpose three prepolymers were formed as described in section 2.8.8., the third one being however too viscous resulting in inhomogeneous mixing and was therefore not suitable for analysis. Table 3-16 shows the NCO values and the viscosity of the prepolymers used in this study.

Table 3-17: Characteristic values for the B-components used in this study.

B-component	Iscocyanate: Methanol	%NCO	Viscosity [mPa.s/25°C]
M 20A	100:0	31.50	201
Prepolymer 1	100:2	27.82	720
Prepolymer 2	100:4	24.80	3017
Prepolymer 3	100:6	21.91	>>5000

The A-component B(I/i) was foamed in the usual way using the prepolymers detailed in Table 3-17 as the B-components. An increase number of finer cells were nucleated with decreasing %NCO (Fig. 3-47) leading to nucleation numbers on a par with levels obtained with the perfluorohexane – blown (emulsion) system (Fig. 3-48). It was also observed that with decreasing %NCO there was an improvement in the compatibility between components A and B. This is clearly seen in the photomicrographs in Fig 3-49. This presumably aided the formation of an increase number of smaller nuclei as can be seen in Fig. 3-48. This increase of 60% was considered significant.

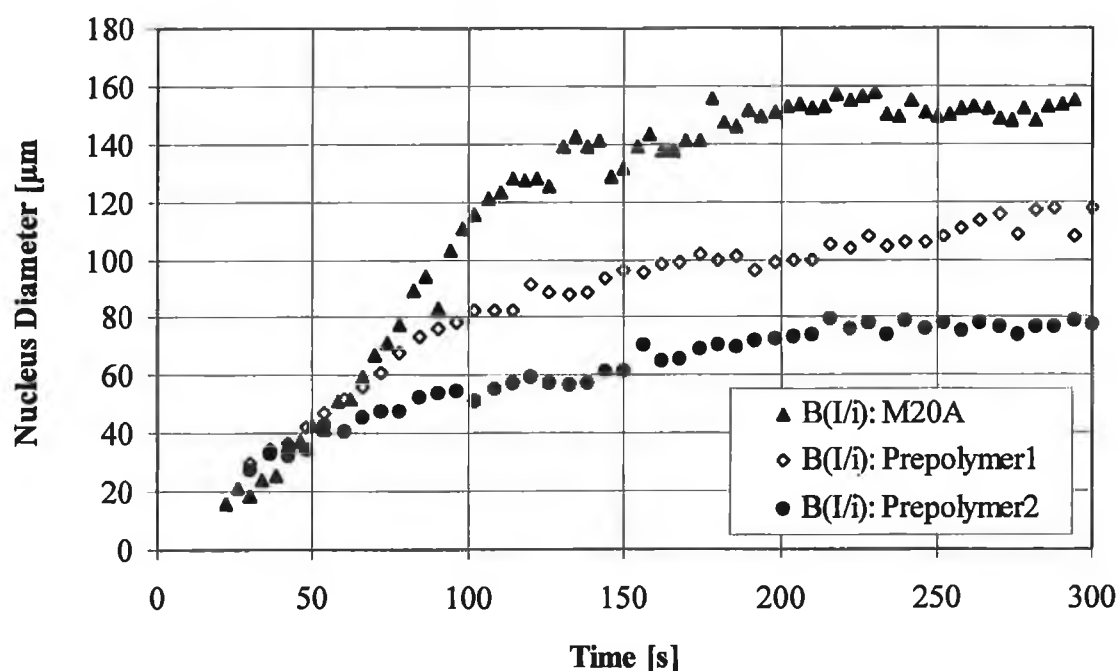


Fig. 3-47: The average nucleus diameter with respect to time for foaming of the A-component B(I/i) with the various B-components: M20A, prepolymer 1 and prepolymer 2. Cream time and gel time for all foams were 60s and 200s. Density of all foams $\approx 55\text{g/l}$.

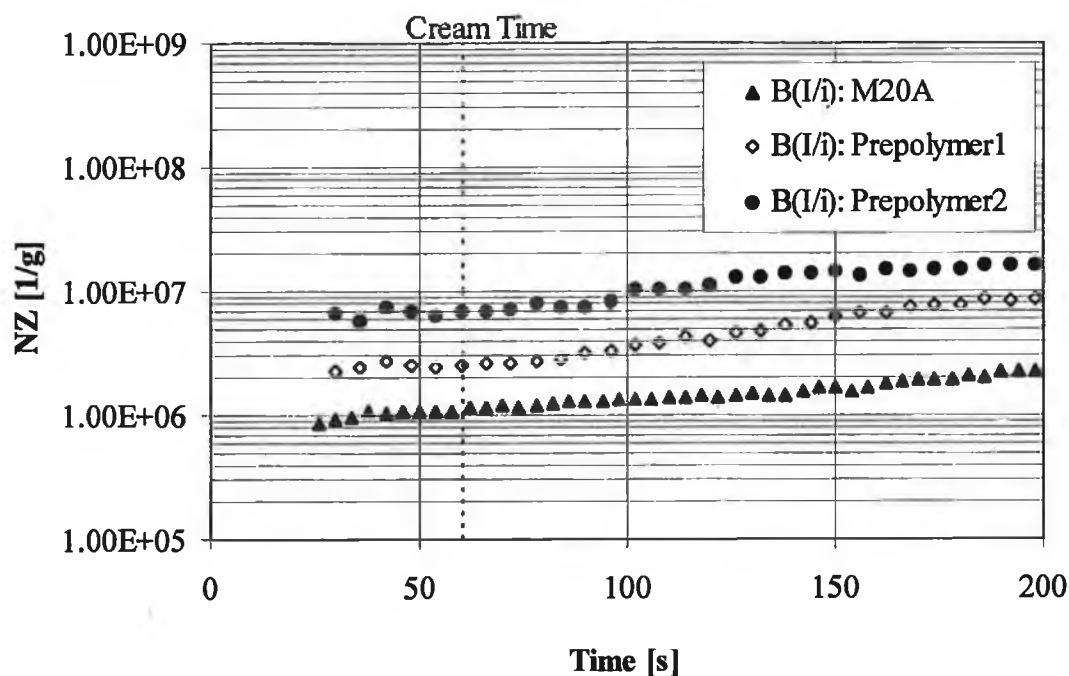


Fig. 3-48: The nucleation number [1/g] with respect to time for foaming of the A-component B(I/i) with the various B-components as discussed in Fig. 3-47. Cream time and gel time for all foams were 60s and 200s. Density of all foams $\approx 55\text{g/l}$.

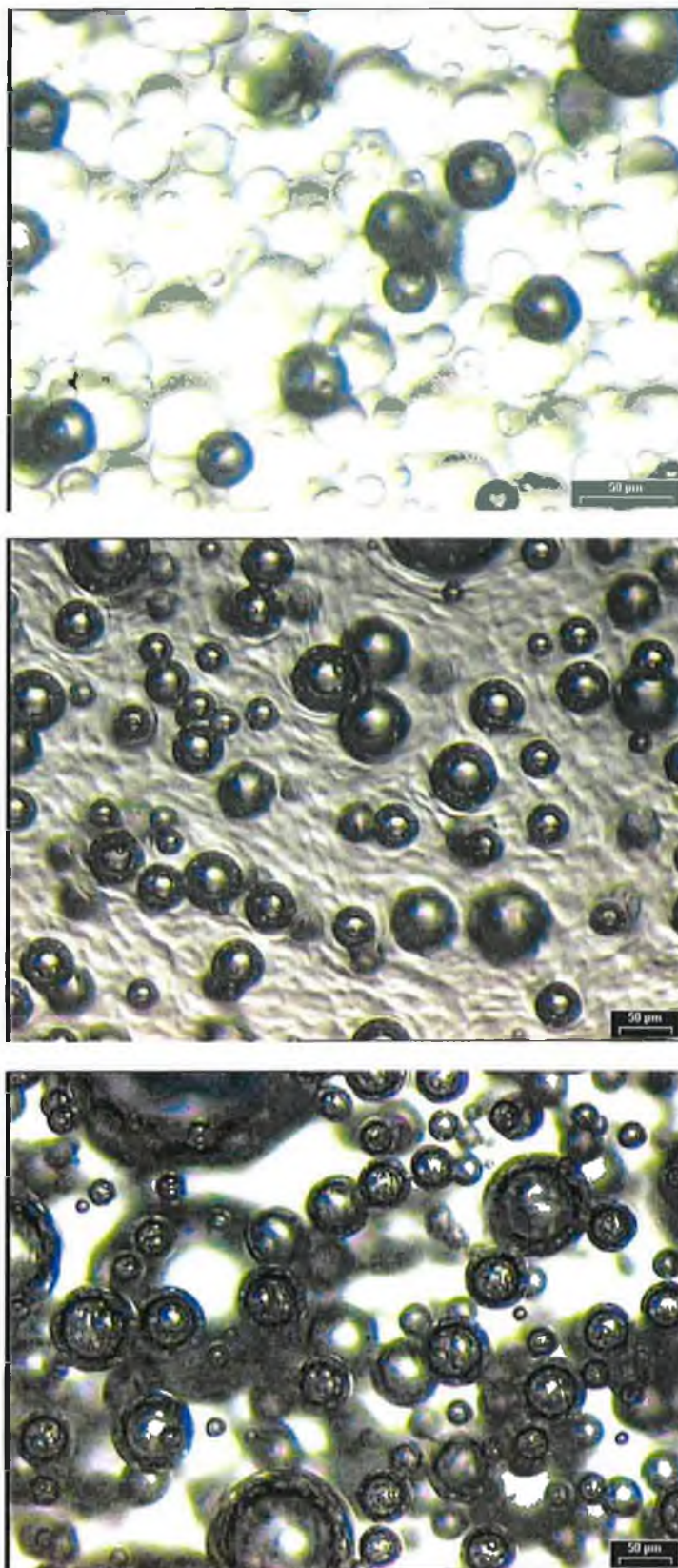


Fig. 3-49: Photomicrographs of the foaming of the A-component B(I/i) with the various B-components Isocyanate (top), prepolymer 1 (middle) and prepolymer 2 (bottom) taken at cream time (60s). Increase compatibility with decreasing free NCO%.

This prompts a method in producing finer cells. Of course, other foam properties such as mechanical strength, its ability to flow etc. would also be altered, the realms of which could form the bases of a further study.

The surface tension of the B-components with and without surfactant were measured. Here it was noted that the surface tensions of the various B-components remained relatively constant ($47\text{mN/m} \pm 1\text{mN/m}$). The addition of the surfactant reduced the surface tension in all cases, however, increasing the value from 23.2mN/m to 30.6mN/m , with decreasing %NCO. These results are illustrated in Fig. 3-50, where the surface tension of the A-component B(I/i) is also depicted. As already stated the compatibility of the two components increases with decreasing free %NCO. This is despite an increase in the difference in surface tensions between the A- and B-component. Logic would expect that components with similar surface tensions would be more compatible.

Correlating these results with the nucleation numbers obtained, again contradicted theory¹⁰ by showing an improvement in nucleation with decreasing %NCO despite an increase in surface tension.

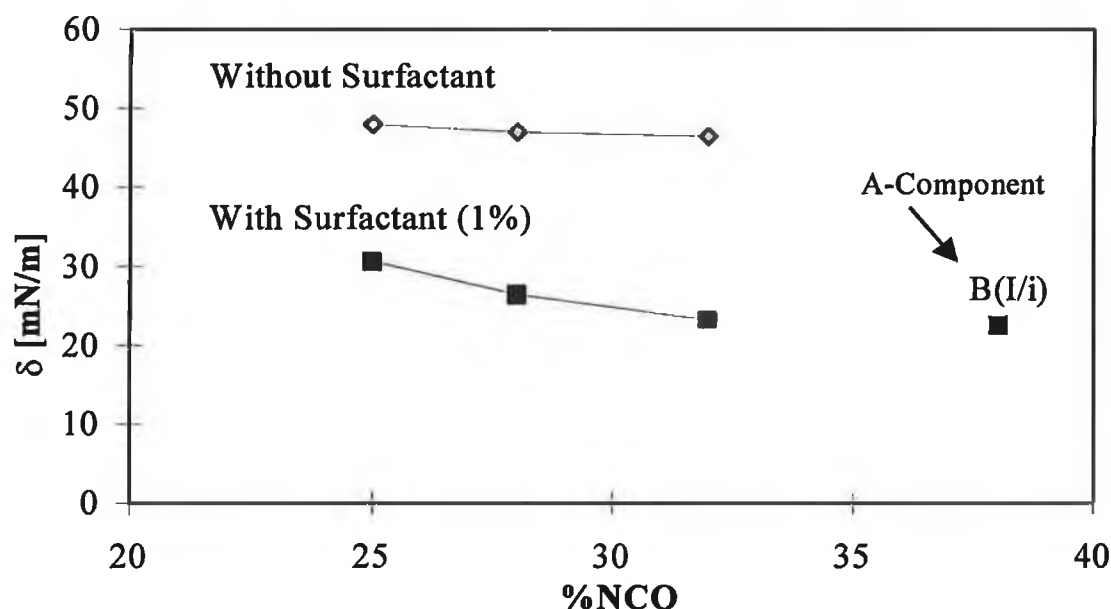


Fig. 3-50: The surface tension of the B-components with and without 1% of surfactant I. The A-Component, B(I/i), has a surface tension of 22.57mN/m .

Table 3-18: *Effect of the prepolymer on the end cell diameter and the estimated nucleation number (NZ_{cal}). Each sample foamed with B(I/i).*

Prepolymer	Cell Diameter [μm]	NZ_{cal} [1/g]
M 20A	444.70	3.73×10^5
Prepolymer 1	384.17	5.79×10^5
Prepolymer 2	373.07	6.45×10^5

The end cell diameter was measured as described in section 2.9. from which the NZ_{cal} was calculated (see Table 3-18). These lay in good agreement (although having a lower tendency) with the experimental results. The calculated nucleation number increased with decreasing free %NCO from 3.73×10^5 [1/g] to 6.45×10^5 [1/g]. These calculated nucleation numbers are comparable to that of the system foamed with the A-component C(VI/i) which exhibited the homogeneous nuclei and as a result the finest cell structure. It had a calculated nucleation number of 1.63×10^6 [1/g] (see Table 3-7).

The implementation of prepolymers proved to be a valid method in improving the nucleation number of the foaming process. This was as a direct result of the increase compatibility due to the reduction in the percentage free NCO. Further compatibility studies of various B-components is recommended.

3.5.10. Influence of Filler on the Nucleation Process

Heterogeneous nucleation at the liquid/liquid interface is the main type of nucleation in the foaming process²⁰. Another type of nucleation that is possible is heterogeneous nucleation at a solid/liquid interface. These interfaces are produced by the insertion of organic fillers into the A-component. Fillers are not generally used in polyurethane rigid foams because they negatively influence the mechanics of the foam and cause problems such as abrasion in the machines on the production line.

All A-components analysed were clear, eliminating the possibility of a dispersion, which could induce heterogeneous nucleation at a liquid/solid interface. Fillers, latex and graphite, were added separately to two A-components of the type A(I/i) and subsequently reacted with the B-component in the usual manner.

The presence of a filler had no effect on the initial number of nuclei regardless of type. This can be seen in Fig. 3-52. The size of the nuclei remained similar up until cream time (Fig. 3-51), when the rate of growth deviated resulting in diameter size differences at gel time from circa 140 μ m for the system without a filler to 110 μ m and 70 μ m for the systems with latex and graphite respectively. This indicates that the presence of a filler does not influence the nucleation process but effects the subsequent stabilising of the nuclei, spatially hindering foam growth.

It was not possible to ascertain whether the nuclei were formed at a liquid/liquid interface or a liquid/solid interface. Interesting was to note that the graphite gathered in the struts of the foam aiding the homogeneity of the cells by acting as a form of scaffolding for the cell structure. Unlike the graphite (7 μ m), it was not possible to observe the latex itself (0.3 μ m) under the microscope as the limit of observance is 1 μ m.

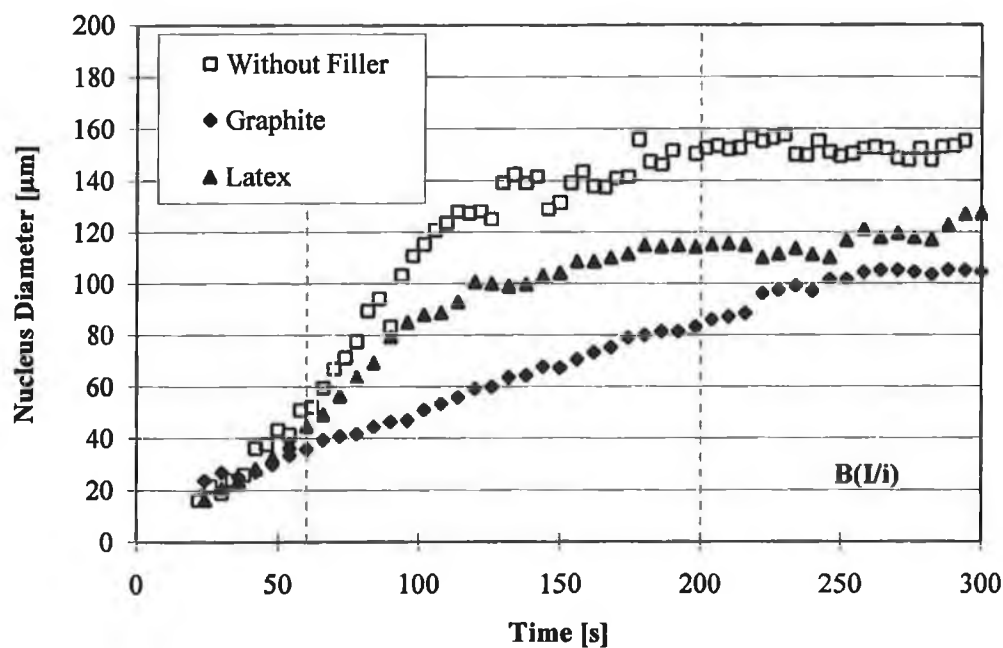


Fig. 3-51: The average nucleus diameter with respect to time for the foaming of the A-components B(I/i) containing 1% filler, graphite and latex. Cream time and gel time are 60s and 200s respectively; density $\approx 55\text{g/l}$.

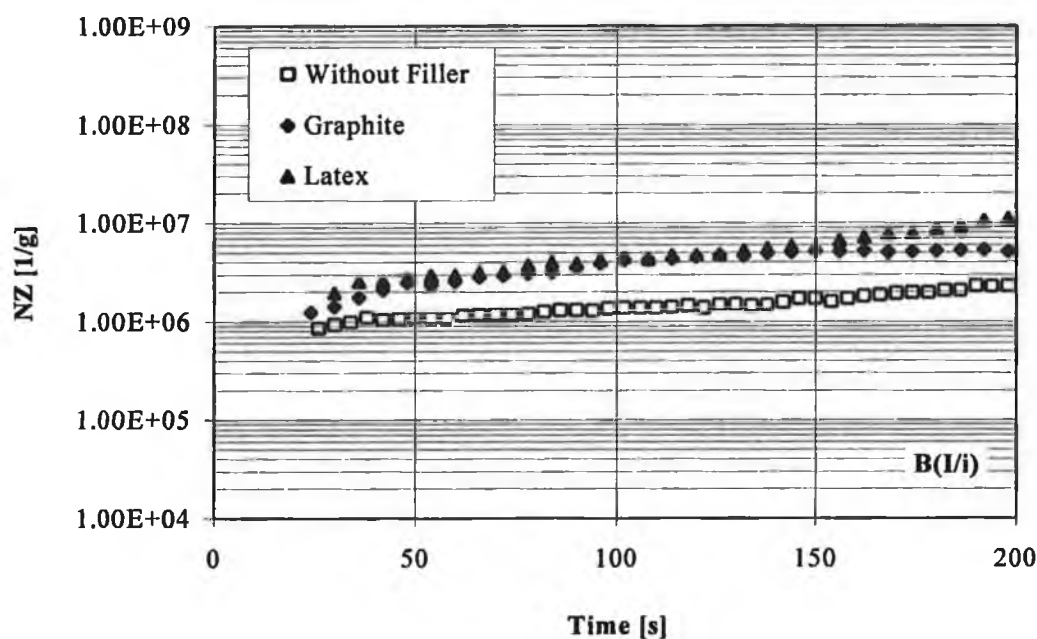


Fig. 3-52: The nucleation number with respect to time for the same system as described in Fig. 3-51. Cream time and gel time are 60s and 200s respectively; density $\approx 55\text{g/l}$.

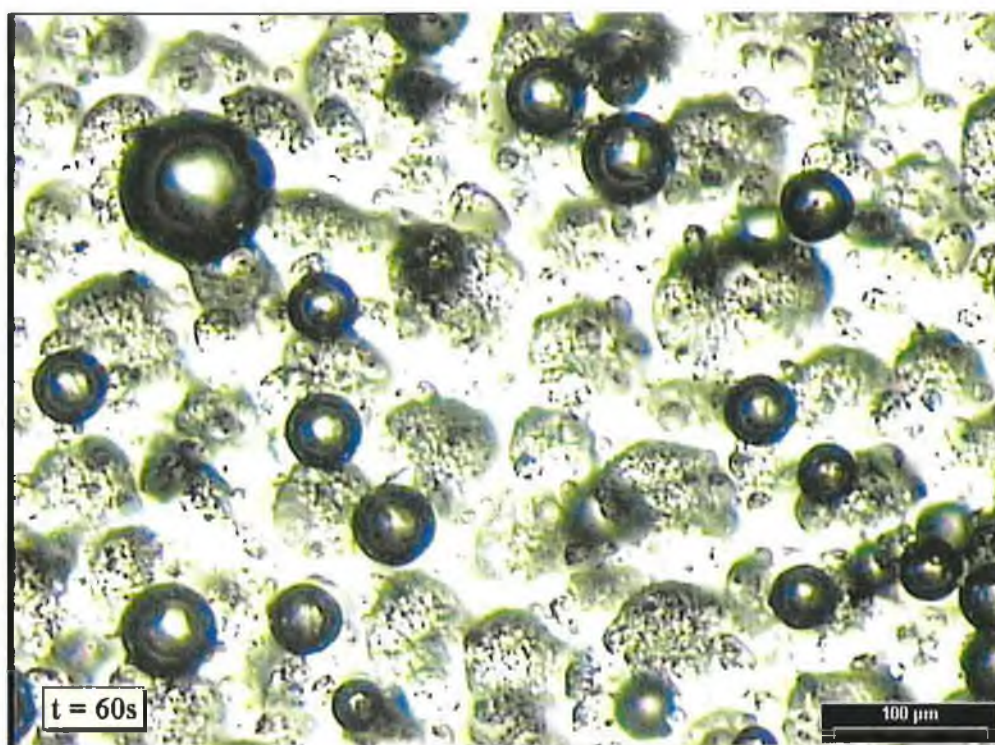
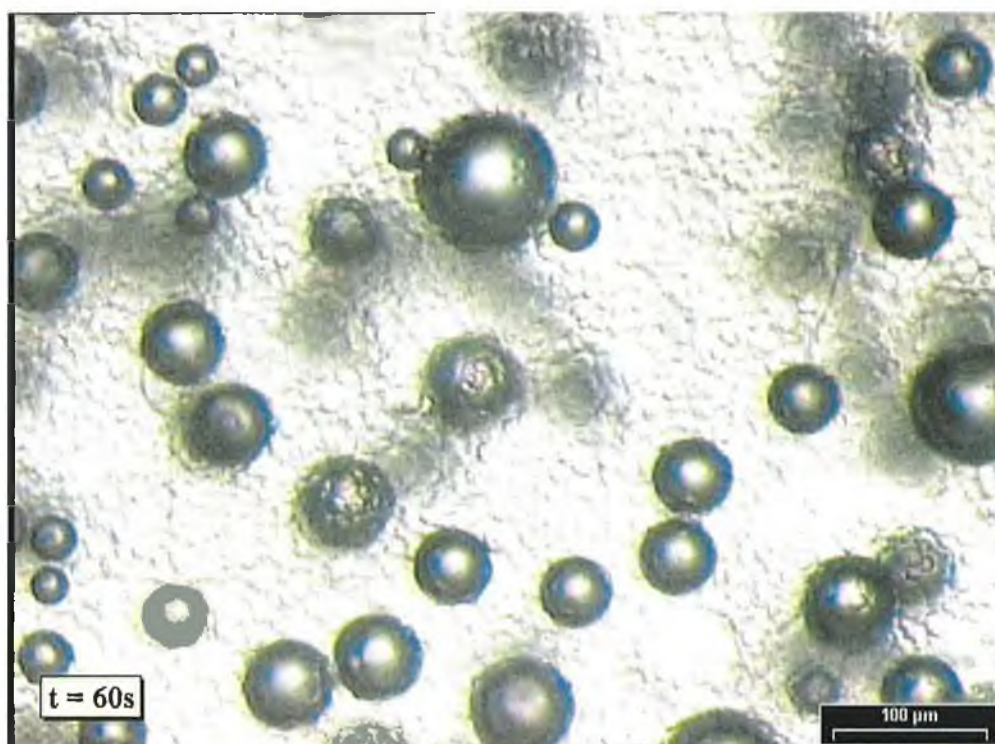


Fig. 3-53: Photomicrographs indicating the effect of a filler on the nucleation process; top: latex, bottom: graphite. The black graphite is clearly seen however, the latex size ($0.3\mu\text{m}$) prohibits its observation.

Table 3-19: *The effect of a filler on the surface tension, δ , cell diameter and calculated nucleation number.*

Filler	δ [mN/m]	Cell Diameter [μm]	NZ_{cal} [1/g]
No filler	22.57	444.47	3.74×10^5
Graphite	22.80	416.77	4.54×10^5
Latex	22.72	427.72	4.50×10^5

The presence of filler had a negligible influence on the surface tension with an average value of 22.70mN/m. The surface tension values are tabulated (see Table 3-18) along with the measured end cell diameters and the calculated nucleation numbers. The values, however, are not consistent with the initial nucleation numbers obtained from the in-situ study but reflect the end cell diameter tendencies. This is a direct result of using the end cell diameters for the calculation, which, as already stated, effectively ignores processes prior to curing.

3.5.11. CO₂ Solubility

As described in the theoretical section (section 1.5.1.) the gas dissolution stage is the first step in forming nucleation sites. The solubility of CO₂ was analysed to establish the dependency of the amount and/or type of surfactant in the system on the formation of these nucleation sites. The solubility is considered as the maximum concentration of gas in the polymer.

Implementing the IR method as described in section 2.14., the following three A-components were analysed: The A-component A(0/i) containing no surfactant, A-components A(I/i) and A(II/i). Particular emphasis was placed on the CO region of the spectrum i.e. between 2360-2300 cm⁻¹.

Table 3-20: *The effect of the surfactant on the solubility of CO₂. The A-components A(0/i)(without surfactant), A(I/i) and A(II/i) were analysed as described in the text.*

Sample	Surfactant [%]	Extinction 2360-2300cm ⁻¹	Integration 2360-2300cm ⁻¹
A(0/i)	0	0.989	7.464
A(I/i)	1	0.960	7.234
A(II/i)	1	0.988	7.429

A comparison of the spectra to their respective background spectra showed no increase in the CO peak (see Fig. 3-54) and therefore no influence from the surfactant was established. Integration of all three peaks resulted in equal areas under the curves (see Table 3-20), indicating no influence from the type of surfactant.

Perhaps the B-component influences the solubility of the CO₂. However, the analysis of the solubility of CO₂ in the B-component is limited as the isocyanate and CO₂ peaks overlap in an IR spectrum.

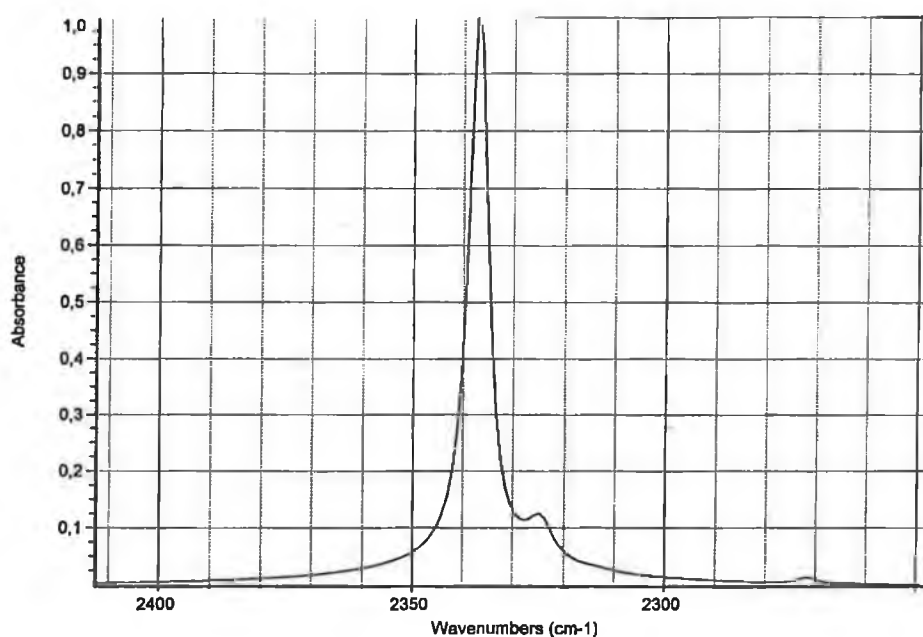


Fig. 3-54: The IR spectrum in the ranges between 2360-2300cm⁻¹ for the analysis of solubility of CO₂ in the A-components. Peaks for the three samples (A-components with and without surfactant) overlapped.

The results were verified by comparing them to those obtained from the method of partial pressures. It should be noted that three times the amount of surfactant was used in A(I/i) for this experiment so as to observe a dramatic difference between the samples. The initial values for the total pressure (0.011bar) were obtained from the vapour pressure analysis conducted as described in section 2.13. The solubility coefficient, α , was calculated using the following formula⁵⁸:

$$\alpha = \frac{w(\text{CO}_2)}{(p - p_0)} \quad (57)$$

where, p is the total pressure of the sample, p_0 is the vapour pressure of the sample and $w(\text{CO}_2)$ is mass of CO₂ in the liquid phase. This resulted in α -values of 0.00274bar⁻¹ and 0.00270bar⁻¹ for A(0/i) and A(I/i) respectively (see Table A10-1 in Appendix 10), i.e. the amount of surfactant has no influence on the solubility of carbon dioxide into the system. As can be seen from Fig. 3.55 this is valid for vapour pressures in the temperature range during nucleation, i.e. between 20°C – 40°C (see thermal analysis in section 3.2.2).

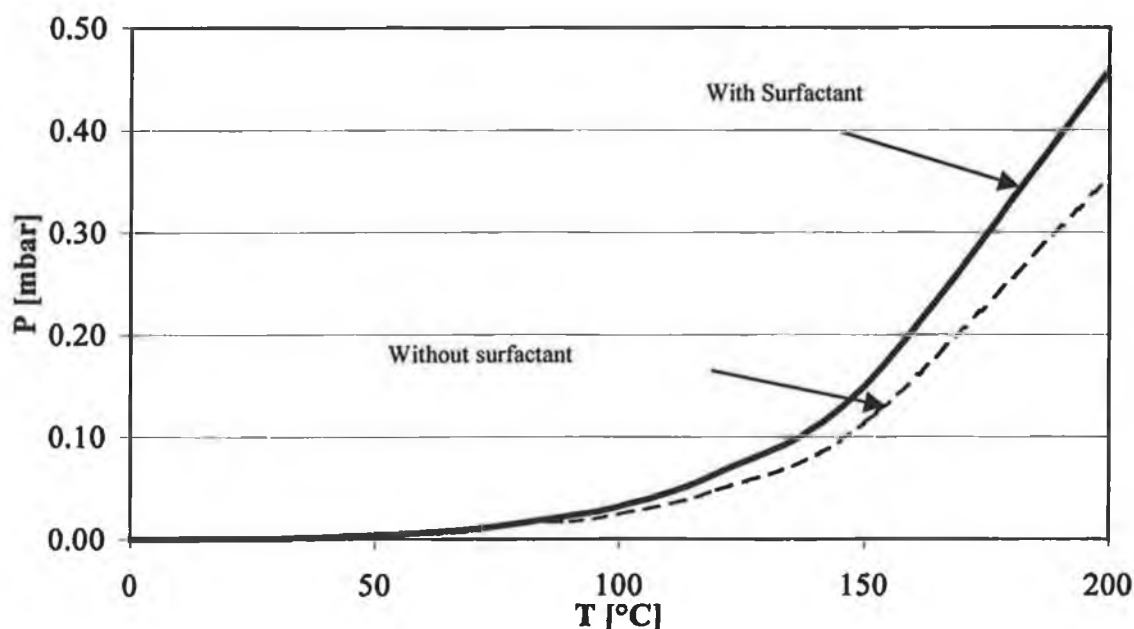


Fig. 3-55: Experimental values for vapour pressures of CO_2 in the A-component A(I/i) (with (3%) and without surfactant) across a given temperature range.

Deviations in vapour pressures occur only after circa. 100°C, which is normally reached after gel time. Therefore it is possible to deduce, supporting the IR results, that solubility of the blowing agent carbon dioxide in the A-component does not influence the nucleation process which is in the temperature range of 25°C.

3.5.12. Optimisations

As a consequence of the results obtained from the in-situ microscopic analysis developed in this work, the following systems were considered as a way of optimising the nucleation number.

The first method was an optimisation of the surfactants. It was proven that the surfactant has no influence on the nucleation process and that it is the surfactants emulsifying and/or stabilising abilities which effect the foaming process and consequently the end cell size. Therefore, the surfactants which showed the greatest emulsifying and stabilising ability, i.e. V and III were added in the ratio of 1:1 (total 1%) to the model A-component forming the new optimised A-component B(III:V/i). This optimised A-component was foamed with the B-component M20A under the usual conditions. Fig. 3-55 shows that the A-component B(III:V/i) resulted in similar initial nuclei sizes, again indicating that the surfactant has no influence on the nucleation process. The stabilising ability of the surfactant mixture improved the average nucleus size however not significantly. However, the foaming system was more stable than the system foamed with B(V/I) as the A-component as indicated by the constant nucleation number for the optimised system in Fig. 3-56

It has been found⁷⁰ that a complex interaction takes place between the surfactants and that it is not possible to simply “add together” positive properties of separate surfactants. This optimised system showed no increase in the nucleation number as would have been expected through the emulsification ability of surfactant V (as seen for the foaming of B(V/i) in Fig. 3-56 – middle photomicrograph). The foam’s overall stability improved from that of the unstable system B(V/i). Thus proving that the interaction between surfactants is complex and the addition of positive properties is not possible.

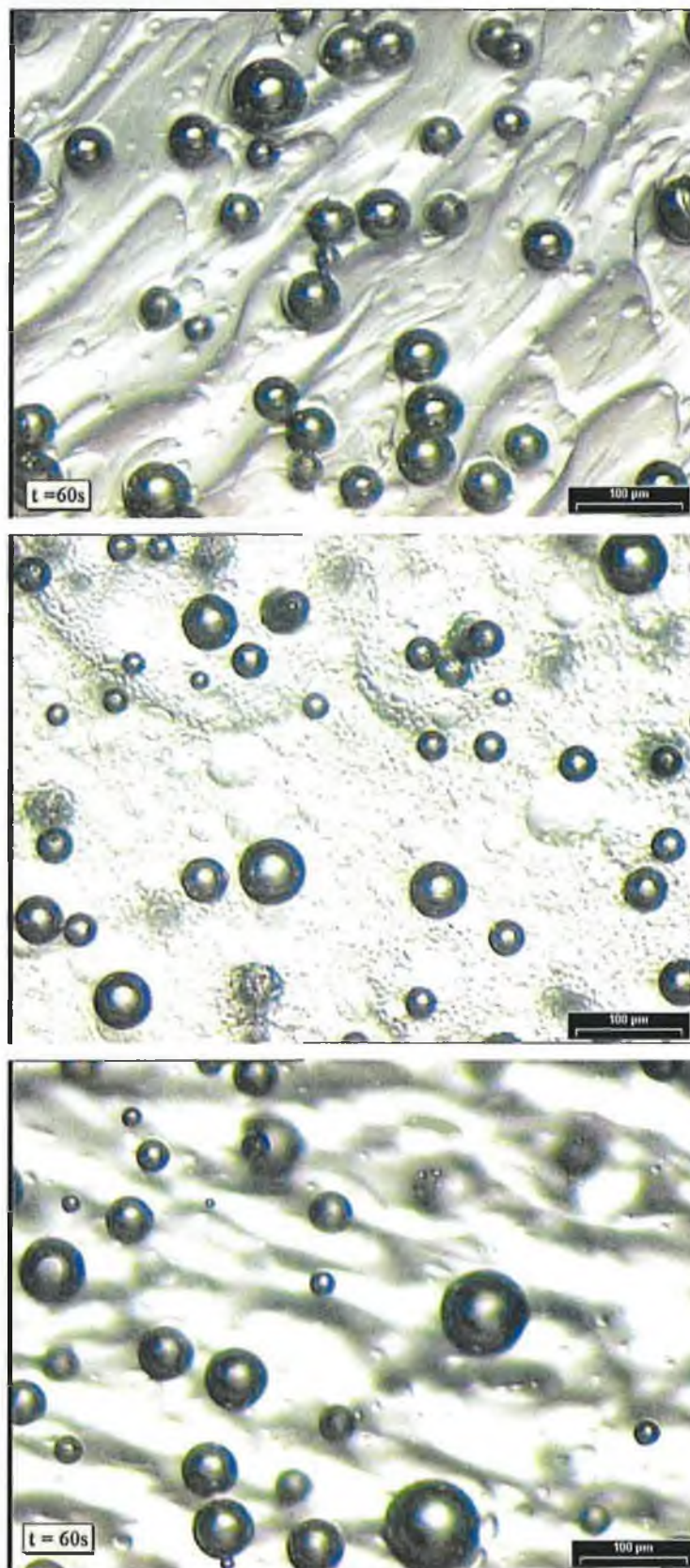


Fig. 3-56: Photomicrographs of the foaming of the A-component B(III/i) (top) and B(V/i) (middle) compared to the optimised A-component B(III:V/i) (bottom). All foamed with M20A as the B-component.

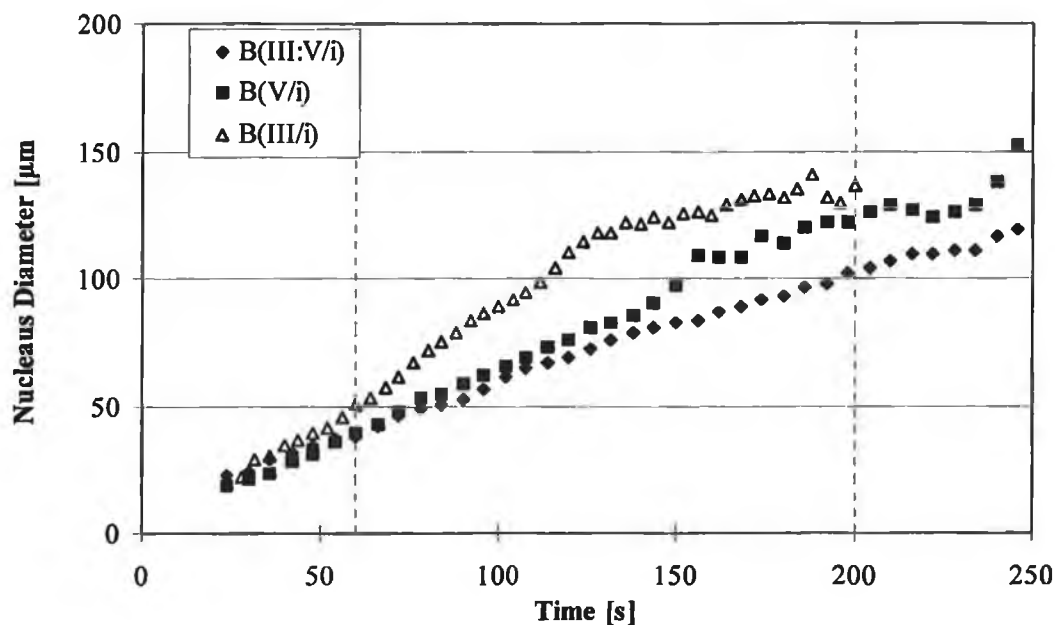


Fig. 3-57: Optimisation: The nucleus diameter with respect to time for foaming with a A-components containing 1% of surfactants III, V and a total of 1% of surfactants III:V. The B-component in each case was M20A. Cream time \approx 30s, gel time \approx 200s, density \approx 55g/l.

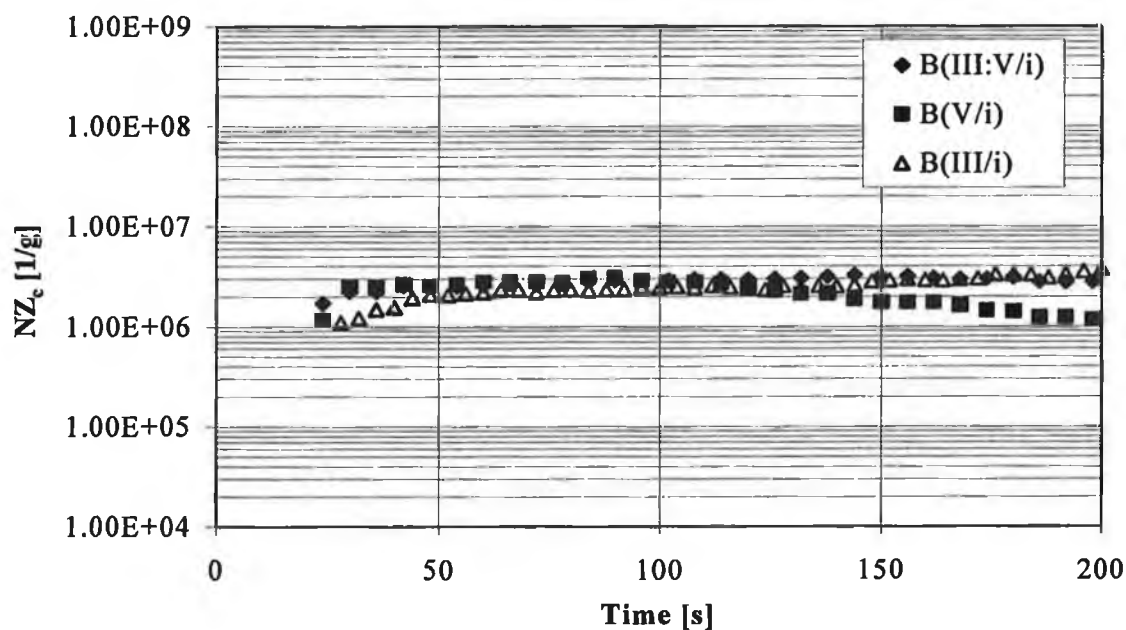


Fig. 3-58: Optimisation: The nucleation number (NZ_c) with respect to time for the foaming of the systems described in Fig.3-56. Cream time \approx 30s, gel time \approx 200s, density \approx 55g/l.

The possibility of increasing the nucleation number by improving the compatibility between A- and B-components was shown in the results obtained from the prepolymer studies. With this in mind a second optimisation was tested. Using prepolymer 1 as the B-component and B(V/i) as the A- component, surfactant V showing the most emulsifying tendencies of the surfactants analysed. Prepolymers also showed a stabilisation tendency. By exploiting the stabilisation ability of the former and the emulsifying ability of the latter it was hoped to produce a stable foam with a high nucleation number.

The A-component B(V/i) was foamed with prepolymer 1 as the B-component in the usual manner. As usual, cream time was set to 30s, gel time to 200s and the core density of the foam was 55g/l comparable to all other foams.

This optimisation led to the formation of the same number of initial nuclei as for the foaming of the A-component B(V/I) with M20A (see Fig. 3-60). The increase in compatibility between the A- and B-component is seen in Fig. 3-59. The improvement in stability is clearly visible in Fig. 3-60 and Fig. 3-61, totally eliminating coalescence and disproportionation which occurred during the foaming of the A-component B(V/i) with M20A as the B-component. End nuclei diameters in Fig. 3-60 and nucleation numbers $[NZ_c]$ in Fig. 3-61 are in the range of those obtained from the foamed system with B(I/i) as the A-component and prepolymer 1 as the B-component (see section 3.5.9).

As already stated in section 3.5.9. prepolymers are not implemented in polyurethane rigid foam formation as these delay curing. For our purposes these were implemented to study the effect of the improvement of compatibility between A- and B- components on the nucleation process. It has been proven that increase in compatibility improves the nucleation numbers. Further research should be carried out on other methods and foam formulations for the improvement of compatibility between A- and B- components.

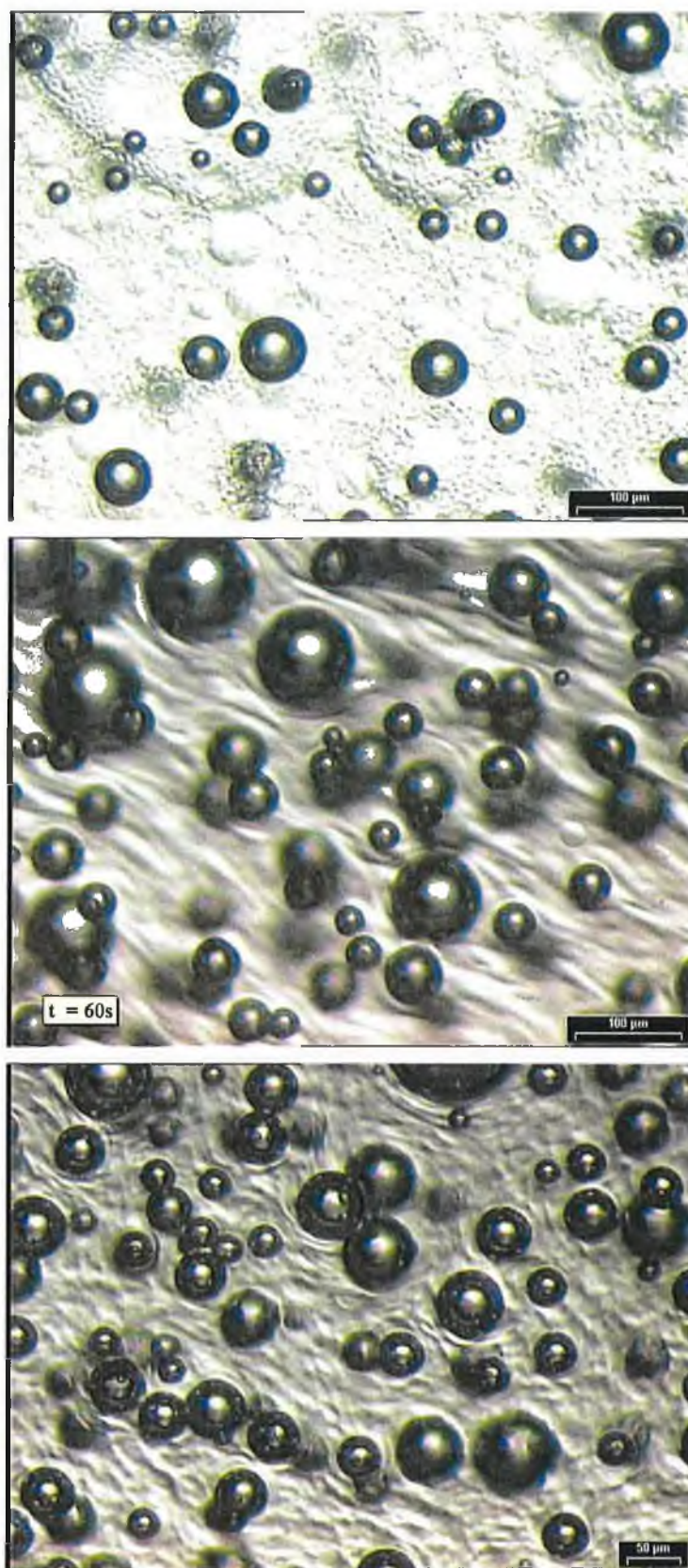


Fig. 3-59: Foaming with the A-component B(III/i), B-component M20A (top); the A-component B(I/i) foamed with prepolymer 1 (middle) compared to the optimised system of the A-component B(III/i) foamed with prepolymer 1 (bottom). Photomicrographs all taken at 60s.

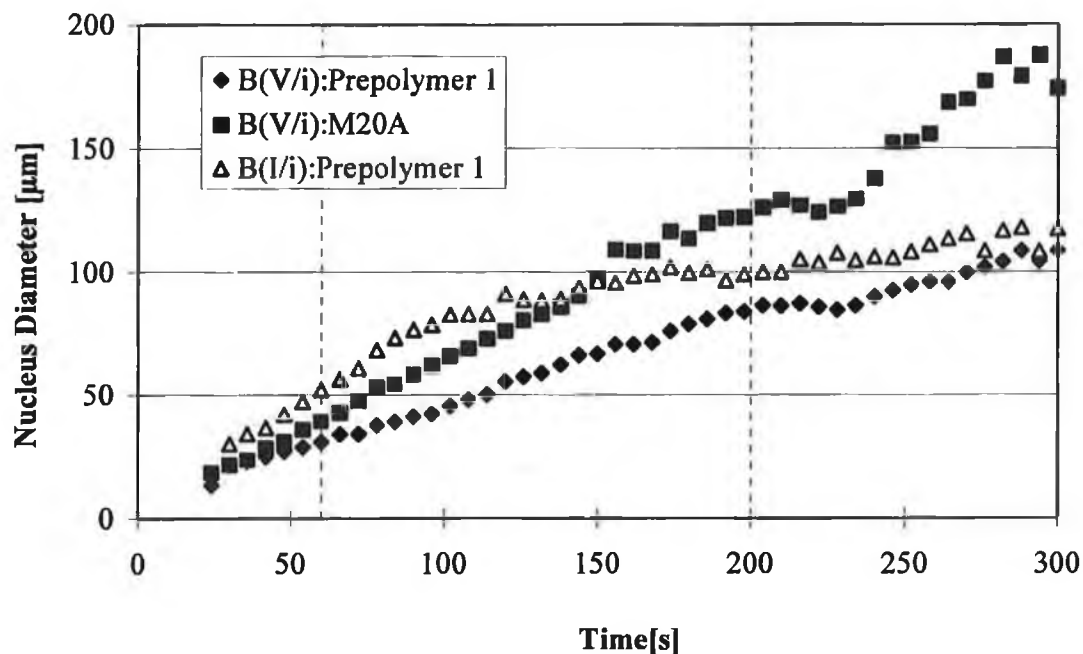


Fig. 3-60: The average nucleus diameter with respect to time for the foaming of the optimised system of the A-component B(V/i) with the B-component prepolymer 1. Cream time ≈ 60 s, gel time ≈ 200 s, density ≈ 55 g/l.

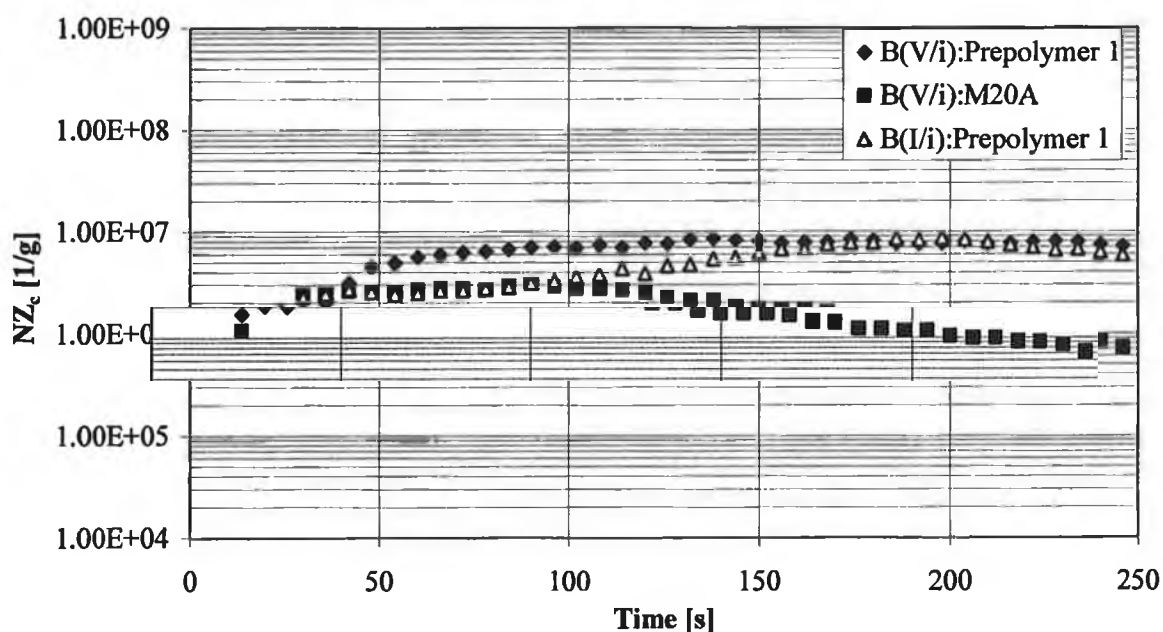


Fig. 3-61: The nucleation number (NZ_c) with respect to time for the foaming of the optimised system of the A-component B(V/i) with the B-component prepolymer 1. Cream time ≈ 30 s, gel time ≈ 200 s, density ≈ 55 g/l.

4.1. Applicability to Commercial Systems

Foaming in a beaker leads to foam cells which are larger than when foamed on the production line with high pressure machines. Nevertheless, beaker tests are used as a general overview for the characteristic times of foaming as well as for calculating core densities and measuring temperature and pressure reactions. During the in-situ analysis, however, only a sample from the beaker was analysed. Moreover, the A-components in this work were model systems with very slow reaction times, leading to the question – how applicable are the results to commercial systems? From the good correlation between the calculated nucleation numbers (which uses end cell values from the beaker) and the observed nucleation values it was proven that the results from the in-situ analyses are representative of the process which happens in the beaker test. However, more importantly, do these results represent values from the production line using commercial systems?

Firstly, we looked at the developed systems 1. Generation, 2. Generation and 3. Generation which are commercialised under the names Elastopor[®]H210/147, Elastopor[®]H2030/13 and Elastopor[®]H2030/40. These are thermal insulation foams for refrigeration appliances which are fully C_5H_{10}/H_2O blown foams. These are on the market and have published thermal conductivity values of 20.8mW/m·K, 20.1mW/m·K and 19.3mW/m·K respectively⁸. This is partly as a result of their cell size, details of which are shown in the Table 4-1. On measuring the surface tensions of these systems the indirect proportionality to the cell size, as was seen with the model systems, was highlighted. This, yet again, showed that despite an increase in surface tension, the 3. Generation had smaller cell sizes and therefore a better thermal conductivity value. One can deduce that it is not the surface activity of the surfactant, i.e. its ability as a stabiliser, which influences the formation of finer cells but rather its ability as an emulsifier or a combination of both.

Once again, this highlighted the unsuitability of the surface tension measurements as a gauge for optimising foam formulations for the formation of finer cells.

Table 4-1: The applicability of the in-situ study to retail systems 1., 2. and 3. generations.

Cell diameter and thermal conductivity values were obtained from reference 8.

System	δ [mN/m]	Cell Diameter [μm]	NZ_{cal} [1/ μg]	λ [mW/m·K]
1. Generation	25.00	267	3.04	20.80
2. Generation	29.00	226	4.31	20.10
3. Generation	33.00	220	4.56	19.30

It was then decided to test the effects of different amounts of surfactant in a retail system, Elastopor[®]H2030/62. For this purpose the amounts of two surfactants X and Y were varied in the system Elastopor[®]H2030/62. Surface tension curves, although somewhat higher, correlated well with that of the model system B(I/i). At concentrations greater than the critical micelle concentration, which lay between 0.2-0.3%, there is no great effect of the surfactant concentration on the surface tension. This is also true for the cell sizes as tabulated above.

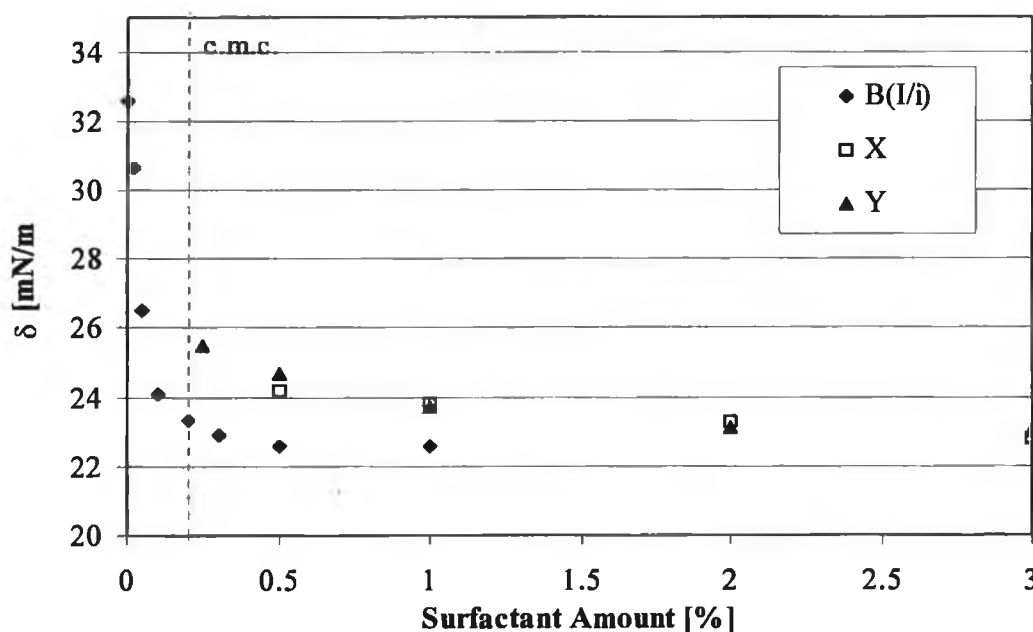


Fig. 4-1: The surface tensions of the commercial system Elastopor[®]H2030/62 with various amounts and types of surfactants X and Y. Critical micelle concentration (CMC) lies in agreement to that of the model system B(I/i).

Table 4-2: The effect of various surfactant types [1%] on the surface tension, δ , end cell diameter, nucleation number and thermal conductivity value, λ , for the commercial system Elastopor®H2030/62.

Surfactant	δ [mN/m]	Cell Diameter [μm]	NZ _{cal} [1/ μg]	λ [mW/m·K]*
W	24.30	254.8	2.97	19.9 \pm 0.2
X	23.80	285.5	2.10	19.5 \pm 0.5
Y	23.70	303.5	1.83	19.9 \pm 0.3
Z	23.80	339.4	1.24	19.4 \pm 0.4

* λ is an average of the thermal conductivity values measured at the beginning, middle and end of a Brett-mould.

The effects of different types of surfactants in the retail system Elastopor®H2030/62 were also studied, the results of which are tabulated in Table 4-2. The cell sizes do not correlate with the surface tension values. A-components containing surfactant X and Z have equal surface tension values of 23.8mN/m but their cell diameters deviate from each other. The cell size can be influenced by the surfactant type. This influence however is not quantifiable by means of the surface tension.

Fig. 4-2 indicates once again the complexity of the nucleation process. Here the influence of the polyols and their compositions is highlighted. The commercial system Elastopor®H2030/62 with different surfactants X and Y have similar nucleation numbers. However, changing the polyol composition to that of another commercial system, Elastopor®H2030/68, increases the nucleation number. The surfactant type and amount remains the same illustrating the influence of the composition of the polyol on the nucleation process. This is an area of possible study for the future.

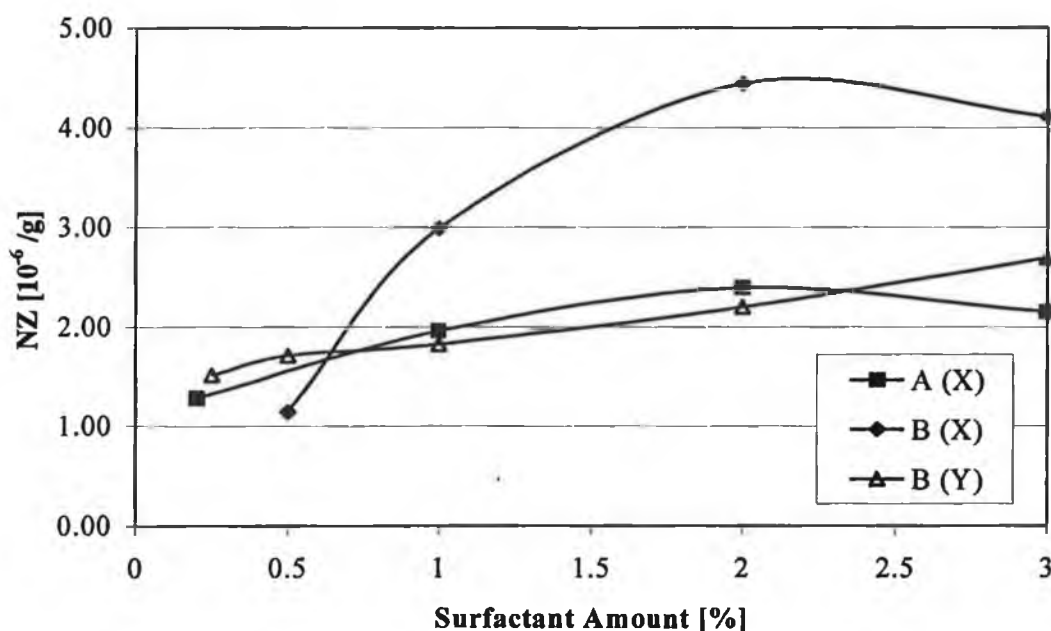


Fig. 4-2: The effect of the surfactant on the (calculated) nucleation number of various systems. Here A = Elastopor[®]H2030/68 and B = Elastopor[®]H2030/62 analysed with various surfactants X and Y.

To summarise, the surface tension of commercial systems is not an indication of its ability to nucleate. Surface tension values are not directly proportional to cell sizes reinforcing the proposition developed by this work that a lowering of the surface tension does not automatically result in a higher nucleation number. The nucleation process is complex, being influenced by not only the composition of the components of the formulations but also by the interaction of the components with each other. In Conclusion, we can say that deductions drawn from experimental apply to commercial systems.

5.1. Conclusion

After many studies into the various factors influencing the properties of polyurethane rigid foam^{6,8}, it is now widely accepted that the foam morphology has a major influence on the thermal conductivity. A large potential to reduce the thermal conductivity lies in the possibility of reducing the IR radiation contribution through the cell size. From these studies the importance of the understanding of the foam formation process, and in particular the nucleation process, has been highlighted. The nucleation process is considered as the process whereby the gas nuclei, which expand to form the cells of the foam, are formed. It has therefore a direct influence on the foam morphology, i.e. cell size and shape. With the aim of gaining a deeper understanding of foam formation and the nucleation process, in order to develop possibilities in influencing it and to ultimately reduce the thermal conductivity, a method was developed for the in-situ analysis of the nucleation process.

With the aid of a stereomicroscope coupled to a pc-controlled imaging system, the nucleation process was systematically analysed. The measured number and size of nuclei per observed area were corrected, taking such factors as sample and density growth into consideration. This allowed for an accurate evaluation of the nucleation number per unit polymer mass. The method was optimised leading to the following advantages as a method of analysis of foaming:

1. Target orientated.
2. Process sensitivity can be estimated.
3. Critical process factors can be identified.
4. Avoidance of costly trials on a larger scale and minimising the number of experiments.
5. An aid in achieving optimal products.

Three primary model systems were analysed, A(I/i), B(I/i) and C(VI/i). The influences of the various reagents such as, blowing agents, surfactants, catalysts, fillers, and prepolymers, on the nucleation process was investigated, giving the following results:

Nucleation in all experiments carried out was homogeneous. Perfluorohexane-blown foams C(VI/i) showed finer and more nuclei in comparison to water/carbon dioxide-blown A(I/i) and cyclopentane-blown B(I/i) foams. The formation of the nuclei however, is only possible in the presence of an emulsifier as the surfactant VI does not have the ability, being hydrophilic inclined, to emulsify the blowing agents droplets that disperse in the system. Foams blown with the A-component A(I/i) showed a tendency for coalescence, while foams foamed with the A-component B(I/i) showed a tendency for disproportionation. Foaming with C(VI/i) resulted in a stable foam unaffected by either coalescence or disproportionation. These phenomena are a sign of an unstable system and are influenced by surfactant type and amount.

An in detail analysis of the surfactants influence on the nucleation process of polyurethane rigid foam was presented in sections 3.5.5. and 3.5.6. Silicone surfactants have little influence on the nucleation number. In fact, they show negative tendencies. The surfactants can be classified as having either an emulsifying or a stabilising ability. Once the nucleus is formed the surfactant aids the stabilising of that nucleus. When the surfactant amount lies under the critical micelle concentration the system is unstable as not enough surfactant is present and coalescence and disproportionation prevails. Even with sufficient surfactant (i.e. surfactant concentrations greater than the critical micelle concentration) coalescence (however negligible) is more prevalent in H₂O-blown foams, diproportionation being more prevalent in C₅H₁₀-blown foams. As already discussed neither processes occur in the stable C₆F₁₄-blown foams.

The varying degrees of stabilisation were analysed by means of the hydrophile-lypophile balance (HLB). The higher the percentage ethylene oxide groups in the surfactant compound the more hydrophilic the compound and vice versa. The hydrophobic Si backbone should not be too long and the molecular weight of the surfactant should not be too large. It was proven that the more hydrophobic the surfactant the more it acted as a stabiliser while the less hydrophobic the surfactant the more it acted as an emulsifier. An ideal surfactant would have the perfect balance of both. The alternative use of two surfactants, one which is highly stabilising and the other highly emulsifying, does not automatically ensure an additive effect of the positive properties. A-components with the hydrophilic surfactants proved under microscope to act more as an

emulsifier, indicating insufficient stabilising abilities by the presence of coalescence etc. Surfactants with emulsifying tendencies show a nucleation bias. However, the hydrophilic strength of the surfactants in this study was not enough to considerably increase the nucleation number. A separate emulsifying agent is perhaps necessary. On the other hand, hydrophobic surfactants, in amounts above the critical micelle concentration, lend extreme stability to the foaming system. In this way the surfactants influence the end cell morphology but not the nucleation process. The size of the initial nucleation sites remained constant regardless of surfactant type. The type of surfactant and their effect on the nucleation process is schematically illustrated in Fig.5-1.

Results obtained proved that the surface tension is not an indication of the nucleating ability of the system. Surprisingly, systems with higher surface tensions tend to have the finest cell size. Therefore, surface tension measurements should not be a gauge for the nucleation ability of a foaming system.

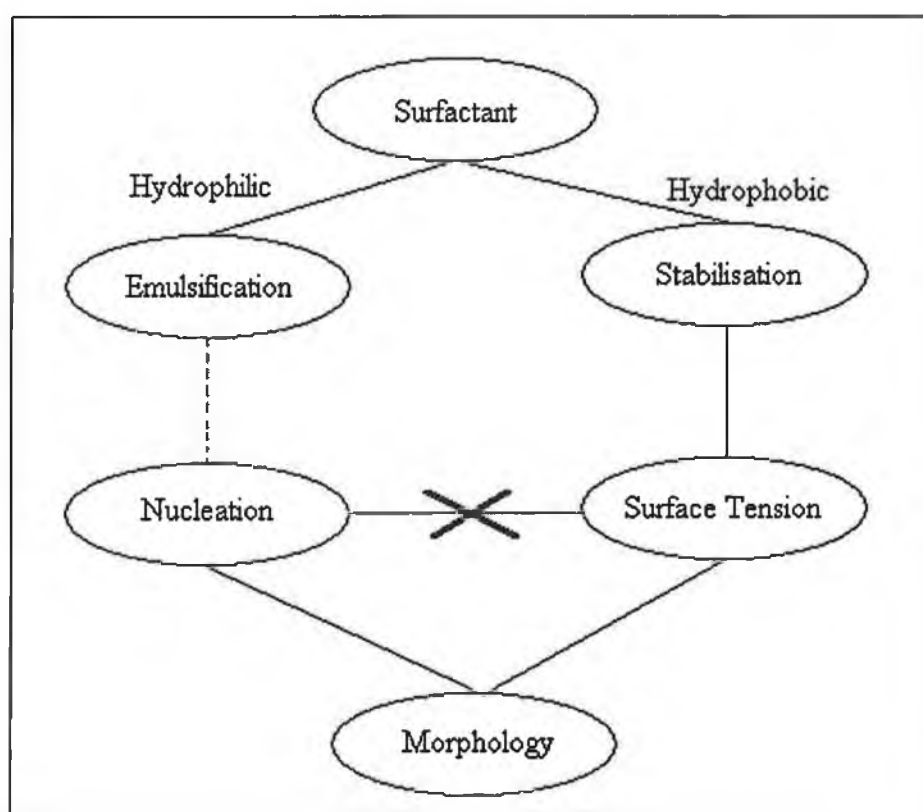


Fig. 5-1: Depending on their hydrophobic / hydrophilic strengths, surfactants have either emulsifying or stabilising abilities. Stabilising strengths is observed in surface tension measurements. These have however, no influence on the nucleation process but aid foam

morphology formation. Emulsifying surfactants only slightly increase nucleation numbers.

Critical radii, r_b^* and consequently critical free energies, ΔF^* , were calculated for the model A-components B(I/i), B(II/i); B(III/i), B(IV/i) and B(V/i). Experimental results contradicted the theoretical results. This is possibly due to the surface tension dependency of r_b^* and ΔF^* when using theory. In reality we have shown that the nucleation number of polyurethane rigid foam is not dependent on the surface tension of the A-component. Future work on the measurement of the interfacial tension between A- and B-components is suggested.

The viscosity of the system has no direct influence on the nucleation process. A-components which have lower viscosities are easier to mix, possibly improving the number of possible nucleation sites. On the other hand, higher viscosities prevent the coalescence of formed nucleation sites.

Catalysts, not being surface active, have no influence on the surface tension. Catalysts affect the nucleation process by speeding up the reaction rates, allowing a fast pressure change needed for nucleation. The faster the pressure change the more homogeneous the cell size. The faster the reaction the finer the cells produced.

The implementation of prepolymers as the B-component improves the compatibility between the A- and B-components by decreasing the %NCO in the B-component. In-situ analysis in section 3.5.9. showed that decreasing the percentage free NCO the compatibility of the components increased which subsequently increased the nucleation number. Further compatibility studies with other prepolymers are suggested.

Surfactants lower the surface tension of the B-component. However, decreasing free %NCO increases the surface tension. This reinforces the proposition that the surface tension does not indicate the nucleation ability of the system.

Fillers were implemented with the aim of analysing heterogeneous nucleation at a liquid/solid interface as described in reference 20. Unfortunately it was not possible to differentiate between heterogeneous nucleation at the liquid /liquid interface and at the

liquid/solid interface. The heterogeneous properties of A- and B-components out weighed these effects. Fillers showed no influence on the nucleation number.

The solubility of CO₂ in the A-component over the reaction's temperature range is independent of the presence of surfactant. This was tested in section 3.5.11. using IR spectroscopy and vapour pressure measurements of A-components with and without surfactant.

At the beginning of the experimental, Fig.2-1 showed a schematic representation of the questions posed at the start of this work. In Fig. 5-2 below these questions have been solved.

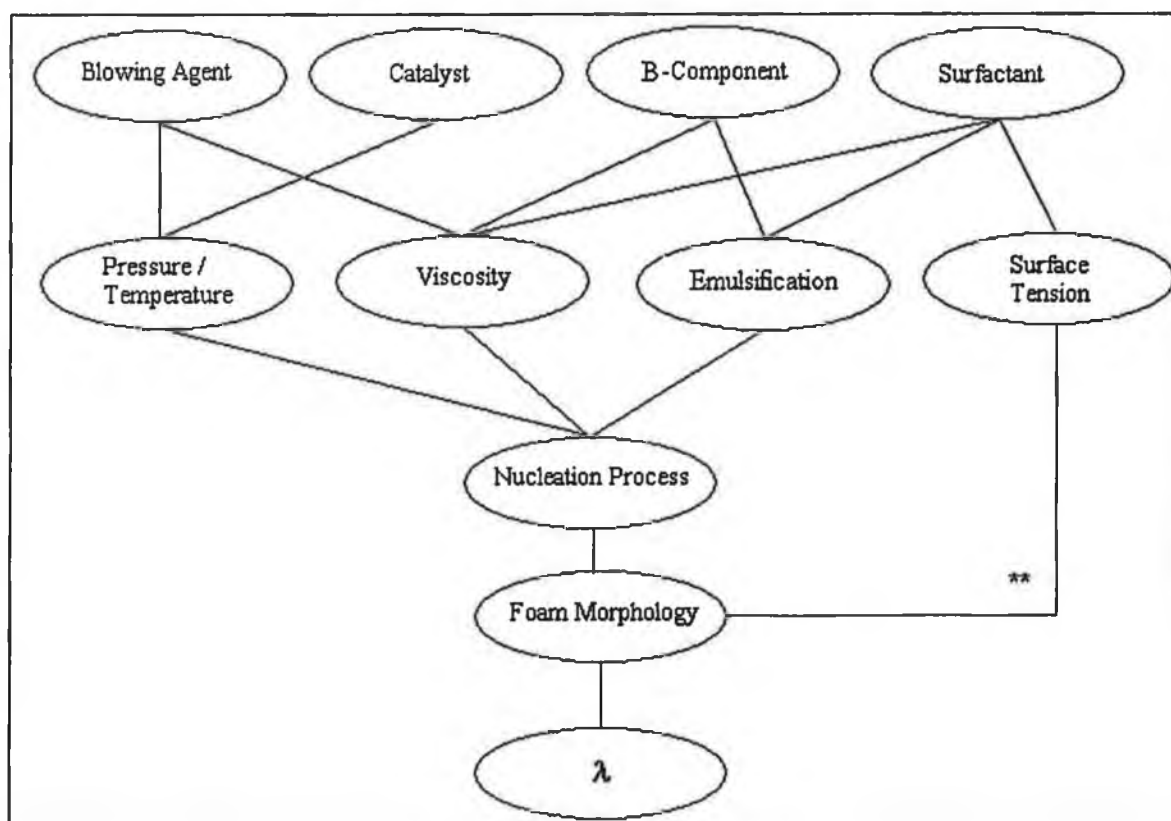


Fig. 5-2: Schematic representation of the results. See text for detailed explanation. **see Fig 5-1 for clarification.

The blowing agent influences the nucleation process by influencing the local temperature, pressure and viscosity. By controlling the rate of pressure and temperature change the catalyst can also positively influence the nucleation process. A faster rate in

temperature or pressure change results in a more simultaneous nucleation of finer cells. The influence from the B-component was studied by implementing prepolymers. Decreasing the %NCO resulted in an increase in nucleation number through an improved compatibility and an increase in viscosity. It is not possible to mathematically quantify compatibility between A- and B-components. However, with the aid of the method developed it was possible to optically estimate compatibility by microscopic analysis. This was also necessary during the study of the surfactants effect on the nucleation process. Here though, with the aid of the HLB-values, the emulsification ability or the stabilising strength of the surfactant was verified. This has already been discussed with respect to Fig. 5-1.

In order to prove that the admittedly small sample analysed was representative of the nucleation in the bulk, commercial systems which were foamed on the production line with high pressure equipment. For this purpose the commercial systems Elastopor[®]H210/147, Elastopor[®]H2030/13, Elastopor[®]H2030/40, Elastopor[®]H2030/62, Elastopor[®]H2030/68 were analysed with respect to cell size, surface tension, nucleation number and thermal conductivity values. Surface tensions were indirectly proportional to the nucleation number. Critical micelle concentrations lay between 0.2-0.3% surfactant, in good agreement to the experimental model systems. The end cell size and consequently the nucleation number is directly proportional to the thermal conductivity value. Results were in agreement to results obtained during the study of the model system proving that conclusions drawn from the method of analysis developed are applicable to commercial systems.

6.1. Future Work

The in-situ microscopic study of the nucleation and foaming process proved to be a useful tool in this work. The experiment is quick and the results showed to be representative of that which happens in practice. Therefore, this method can be implemented as a tool for the prediction of foam properties in the regulation of new foams.

Such experiments have already been carried out. During the testing of a new formulation it was noted that even a minute amount [0.05%] of a certain acrylate-type leveller prevented foaming. Levellers are used to improve the distribution of dye coverage on metal surfaces, eliminating the presence of gaps or voids. Microscopic analysis showed that this was due to rapid coalescence indicating a destabilising property of the leveller. Similarly, another acrylate-type leveller was also tested. This leveller aids foaming. Under the microscope the system demonstrated stability. However, the leveller fell out of the system and particles ($<1.0\mu\text{m}$) were observed on the surface of the bubbles. These particles perhaps served as additional heterogeneous nucleation sites, improving foaming. The photomicrographs taken during the analysis are shown in Fig. 6-1. Further in-situ analysis on the formation of voids is also possible.

In the future, the following points should be taken into consideration with respect to the nucleation process during the foaming of polyurethane rigid foam:

- Perfluoroalkane-blown foams have more nuclei from the start
- Nucleation is highly dependent on emulsification.
- Surfactants have a negligible influence on the nucleation process.
- Surfactants improve the stability of the foam and thereby improve the foam morphology.
- Increasing the compatibility between A- and B-components increases the nucleation number.

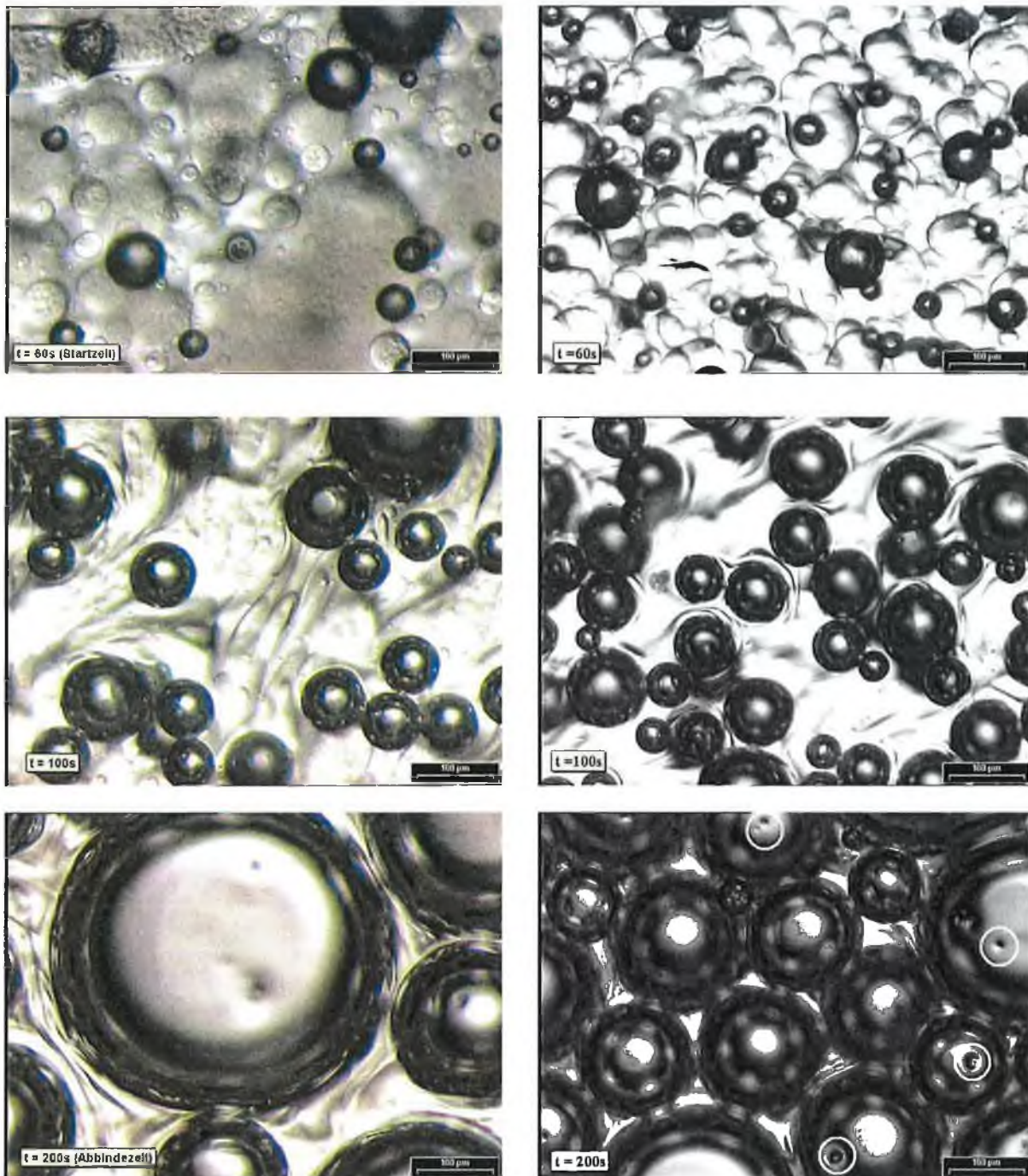


Fig. 6-1: Left, from top to bottom: foaming with an acrylate leveller which inhibits stabilisation, resulting in coalescence and foam destruction. Right, from top to bottom: the foaming of a stable system with a different type of acrylate leveller which aids foaming. The rings indicate where the particles are sitting on the surface of the cell.

With these points in mind the following could be considered worthy of investigation:

- The influence of the polyol on the nucleation process. This was beyond the scope of this work but results indicated a possible polyol dependency.
- As already stated in the work, the determination of the catalysts' influence on the isocyanate-hydroxyl and/or the water-isocyanate reaction with respect to nucleation is also worth analysing.
- Also highlighted was the increased nucleation due to prepolymers. Maintaining other properties of rigid foam such as mechanical strength and its ability to flow, the implementation of prepolymers could be exploited.
- Interesting would be experiments carried out under high pressures and if possible in-situ photomicrographs during the production of commercial systems on high pressure machines.
- A method to measure dynamic surface tension during foaming could improve the understanding of the role of the surfactant. An analysis of the interfacial tension between A- and B-component would also be interesting.

7.1. Nomenclature

A	m ²	Interfacial area
A ₆₀	m ²	Sample area at 60s
A ₂₀₀	m ²	Sample area at 200s
A _{ij}	-	Wassiljewa constant
A _l	-	Lateral amplification
a	μm	d perpendicular to temperature gradient
b	μm	d parallel to temperature gradient
C ₀	moles	Gas molecule concentration
C ₀ *	moles	Reduced concentration of gas molecules
C	mol	Concentration of dissolved gas
c	μm	Cell wall thickness
d	μm	Cell diameter
d _o	mm	Object distance
d' _o	mm	Image distance
D	m ² /s	Diffusivity of gas
E	N/m	Film elasticity
ΔF	kJ/mol	Helmholtz free energy change
ΔF*	kJ/mol	Critical free energy
F	mol/m ²	Molar rate of diffusion
F ⁺	mN	Force
f	mm	Focal distance
f _{gr}	-	Sample growth factor
f _s	%	Fraction of polymer in the struts
f ₀	%	Frequency factor for homogeneous nucleation
ΔG	kJ/mol	Free Enthalpy
h	m	Height of cylinder
J	cm ³ /s	Rate of nucleation
J _{het}	cm ³ /s	Heterogeneous nucleation rate
J _{mod}	cm ³ /s	Modified homogeneous nucleation rate
K	cm ⁻¹	Extinction coefficient
K _{strut}	cm ⁻¹	Extinction coefficient of strut

K_{wall}	cm^{-1}	Extinction coefficient of wall
k	JK^{-1}	Boltzmann constant ($1.38 \times 10^{-23} JK^{-1}$)
k_b	$Wm^{-2}K^{-4}$	Stefan-Boltzmann constant ($5.67 \times 10^{-8} Wm^{-2}K^{-4}$)
L	m	The mean free path of air
M	mol/kg	Molar mass
M_h	g	Hydrophilic molecular mass
M_{obj}	-	Magnification of objective lens
M_{oc}	-	Magnification of ocular lens
M_t	-	Total magnification
m_c	kg	Mass of gas molecule in the critical nucleus
N_c	-	Number of components
N_v	-	Number of particles per unit volume
NZ	$1/m^2$	Nucleation number
NZ_c	$1/g$	Nucleation number corrected
NZ_{cal}	$1/g$	Nucleation number calculated
n_b	$J/mol K$	Gas mole number
P	bar	Pressure
P_0	bar	Environmental pressure
P_b	bar	Gas pressure inside the bubble
P_s	bar	Saturation pressure
P_{max}	bar	Maximum pressure
p_0	bar	Vapour pressure
q_A	-	Tube factor
r	μm	Radius of cell / bubble
R	$J/mol K$	Universal gas constant ($8.31441 J mol^{-1} K^{-1}$)
r_b^*	μm	Critical radius
Re	-	Reynolds number
S	kg/m^3	Solubility
$S(m_c)$	μm^2	Surface area of the critical nucleus
T	K	Temperature
T_s	K	Gas saturation temperature
T_{max}	K	Maximum temperature
t	s	Time

t_D	s	Time scale for diffusion
t_n	s	Time scale for nucleation
V	μm^3	Cell envelope divided by $(4\pi/3)$
V_b	μm^3	Volume of bubble
V_z	μm^3	Volume of cell
V_g	μm^3	Volume of gas
V_f	μm^3	Volume of foam
x	m	Distance in the direction of diffusion
y_i	-	The mole fraction of the i^{th} component
Z	-	Zeldovich non-equilibrium factor

7.2. Greek Symbols

α	bar ⁻¹	Solubility coefficient
β	-	Correction factor (tensiometer)
ε	cm ⁻¹	Emissivity
γ	mN/m	Surface tension
γ^*	m ²	Collision diameter of air (4×10^{-10} m ²)
γ_0	mN/m	Surface tension of initial pure liquid
η	mPa*s	Viscosity
λ	mW/m*K	Thermal conductivity
λ_g	mW/m*K	Thermal conductivity through the gas
λ_{g0}	mW/m*K	Thermal conductivity of air at atmospheric pressure
λ_{gi}	mW/m*K	Thermal conductivity of the pure <i>i</i> th component
λ_{mix}	mW/m*K	Thermal conductivity of a gas mixture
λ_p	mW/m*K	Thermal conductivity of the compact polymer
λ_r	mW/m*K	Radiative heat transfer
λ_s	mW/m*K	Thermal conductivity through the solid
μ	-	Average value
π	bar	Spreading pressure of an adsorbed surfactant(= $\gamma_0 - \gamma$)
ρ	kg/m ³	Density
ρ_f	kg/m ³	Foam density
ρ_s	kg/m ³	Density of solid polymer
σ	-	Standard deviation
ω	kg/m ³	Porosity
τ	s	Induction period
ς	Pa	Macroscopic gas density
δ	mN/m	Surface tension

8.1. Acknowledgements

Firstly, I would like to thank my supervisor at BASF Schwarzheide GmbH, Germany Dr. Biedermann who provided the topic of research. Anja, many thanks for your support, help, and patience with what we affectionately called our “Sisyphus” project. Thank you to Prof. Vos, Dublin City University for accepting the task of supervising me from afar.

I would like to thank Dr. Rotermund and Dr. Schlegel for the informative discussions on polyurethane chemistry and microscopy at the earlier stages of my research. I greatly appreciate the help of the research department of BASF Schwarzheide, not just from the research point of view but also for their support and help outside of working hours. A special thanks to the analytical department - Fr. Scheel (surface tension), Fr. Franzke (electron microscope images), Fr. Thierling (cell diameter measurements), Fr. Kudoke, Fr. Schlüter, Fr. Kirmis (spectroscopy) and Fr. Merten (vapour pressure and thermal conductivity values). Many thanks to the former rigid foam research group, including Fr. Fischer for her help in the formulating of the model systems. I gratefully acknowledge Fr. Murrar for beneficial discussions on prepolymers. Thank you Mirko for saving my computer (several times) from a quick death and for sacrificing your weekend to help me count bubbles. Thanks to my proof readers, Andreas and Mike, for their tips and suggestions.

From BASF AG Ludwigshafen I would like to thank the following people: Dr. Heckmann (providing heating mantle), Hr. Woll (vapour pressure and CO₂ solubility measurements) and Dr. Kluge (surfactant analysis). Thanks also to Hr. Huntermann (rheological studies) and Fr. Giesker (values for commercial systems) from Elastogran Lemförde GmbH.

Alexandra, Annett, Antje, Thomas, Raimund, Mirko (again) and Monika, thanks for your friendship and help (and for the odd visit to the Irish Pub in Lauchhammer!). Thanks to the lads back in DCU for emailing, visiting and generally encouraging me during my three years in Germany. A special thanks to Kevin for his constant support and encouragement without which life would have been more difficult.

Most importantly, I would like to thank my family, especially my parents who have supported and guided me in every way throughout my education.

9.1. Literature

- [1] Handbook of Polymeric Foams and Technology; D. Klempner, K.C. Frisch; Hanser 1991.
- [2] S. Adams, O.Volkert, W. Wiegmann; Utech 1994 Paper 24.
- [3] C. Cecchini, B. Cellarosi, M. Brocci; Utech 1194 Paper 30.
- [4] V. P. Valujskich, J.L. Esipov; Plaste und Kautschuk **36** 12 1989.
- [5] A. Cunningham; Polymer **22** 882 1981.
- [6] Low Density Cellular Plastics Physical Basis of Behaviour; N. C. Hilyard, A. Cunningham; Chapman & Hall 1994.
- [7] Polyurethane: Chemistry and Technology; Vol. XVI, Part II Technology, J. H. Saunders, K. C. Frisch; Interscience Publishers 1964.
- [8] A. Biedermann, C. Kudoke, A. Merten, E. Minogue, U. Rotermund, H.-P. Ebert, U. Heinemann, J. Fricke and H. Seifert; Polyurethanes Expo 405 1999.
- [9] Silicone Surfactants; R.M. Hill; Marcel Dekker 1999.
- [10] B. Kanner, T.G. Decker; J. Cell. Plast.; **32** Jan 1969.
- [11] G.R. Rossmly, H.J. Kollmeier, W. Lidy, H. Schator, M. Wiemann; J. Cell. Plast. 26 1977.
- [12] H.J. Kollmeier, H. Schator; J. Cell. Plast. 239 1985.
- [13] H.J. Kollmeier, H. Schator, P. Zaeske; J. Cell. Plast. 255 1983.
- [14] J.G. Dubjuga, G. Titarowa, O.G. Tarakanow, H. Hamann, G. Tschernko; Plaste und Kautschuk **26** 11 616 1979.
- [15] H. Hamann, J. Ritter; Plaste und Kautschuk **30** 7 364 1983.
- [16] Makromoleküle; H.-G. Elias; Hüthig & Wepf Verlag Basel- Heidelberg 1975.
- [17] T. Ota; PhD. Thesis, Microcellular Polyurethane Foaming by Modified Reaction Injection Moulding; Massachusetts Institute of Technology, 1995.
- [18] N.S. Ramesh, D.H. Rasmussen and G.A. Campbell; Polym. Eng. Sci., **34** 1685 1994.
- [19] H. Park and J.R. Youn; Polym. Eng. Sci., **35** 1899 1995
- [20] J. R. Youn and N.P. Suh; Polym. Comp., **6** 175 1985.
- [21] S.K. Goel and E.J. Beckman; Polym. Eng. Sci., **34** 1148 1994.
- [22] K.C. Russell; Adv. in Coll. and Int. Sci. **13** 205 1980.
- [23] A. Prins; Chem. Ing. Tech. **64** 1 73-75 1992.
- [24] J.S. Colton, N.P. Suh; Polym. Eng. **27** 7 1987.

- [25] W.A. Amon, C.D. Denson; Poly. Eng. Sci., **13** 1026 1984.
- [26] A. Arefmanesh, S.G. Advani, Rheol. Acta, **30** 274 1991.
- [27] A. Arefmanesh, S.G. Advani, E. E. Michaelides; Int. J. Heat Mass Transfer **35** 1711 1992.
- [28] C. B. Park, D. F. Baldwin, N. P Suh; ASME **46** 537-552 1993.
- [29] A. Biedermann; Private Communications 04/97.
- [30] Ullmann's Encyclopaedia of Industrial Chemistry, Vol. A25 747 VCH Verlag 1994.
- [31] The Physics and Chemistry of Surfaces; N.K. Adam; 3rd Edt., Oxford University Press, London 1941.
- [32] Introduction to Colloid and Surface Chemistry; D.J. Shaw; 4th Edt., Butterworth-Heinemann 1992.
- [33] A. Biedermann, U. Rotermund; Private Communications 01/1999.
- [34] University Physics; F.W. Sears, M.W. Zemansky, H.D. Young; 6th Edt. Adison-Wesley 1982.
- [35] Physical Chemistry; P.W. Atkins; 5th Edt. Oxford University Press 1994.
- [36] R.B. Turner, J.B. Nichols, R.A. Kuklies; J. Cell. Plast. **25** 2 117 1989.
- [37] M. A. Schuetz, L.R. Glicksmann; J. Cell. Plast. **20** (2) 114 1984.
- [38] R.E. Skochdopole; Chem. Eng. Progr., **57** 10 1961.
- [39] D. J. Doherty, R. Hurd, G.R. Lester; Chem and Ind. **30** 1340 1962.
- [40] R. De Vos, D. Rosbotham, J. Deschaght; 35th Annual Polyurethanes Technical/Marketing Conference, 194 1994.
- [41] W. Wacker, A. Christfreund, D. Randall, N.W. Keane; Polyurethanes Expo 35 1996.
- [42] C.P. Gonatas, J.S. Leigh, A.G. Yodh; Physical Review Letters, Am. Phys. Soc. **75** 3 573 1995.
- [43] P.N. Segrè, W. Van Megen, P.N. Pusey, K. Schätzel, W. Peters; J. Mod. Opt. **42** 9 1929 1995.
- [44] Handbook of Microscopy, Methods I; S. Amelinckx, D. van Dyck, J. van Landuyt, G. van Tendeloo; VCH Verlag, Weinheim 1997.
- [45] Ullmann's Encyclopaedia of Technology; Vol. B2 24-1, VCH Verlag 1997.
- [46] Handbook of Microscopy, Methods II; S. Amelinckx, D. van Dyck, J. van Landuyt, G. van Tendeloo; VCH Verlag, Weinheim 1997.
- [47] The Image Processing Handbook; 3rd Edt.; J.C. Russ; CRC & Springer Verlag 1998.
- [48] N.V. Schwarz, M.T. Bomberg; J.Them. Insul. **15** 153 1991.

- [49] T. Baumann, TU Berlin; Videomikroskopie als Methode zur Untersuchung heterogen katalysierter Gasphasenpolymerisation; Presentation at BASF Scwarzheide GmbH, Oct. 1999.
- [50] Statistik in der Analytischen Chemie; K. Doerffel; VEB Deutscher Verlag für Grundstoffindustrie, 1966.
- [51] U. Rotermund, J. Rüderich, K. Schlegel; Plaste und Kautschuk **21** 2 109 1974.
- [52] U. Rotermund, J. Läuter, W. Gräfe; Plaste und Kautschuk **26** 5 244 1979.
- [53] E. Scheil; Zeitschrift für Metallkunde; **27** 9 199 1935.
- [54] D. Niyogi, R. Kumar, K.S. Gandhi; AIChE Journal, **38** 8 1170 1992.
- [55] K. Kodama, K. Yuge, Y. Masuda, Y. Tanimoto; J. Cell. Plast. **31** 24 1995.
- [56] K. Lunkenheimer, K.D. Wantke; J. Coll. Int.Sci. **66** 3 579 1978.
- [57] Surfactants and Interfacial Phenomena; 2nd. Edt.; M.J. Rosen; Wiley Interscience, 1989.
- [58] Methoden der Organischen Chemie; Band III Physikalische Forschungsmethoden; Teil 1 Houben-Weyl; 252 1955.
- [59] H.J.M. Grünbauer, J.A. Theon, J.C.W. Folmer, H.C. Lieshout; J. Cell. Plast. **28** 36 1992.
- [60] M.J. Elwell, A.J. Ryan, H.J.M. Grünbauer, H.C. Van Lieshout; Macromolecules **29** 2960 1996.
- [61] R.A. Neff, C.W. Macosko; Rheol Acta **35** 656 1996.
- [62] Rheologie der Kunst; R. S. Lenk; Karl Hanser Verlag München, 1971.
- [63] M.D. Bessette, D.W. Sundstrom; Poly. Proc. Eng. **3** (1&2) 25 1985.
- [64] E. Mora, L.D. Artavia, C.W. Macosko; J. Rheol. **35** 921 1991.
- [65] Patent No.: OZ 0050/48762; Preparation of Rigid Polyurethane Foams Having Small Cell Diameter; O. Volkert.
- [66] VDI-Wärmeatlas, 6. Auflage Dc27 1991.
- [67] O. Volkert; Polyurethanes World Congress 1983, 29.
- [68] A. Merten; Private Communications 08/2000.
- [69] J.S. Colton; PhD. Thesis, The Nucleation of Microcellular Thermoplastic Foam; Massachusetts Institute of Technology, 1985.
- [70] A. Biedermann; Private Communications 07/2000.
- [71] B.J. Pangrle, X.D. Zhang, C.W. Macosko, B.E. Hammer, N.P. Bidault, M.L. Listemann, R.E. Stevens; Polyurethanes Expo Sept.17 - 20 247 1988.

Appendix 1

Key to Composition of Systems Used

B-Component:

The principal B-component was M20A, an MDI-type polyisocyanate with a free NCO content of 31.5%. Other B-components used were prepolymers 1 and 2 whose data are presented in the table below:

Table A1-1 : The %NCO and the viscosity of B-Components used in this study.

B-component	Isocyanate :Methanol	%NCO	Viscosity [mPa.s] @25°C
M 20A	100:0	31.50	201
Prepolymer 1	100:2	27.82	720
Prepolymer 2	100:4	24.80	3017

A-Component:

The A-component was varied according to experiment. The various formulations are tabulated on the next page in Table A1-2. In Table A1-3 the viscosity and density at 25°C of the A-components A(I/i), B(I/i) and C(VI/i) with and without their respective surfactants are tabulated. It was important each systems formulation was set such that the following characteristic times and density applied to each system when foamed:

Cream time	=	60s ±10s
Gel time	=	200s ±10s
Rise time	=	300s ±10s
Density	=	55g/l ± 1g/l

Table A1-2: Clarification of the formulations of the A-components used throughout this work.

	A(I/i)	B(I/i)	B(II/i)	B(III/i)	B(IV/i)	B(V/i)	B(I/ii)	B(I/iii)	B(I/iv)	C(VI/i)
A-Component										
Polyol 1	✓	✓	✓	✓	✓	✓	✓	✓	✓	✓
Polyol 2	✓	✓	✓	✓	✓	✓	✓	✓	✓	✓
DPG*	✓	✓	✓	✓	✓	✓	✓	✓	✓	✓
Water	✓✓	✓	✓	✓	✓	✓	✓	✓	✓	✓
Cyclopentane		✓	✓	✓	✓	✓	✓	✓	✓	
Perfluorohexane										✓
Surfactant										
(HLB-Value):										
I (1.38)	✓	✓					✓	✓	✓	
II (1.15)			✓							
III (1.77)				✓						
IV (4.18)					✓					
V (5.35)						✓				
VI (0.87)										✓
Catalyst:										
C ₈ H ₁₇ N	✓	✓	✓	✓	✓	✓				✓
C ₆ H ₁₂ N ₂							✓			
C ₁₁ H ₂₁ O ₂ N								✓		
C ₃₂ H ₆₄ O ₄ Sn									✓	
Emulsifier:										
C ₁₂ H ₁₀ O ₃ SF ₁₇										✓

Polyol 1 = a polyol with starter materials of sucrose, glycerine and propylene oxide; OH No. 380-420.

Polyol 2 = a polyol with starter materials of propylene glycol and propylene oxide; OH No. 235-260.

*DPG = dipropylene glycol

Table A1-3: The viscosity and density of the A-components A(I/i), B(I/i) and C(VI/i) with (1%) and without (0%) their respective surfactants.

A-Component	Viscosity [mPa.s] @25°C		Density[g/cm³] @25°C	
	1%	0%	1%	0%
A(I/i)	819	802	1.069	1.069
B(I/i)	240	208	1.021	1.011
C(VI/i)	967	973	1.101	1.096

Appendix 2

Example of Gaussian Distributions Obtained from In-Situ Analyses

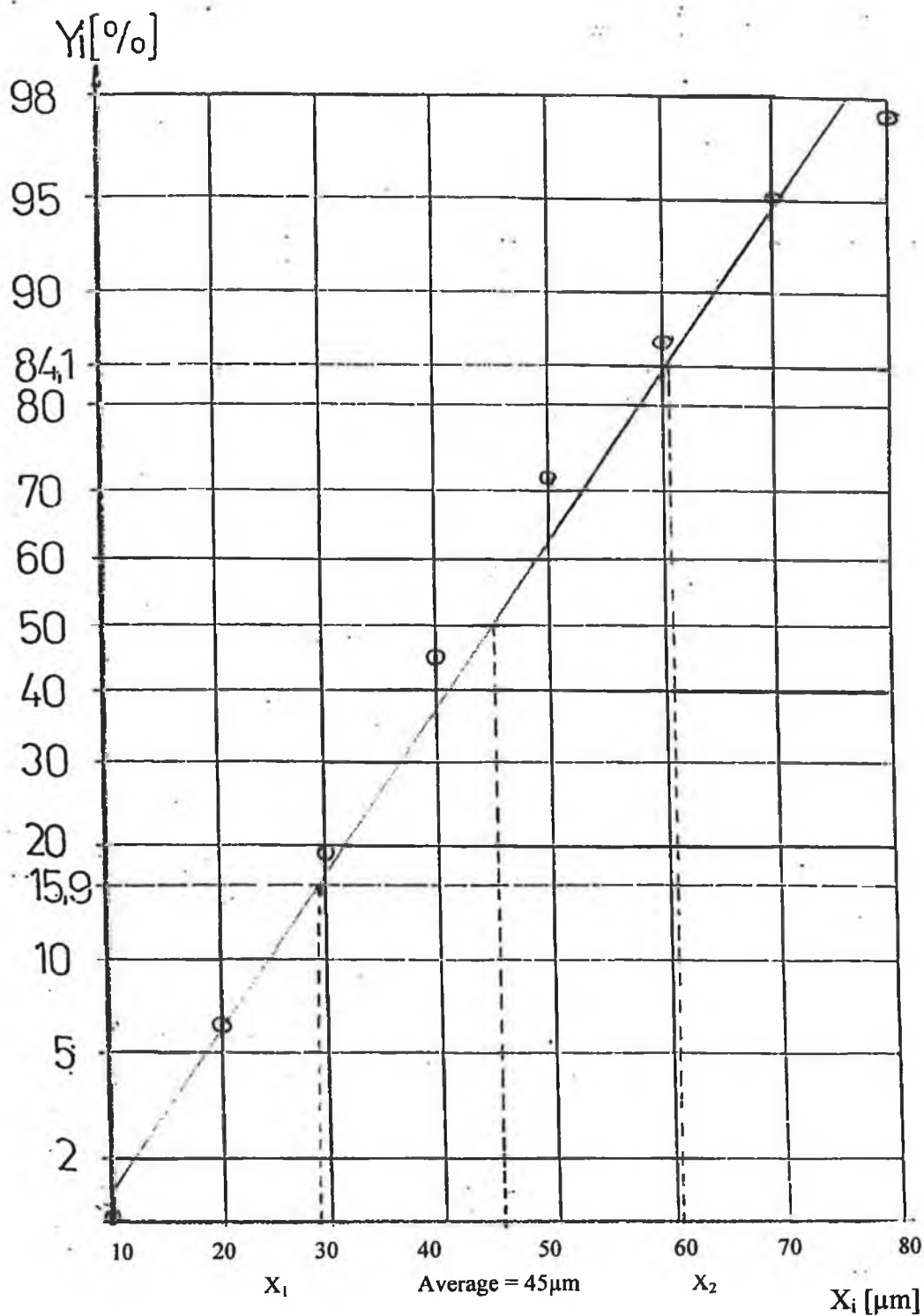


Fig. A2-1: The probability net³⁰ of the nucleus size distribution of a sample foamed using the A-component B(I/i) with the B-component M20A at cream time of 60s. Where $y = 50$, $x =$ average value, μ . Standard deviation, $\sigma = (x_2 - x_1)/2$.

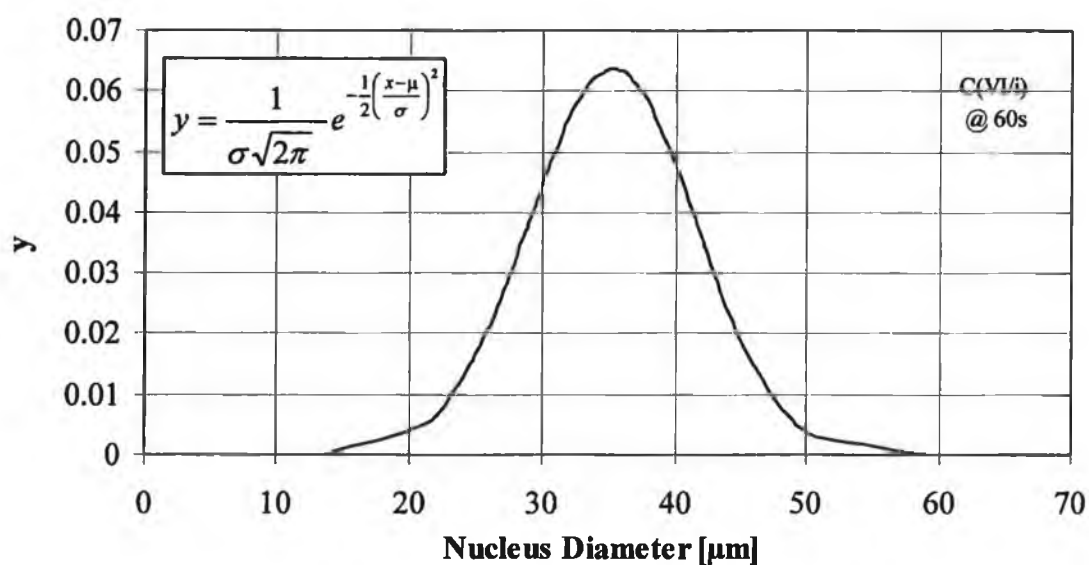
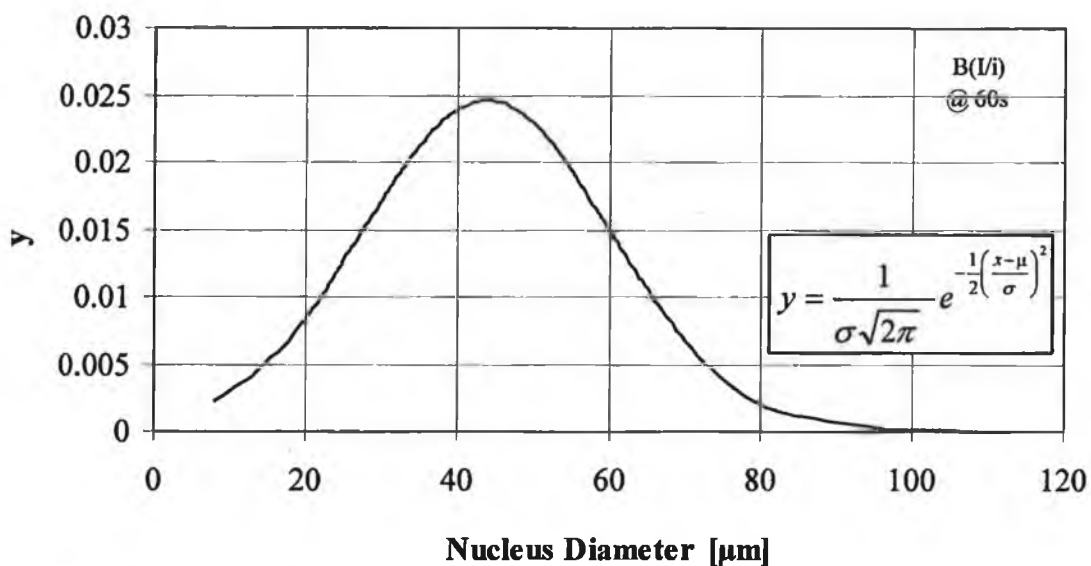
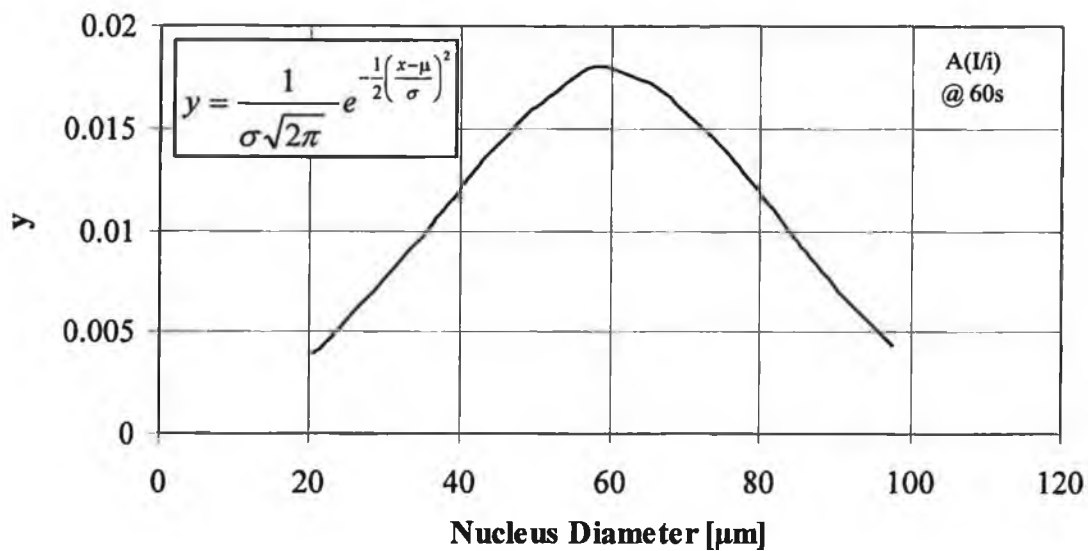
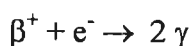


Fig. A2-2: The average nucleus diameter, μ and standard deviation, σ of the various systems were obtained from their respective probability nets and their values substituted into the given formula to form typical bell-shaped Gaussian distributions.

Appendix 3

Positron Emission Tomography Results

Clinical tests such as magnetic resonance imaging (MRI) have previously been implemented in the study of a very slow (12h) evolving gelatine foam⁴². It was possible to analyse the foam interior and to reconstruct the topology at set intervals. The reaction of polyurethane foaming takes place in a matter of seconds and although a system was regulated, which would be considered very slow, it still had a rise time of only 5mins. Therefore, this method was considered unsuitable. However, an attempt was made to examine the formation of PU rigid foam by means of another clinical radio chemical application - positron emission tomography (PET). PET involves the use of radio-labelled compounds that decay by positron emission. In this decay process, a positron is emitted from the nucleus and is annihilated in a collision with a negatively charged orbital electron. In the annihilation reaction, the two particles are converted into two γ -rays, which travel away from each other at an angle of 180° where two opposing detectors detect them simultaneously. Therefore, it was possible to obtain a 3D image of the foaming process.



According to the reaction schemes previously described (section 2.4.), by means of the two radio-labelled compounds [¹⁵O]H₂O and [¹⁵O]butanol, the foaming process was analysed. Due to the increased number of hydroxyl groups in the tracer mixture it was necessary to reduce the amount of the polyetherpolyol in the system (A/i) by the equivalent 2g. This ensured foaming without collapse.

It was possible to visualise the foaming process by PET, producing a radioactive portrait of the foaming. Fig. A4-1 shows an overview of the PET images obtained at set intervals using [¹⁵O]H₂O as the tracer. Going from left to right, top to bottom the foam growth can be seen. Moreover, the technique failed to follow the various stages of nucleation and foam formation including coalescence and/or disproportionation. This was because of bad spatial resolution. An additional disadvantage was the speed of the system. Despite this slow foaming system, the 2s timeframes of the PET-scanner were much too

long. The dynamic growth of the polymer framework results in a continuous dilution of the radioactivity. The former coupled with the later culminates in bad statistics for the counting of the radioactive decay. A difference in the PET data obtained with $[^{15}\text{O}]\text{H}_2\text{O}$ and $[^{15}\text{O}]\text{butanol}$ was not observed.

Therefore, PET has been proven an unsuitable method for the analysis of the nucleation process due to bad spatial resolution of the PET technique and the velocity of the foaming process. For a better spatial resolution computerised tomography, CT, another medical imaging process, is possible. Pangrle et al⁷¹ have implemented this technique on prefoamed PU flexible foam in order to analyse the end morphological structure. However, in -situ studies have not been carried out primarily due to the addition of heavy atoms such as iodine for the production of a contrast.

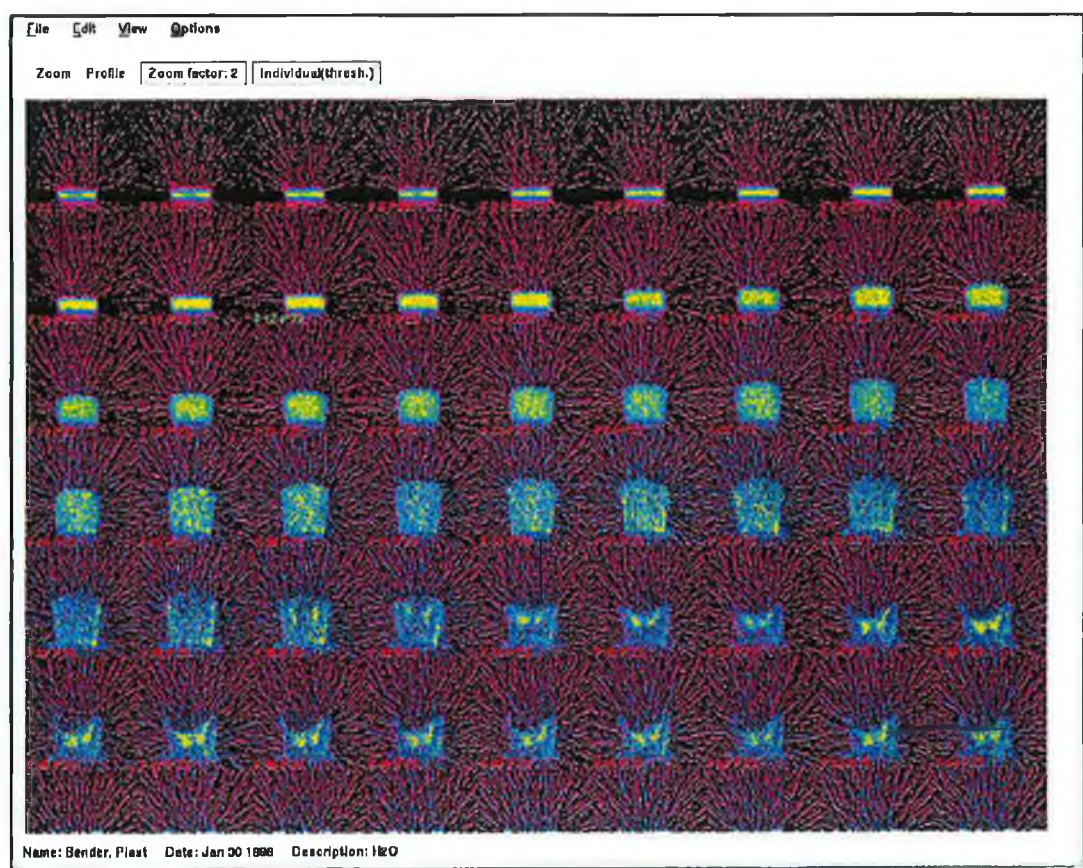


Fig. A4-1: An overview of the positron emission tomographical images of the foaming process of the radio active A-component A(I/i) with M20 as the B-component using H_2^{15}O ; growth proceeding from left tot right, top to bottom.

Appendix 4

Two-Coloured Dynamic Light Scattering⁴³ Results

Dynamic light scattering (DLS) is an effective technique for investigating the dynamics of a wide range of systems such as colloidal suspensions, solutions of polymers and amphiphilic systems. It is necessary, however, for the sample to be relatively transparent so that single scattering dominates and for the measurements obtained to relate to properties of the medium. The light scattered by a turbid media, such as that produced during polyurethane foaming, contains contributions from both single and multiple scattering with complex results. Thus the traditional application of DLS is restricted to transparent media. Two-colour dynamic light scattering, however, suppresses multiple scattering and allows the study of the (Brownian) dynamics of optically turbid systems. The technique operates by cross-correlating scattered light of two different colours. With the appropriate scattering geometry, only single scattered light contributes to the time-dependent part of the measured intensity cross-correlation function thus allowing straightforward interpretation of the data.

This, however, was not possible with the data obtained from the foaming process of polyurethane rigid foam. This was primarily due to the simultaneous nucleation of cells with various diameter sizes after start time, through which a very complicated feed back was obtained. Despite the sensitivity of measurement in the μm -area, the velocity at which the initial nuclei grew was too fast, hindering the experimental measurement of the critical radius, r_b^* . Therefore two-coloured Dynamic Light Scattering was also considered ineffective in the analysis of the formation of PU rigid foam.

Appendix 5

A Method to Calculate the Maximum Number of Possible Nucleation Sites

In order to ascertain the maximum possible number of nucleation sites for the ideal scenario, the following calculations were carried out. Assuming that

1 H₂O → 1 CO₂ (the second oxygen comes from the isocyanate, see reaction 1.4)

In model A-component A(I/i):

2.7% H₂O present ≈ 9.03 × 10²² molecules H₂O in 100g

Mixing ratio A: B = 40:60

→ 2.53 × 10²² molecules in A.

A + B = 70g

→ 2.53 × 10²² in 70g reaction mixture.

= 3.61 × 10²⁰ [1/g]

Every molecule of H₂O formed one molecule of CO₂

→ 3.61 × 10²⁰ molecules of CO₂ per gram of reaction mixture are formed.

If for formation of a nucleus, a critical radius of 450nm is needed (see section 3.5.6.)

→ critical diameter = 900nm

molecular diameter of CO₂ = 3.34 × 10⁻⁸cm

→ 26 molecules CO₂ necessary for each critical radius.

The number of nucleation sites is then equal to the number of CO₂ molecules formed divided by the number of CO₂ molecules necessary for a critical radius:-

$$\frac{3.61 \times 10^{20}}{26.94} = 1.3 \times 10^{19} [1/g]$$

This assumes that all nucleation happens simultaneously and ignores external parameters such as rate of reaction, influence of increasing temperature or pressure.

Appendix 6

Opened-Cell Polyurethane Foam Results

As described in the introduction polyurethane rigid foam can have a closed or an opened cell structure (see Fig. 1-2). During the initial stages of foam rise the nuclei (cells) are closed. Opening occurs when one or more cell wall ruptures, usually due to excessive thinning so that the strength of the wall cannot resist the pressure in the cell. It was hoped to microscopically observe the nucleation and foam formation of an opened celled rigid foam. For this purpose an A-component which produces opened celled foams was foamed with M20A as the B-component and analysed under the microscope. However, neither the open cells nor the rupturing process leading to cell opening, could be microscopically observed using the in-situ method of analysis.

Appendix 7

Surface Tension

Surfactants when present at low concentrations in a system adsorb onto the surface or interfaces of the system and therefore alter the systems surface tension or interfacial tension. In other words, surfactants significantly reduce the amount of work required to expand the interfaces and in the case of foaming some questions with respect to this need to be answered. Do surfactants play a significant role in the nucleation / foaming process and if so under what conditions? How and why do certain surfactants work as they do?

The surface tensions, δ [mN/m], of the model system A(I/i), containing various amounts of surfactant (I) were measured using the following three methods as described in the experimental (see section 2.11.):

1. The Lecomte du Noüy Tensiometer
2. The Pendant Drop Method
3. Maximum Bubble pressure Method

1. The Lecomte du Noüy Method

The surface tensions of each of the model A-components A(I/i), B(I/i), and C(I/i) containing various amounts of surfactant (I) were measured using the ring method. Results lay in good agreement with theory and a critical micelle concentration of 0.2 – 0.3% was obtained. See for reference Table A7-1 and Fig.3-38 in section 3.5.6.

2. The Pendant Drop Method

The surface tension of system A(I/i) with various amounts of surfactant was measured using the described pendant drop method. The results obtained compared well to those from the DeNoüy method (see Fig A7-1 below) indicating that the available tensiometer was accurate and sufficient for the analysis of the surface tension of the systems.

Table A7-1: The surface tensions measured of the various systems A(I/i), B(I/i) and C(I/i) containing various amounts of surfactant (I) using the Lecomte du Noüy Tensiometer.

Surfactant (I)	Surface Tension [mN/m]		
	A(I/i)	B(I/i)	C(I/i)
[%]			
0.00	34.08	32.60	34.30
0.05	-	26.51	22.40
0.10	24.48	24.08	-
0.20	24.27	23.36	22.20
0.30	23.81	22.92	-
0.50	23.50	22.60	22.20
1.00	23.19	22.57	21.00
1.50	-	-	21.30
2.00	-	-	21.70

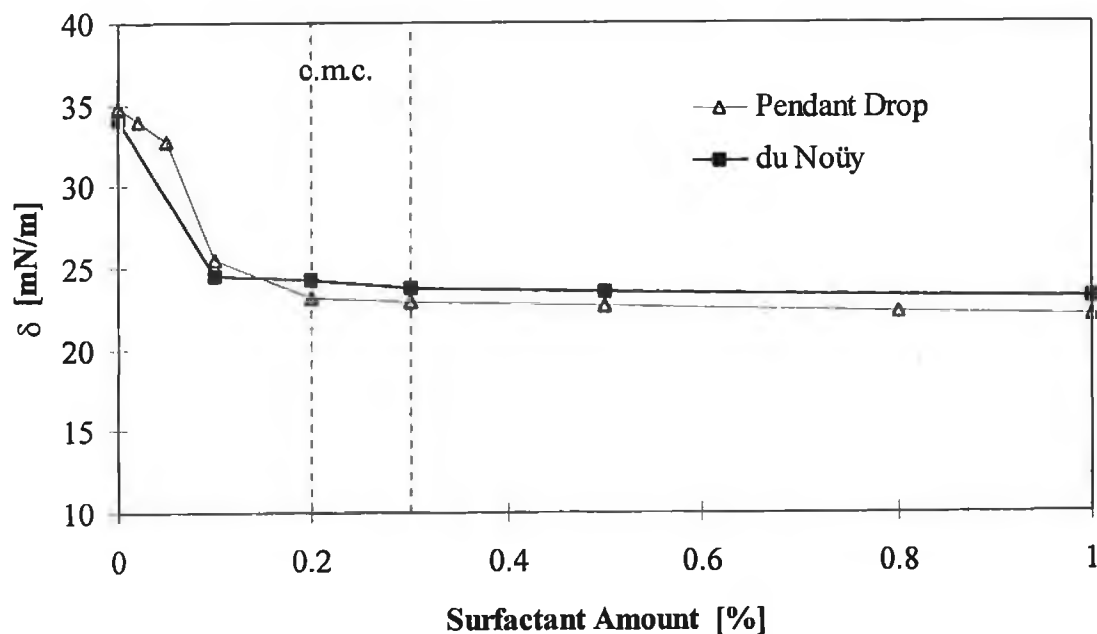


Fig. A7-1.: The surface tensions of the A-component A(I/i) with various amounts of surfactant measured using the pendant drop and the du Noüy ring methods. There is an agreement in the results obtained from the two independent methods.

3. Maximum Bubble Pressure Method

In an attempt to mimic the actual nucleation process, i.e. the formation of gas nuclei in the liquid bulk, the maximum bubble pressure method was tested on the A-components A(I/i), B(I/i) and C(V/i). This method, which is primarily based for aqueous media, obtained consequently higher surface tension values than in the previous two methods and general values quoted in the literature¹⁰. The values obtained using this instrument, especially with samples with high viscosities are not very accurate. However, the trend is the same, which reinforces the assumption that the surfactant molecules move quickly from the bulk to the liquid/gas interface under these experimental conditions. Measurements during foaming could not be carried out due to the unsuitability of the process.

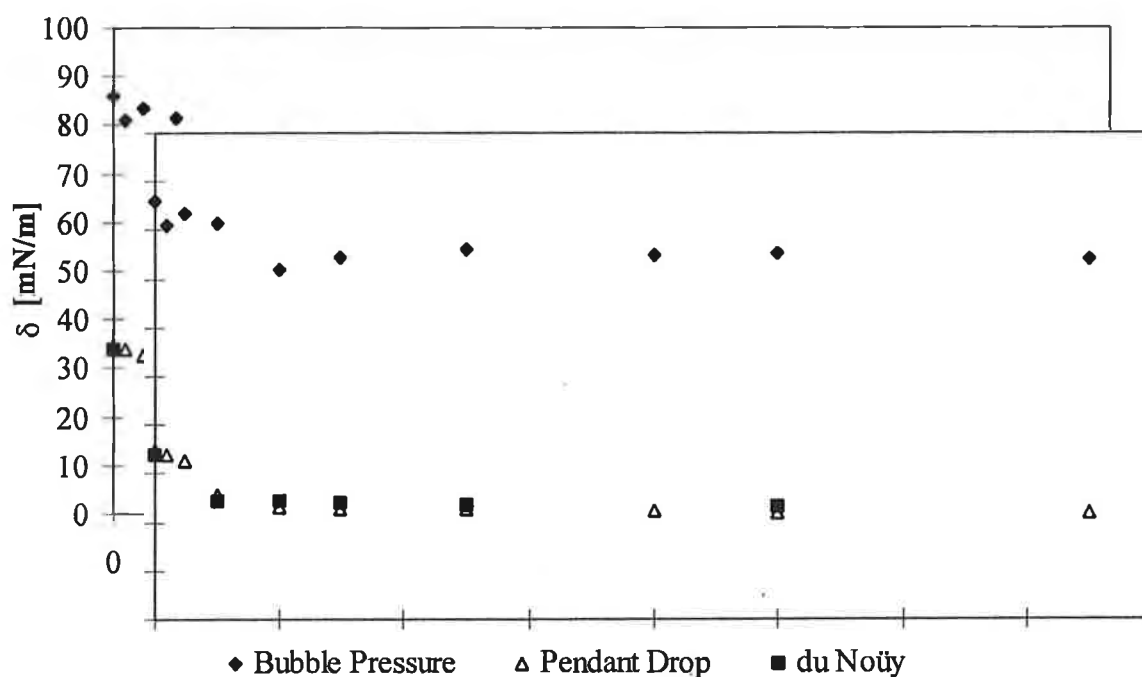


Fig. A7-2: A comparison of the all three surface tension measurement methods of the A-component A(I/i) with various amounts of surfactant.

Surface Tension Measurements with a Cyclopentane in Equilibrium

A further attempt was made to reproduce the environment of the nucleation process and to estimate the surface tension of the liquid / vapour interface. For this purpose a method was developed to induce a cyclopentane atmosphere over the sample (which also contained excess cyclopentane) to be measured. In this way a saturated solution of cyclopentane was simulated, avoiding loss of cyclopentane gas from the sample to its immediate environment, i.e. the cyclopentane is in equilibrium. This resulted in approx. 0.15% volume vapour of the total volume of cyclopentane heated, a relatively small amount. Increased heating was avoided due to its low boiling point.

The next task was to establish an adequate amount of time for the promotion of cyclopentane vapour. For this purpose the apparatus was set up as in Fig. 2-28 and cyclopentane vapour was produced as previously described. The surface tension was measured at zero time, after 30 minutes, 60 minutes and every hour for five hours. As can be seen from Fig. A7-3, a plateau is reached after one hour and the surface tension value remains steady. Therefore, a promotion time of one hour was accepted. However, it was noted that even after five hours only a small percentage weight of cyclopentane was gone from the sample at a rate of approximately 0.5g/hr and was considered negligible. The weight loss of the sample (at 25°C) was estimated at 0.04%/hr.

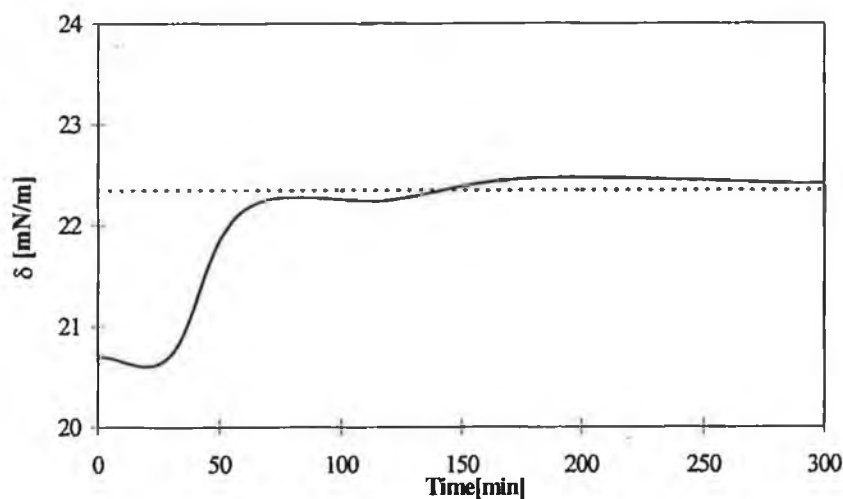


Fig. A7-3: The effect of increase cyclopentane concentration in the atmosphere on the surface tension – reaching a sample-atmosphere equilibrium after approx. 1h.

The surface tension of the system B(I/i) with various amounts of surfactant was measured after one hour of production of a cyclopentane sample-atmosphere equilibrium. The results are shown in Table A7-2 below:

Table A7-2: Surface tensions [mN/m] of B(I/i) containing various amounts of surfactant with and without cyclopentane in equilibrium.

Surfactant [%]	Surface Tension [mN/m]		$\Delta\delta$
	Without Equilibrium	In Equilibrium	
0.0	36.12	36.01	0.11
0.3	24.03	24.12	0.09
0.5	23.74	24.02	0.28
1.0	24.32	24.40	0.08

It was expected that the surface tension would increase due to increasing viscosity in a cyclopentane vapour equilibrium. This was not observed, values of which are shown in Table A7-2. The largest difference of 0.28 mN/m can be considered a result of the biggest disadvantage of the method - the instability of the ring in a gas current.

As the difference between the surface tension values obtained with cyclopentane in equilibrium and an open system was negligible, it was decided to measure the surface tension of all other systems using the traditional method with a bell cap for added environmental protection.

The surface tension proved to be independent of the amount and / or type of catalyst. Surfactants decreased the surface tension of the B-component. Prepolymers decreasing in free %NCO showed increasing surface tensions (see Fig.3-49).

Appendix 8

Surfactant Analysis

Structural analysis was carried out using quantitative ^{29}Si -NMR and ^1H -NMR providing values for the length of the siloxane backbone, the number of polyol sidechains and the ratio of ethyleneoxide to propylene oxide (EO:PO).

For the evaluation of x, y, m and n the following example has been explained. From the integration of the peaks in the ^{29}Si NMR spectrum in Fig A8-1, signal **a** at 0.1ppm represents the methyl groups:

$$6x + 3y + 18 = 100$$

where, 6x, 3y and 18 represent the trimethylsilyl groups, the alkylmethyl groups and the trimethylsilyl end groups. The intensity of the protons on the polyether sidechain can be got from the peak marked **b** (0.5ppm) (CH_2 groups on Si):

$$2y = 3.56$$

$$y = 1.78$$

Insertion of y value into previous equation yields a value of 12.78 for x.

From the ^{29}Si -NMR spectrum and the ratio of x:y obtained from the former spectrum the average chain length of the siloxane backbone can be obtained:

$$x + y = 44$$

$$x:y = 12.78:1.78$$

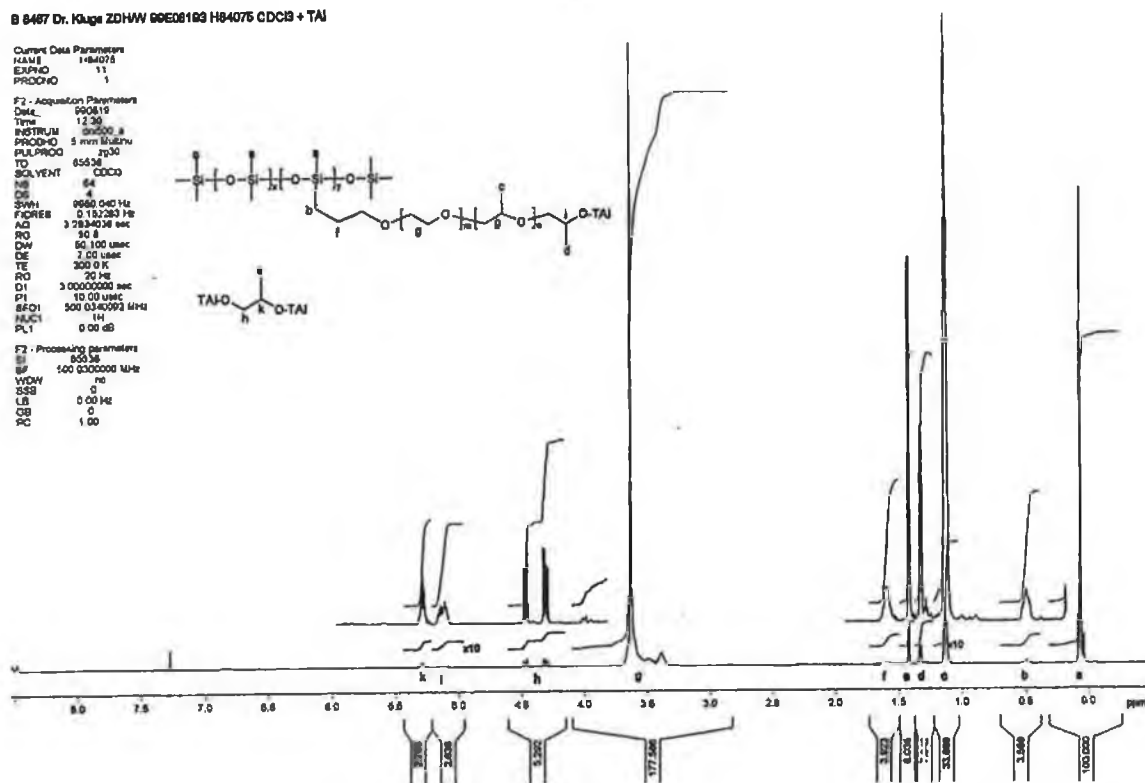
$$x = 38.62 \quad y = 5.38$$

B 8487 Dr. Kuge ZDHW 90E08103 H84076 CDCB + TAI

Current Data Parameters
NAME 184076
EXPNO 11
PROCNO 1

F2 - Acquisition Parameters
Date_ 090819
Time 12:30
INSTRUM spect
PROBHD 5 mm BBO
PULPROG zgpg30
TD 65536
SOLVENT CDCl3
NS 64
DS 4
SWH 6580.040 Hz
FIDRES 0.132283 Hz
AQ 1.283458 sec
RG 36
DM 50.100 usec
DE 1.00 usec
TE 300.0 K
RO 20 Hz
D1 3.00000000 sec
P1 10.00 usec
SFO1 500.000000 MHz
NUC1 1H
PL1 0.00 dB

F2 - Processing parameters
SI 32768
SF 500.000000 MHz
WDW no
SSB 0
LB 0.00 Hz
GB 0
PC 1.00



B 8487 Dr. Kuge ZDHW 90E08103 5207
CDCB + Cress

Current Data Parameters
NAME 5207
EXPNO 1
PROCNO 1

F2 - Acquisition Parameters
Date_ 090820
Time 8:37
INSTRUM spect
PROBHD 5 mm BBO
PULPROG zgpg30
TD 32768
SOLVENT CDCl3
NS 4096
DS 4
SWH 6580.040 Hz
FIDRES 0.132283 Hz
AQ 1.283458 sec
RG 36
DM 50.100 usec
DE 1.00 usec
TE 300.0 K
RO 20 Hz
D1 3.00000000 sec
P1 10.00 usec
SFO1 500.000000 MHz
NUC1 1H
PL1 0.00 dB

F2 - Processing parameters
SI 32768
SF 500.000000 MHz
WDW no
SSB 0
LB 0.00 Hz
GB 0
PC 1.00

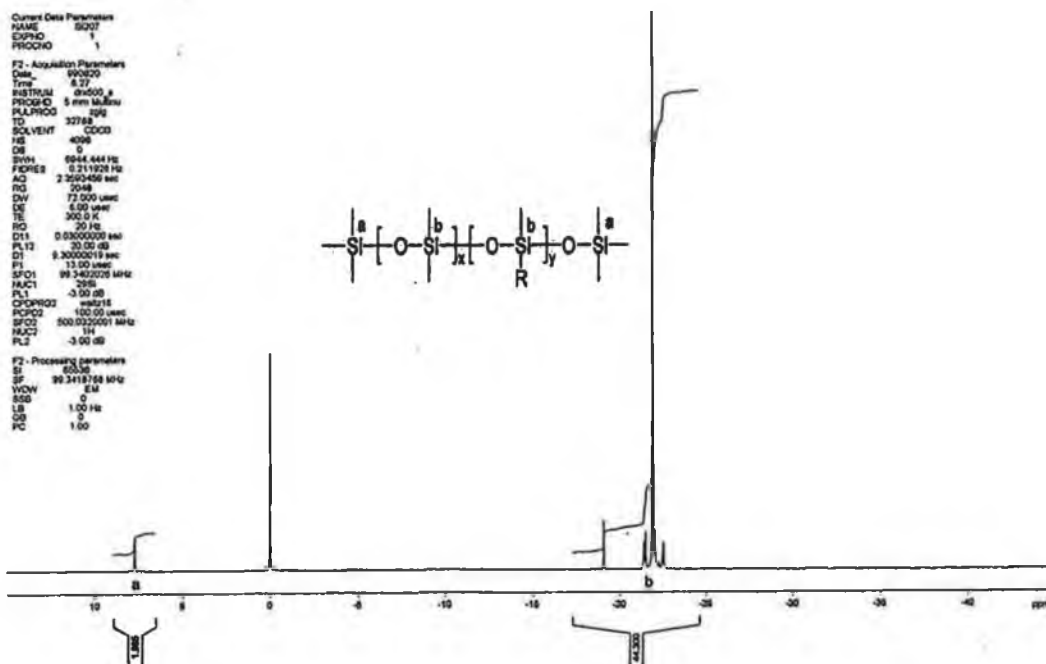


Fig. A8-1: The ^1H - and ^{29}Si -NMR spectra of the surfactant I.

In order to calculate the values for m and n the following peak intensities in the ^1H -NMR spectrum have to be taken into account: **c**, **d**, **g** and **i**. The peak at **g** (177.59) is made from contributions from 4 EO-protons and 3 PO-protons (CH and CH_2 beside O). Peaks **c** (33.67) and **d** (7.84) are from the CH_3 groups of the PO. The signal at **i** (2.638) represents the secondary alcohol, which was esterified using trichloroacetyl isocyanate.

The total intensity of the EO-protons, I_{EO} , is

$$I_{\text{EO}} = 177.59 - (33.67 + 7.84) = 136.08$$

Dividing this value by the intensity of the proton at **i** gives the number of EO-proton sidechains. Further dividing by 4 results in the number of EO units per sidechain:

$$136.08 \div 2.64 = 51.55$$

$$51.55 \div 4 = 12.9$$

Similarly the PO-protons can be calculated:

$$I_{\text{PO}} = (33.67 + 7.84) \div 2.64 = 15.72$$

$$15.72 \div 3 = 5.2$$

Therefore the ratio of EO:PO is 12.9 : 5.2 or 1 : 0.4.

Substituting the values for x, y, m and n into the structure results in a molecular weight of 8300g.

Appendix 9

Measured Cell Diameter in Finished Foam

The cell diameter of the finished foam was measured perpendicular (\perp) and parallel (\parallel) to the direction of foaming. As expected, the cells are smaller in the perpendicular direction.

Table A9-1: The cell sizes measured perpendicular (\perp) and parallel (\parallel) to the direction of foaming.

Blowing Agent:	H ₂ O / CO ₂		C ₅ H ₁₀		C ₆ F ₁₄	
Surfactant (I)	\perp	\parallel	\perp	\parallel	\perp	\parallel
[%]	[μ m]	[μ m]	[μ m]	[μ m]	[μ m]	[μ m]
0.00	1700.5	2254.1	1966	2395	351.7	485.2
0.10	509.8	646.3	604.1	827.8		
0.20	448.7	649.9	556.4	764.1	287.0	361.8
0.30	430.3	592.8	492.7	671.9		
0.50	429.2	633.7	501.8	679.9	279.8	360.5
1.00	399.5	554.9	444.7	625.5	272.3	322.1

Table A9-2: Influence of surfactant type and amount on the end cell diameter sizes measured perpendicular (\perp) and parallel (\parallel) to the direction of foaming.

Surfactant	Cell Diameter [μ m]									
	B(I/i)		B(II/i)		B(III/I)		B(IV/i)		B(V/i)	
	\perp	\parallel	\perp	\parallel	\perp	\parallel	\perp	\parallel	\perp	\parallel
[%]	[μ m]	[μ m]	[μ m]	[μ m]	[μ m]	[μ m]	[μ m]	[μ m]	[μ m]	[μ m]
0.00	1966	2395	1966	2395	1966	2395	1966	2395	1966	2395
0.20	556.4	764.1	526.2	718.6	643.3	981.8	655.7	869.4		
0.50	501.8	679.9	483.8	679.8	529.2	718.7	590.6	752.2	731.0	919.9
1.00	444.7	625.5	488.6	635.7	424.2	584.1	542.2	706.4	655.2	935.4
1.50			471.4	620.2	501.5	678.8	507.5	674.8		

Appendix 10

CO₂ Solubility – Method of Partial Pressures

Table A10-1: The solubility of CO₂ in A(0/i) (without surfactant) and A(I*/i). (* indicates 3% surfactant instead of 1%). p is the total sample pressure, p_0 is the vapour pressure of the sample, $w(\text{CO}_2)$ is the mass of CO₂ in the liquid phase and α is the solubility of CO₂ calculated from equation (56) in section 3.5.11.

Sample	Total Pressure p [bar]	CO ₂ -Partial Pressure $(p-p_0)$ [bar]	$w(\text{CO}_2)$	Solubility Coefficient α [bar ⁻¹]
A(0/i)	0.011	0.000	0	0.00274
	0.118	0.107	0.000297	
	0.380	0.369	0.00101	
	0.880	0.869	0.00237	
	1.610	1.599	0.00428	
	2.320	2.309	0.00614	
	3.074	3.063	0.00812	
	4.474	4.463	0.0118	
	5.968	5.957	0.0157	
	7.645	7.634	0.0201	
A(I*/i)	0.011	0.000	0	0.00270
	0.125	0.114	0.00321	
	0.370	0.359	0.000967	
	0.857	0.846	0.00226	
	1.542	1.531	0.00408	
	2.236	2.225	0.00590	
	2.923	2.912	0.00772	
	4.319	4.308	0.0114	
	5.793	5.782	0.0151	
	7.390	7.379	0.0195	

Appendix 11

Publications

The following is a list of publications and posters which were (co-) published with regard to this work by the author during the time of research:

- A. Biedermann, C. Kudoke, A. Merten, E. Minogue, U. Rotermund, H.-P. Ebert, U. Heinemann, J. Fricke and H. Seifert; *Analysis of Heat Transfer Mechanisms in Polyurethane Rigid Foam*; Polyurethane Expo, Florida 1999 405-412.
- A. Biedermann, C. Kudoke, A. Merten, E. Minogue, U. Rotermund, H.-P. Ebert, U. Heinemann, J. Fricke and H. Seifert; *Analysis of Heat Transfer Mechanisms in Polyurethane Rigid Foam*; High Temperatures – High Pressures; 15th European Conference on Thermophysical Properties, Würzburg 1999.
- *A Study Into the Improvement of the Thermal Properties of Polyurethane Rigid Foam*; E. Minogue, A. Biedermann, H. Vos; The Fifty Second Irish Universities Chemistry Research Colloquium, Cork 2000.
- *Nucleation Process in Polyurethane Rigid Foam*; A. Biedermann, E. Minogue; Polyurethanes 2000; Advances in the Science of Polyurethanes, Annapolis 2000.
- *An In-Situ Study of the Nucleation Process of Polyurethane Rigid Foam*; A. Biedermann, E. Minogue; Polyurethanes Expo, Boston 2000.

	A(I/i)	B(I/i)	B(II/i)	B(III/i)	B(IV/i)	B(V/i)	C(VI/i)
A-Component							
Polyol 1	✓	✓	✓	✓	✓	✓	✓
Polyol 2	✓	✓	✓	✓	✓	✓	✓
DPG*	✓	✓	✓	✓	✓	✓	✓
Water	✓✓	✓	✓	✓	✓	✓	✓
Cyclopentane		✓	✓	✓	✓	✓	
Perfluorohexane							✓
Surfactant							
(HLB-Value):							
I (1.38)	✓	✓					
II (1.15)			✓				
III (1.77)				✓			
IV (4.18)					✓		
V (5.35)						✓	
VI (0.87)							✓
Catalyst:							
C ₈ H ₁₇ N	✓	✓	✓	✓	✓	✓	✓
C ₆ H ₁₂ N ₂							
C ₁₁ H ₂₁ O ₂ N							
C ₃₂ H ₆₄ O ₄ Sn							
Emulsifier:							
C ₁₂ H ₁₀ O ₃ SF ₁₇							✓

Polyol 1 = a polyol with starter materials of sucrose, glycerine and propylene oxide;
OH No. 380-420.

Polyol 2 = a polyol with starter materials of propylene glycol and propylene oxide;
OH No. 235-260.

*DPG = dipropylene glycol

	B(I/i)	B(I/ii)	B(I/iii)	B(I/iv)
A-Component				
Polyol 1	✓	✓	✓	✓
Polyol 2	✓	✓	✓	✓
DPG*	✓	✓	✓	✓
Water	✓	✓	✓	✓
Cyclopentane	✓	✓	✓	✓
Perfluorohexane				
Surfactant				
(HLB-Value):				
I (1.38)	✓	✓	✓	✓
II (1.15)				
III (1.77)				
IV (4.18)				
V (5.35)				
VI (0.87)				
Catalyst:				
$C_8H_{17}N$	✓			
$C_6H_{12}N_2$		✓		
$C_{11}H_{21}O_2N$			✓	
$C_{32}H_{64}O_4Sn$				✓
Emulsifier:				
$C_{12}H_{10}O_3SF_{17}$				

Polyol 1 = a polyol with starter materials of sucrose, glycerine and propylene oxide;
OH No. 380-420.

Polyol 2 = a polyol with starter materials of propylene glycol and propylene oxide;
OH No. 235-260.

*DPG = dipropylene glycol